Application of Ionizing Radiations in Conjunction with Biological Treatment for the Degradation of Pharmaceutical Effluents

A Thesis submitted in partial fulfilment of the requirement for the award of the degree of

DOCTOR OF PHILOSOPHY

By:

RAHIL CHANGOTRA

(Regd. No. 901514001)

School of Energy and Environment

Thapar Institute of Engineering and Technology

Patiala- 147004, India

October, 2019

DECLARATION

This is to declare that the research work which is being presented in this thesis entitled "**Application of Ionizing Radiations in Conjunction with Biological Treatment for the Degradation of Pharmaceutical Effluents**" in fulfilment of requirement of the degree of 'Doctor of Philosophy' in School of Energy and Environment, Thapar Institute of Engineering and Technology, Patiala, India, is an authentic record of my own research work carried out under the supervision of Dr. Amit Dhir (Associate Professor, School of Energy and Environment, TIET, Patiala, India). The matter presented in this thesis has not been submitted, in part or full, to any other institute in India or Abroad for the award of any degree. Works of other authors cited in this thesis have been duly acknowledged under reference section of this thesis.

Rahil Changotra
(Regd. No. 901514001)

I

CERTIFICATE

This is to certify that the thesis entitled **"Application of Ionizing Radiations in Conjunction with Biological Treatment for the Degradation of Pharmaceutical Effluents"** which has been submitted by Mr. Rahil Changotra in the fulfilment of the requirements for the award of the degree of 'Doctor of Philosophy' in School of Energy and Environment, Thapar Institute of Engineering and Technology, Patiala, India, is a record of the candidate's own independent and original research work carried out by him under my supervision and guidance. The matter embodied in this thesis has not been submitted, in part or full, to any other institute for the award of any degree in other University or Institute.

Supervisor

Dr. Amit Dhir

Associate Professor & Head

School of Energy and Environment

TIET, Patiala, India

II

ACKNOWLEDGEMENT

First and foremost, I would like to express my sincere gratitude to my supervisor ***Dr. Amit Dhir,*** *Associate Professor & Head, School of Energy and Environment, TIET, Patiala, for his continuous support in my Ph.D. study and related research. I appreciate all his contributions of time, ideas, motivation, knowledge and funding to make my Ph.D. experience productive and stimulating.*

I express my heartfelt gratitude to ***Dr. Prakash Gopalan****, Director, TIET, Patiala, for providing the opportunity to work in this esteemed organization. Without the precious support it would not be possible to conduct this research. I feel special gratitude towards* ***Dr. Rafat Siddique****, Dean, Research and Sponsored Projects, TIET, Patiala for his valuable guidance and support during my research work. I am very thankful to* ***Dr. N.Tejo Prakash****, the former Head of School of Energy and Environment, Thapar University for providing me access to the laboratory and research facilities.*

I gratefully acknowledge the funding sources that made my Ph.D. work possible. A very special gratitude goes out to ***Department of Atomic Energy-Board of Research in Nuclear Sciences (DAE-BRNS), Government of India (Project No. 35/14/48/BRNS-2014)****, for providing the fellowship and funding for the work. I am grateful to* ***Dr. Jhimli Paul Guin****, Scientific officer, Bhabha Atomic Research Centre, Mumbai for her valuable knowledge, time, interest, and helping nature during experimentation at BARC, Mumbai. I am also thankful to* ***Dr. Lalit Varshney****, Head, Radiation Technology and Development Division, BARC for providing the necessary research facilities at BARC. I would also like to acknowledge the Board of Radiation & Isotope Technology, Navi Mumbai where I performed electron beam experiments. I am thankful to* ***Dr. S.A. Khader,*** *Scientific Officer and* ***Mr. Ravindra Patkari,*** *Scientific Assistant, Electron Beam Processing Section (EBPS), BARC for their kind support in carrying out electron beam irradiation experiments.*

Beside my advisors, I would like to thank the rest of my doctoral committee: ***Dr. Anita Rajor****,* ***Dr. J.P. Kushwaha*** *and* ***Dr. V.K. Sangal*** *for their insightful comments and encouragement, but also for their keen interest in me at every stage of my research work from various perspectives.*

I am thankful to ***Mr. Suhail****,* ***Mr. Gurpreet Singh*** *and* ***Mr. Bharat*** *for their constant support and kind help throughout my research work. This research work would have not*

come to a successful completion without the help I received from SAI Labs, TIET, Patiala, SAIF, PU, Chandigarh and MRC, MNIT, Jaipur.

I take this opportunity to thank my special lab-mates ***Mr. Vagish Dwibedi, Mr. Pali Rosha, Dr. Sumit Jaiswal, Dr. Noorpreet Dhanjal, Ms. Palak, Ms. Jayishnu and Ms. Harleen*** *for the stimulating discussions, cheerful support, cooperation, and for all the fun that we have had together. The group has been a source of friendships as well as good advice and collaboration.*

I feel a deep sense of gratitude for ***Ms. Rupali Dhir*** *for her kind support, encouragement and blessings.*

I am very much indebted to my ***father*** *for always showering his blessings from above. I would like to thank my family for all their love and encouragement. For my parents, who have raised me with love and supported me in all my pursuits. And most of all for my loving, supportive, encouraging, and patient person* ***Ms. Himadri Rajput*** *whose faithful support during the every stage of this Ph.D. is so appreciated. Thank you.*

I am very grateful to my in-Laws, who have constantly provided the moral and emotional support in my life. I am also grateful to my other family members and friends who have supported me along the way.

Above all, I owe it all to the Almighty God for granting me the wisdom, health and strength to undertake this research task and enabling me to its completion.

Rahil Changotra

ABSTRACT

Due to rapid urbanization and steep population growth, the advancement in medical field has dramatically increased the consumption of pharmaceuticals in developing country like India. Pharmaceutical compounds are a group of man-made chemicals of utmost concern, as they may infuse into our environment. During pharmaceutical manufacturing, high volume of clean water is consumed with the generation of enormous volumes of complex and hazardous wastewater. In most of the existing pharmaceutical industry, the dilute aqueous streams from the plants are generally treated by conventional biological treatment. However, these treatment processes are ineffective in removal of the persistent and biological resistant pharmaceutical contaminants. In addition, evaporation technique is used to treat the refractory and high strength effluents which is energy and cost intensive process. Thus, there is stringent requirement to employ methods and technologies to treat wastewater in order to enhance its reuse or recyclability.

In this regard, advanced oxidation processes (AOPs) are considered to be competent and effective approach, which is based on the generation of reactive radical species i.e., hydroxyl radical ($HO^{\bullet}$). Among various AOPs, Fenton and photo-assisted Fenton processes have been regarded as an efficient treatment for the degradation of pharmaceuticals and there is growing interest in the applications of heterogeneous Fenton-like processes using iron oxides and other naturally occurring minerals. Radiolytic degradation process using ionizing radiations i.e., gamma radiation and high electron beam (E-beam) have received much attention due to their ability to degrade recalcitrant organic contaminants without use of any additional oxidant and chemicals. Thus, the present study was aimed to explain the degradation of selected pharmaceuticals *viz*. amoxicillin (AMX), ofloxacin (OFX) and ornidazole (ORZ) as well as real pharmaceutical wastewater with independent Fenton/photo-Fenton, gamma and E-beam treatment. In addition, a coupled system involving gamma/E-beam irradiations along with biological treatment have been explored to study the feasibility of integrated approach on real pharmaceutical industrial wastewater.

For the Fenton based treatment of model compounds, hematite (α-Fe_2O_3), graphene oxide-pyrite (GO-FeS_2) nanocomposites and natural available soil were utilized as catalyst. Hematite particles of different shaped (rod, spherical and cubical) and graphene oxide-pyrite (GO-FeS_2) nanocomposites were synthesized using sol-gel and hydrothermal procedure, respectively and were characterized for morphological properties. Complete removal (98%)

of ORZ (0.22 mM) was achieved in solar-Fenton treatment with cubical hematite under the optimum operating conditions *viz*. 10 mM H_2O_2, 0.13 g L^{-1} α-Fe_2O_3 at pH 3 within 180 min. The highest concentration of leached iron in the aqueous solution confirms cubical hematite to be the most photoactive form among the various synthesized hematite particles. Highly dispersive iron oxide i.e., FeS_2 fabricated on GO layer was utilized in solar-Fenton treatment of AMX (0.1 mM) and OFX (0.1 mM) leading to 97 and 80% degradation, respectively under the optimized conditions *viz.* 1 g L^{-1} GO-FeS_2, 10 mM H_2O_2 at pH 5 within 180 min. The rate of H_2O_2 degradation and $HO^{\bullet}$ concentration was investigated during the treatment process.

The potential viability of soil as a cost-free catalyst was investigated in photo-Fenton degradation of ORZ (0.09 mM) and OFX (0.05 mM). Soil was found to be enriched with various iron oxides like hematite, magnetite, goethite, pyrite and wustite, which contributes toward enhanced dissolution of Fe^{3+} than Fe^{2+} in the aqueous solution. Elevated degradation efficiencies (95% ORZ and 92% OFX) were achieved due to Fe^{2+}/Fe^{3+} cycling, producing more $HO^{\bullet}$ leading to the co-existence of homogeneous and heterogeneous process simultaneously. Continuous scale studies conducted by employing soil in the form of soil beads and as a thin layer spread on the surface of baffled reactor lead to effective treatment of ORZ and OFX. Soil beads were found to have satisfactory reusability and stability. HPLC, mineralization and toxicity assessment confirmed the efficient removal of both the compounds.

Gamma and E-beam radiolytic degradation of OFX (0.1 mM), AMX (0.1 mM) and ORZ (0.22 mM) was studied under different experimental conditions. The parameters *viz.* initial concentration, pH, dose and the concentrations of various additives were optimized and it was observed that degradation followed pseudo first-order reaction kinetics. Degradation rate of model compounds was significantly increased with increase in the absorbed dose and decrease with the initial concentration under acidic condition when compared to neutral or alkaline condition. Presence of different scavengers showed decrease in the dose constant, mainly owing to the competition reactions between model compounds and scavengers with the radiolytically generated reactive species. The addition of H_2O_2 had a synergistic effect on the degradation and mineralization extent of model compounds. Based on the LC-QTOF-MS analysis, it was inferred that OFX and ORZ radiolytic degradation was mainly attributed to oxidative $HO^{\bullet}$ radicals and the direct cleavage of these molecules. Cytotoxicity assessment showed that the degradation products of OFX, AMX and ORZ did not exhibited any toxicity after irradiation treatment. The cost of energy consumed during gamma and E-beam irradiation treatment of model compounds was also evaluated. Overall, all the treatment

technologies applied in the treatment of model compounds were effective in their degradation; however, the use of E-beam was effective in degradation of model compounds in term of treatment time. Moreover, the use of irradiation based treatment has eliminated the use of additional chemicals as well as sludge formation in comparison to photo-Fenton treatment.

High strength wastewater (HSW) and low strength wastewater (LSW) collected from representative manufacturing unit were subjected to independent Fenton/photo-Fenton, gamma and E-beam treatment. For both the HSW and LSW, dark-Fenton (DF) and solar driven photo-Fenton (PF) were utilized as pre-treatment technologies to enhance the biodegradability and reduce the organic load of wastewater through simultaneous oxidation and coagulation. The operational parameters like pH, H_2O_2 dosage and Fe^{2+} concentration were optimized in case of DF and PF processes. Overall results indicated that treatment of wastewaters with PF lead to better COD and TOC removal efficiency with subsequent biological degradation when compared to DF treatment. For the effective treatment of LSW and HSW under gamma/E-beam irradiation, hybrid approach including coagulation, gamma/E-beam irradiation and biological treatment were employed individually and in sequence to determine the effective remediation of real wastewater. Effect of parameters like pH, irradiation dose and oxidants were investigated during gamma/E-beam irradiation treatment. To compare process performance, gamma-irradiation was employed as pre- and post-treatment to biological treatment. Use of H_2O_2 irradiation based treatment lead to enhanced COD and TOC removal efficiency when compared to $K_2S_2O_8$ in independent gamma/E-beam irradiation. The sequential approach of coagulation, gamma and biological treatment accounts for the synergistic degradation and detoxification of wastewaters, and lead to overall 92 and 90% COD removal of LSW and HSW, respectively. Sequential coagulation, E-beam and biological treatment lead to overall COD removal of 94 and 89% for LSW and HSW, respectively. Cytotoxicity and cost assessment of the gamma/E-beam treatment process for LSW and HSW were examined. Considering the high dose rate of E-beam accelerators and capacity to treat large volume of wastewater, E-beam technology followed by existing aerobic biological treatment could be utilized as an effective technique for the degradation of real pharmaceutical industry wastewater in the common effluent treatment plant (CETP).

Dedicated to my papa

LIST OF TABLES

Table No.	Tittle	Page No.
1.1	Properties of AMX, OFX and ORZ	13
2.1	Results of different AOPs utilized for the treatment of selected model compounds	19
4.1	EDS analysis of synthesized α-Fe_2O_3	53
4.2	BET surface area and porosity details of the synthesized catalyst	54
4.3	EDS analysis of soil	62
4.4	TOC removal vs. Reaction time in solar-induced batch mode [For ORZ, 0.033 g L^{-1} soil dosage, 1 mM H_2O_2, pH 3, 150 mL solution volume; For OFX, 0.020 g L^{-1} soil dosage, 2 mM H_2O_2, pH 3, 150 mL solution volume]	68
4.5	Statistical analyses (ANOVA and Tukey's) on different irradiation sources for the degradation of ORZ	72
4.6	Statistical analyses (ANOVA and Tukey's) on different irradiation sources for the degradation of OFX	72
4.7	EDS analysis of synthesized GO-FeS_2 nanocomposite	77
4.8	Data from gamma radiolytic experiments of ofloxacin: Influence of initial concentration, pH and various additives. [(G-(OFX)) values calculated for 1.0 kGy absorbed dose using Eq. 3.1]	85
4.9	Data from gamma radiolytic experiments of ORZ: Influence of initial concentration, pH and various additives. [*G*-value calculated for 1 kGy dose using the Eq. 3.1]	85
4.10	Data from gamma radiolytic experiments of AMX: Influence of initial concentration, pH and various additives. [*G*-value calculated for 2.5 kGy dose using the Eq. 3.1]	86
4.11	Intermediate compounds during gamma-radiolytic degradation of ORZ	104
4.12	Cost involved during gamma radiolysis of model compounds	108
4.13	Experimental data from E-beam induced treatment of OFX: Influence of various parameters. [G-(OFX) calculated for 1.0 kGy dose using Eq. 3.1]	112
4.14	Experimental data from E-beam induced treatment of ORZ: Influence of	113

	various parameters. [G-(ORZ) calculated for 1.0 kGy dose using Eq. 3.1]	
4.15	Experimental data from E-beam induced treatment of AMX: Influence of various parameters. [G-(AMX) calculated for 2.5 kGy dose using Eq. 3.1]	114
4.16	Chemical composition of the selected water matrices and the results of inhibition rates of $HO^{\bullet}$, e_{aq}^{-} and $H^{\bullet}$ for E-beam radiolytic degradation of OFX	124
4.17	Chemical composition of the selected water matrices and the results of inhibition rates of $HO^{\bullet}$, e_{aq}^{-} and $H^{\bullet}$ for E-beam radiolytic degradation of ORZ	124
4.18	Calculations of power of E-beam accelerator and volume of model compound solution treated	138
4.19	The cost of electrical energy involved in E-beam radiolysis of OFX in different water matrices (UW: ultrapure water; SW: surface water; WW: wastewater)	138
4.20	The cost of electrical energy involved in E-beam radiolysis of ORZ in different water matrices (UW: ultrapure water; SW: surface water; WW: wastewater)	138
4.21	The cost of electrical energy involved in E-beam radiolysis of AMX	139
4.22	Comparative results of employed treatments for model compounds	140
4.23	Physicochemical characteristics of raw low and high strength wastewater	141
4.24	Physicochemical characteristics of low strength wastewater before and after coagulation treatment with 3 g L^{-1} of coagulant dose	157
4.25	Physicochemical characteristics of high strength wastewater before and after coagulation treatment with 4 g L^{-1} of coagulant dose	157
4.26	The cost of energy involved in gamma radiolysis of low strength pharmaceutical wastewater	174
4.27	The cost of energy involved in gamma radiolysis of high strength pharmaceutical wastewater	175
4.28	Physicochemical characteristics of low and high strength wastewater before and after coagulation treatment with $FeCl_3$	176
4.29	The cost of energy involved in E-beam radiolysis of low strength pharmaceutical wastewater	187
4.30	The cost of energy involved in E-beam-radiolysis of high strength	187

	pharmaceutical wastewater	
4.31	The total operating cost involved in E-beam radiolysis + biological treatment of pharmaceutical wastewater	188
4.32	Evaluation of total cost of E-beam facility for industrial applications of wastewater treatment	189
4.33	Comparative results of employed treatments for real wastewater	190
4.34	Comparative results of employed treatments for real wastewater in conjunction with biological treatment	190

LIST OF FIGURES

Figure No.	Tittle	Page No.
1.1	Fate and transport of the pharmaceuticals in the environment. ETPs: Effluent treatment plants, DWTPs: Drinking water treatment plants.	4
1.2	Classifications of AOPs	7
1.3	E-beam accelerator: view (left) and scheme (right)	10
3.1	ETP layout of representative industry (MEE: Multiple Effect Evaporator; PSF: Pressure Sand Filter; ACF: Activated Carbon Filter)	35
3.2	Schematic representation of UV tubes chamber	36
3.3	Schematic representation of continuous baffled reactor	36
3.4	Schematic representation of gamma chamber (*Source:* BARC, Mumbai)	37
3.5	View of electron beam accelerator unit at BRIT, Navi Mumbai [1: Electron exit window; 2: Conveyor: 3: Stainless steel tray]	37
3.6	Schematic layout of batch mode biological reactor	38
3.7	Schematic diagram of experimental setup for activated sludge treatment of wastewater. P1: Peristaltic pump for sludge recirculation; P2: Peristaltic pump for influent of wastewater	38
3.8	Synthesis procedure of graphene oxide	40
3.9	Synthesis procedure of graphene oxide-pyrite (GO-FeS_2) nanocomposite	41
4.1	XRD patterns of the α-Fe_2O_3 with different shapes: (a) R-α-Fe_2O_3 (b) C-α-Fe_2O_3 and (c) S-α-Fe_2O_3	53
4.2	SEM (a: Rod-shaped α-Fe_2O_3; b: Cubical-shaped α-Fe_2O_3; c: Spherical-shaped α-Fe_2O_3), TEM (d: Rod-shaped α-Fe_2O_3; e: Cubical-shaped α-Fe_2O_3; f: Spherical-shaped α-Fe_2O_3) and EDS (g: Rod-shaped α-Fe_2O_3; h: Cubical-shaped α-Fe_2O_3; i: Spherical-shaped α-Fe_2O_3) analysis of α-Fe_2O_3 microstructures	54
4.3	Factorial effects of heterogeneous photo- Fenton reaction on ORZ degradation: (a) C-α-Fe_2O_3 dosage, (b) H_2O_2 dosage, and (c) pH	56
4.4	Time trend of total dissolved Fe upon solar irradiation	58
4.5	Schematic diagram depicting the degradation process using hematite particles	58
4.6	Activity comparison of different α-Fe_2O_3 under solar and UV irradiations	59

4.7	HPLC of initial and treated samples using different α-Fe_2O_3 under solar/UV irradiations	60
4.8	Time dependent TOC removal of ORZ using synthesized catalyst under solar and UV irradiations	61
4.9	SEM micrograph (a & b) and EDS pattern of soil (c & d)	62
4.10	XRD pattern of soil	63
4.11	Preliminary experimental results of (a) ORZ (b) OFX	63
4.12	Variation of process parameters (a) soil dosage (1 mM H_2O_2, pH 3) (b) H_2O_2 (0.033 g L^{-1} soil, pH 3) and (c) pH (0.033 g L^{-1} soil, 1 mM H_2O_2), for the degradation of 150 mL ORZ solution and (d) soil dosage (1 mM H_2O_2, pH 3) (e) H_2O_2 (0.020 g L^{-1} soil, pH 3) and (f) pH (0.020 g L^{-1} soil, 2 mM H_2O_2), for the degradation of 150 mL OFX solution	66
4.13	PL spectrum for $HO^{\bullet}$ determination (a) ORZ under UV-A, (b) OFX under UV-A, (c) ORZ under UV-B, (d) OFX under UV-B, (e) ORZ under solar and (f) OFX under solar. [ORZ 0.09 mM and OFX 0.05 mM; 150 mL solution volume]	67
4.14	pH profile of ORZ and OFX degradation with time in solar-induced batch mode [For ORZ, 0.033 g L^{-1} soil dosage, 1 mM H_2O_2, pH 3, 150 mL solution volume; For OFX, 0.020 g L^{-1} soil dosage, 2 mM H_2O_2, pH 3, 150 mL solution volume]	69
4.15	Leaching of iron in solar-induced batch degradation of (a) ORZ (0.033 g L^{-1} soil, 1 mM H_2O_2 and pH 3) and (b) OFX (0.020 g L^{-1} soil, 2 mM H_2O_2 and pH 3)	70
4.16	Schematic diagram depicting the occurrence of simultaneous homogeneous and heterogeneous reactions	70
4.17	Degradation profile with time under different irradiation sources (a) ORZ [0.033 g L^{-1} soil dosage, 1 mM H_2O_2, pH 3, 150 mL solution volume] (b) OFX [0.020 g L^{-1} soil dosage, 2 mM H_2O_2, pH 3, 150 mL solution volume]	71
4.18	Degradation and reusability in continuous immobilized mode [For ORZ, 0.033 g L^{-1} soil dosage, 1 mM H_2O_2, pH 3, 5 L solution volume; For ORZ, 0.020 g L^{-1} soil dosage, 2 mM H_2O_2, pH 3, 5 L solution volume]	74
4.19	HPLC chromatograms of ORZ (Batch: 0.033 g L^{-1} soil, 1 mM H_2O_2, pH	75

3, 150 mL ORZ solution; Continuous: 0.033 g L^{-1} soil, 1 mM H_2O_2, pH 3, 5 L ORZ solution) and OFX (Batch: 0.020 g L^{-1} soil, 2 mM H_2O_2, pH 3, 150 mL OFX solution; Continuous: 0.020 g L^{-1} soil, 2 mM H_2O_2, pH 3, 5 L OFX solution)

4.20 HR-TEM analysis of (a) FeS_2 (b, c & d) GO-FeS_2 nanocomposite 76

4.21 XRD patterns of FeS_2 and GO-FeS_2 nanocomposite 77

4.22 Degradation profile of (a) OFX and (b) AMX using synthesized GO-FeS_2 nanocomposite 78

4.23 (a) Profile of H_2O_2 decomposition and $HO^{\bullet}$ concentration in GO-FeS_2 photo-Fenton treatment (b) TOC profile of AMX and OFX in GO-FeS_2 photo-Fenton treatment 79

4.24 (a) Change in concentration (C/C_o) of OFX as a function of absorbed dose (b) Change in concentration (C/C_o) of ORZ as a function of absorbed dose (c) Change in concentration (C/C_o) of AMX as a function of absorbed dose 81

4.25 (a) Pseudo first-order kinetics of OFX degradation as a function of absorbed dose (b) Pseudo-first-order kinetics of ORZ degradation as a function of absorbed dose (c) Pseudo-first-order kinetics of AMX degradation as a function of absorbed dose 82

4.26 (a) G-(OFX) and degradation efficiency (%) of OFX using gamma radiation with $[OFX]_o$=0.1 mM and pH 6.5 (b) G-(ORZ) and degradation efficiency (%) of ORZ using gamma radiation with $[ORZ]_o$=0.22 mM and pH 6.5 (c) G-(AMX) and degradation efficiency (%) of AMX using gamma radiation with $[AMX]_o$=0.1 mM 84

4.27 Effect of pH on gamma radiolytic degradation of (a) OFX (b) ORZ and (c) AMX 88

4.28 Effect of CO_2^{3-} on gamma radiolytic degradation of (a) OFX and (b) ORZ; Effect of *t*-BuOH on gamma radiolytic degradation of (c) OFX and (d) ORZ [$(OFX)_o$ =0.1 mM; pH = 6.5] [$(ORZ)_o$ =0.22 mM; pH = 6.5] 89

4.29 Effect of additives on radiolytic degradation of AMX [$(AMX)_o$ =0.1 mM; pH = 6.5] 90

4.30 Effect of H_2O_2 on gamma radiolytic degradation of (a) OFX and (b) ORZ 94

4.31 Effect of H_2O_2 on gamma radiolytic degradation of AMX 95

4.32	Effect of absorbed dose and initial H_2O_2 concentration on TOC reduction of (a) OFX (b) ORZ and (c) AMX	97
4.33	(a) & (b) Total ion current chromatograms and ESI mass spectra recorded for aqueous solution of irradiated OFX at 1.0 kGy (c) & (d) Total ion current chromatograms and ESI mass spectra recorded for aqueous solution of irradiated OFX at 2.0 kGy	99
4.34	Proposed transformation pathways of gamma radiolytic degradation of OFX	101
4.35	ORZ molecule structure and its charge distribution	102
4.36	The main degradation pathways of ORZ during gamma radiolysis	105
4.37	Cytotoxicity activity of aqueous solutions of OFX under gamma radiation (a) before irradiation (b) after 2.0 kGy absorbed dose and (c) after 3.0 kGy absorbed dose	105
4.38	Inhibition rate of activity of ORZ solutions before and after gamma irradiation against (a) *B. subtilis (b) P. aeruginosa (c) E. coli*	106
4.39	Inhibition rate of activity of AMX solutions before and after gamma irradiation against (a) *B. subtilis (b) P. aeruginosa (c) E. coli*	107
4.40	(a) Concentration change of OFX as a function of dose [Inset: Degradation kinetics study of OFX] (b) Concentration change of ORZ as a function of dose [Inset: Degradation kinetics study of ORZ] and (c) Concentration change of AMX as a function of dose [Inset: Degradation kinetics study of AMX]	109
4.41	(a) Absorption spectrum of OFX at 190–400 nm after E-beam irradiation treatment (b) Absorption spectrum of ORZ at 190–400 nm after E-beam irradiation treatment	110
4.42	(a) G-values for the degradation of different initial concentration of OFX as a function of dose (b) G-values for the degradation of different initial concentration of ORZ as a function of dose using E-beam irradiation	111
4.43	(a) G-values and degradation extent (%) of OFX using E-beam irradiation with $[OFX]_o$=0.1 mM (b) G-values and degradation extent (%) of ORZ using E-beam irradiation with $[ORZ]_o$=0.22 mM (c) G-values and degradation extent (%) of AMX using E-beam irradiation with $[AMX]_o$=0.1 mM	112

4.44	Effect of different pH solutions on (a) OFX and (b) ORZ (c) AMX degradation using E-beam irradiation	115
4.45	Effect of NO_2^- and NO_3^- on E-beam radiolytic degradation of (a) OFX (b) ORZ; and Effect of 2-propanol on E-beam radiolytic degradation of (c) OFX (d) ORZ	117
4.46	Effect of thiourea on E-beam radiolytic degradation of (a) OFX (b) ORZ	118
4.47	Effect of different additives on E-beam radiolytic degradation of AMX	119
4.48	Effect of H_2O_2 concentrations on E-beam radiolytic degradation of (a) OFX (b) AMX and (c) ORZ	121
4.49	Effect of H_2O_2 concentrations on mineralization efficiency of (a) OFX and (b) ORZ (c) AMX	122
4.50	Effect of water matrices on E-beam radiolytic degradation of (a) OFX and (b) ORZ [UW: ultrapure water; SW: surface water; GW: ground water and WW: wastewater]	123
4.51	OFX molecule structure and its charge distribution	126
4.52	(a) & (b) Total ion current chromatogram and mass spectrum recorded for OFX with initial concentration of 0.1 mM (c) & (d) Total ion current chromatogram and mass spectrum recorded for aqueous solution of OFX E-beam irradiated with 2.0 kGy	127
4.53	(a) Total ion current chromatogram and (b), (c) & (d) mass spectrum recorded for aqueous solution of OFX E-beam irradiated with 3.0 kGy	128
4.54	The possible pathways of E-beam induced radiolytic degradation of OFX	130
4.55	Total ion current chromatogram and mass spectrum recorded for aqueous solution of ORZ (0.22 mM) E-beam irradiated with 2.0 kGy dose	132
4.56	Total ion current chromatogram and mass spectrum recorded for aqueous solution of ORZ (0.22 mM) E-beam irradiated with 3.0 kGy dose	133
4.57	The possible pathways of E-beam induced radiolytic degradation of ORZ	135
4.58	Inhibition rate of activity of OFX solutions before and after E-beam irradiation against (a) *E. coli* (b) *B. subtilis* (c) *P. aeruginosa*	136
4.59	Inhibition rate of activity of AMX solutions before and after E-beam irradiation against (a) *E. coli* (b) *B. subtilis* (c) *P. aeruginosa*	137
4.60	Effect of Fe concentration on COD removal efficiency of (a) LSW and (d) HSW; Effect of H_2O_2 on COD removal efficiency of (b) LSW and (d)	144

HSW; Effect of pH on COD removal efficiency of (c) LSW (f) HSW during dark-Fenton treatment

4.61 Effect of optimized conditions on COD and TOC removal efficiency of wastewaters during dark-Fenton treatment [LSW: Low strength wastewater with 0.25 M H_2O_2 and 0.025 M Fe^{2+} at pH 3.0; HSW: High strength wastewater with 1 M H_2O_2 and 0.15 M Fe^{2+} at pH 3.0] 145

4.62 Effect of Fe concentration on COD removal efficiency of (a) LSW and (d) HSW; Effect of H_2O_2 on COD removal efficiency of (b) LSW and (d) HSW; Effect of pH on COD removal efficiency of (c) LSW (f) HSW during photo-Fenton treatment 147

4.63 Effect of optimized conditions on COD and TOC removal efficiency of wastewaters during photo-Fenton treatment [LSW: Low strength wastewater with 0.25 M H_2O_2 and 0.05 M Fe^{2+} at pH 3.0; HSW: High strength wastewater with 1 M H_2O_2 and 0.1 M Fe^{2+} at pH 3.0] 148

4.64 COD and TOC profile using post-biological treatment of LSW and HSW pre-treated with dark-Fenton. [Left axis: Low strength wastewater with 20% (v/v) sludge concentration at 27 °C] and [Right axis: High strength wastewater with 25% (v/v) sludge concentration at 27 °C] 151

4.65 COD and TOC profile using post-biological treatment of LSW and HSW pre-treated with photo-Fenton. [Left axis: Low strength wastewater with 20% (v/v) sludge concentration at 27 °C] and [Right axis: High strength wastewater with 25% (v/v) sludge concentration at 27 °C] 152

4.66 Cytotoxic potential of (a, b and c) LSW and (d, e and f) HSW treated with Fenton treatments 154

4.67 Cytotoxic potential of (a, b and c) LSW and (d, e and f) HSW treated with Fenton treatment and subsequent biological treatment 154

4.68 Effect of different coagulants on COD reduction and biodegradability index of (a, d, c) Low strength wastewater and (d, e, f) high strength wastewater 156

4.69 Results of pH and contact time of $FeCl_3$ treatment of (a) LSW and (b) HSW for reduction in COD 156

4.70 Effect of sludge concentration and temperature on COD reduction of (a) LSW at 20 °C (b) LSW at 27 °C (c) LSW at 37 °C (d) HSW at 20 °C (e) 159

	HSW at 27 °C and (f) HSW at 37 °C	
4.71	(a) COD and TOC profile of low strength wastewater under biological degradation with 20% (v/v) sludge concentration at 27 °C (b) COD and TOC profile of high strength wastewater under biological degradation with 25% (v/v) sludge concentration at 27 °C	161
4.72	Effect of solution pH and dose on COD removal efficiency of pre-bio treated (a) LSW and (b) HSW under gamma radiolysis	162
4.73	Effect of H_2O_2 on COD and TOC removal of gamma irradiation treatment of (a & b) LSW (d & e) HSW; Effect of $K_2S_2O_8$ on COD removal of (c) LSW (f) HSW	163
4.74	Effect of oxidants on COD and TOC profile of pre-bio treated (a) LSW (b) HSW under gamma radiolysis	165
4.75	Effect of solution pH and dose on COD removal efficiency of pre-coagulant treated (a) LSW and (b) HSW under gamma radiolysis	166
4.76	Effect of H_2O_2 on COD and TOC removal of pre-biological and post-gamma irradiation treatment of (a & b) LSW (d & e) HSW; Effect of $K_2S_2O_8$ on COD removal of (a) LSW (b) HSW	167
4.77	Effect of oxidant on COD and TOC profile of pre-coagulant treated (a) LSW (b) HSW under gamma radiolysis	169
4.78	(a) COD and TOC profile of low strength wastewater using post-biological treatment with 20% (v/v) sludge concentration at 27 °C (b) COD and TOC profile of high strength wastewater using post-biological treatment with 25% (v/v) sludge concentration at 27 °C	170
4.79	Cytotoxic potential of (a, b and c) LSW and (d, e and f) HSW treated with pre-biological followed by post-gamma irradiation treatment	173
4.80	Cytotoxic potential of (a, b and c) LSW and (d, e and f) HSW treated with pre-gamma irradiation followed by post-biological treatment	174
4.81	Effect of solution pH on COD removal of (a) LSW and (b) HSW under E-beam radiolysis	177
4.82	Effect of H_2O_2 on COD and TOC removal of E-beam irradiation treatment of (a & b) LSW (d & e) HSW; Effect of $K_2S_2O_8$ on COD removal of (c) LSW (f) HSW	178
4.83	Effect of oxidants on COD and TOC removal of (a) LSW and (b) HSW	179

	under E-beam irradiation treatment	
4.84	Profile of COD and TOC concentration at the effluent of ASP reactor operating under continuous mode at constant Q_{feed} of 0.15 L h^{-1} for pre-coagulant treated (a) L_{OSW} and (b) H_{OSW}	182
4.85	Profile of COD concentration and pH at the effluent of ASP reactor (b) TOC profile at the effluent of ASP reactor operating in continuous mode at constant Q_{feed} of 0.15 LPH and feed COD (I) 1000 (II) 2000 and (III) 3000 mg L^{-1} LSW	183
4.86	Variation of MLSS and SVI during continuous mode operation of ASP reactor at constant Q_{feed} of 0.15 LPH and varied COD concentration for (a) LSW and (b) HSW	184
4.87	Profile of COD concentration and pH at the effluent of ASP reactor (b) TOC profile at the effluent of ASP reactor operating in continuous mode at constant Q_{feed} of 0.15 LPH and feed COD (I) 4000 (II) 8000 and (III) 12000 mg L^{-1} HSW	185
4.88	Cytotoxic potential of (a, b and C) LSW and (d, e and f) HSW treated with sequential E-beam irradiation followed by biological treatment	186

TABLE OF CONTENTS

S.No.	Topic	Page No.
	Declaration	I
	Certificate	II
	Acknowledgement	III
	Abstract	V
	List of tables	IX
	List of figures	XII
1.0	**Introduction**	**1-14**
1.1	Overview of pharmaceutical industry and its waste	1
1.2	Fate and transport of pharmaceuticals in the environment	2
1.3	Treatment technologies employed in pharmaceutical industries	4
1.4	Advanced oxidation processes (AOPs): an overview	6
	1.4.1 Applications of Fenton treatment	8
	1.4.2 Applications of Ionizing radiations	9
	1.4.2.1 Gamma radiations	9
	1.4.2.2 High electron beam	10
	1.4.2.3 Radiolysis of aqueous solution	11
1.5	Integration of AOPs with biological treatment	11
1.6	Overview of representative pharmaceutical industry	12
1.7	Target pharmaceutical compounds and wastewater	13
1.8	Aim of the proposed study	14
2.0	**Review of Literature**	**15-32**
2.1	Impacts of pharmaceuticals on environment	15
2.2	Biological treatment	16
2.3	Advanced oxidation processes for pharmaceuticals treatment	18
	2.3.1 Applications of Fenton's oxidation for pharmaceuticals wastewater	20
	2.3.2 Applications of ionizing radiation for pharmaceuticals wastewater	23
2.4	Integration of ionizing radiations with biological treatment	27
2.5	Research Gaps	29
2.6	Objectives of the study	31

3.0 Materials and Methods 33-51

3.1 Materials 33

3.1.1 Model compounds and chemicals 33

3.1.2 Wastewater and sludge collection 34

3.2 Instruments and reactors 35

3.2.1 UV reactor chamber 35

3.2.2 Continuous baffled reactor 36

3.2.3 Gamma chamber 36

3.2.4 Electron beam accelerator 37

3.2.5 Biological reactor 37

3.3 Methods 39

3.3.1 Synthesis of hematite 39

3.3.2 Collection of red soil 39

3.3.3 Synthesis of graphene oxide-pyrite nanocomposite 40

3.3.4 Characterization of hematite, GO-pyrite and red soil 41

3.4 Mode of experiments for model compounds 41

3.4.1 Photo-Fenton treatment of model compounds 42

3.4.1.1 Batch experiments for photo-Fenton oxidation using hematite 42

3.4.1.2 Batch experiments for photo-Fenton oxidation using soil particles 42

3.4.1.3 Continuous experiments for photo-Fenton oxidation using soil 43

3.4.1.4 Batch experiments for photo-Fenton oxidation using GO-FeS_2 43

3.4.2 Gamma irradiation treatment of model compounds 44

3.4.3 E-beam irradiation treatment of model compounds 45

3.4.4 G-value and dose constants calculations 45

3.5 Mode of experiments for real pharmaceutical wastewater 46

3.5.1 Pre-coagulant treatment of wastewater 46

3.5.2 Applications of gamma irradiation for pharmaceutical wastewater treatment 46

3.5.3 Applications of E-beam irradiation for pharmaceutical wastewater treatment 46

3.5.4 Applications of Fenton technologies for pharmaceutical wastewater treatment 47

3.6	Biological treatment	48
	3.6.1 Biological treatment in batch mode	48
	3.6.2 Biological treatment using continuous mode	49
3.7	Analytical techniques	49
3.8	Toxicity assessment	51
4.0	**Results and discussions**	**52-189**
4.1	Photo-Fenton treatment of model compound using hematite particles	52
	4.1.1 Characterization of hematite (α-Fe_2O_3) particles	52
	4.1.2 Catalytic activity of the α-Fe_2O_3	55
	4.1.3 Effect of variation of C- α-Fe_2O_3 dose	55
	4.1.4 Effect of H_2O_2 concentration	55
	4.1.5 Effect of pH	56
	4.1.6 Leaching of iron	57
	4.1.7 Comparison of α-Fe_2O_3 activity	59
	4.1.8 HPLC and mineralization study	59
4.2	Photo-Fenton treatment of model compounds using soil particles	61
	4.2.1 Characterization of Soil	61
	4.2.2 Degradation of model compounds under batch mode	63
	4.2.2.1 Effect of experimental conditions	64
	4.2.2.2 Influence of leached iron	68
	4.2.2.3 Effect of different irradiation sources	71
	4.2.3 Degradation of model compounds under continuous mode	73
	4.2.4 HPLC and mineralization study	74
	4.2.5 Toxicity assessment	75
4.3	Photo-Fenton treatment of model compounds using GO-pyrite nanocomposite	75
	4.3.1 Characterization of GO-pyrite nanocomposite	76
	4.3.2 Catalytic activity of GO-FeS_2 in photo-treatment of model compounds	77
4.4	Gamma irradiation treatment of model compounds	80
	4.4.1 Gamma radiolytic degradation of model compounds	80
	4.4.2 Effect of solution pH on gamma radiolytic degradation of model	87

compounds
4.4.3 Effect of additives on gamma radiolytic degradation of model compounds 88
4.4.4 Effect of oxidant on gamma radiolytic degradation of model compounds 94
4.4.5 Effect of oxidant on mineralization efficiency of model compounds 96
4.4.6 LC-MS analysis of gamma irradiated solutions of OFX 98
4.4.7 LC-MS analysis of gamma irradiated solutions of ORZ 102
4.4.8 Toxicity analysis of gamma irradiated solutions of model compounds 105
4.4.9 Cost analysis of gamma irradiated treatment of model compounds 107
4.5 E-beam irradiation treatment of model compounds 108
4.5.1 E-beam radiolytic degradation of model compounds 108
4.5.2 Effect of solution pH on E-beam radiolytic degradation of model compounds 114
4.5.3 Effect of different additives on E-beam radiolytic degradation of model compounds 116
4.5.4 Effect of oxidant on E-beam radiolytic degradation of model compounds 119
4.5.5 Effect of oxidant on mineralization efficiency of model compounds 121
4.5.6 Influence of water matrices on degradation efficiency of model compounds 123
4.5.7 LC-MS analysis of E-beam irradiated solutions of OFX 125
4.5.8 LC-MS analysis of E-beam irradiated solutions of ORZ 131
4.5.9 Cytotoxicity assessment 135
4.5.10 Cost evaluation of treatment process 137
4.6 Comparison of treatment technologies for degradation of model compounds 139
4.7 Applications of Fenton's technologies for wastewater treatment 140
4.7.1 Physicochemical characteristics of wastewaters 141
4.7.2 Fenton treatment 141
4.7.3 Photo-Fenton treatment 146
4.7.4 Biological treatment 150

	4.7.5 Toxicity analysis	153
4.8	Gamma irradiation treatment of real pharmaceutical wastewater	155
	4.8.1 Chemical coagulation treatment	155
	4.8.2 Integrated Bio-Gamma treatment of wastewater	158
	4.8.3 Integrated Gamma-Bio treatment of wastewater	166
	4.8.4 Cytotoxicity assessment of wastewater	172
	4.8.5 Cost associated with irradiation treatment for wastewater	174
4.9	E-beam irradiation treatment of real pharmaceutical wastewater	175
	4.9.1 Chemical coagulant treatment of wastewater and its characterization	175
	4.9.2 E-beam irradiation treatment	176
	4.9.3 Biological treatment using lab-scale activated sludge process (ASP) reactor	180
	4.9.4 Toxicity analysis	185
	4.9.5 Cost analysis and environmental implications	186
4.10	Comparison of treatment technologies for degradation of real wastewater	189
5.0	**Conclusion**	**193-194**
	Future recommendations	195
	References	196
	List of contributions	234
	Annexure	236

Chapter 1.0 Introduction

Increasing demand for water, energy and food are emerging as imperative and vital issues worldwide. India represents 16% of the world population and accounts for 2.45% of land area and 4% of water resources of the world. Due to industrialization, urbanization and agricultural growth, most of the river basins are facing moderate to severe water shortages. The population of India is anticipated to surpass the 1.5 billion mark by 2050 with the current population growth-rate (1.9% per year). Due to increasing development and population in the country, the availability of per capita average annual freshwater has reduced since 1951 from 5176 m^3 to 1870 m^3, in 2001 and 1589 m^3, in 2010. It is likely to further decrease to 1340 m^3 and 1140 m^3 in 2025 and 2050, respectively (CWC, 2010). Henceforth, there is an imperative need for the management of efficient water resources through better water reusability and recyclability.

1.1 Overview of pharmaceutical industry and its waste

India is in grip of severe water pollution crisis. The number of waterways has been contaminated in the past years and half of the country's rivers are polluted. Several factors have contributed to this alarming situation, particularly the staggering quantities of untreated wastewater generated in this country. Another major cause is effluents generated from water intensive industries. The advancement in medical field has dramatically increased the consumption of pharmaceuticals in developing country like India. The pharmaceutical industry is one of the fastest growing sectors of the Indian economy and has encountered rapid and sustained expansion since the second half of the 20th Century. After North America and Europe, Indian pharmaceutical industry sector is third largest producers of pharmaceuticals in the world, with an anticipated turnover of USD 75 billion per year by 2020 (KPMG International, 2006). In other words, every third pill consumed in the world is manufactured in India. The organized pharmaceutical sector of India consists of 250 large scale and 8000 small scale companies, with the growing export of drugs to 30% annually (KPMG International, 2006).

The water quality monitoring conducted by the Central Pollution Control Board (CPCB) for the year 1995-2009 indicated the presence of organic, inorganic and bacterial contamination in the water bodies in India (Murty and Kumar, 2011), which is continuously rising every year. The leading cause of water pollution is the mixing of industrial and domestic wastewater in the water bodies without being efficiently treated through the treatment plants as only 30-31% gets treated by these plants (Kurunthachalam, 2012).

Considering the industrial wastewater, pharmaceutical manufacturing activity has been classified as a "red category" owing to the huge volume, complexity and hazardous waste it produces. The term "pharmaceutical wastewater" primarily refers to the wastes and effluents generated during the pharmaceutical manufacturing. In manufacturing unit, synthesis of bulk drugs involves a number of reactants with or without fermented natural antibiotics depending on the type of bulk drugs being synthesized. The very characteristics of effluent generated during bulk drug manufacturing involving organic synthesis show that effluent has a very high level of COD & TDS. The major COD is contributed by high degree of solvent contamination. A list of commonly used solvents which may participate also as a reactant, in some cases, is represented *Annexure 1.1* with their chemical formula, boiling points and toxicity level. Thus, the presence of such solvents in the effluents of pharmaceutical industries increases both the COD and BOD load significantly along with the high degree of toxicity.

Moreover, the increasing rate of unused medicines from hospitals and households and its disposal malpractices have also been considered as a source of pharmaceutical waste (Santos *et al.* 2007; Tong *et al.* 2011; Vellinga *et al.* 2014). The effective disposal and management of pharmaceutical waste and wastewater poses a serious challenge for the scientific research community particularly due to the occurrence of pharmaceuticals and its metabolites in the outlets wastewater treatment plants; which may find their pathways to enter in aquatic environment. Knowing the existence of pharmaceuticals compounds in the aquatic environment, there is growing concerns to explore their fate, transport, effects and toxicity as well as treatment technologies for the effective removal of these compounds from the different water sources.

1.2 Fate and transport of pharmaceuticals in the environment

The pharmaceuticals comprise of non-steroidal anti-inflammatory drugs, antibiotic, analgesics, antiepileptic, hormones, steroids, toxic substances, volatile organic compounds (VOCs) and surfactants etc. These pharmaceuticals despite of being intended to treat certain ailments in animals and human have exhibited adverse impacts on the ecosystem due to their existence in wastewater, surface water, groundwater and also drinking water. The previous years have witnessed significant and wide research on the detection of more than 160 different pharmaceuticals and their metabolites in the various environment samples ranging from few ng L^{-1} to several µg L^{-1} (Kümmerer, 2010; Sangion and Gramatica, 2016; Kanakaraju *et al.* 2017) and as a result these pharmaceuticals are now categorized as an emerging pollutant in various water bodies. Pharmaceuticals enter into the environment from

the pharmaceutical production industries, direct and improper disposal of unused/expired medicines by humans and through human urine or faeces, through the hospital wastes and household sewage and enter into the influent of wastewater treatment plants (WWTPs) in un-metabolized form or as moderately active metabolites (Heberer, 2002; Mompelat *et al.* 2009). It has been reported that about 10 to 90% of the administrated dose of pharmaceutical drug is excreted from the human body as a parent compound, whereas the rest is excreted as metabolites and/or in transformed forms (Kümmerer, 2009). The recent research showed that that numerous pharmaceutical manufacturing units were found to be sources of surpassing pharmaceuticals concentrations into the aquatic environment than those caused by the usage of pharmaceutical drugs (Kessler, 2010). The excreted pharmaceuticals reach the WWTPs and finally discharged as raw or treated wastewater into the rivers, surface water, groundwater, oceans and soil (Fig. 1.1).

The pharmaceuticals and its metabolites have been detected in all types of surface water, ground water, rivers and the oceanic environment in the past few decades (Swati *et al.* 2010; WHO, 2011, Veach and Bernot, 2011; Luo *et al.* 2014; Balakrishna *et al.* 2017). The presence of pharmaceutical compounds can induce toxicity to certain aquatic organisms causing allergic and hormonal disturbances in humans and animals, and promoting pathogens resistance to antibiotics (Xiao *et al.* 2001; Kolpin *et al.* 2002; Kidd *et al.* 2007; Behera *et al.* 2011; Kristiansson *et al.* 2011). Hence, it is essential to explore the advanced treatments that might help to decrease or eliminate their release into the aquatic environment (Bui *et al.* 2016). The consideration of such treatment options is that water will become progressively scarce in several regions of world and wastewater reuse is being encouraged as a valuable alternative for augmenting the availability of water (Urkiaga *et al.* 2006; Miller, 2006; Rodriguez *et al.* 2009).

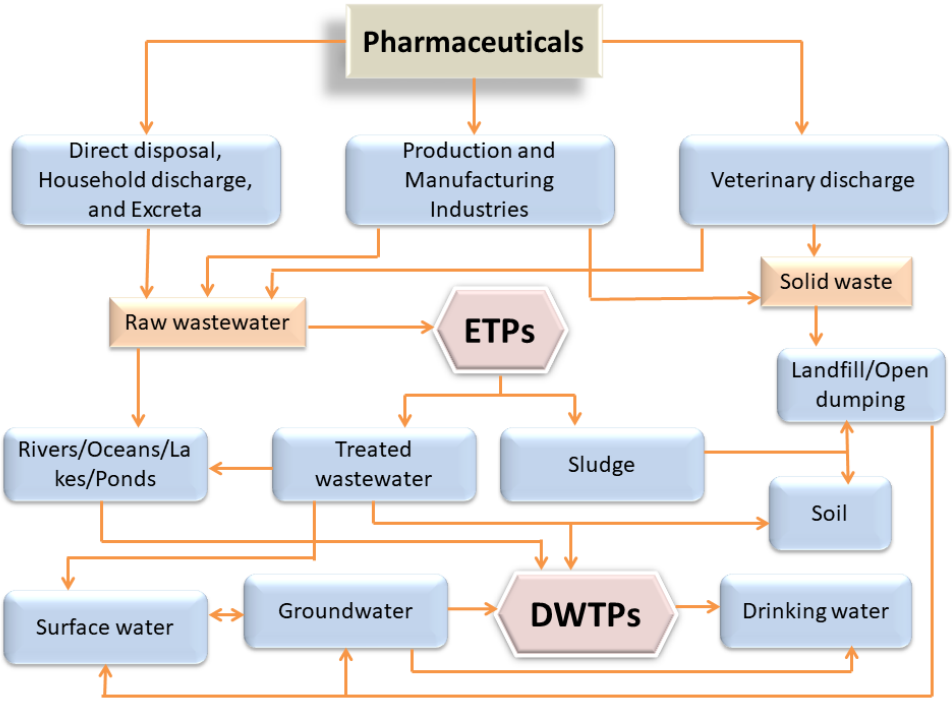

Fig. 1.1 Fate and transport of the pharmaceuticals in the environment. ETPs: Effluent treatment plants, DWTPs: Drinking water treatment plants.

The major pathway of pharmaceutical presence in the environment is considered to be WWTPs as they accumulate discharges from pharmaceutical industries, hospitals, household discharges, veterinaries and pharmacies (Heberer, 2002a; Onesios *et al.* 2009; Celle-Jeanton *et al.* 2014; Lee *et al.* 2017; Tarpani and Azapagic, 2018). This is due to the inefficient removal of pharmaceuticals in the conventionally used treatment technologies which are intended to treat biodegradable, non-polar and large compounds, as opposed to polar tendency, small compounds and non-biodegradable nature of pharmaceuticals compounds (Daughton, 2001; Richardson *et al.* 2005; Ratola *et al.* 2012; Tarpani and Azapagic, 2018). Moreover, numerous transformation products and metabolites are also likely to form in WWTPs as a consequence of numerous chemical reactions in the course of treatment (Quintana *et al.* 2005; Zuccato *et al.* 2005; Schuman *et al.* 2008) that could facilitate synergetic effects and become more bioactive when compared to parent compounds. Furthermore, improper disposals of effluents from the pharmaceutical industries are considered to be the major pathways for the antibiotics drugs to enter in aquatic environment in the developing country like India (Gothwal and Shashidhar, 2017).

1.3 Treatment technologies employed in pharmaceutical industries

In order to meet the strict regulatory discharge limits, the pharmaceutical industry

need enormous volume of high-quality water for manufacturing and efficient wastewater treatment methods to treat the generated wastewater. The process involved in pharmaceutical manufacturing industry includes, manufacture, extraction, processing, purification, and packaging of solids and liquids materials to be utilized for the ailments of humans and animals. Wastewater generation in a pharmaceutical industry typically originate during the synthesis and formulation of the pharmaceutical drugs. Wastewater generated in pharmaceutical manufacturing industries can be severely loaded with toxins, contaminants, and organics with high biological oxygen demand (BOD), chemical oxygen demand (COD), total dissolved solids (TDS), total organic carbon (TOC) oil content and pH values ranging from 1 to 11, suggesting different challenges in terms of treatment taking into account the stringent regulations (Gadipelly *et al.* 2014). It has been observed that approximately 50% of water used in pharmaceutical industries is going as a waste (Gadipelly *et al.* 2014). In order to treat the wastewater, most of the pharmaceutical industry utilized general approaches like recovery of pharmaceutical drugs which are expected to be present in wash waters and solvents; physicochemical treatments like sedimentation or floatation; conventional treatment technologies like aerobic/anaerobic biological treatment; inactivation of active compounds using UV oxidation; sterilization or inactivation of bioactive substances; and a new hybrid technology specific to pharmaceutical industry (Gadipelly *et al.* 2014).

In India, industries are the major contributor of wastewater generation apart from domestic sewage. Common Effluent Treatment Plants (CETPs) has been installed for group of small scale industries that might not be able to afford the wastewater treatment plant (CPCB, 2005). The treatment methods used in these plants includes dual media filter, air floatation, sand filtration, activated carbon filter, clariflocculator, flash mixer, secondary clarifiers, stabilization tank and sludge drying beds, etc. The treated effluents from these CETPs are disposed in rivers. For instance, 10 CETPs of 133 MLD capacity dispose their treated effluent in Yamuna River (Kaur *et al.* 2012). Furthermore, the conventional wastewater treatment plants involve complex operations and maintenance. For the entire domestic wastewater, the total cost for setting-up a treatment plant is approximately 7,650 crores INR (CPCB, 2005), which is about 10 times the cost which Government of India plans to spend (Kumar, 2003). Due to inadequate design, complex operations, lack of technical manpower and frequent electricity break downs, the treatment plants do not function appropriately (CPCB, 2007). Moreover, the direct economic return associated with the available technologies is one of the major problems with the WWTPs. According to CPCB report, a performance evaluation of 92 Sewage Treatment Plants (STPs) studied, 26 STPs did

not met prescribed standard thus making the discharged water unsuitable for household or domestic purpose (Trivedy and Nakate, 2001).

In most of the existing pharmaceutical industry, the dilute aqueous streams coming from the plants are generally treated by biological treatment methods including anaerobic and aerobic treatments. Available biological treatments take account of the activated sludge process, trickling filtration, membrane bioreactor, sequencing batch reactor and the anaerobic hybrid reactor. However, these conventional treatment technologies are ineffective in degradation of pharmaceutical contaminants (Santos *et al.* 2007; Luo *et al.* 2014; Balakrishna *et al.* 2017). In addition, multiple effect evaporators (MEE) are used to manage the residual refractory and high inorganic TDS level in high strength pharmaceutical effluents. Evaporation is an energy intensive process which increases recurring treatment cost. Moreover, the reappearance of trace amount of pharmaceuticals in the treated water samples of ETPs points to the failure of these treatments technologies in the degradation of persistent and recalcitrant pollutants from water streams (Hedgespeth *et al.* 2012). The changing nature of wastewater due to the varying nature of composition of the raw materials for different products is the main problem commonly encountered in the handling of pharmaceutical wastewater of different organic loads. Water differing in physicochemical characteristics from different sections is permitted to mix with each other forming a complex hybrid wastewater with properties along with the problems requiring great efforts in handling, analysis, isolation of the essential components and overall treatment.

Thus, it is mandatory need to employ methods and technologies of recycling and reusability of water in pharmaceutical industries. There is an extensive scope for water reusability and recyclability by employing advanced treatment techniques at the wastewater generation site rather than treating the wastewater at ETP and disposal site.

1.4 Advanced oxidation processes (AOPs): an overview

The commonly employed treatment in pharmaceutical industries are ineffective for complete removal of pharmaceutical compounds due to the low biodegradability of abundant pharmaceuticals and the discharge of treated effluents in different water bodies can lead to the contamination by these micro pollutants. Thus, advanced oxidation processes (AOPs) are considered to be competent and effective approach in the removal of pharmaceuticals contamination. AOPs can be broadly defined as aqueous-phase oxidation methods based on the intermediacy of highly reactive species such as hydroxyl radicals ($HO^{\bullet}$) in the mechanisms primary leading to the degradation of the target contaminant. These $HO^{\bullet}$ radicals are highly reactive, non-selective and powerful oxidizing species with oxidation potential of

2.80 V (Andreozzi *et al.* 1999). The $HO^{\bullet}$ radicals reacts with organic pollutant either by hydrogen abstraction (Eq. (1.1)) from C-H, N-H, or OH groups; or through direct electron transfer (Eq. (1.2)) yielding oxidized intermediates/by-products or, the production of CO_2, H_2O and inorganic acids due to complete mineralization; or through radical-radical interactions, for example, the generation of the peroxyl radical by the addition of molecular O_2 (Eq. (1.3)) (Legrini *et al.* 1993).

$$HO^{\cdot} + RH \rightarrow R^{\cdot} + H_2O \quad (1.1)$$

$$HO^{\cdot} + RX \rightarrow RX^{\cdot +} + HO^{-} \quad (1.2)$$

$$R^{\cdot} + O_2 \rightarrow RO_2^{\cdot} \quad (1.3)$$

AOPs generally applied for the treatment of pharmaceutical wastewater falls into three broad categories *viz.* photochemical processes, non-photochemical processes and hybrid or combined processes (Fig. 1.2). All AOPs comprise of two steps, the *in situ* production of reactive radical species and the reaction of radical species with target pollutant in water/ wastewater. Mechanisms of radical generation depend on process specific parameters and can be affected by the design of treatment system and quality of water/ wastewater. However, these AOPs limits their practical applications due to the production of toxic intermediates/by-products, dependence on the surface properties of the photocatalyst, ineffective mineralization of the intermediate/by-products and production of degraded compounds which are more toxic than the parent compounds (Hapeshi *et al.* 2010; Paul *et al.* 2014; Tay and Madehi, 2015; Bhatia and Dhir, 2016).

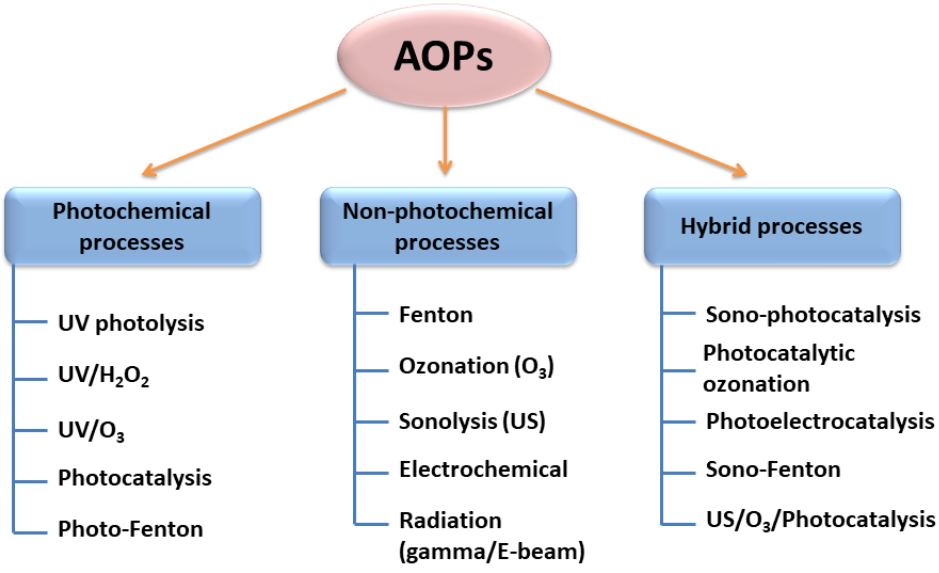

Fig. 1.2 Classifications of AOPs

1.4.1 Applications of Fenton treatment

Among the non-photochemical AOPs illustrated in the Fig. 1.2, Fenton and photo-assisted Fenton processes have been demonstrated as an efficient treatment for the degradation of wider range of pharmaceuticals like antibiotics (Trovo *et al.* 2011; Sirtori *et al.* 2011), anti-inflammatory (Alalm *et al.* 2015), analgesic and antineoplastic drugs (Klamerth *et al.* 2010).

The Fenton reagent, a mixture of Fe salt and hydrogen peroxide (H_2O_2) discovered by Henry J.H. Fenton describes the oxidation power of H_2O_2 on organic pollutant in which $HO^{\bullet}$ radicals are generated from H_2O_2 under the addition of Fe as a catalyst, as shown in Equations (1.4 to 1.7). Photo-Fenton oxidation combines the use of Fenton's reagent and UV-visible light for producing supplementary $HO^{\bullet}$ radicals through photo-reduction of Fe^{3+} to Fe^{2+} ions and photolysis of H_2O_2 (Eq. 1.8-1.9) (Pignatello *et al.* 2006). However, there are some drawback of homogeneous Fenton and photo-Fenton processes that are mainly the (a) pH dependency (2.5-4.0) (Katsumata *et al.* 2005); (b) generation of $Fe(OH)_3$ sludge at pH > 4.0 (Tamimi *et al.* 2008); (c) light penetration in photo-Fenton process due to the generation of sludge (Faust and Hoigne, 1990); (d) recovery of catalyst (Pariente *et al.* 2008) and; (e) cost involved with the additional chemicals for neutralization which may limit the applicability of homogeneous Fenton and photo-Fenton process at industrial scale. However, various studies has shown the practice of homogeneous Fenton process proficient in diminishing load of refractory wastewater to being less toxic and making them susceptible to subsequent biological treatment (Tekin *et al.* 2006; Kulik *et al.* 2008). Thus, Fenton treatment can be considered as pre-treatment process to convert the non-biodegradable organic content of pharmaceutical wastewater into biodegradable content which can be treated by subsequent biological process more efficiently (Alaton *et al.* 2004; Sirtori *et al.* 2009).

$$H_2O_2 + Fe^{2+} \rightarrow Fe^{3+} + OH^- + HO^{\cdot} \quad [k = 76\ L\ mol^{-1}s^{-1}) \tag{1.4}$$

$$H_2O_2 + Fe^{3+} \rightarrow Fe^{2+} + HO_2^{\cdot} + H^+ \quad [k = 0.001 - 0.01\ L\ mol^{-1}s^{-1}) \tag{1.5}$$

$$HO_2^{\cdot} + Fe^{2+} \rightarrow Fe^{3+} + HO_2^- \ [k = 1.3 \times 10^6\ L\ mol^{-1}s^{-1}) \tag{1.6}$$

$$HO_2^{\cdot} + Fe^{3+} \rightarrow Fe^{2+} + O_2 + H^+ \quad [k = 1.2 \times 10^6\ L\ mol^{-1}s^{-1}) \tag{1.7}$$

$$H_2O_2 + Fe^{3+} + h\nu \rightarrow Fe^{2+} + HO^{\cdot} + H^+ \tag{1.8}$$

$$H_2O_2 + h\nu \rightarrow 2HO^{\cdot} \tag{1.9}$$

In order to overcome the shortcomings of homogeneous Fenton and photo-Fenton process, there is growing interest in the applications of heterogeneous Fenton-like process. Since iron oxides are abundantly available minerals, the utilization of iron oxides in Fenton-like process is the most feasible method for the treatment of pharmaceutical wastewater and has been successfully put into perspectives by many researchers. In heterogeneous Fenton-like process, the application of iron oxides like hematite (α-Fe_2O_3), magnetite (Fe_3O_4), pyrite (FeS_2), goethite (α-FeOOH) and maghemite (γ-Fe_2O_3) in pure or structurally modified forms are widely used and have been promising alternatives for remediation of wastewater pollution (Pouran *et al.* 2014). Although, the use of iron oxides in heterogeneous Fenton-like process is an effective for pollutant degradation, however, several practices can be performed to increase the efficiency and degradation rate of pollutant molecules through some modifications in their morphological structure.

1.4.2 Applications of Ionizing radiations

Currently, the focus is on the development of innovative technology that eventually causes destruction of the organic contaminants without use of any oxidant and toxic chemicals. Radiolytic degradation processes using ionizing radiations i.e., gamma radiation or high electron beam (E-beam) have received much attention (Basfar *et al.* 2005). Ionizing radiation is any of several types of rays or particles given off by radioactive material (^{60}Co-gamma radiation source) and any radiation producing machines (high electron beam). In comparison to other AOPs, the use of ionizing radiation offers advantages like it is an effective, clean and fast method to generate $HO^{\bullet}$; does not require the supplementary chemicals or reagents; produces lesser amount of toxic intermediates/by-products; devoid of any sludge production, insensitive to suspended solids and colour in the wastewater. Moreover, recalcitrant compound could be effectively degraded by the reactive oxidative and reductive species produced during *in situ* water radiolysis (Cantwell and Hofmann, 2011; Paul *et al.* 2014; Guin *et al.* 2014; Borrely *et al.* 2016; Guin *et al.* 2017).

1.4.2.1 Gamma radiations

Gamma radiations are emitted by gamma emitting-radionuclide with high energy photons such as ^{60}Co (half-life of 5.26 years and having energy of 1.33 and 1.17 MeV) or ^{137}Cs (half-life of 29 years and energy of 0.66 MeV). Gamma radiations are of extremely high frequency (>10^{19} Hz) and high energy above 100 keV and wavelength less than 10^{-12} m. Gamma radiation is categorized as indirectly ionizing radiation because they have no mass and charge, and it is the electrons that they liberate from atoms that produce most of the ionization.

1.4.2.2 High electron beam

Electron beam (E-beam) treatment refers to the use of high energy electrons coming from an E-beam accelerator to induce chemical changes in molecular structure of compounds in aqueous phase, but is too low to induce radioactivity. E-beam is absorbed almost completely by the target compounds' electron orbital's, consequently increasing the energy level of its orbital electrons to produce changes in the. The main components of E-beam accelerators are shown in Fig. 1.3. The basic mechanism of E-beam irradiation production is enclosed in a sealed container which is kept under high vacuum. A heated emitter (cathode) releases electrons that are accelerated by a passage through a grid under high voltage DC power supply or through radiofrequency (in more compact designs). The way in which the high energy E-beam is directed towards the exit window is mainly controlled by electrostatic and/or magnetic fields (by deflecting and focusing). Electrons arising from the exit window carry energy dependent on the voltage applied to the anode, while their number is governed by the cathode current. By regulating these parameters, it is feasible to control the dose rate and beam penetration of E-beam accelerators. E-beam accelerators employed in the water and wastewater treatment are generally energetically ranged between 600 keV and 1.5 MeV, although accelerators up to 10 MeV have been used (He *et al.* 2014; Wang *et al*. 2016).

Advantage of E-beam accelerator over gamma radiation is that they can be switched off when desired, contrary to other source of radiation that continuously emits radiations and they have high dose rate. Gamma irradiation and high electron beam, as AOPs, can be a competent approach for the treatment of stable organic pollutants as well as real pharmaceutical wastewater.

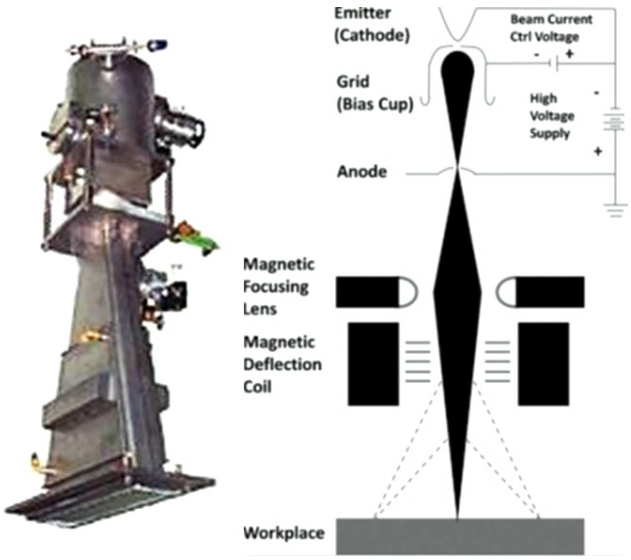

Fig. 1.3 E-beam accelerator: view (left) and scheme (right). (*Source:* Capodaglio, 2018)

1.4.2.3 Radiolysis of aqueous solution

The framework in which water radiolysis occurs by the means of ionizing radiations is now well understood experimentally as well as theoretically (Buxton et *al.* 1988; Spinks and Woods, 1990). Water radiolysis can be written as (1.10):

$$H_2O \overset{\approx}{\rightarrow} HO^{\cdot}(0.28) + e_{aq}^{-}(0.28) + H^{\cdot}(0.06) + H_2O_2(0.073) + H_2(0.047) + H_3O^{+}(0.28) \quad (1.10)$$

In very dilute aqueous solutions, practically all the ionizing radiation is absorbed by water molecule. Thus, within 10^{-16} to 10^{-12} seconds, radiolysis of water through gamma and E-beam leads to the generation of both oxidative ($HO^{\bullet}$, hydroxyl radicals) and reductive species ($H^{\bullet}$, hydrogen atom and e_{aq}^{-}, aqueous electrons) (Eq. 1.10). H_2 will come out from the solution and H_2O_2 will decompose to produce O_2 and H_2O. Therefore, radiolysis of water will produce reactive radical species and water molecule only. In presence of solute, reactive radicals (life time ~ μs) will react with the solute molecules producing stable intermediate products in the short span of time. The values in the parenthesis are the concentration of reactive species generated with absorption of 100 eV of radiation energy and are denoted as G-value of each species (μmol J^{-1}). These generated reactive radical species are considered to be principally accountable for degrading the organic pollutants in aqueous medium. Ionizing radiations can be used as hyphenated processes involving coagulants/oxidants or followed by subsequent biological treatment which might improves the degradation efficiency and reduce the overall cost of real wastewater treatment.

1.5 Integration of AOPs with biological treatment

Biological treatments including aerobic and anaerobic systems has been traditionally engaged in the degradation of industrial wastewater all across the world**.** Although, biological treatments have been regarded as widely utilized treatment options in industries to treat wastewater, but its effect is reduced in presence of non-biodegradable compounds in pharmaceutical wastewater. However, biodegradation processes produces mixed results and are not capable of degrading complex and stable organic compounds. AOPs have been effectively used as pre-treatment technology to enhance the biodegradability of industrial wastewaters prior to biological treatment (Rizzo, 2011). Recent advances in past few years revealed that biological treatment is an energy and cost effective treatment option, in particular if integrated with AOPs such as Fenton (Sirtori *et al.* 2009; Jagadevan *et al*. 2011) and several UV-based AOPs. Radiation based treatment has shown to enhance the biodegradability of wastewater streams by converting biologically resistant compounds into

smaller and more bio-available compounds (Han *et al.* 2012; Rawat and Sarma, 2013). Therefore, a coupled system involving gamma/electron beam irradiations and biological treatment can be effectively applied in the degradation of numerous classes of organic pollutants present in real industrial effluent. Considering the potential applications of radiation technology in degrading various compounds and the environmental benefits, the transference of this technology for real effluents on the centralized wastewater treatment system instead of making scattered efforts at individual level would mitigate the individual problems with better approach and with reduced environmental impact on the ecology.

1.6 Overview of representative pharmaceutical industry

Hyderabad is described as the bulk drug production capital of India, which accounts for more than one-third of India's total bulk drug production with a market share of USD 1.6 million and a target of USD 10-15 billion by 2020 (Balakrishna *et al.* 2017). The Derabassi region has emerged since 2003, and has been a birth place of bulk drugs industries in Punjab with a total annual production of approximately 30,000 MT/annum. Representative pharmaceutical industry is a large scale, research based, pharmaceutical manufacturer and exporter, focusing on manufacturing of Active Pharmaceutical Ingredients (API) and API intermediates located in Derabassi town of Punjab province, India. The major products of industry includes amoxicillin trihydrate, cefuroxime axetil and cepodoxime proxetill etc. The water consumption per unit of production of the industry is 80 m^3 day^{-1} with total discharge of 120 KLD. The discharged water is further treated through the installed effluent treatment plant of the industry.

The manufacturing process at PDL involves a lot of chemicals and solvents which leads to the generation of highly complex and toxic effluent. The complete solution for handling the effluent involves number of stages: like physicochemical, chemical detoxification and biological treatment. Even the combinations of all the techniques are not adequate to meet the required statuary discharge standards. Pharmaceutical wastewater coming from manufacturing plant is segregated into two streams *viz.* high and low strength wastewater. High strength wastewater is treated by chemical treatment followed by biological treatment and tube settlers. The characteristics of effluent generated during pharmaceutical manufacturing involving organic synthesis has a very high level of COD, TOC, TDS & toxicity. High strength wastewater cannot be disposed off, for which evaporation technique are being adopted which require space as well as high investment at individual unit level, which may lead to environmental management problem. Though, most of the units have their own existing effluent treatment plants based on biological, chemical adsorption and

membrane separation processes, in addition to multiple effect evaporators (MEE), still operation of individual waste water treatment to meet statuary standard is an extremely difficult job with insurmountable problems.

1.7 Target pharmaceutical compounds and wastewater

In this study, the high strength wastewater (HSW) and low strength wastewater (LSW) from the ETP of representative pharmaceutical manufacturing unit was collected for the experiment purposes. In addition to real pharmaceutical wastewater, amoxicillin trihydrate (AMX), ofloxacin (OFX) and ornidazole (ORZ) were selected as target pharmaceutical compounds in the study. The chemical structures of AMX, OFX and ORZ along with their properties are presented in Table 1.1

Table 1.1 Properties of AMX, OFX and ORZ

Properties	**AMX**	**ORZ**	**OFX**
Wavelength λ_{max} (nm)	228 and 272	310	288
Molecular weight (g mol^{-1})	419.44	219.63	361.37
Chemical formula	$C_{16}H_{19}N_3O_5S$	$C_7H_{10}ClN_3O_3$	$C_{18}H_{20}FN_3O_4$
Molecular structure	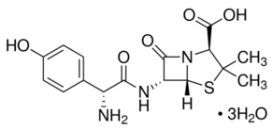	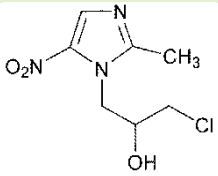	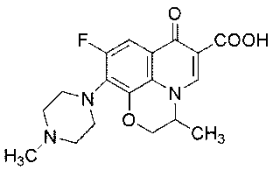

Amoxicillin trihydrate is semi synthetic beta-lactam penicillin that is widely used to treat certain bacterial infections such as nausea, pneumonia, bronchitis and infections of ear, throat, skin and urinary tract (Elmolla and Chaudhuri, 2010). It has been found that AMX is not susceptible to biodegradation and it has slow metabolic rate in humans resulting in 80–90% excretion (Mohammadi *et al.* 2013). OFX is a widely used synthetic fluorinated quinolone-type antibiotic of considerable environmental significance due to its extensive occurrence and genotoxic properties (Kümmerer, 2009). It is persistent against biological degradation and as a result it remains in environment for longer time duration (Hapeshi *et al.* 2013). Moreover, OFX has been characterized as extreme hazardous for aquatic environment due to the reuse of bio-solids for agricultural purposes (Langdon *et al.* 2009; Michael *et al.* 2010). ORZ is an extremely exploited antibiotic for human and veterinary treatment (Zhao *et al.* 2012; Khattab *et al.* 2012). It is reported that ORZ as conjugates and metabolites is

excreted in the urine after being metabolized in the liver and to a smaller amount in the faeces. Within 5 days, 85% of a single oral ORZ dose is eliminated; 63% and 22% in the urine and faeces, respectively (Schwartz and Jeunet, 1976; Solomon *et al.* 2008). Few researchers have reported the existence of OFX and ORZ in different water bodies ranging from few ng L^{-1} to several µg L^{-1} (Radjenović *et al.* 2009; Tamtam *et al.* 2008; Dinh *et al.* 2011).

1.8 Aim of the proposed study

The present study aims to explain the degradation of aqueous solution of selected pharmaceuticals with Fenton/photo-Fenton like processes, gamma and E-beam radiations. Moreover, the study is focused on Fenton/photo-Fenton processes, gamma and E-beam treatment for real pharmaceutical wastewater. The proposed study will be helpful in basic understanding of the degradation of persistent pharmaceuticals in aqueous phase by Fenton/photo-Fenton like processes, gamma and E-beam treatment. The possibility of use of ionizing radiations coupled with biological treatment as an alternative to conventional processes shall be helpful in establishing the potential applicability of treatment technology at common effluent treatment plant in an industrial cluster zone. This study envisage that the combined treatment of ionizing radiations and biological treatment would be more efficient than either alone for the treatment of pharmaceutical wastewater at industrial scale. In addition, the compilation of characterization and treatment processes data will be helpful to the industries, regulatory bodies and Ministry of Environment & Forests.

In the past few decades, pharmaceuticals have been regarded as emerging pollutants and encountered increasing concern worldwide (Jones *et al.* 2005; Rivera-Utrilla *et al.* 2013). Even at trace concentrations in environment, they have adverse effects on human health and ecosystems (Liu and Wong, 2013). However, the risk associated with the exposure of pharmaceutical is essentially vital in areas that practice indirect water reuse, where pharmaceutical effluent is discharged to rivers and streams that are in turn used as a raw water source for the production of drinking water for the living communities (Van Dijk-Looijaard and Van Genderen, 2000). It is notable that pharmaceuticals enter in soil and surface waters, and eventually in ground and drinking water after their excretion (as active metabolites or in un-metabolized form) in urine or feces from humans and animals (Darlymple *et al.* 2007; Klavarioti *et al.* 2009). Besides excretion, pharmaceuticals may find their pathways into water bodies due to the disposal of medicines used in industry, agriculture, households and hospitals. Veterinary pharmaceuticals may directly contaminate soil through manure and surface and ground waters by surface runoff (Bila and Dezotti, 2003; Khetan and Collins, 2007).

2.1 Impacts of pharmaceuticals on environment

Pharmaceuticals are intended to have physiological effects on animals and humans even at trace concentrations. Their chemical structure is stable enough to produce therapeutic activity and due to their constant input they persist in the environment for a longer duration of time; and their existence at trace, low and high concentration is dangerous to the environment and ecosystem (Mendez-Arriaga *et al.* 2009; Chatzitakis *et al.* 2008; Klavarioti *et al.* 2009). These pharmaceuticals are characterized with low volatility and high polarity, and tend to be easily transported and distributed in different water bodies (Zhang *et al.* 2014). Many pharmaceuticals have the potential to bio-accumulate and are highly persistent in environment.

Pharmaceuticals have been detected in various bodies like surface and ground water (Heberer, 2002; Andreozzi *et al.* 2003; WHO, 2011; Mutiyar and Mittal, 2014; Rehman *et al.* 2015; Balakrishna *et al.* 2017; Lee *et al.* 2017), drinking water (Zuccato *et al.* 2000; Ternes *et al.* 2002; Jones *et al.* 2003; Jones *et al.* 2005; Loraine and Pettigrove, 2006; Buffle *et al.* 2006), tap water (Halling-Sorensen *et al.* 1998; Doll and Frimmel, 2003), soil and sediments, ocean water (Halling-Sorensen *et al.* 1998; Klavarioti *et al.* 2009) and sewage influents and effluents (Heberer, 2002; Carballa *et al.* 2004; Lindqvist *et al.* 2005; Arlos *et al.* 2015; Gros

et al. 2017). Additionally, scarce studies confirmed the presence of pharmaceuticals in Indian rivers (Fick *et al.* 2009; Ramaswamy *et al.* 2011; Kristiansson *et al.* 2011; Iyanee *et al.* 2013; Shanmugam *et al.* 2014; Mutiyar and Mittal, 2014; Subedi *et al.* 2015; Archana *et al.* 2016).

Pharmaceuticals discharged in the environment may impose serious toxicity on any level of the biological life i.e., humans, animals, microorganisms, ecosystems, or the ecosphere. They are resistant to biodegradation processes and frequently escape from the conventional treatment plants (Daughton and Ternes, 1999; Santos *et al.* 2007; Bu *et al.* 2013; Luo *et al.* 2014). Moreover, certain pharmaceuticals like antibiotics may cause irreversible change and lasting effect on the microorganisms, making them resistant to antibiotic, even at trace concentrations (Xiao *et al.* 2001; Kidd *et al.* 2007; Bredhult *et al.* 2007; Behera *et al.* 2011; Kristiansson *et al.* 2011; Balakrishna *et al.* 2017). The pharmaceuticals presence in the environment has effects such as retardation of nitrite oxidation and methagenosis, disruption of human endocrine system and increased toxicity of chemical combinations and metabolites (Gadipelly *et al.* 2014). Scientific community is more concerned of the development of antibiotic resistant bacterial strains and the endocrine disrupting effects to aquatic organisms persuaded by pharmaceuticals (Ikehata *et al.* 2006; Homem and Santos, 2011). Hence, the presence of pharmaceuticals or their metabolites in the aquatic environment in particular constitutes a serious environmental problem. Due to these reasons, physicochemical and biological methods have been established to treat and eliminate the pharmaceuticals and their metabolites from aqueous environment.

2.2 Biological treatment

The pharmaceutical manufacturing process involves a lot of chemicals and solvents which leads to the generation of highly complex and toxic effluent. The treatment of effluent has been a great challenge to the environmental scientist's worldwide. In fact, the complete solution for handling the pharmaceutical effluent involves number of stages like physicochemical, chemical detoxification and biological treatment. Physical separation processes adopted are air stripping, steam stripping, air flotation techniques and adsorption. Even the combinations of all the techniques are not adequate to meet the required statuary discharge standards. Therefore, some effluents are required to be treated through Multiple Effect Evaporators (MEE), but the cost of installation and operation of MEE is very high. Efforts are also being made to reduce the volume by process of evaporation, polishing of effluent is also simultaneously required to eliminate the degree of formation of scale in evaporators.

In pharmaceutical industry, the dilute aqueous streams coming from the manufacturing plant are generally treated by the biological treatment including aerobic and anaerobic treatment processes as they utilize the microbes to convert the waste into gases and sludge that can be disposed off harmlessly. In some industries, pre-coagulation and flocculation treatment have been utilized as a pre-treatment method to reduce the organic load of wastewater (Verma *et al.* 2010). The conventional biological treatments employed in the treatment of industrial wastewater are ineffective in degrading and eliminating pharmaceuticals (Raj *et al.* 2004; Joss *et al*. 2005; Clara *et al*. 2005). Studies using anaerobic and aerobic treatment for pharmaceutical wastewater have been proven to be effective in reducing COD but not in removal of antibiotics (Kümmerer *et al.* 2001; Snyder *et al.* 2007).

Studies on the treatment of wastewater comprising antibiotics revealed that antibiotics are not readily biodegradable and their genotoxicity was not eliminated by biological treatment (Alexy *et al.* 2001). The most commonly used activated sludge treatment process cannot remove pharmaceuticals efficiently and entirely that are persistent to biodegradation (Celiz *et al.* 2009). In Japan, Matsuo *et al.* (2011) detected the presence of 100–2000 ng L^{-1} of amoxicillin concentration in an activated sludge based biological treatment of wastewater. Similar presence of amoxicillin was reported in the influent of WWTP involving activated sludge treatment in Australia by Watkinson *et al.* (2007), whereas, 20 times higher concentration was found in the effluent of WWTP comprising biological treatment in Hong-Kong (Minh *et al.* 2009). Mutiyar and Mittal (2013) found the higher concentration of amoxicillin in the wastewater discharged from WWTP in New Delhi. The concentrations of amoxicillin, ofloxacin, sulfamethoxazole, ciprofloxacin and metoprolol were found to be 40 times higher in the treated wastewater of Indian WWTPs when compared to the treated effluents of WWTPs in Europe, Japan, North America and Australia (Balakrishna *et al.* 2017). Although, biological treatment is considered to be effective in abundance of industrial wastewater treatment applications, but its efficacy gets diluted in occurrence of complex and tough pharmaceutical compounds in wastewater. Moreover, the complex design, overall cost and economic return are the major problems associated with the treatment of pharmaceutical wastewater at industrial scale.

Several studies have reported the occurrence of pharmaceuticals and their active metabolites in wastewater from conventional activated sludge based WWTPs in India (Mutiyar and Mittal, 2013; Singh *et al.* 2014; Subedi *et al.* 2015; Akiba *et al.* 2015; Archana *et al.* 2016; Anumol *et al.* 2016; Mohapatra *et al.* 2016; Subedi *et al.* 2017). Thus, potential of biological process in the pharmaceutical effluent treatment is acknowledged to some

extent, but destination of efficient removal of refractory from effluent up to the desired level is still a far cry while designing a zero discharge effluent treatment plant. Thus, there is stringent requirement to utilize other advanced treatment technologies in conjunction with biological treatment to efficiently degrade the recalcitrant and biodegradation resistant pharmaceutical compounds and reduce the overall cost of treatment.

2.3 Advanced oxidation processes for pharmaceuticals treatment

In the past decades, research and development (R & D) activities regarding AOPs has increased immensely due to the variety of technologies involved and the range of potential application. Key AOPs include homogeneous and heterogeneous, photocatalysis based on solar or ultraviolet (UV) light, ozonation, electrolysis, ultrasound, Fenton's and sonolysis, while emerging processes include pulsed plasma, microwaves and ionizing radiation. The basic purpose of all the AOPs is to generated highly reactive radical species (especially $HO^{\bullet}$ radicals) which are accountable for achieving the degradation of recalcitrant organic pollutants. Considering the AOPs, water and wastewater treatment is undoubtedly the most dominant area for R & D activities.

The AOPs have been successfully employed in the treatment of pharmaceuticals and organic pollutants in water and wastewater, including heterogeneous photocatalysis (Tanizaki *et al.* 2002; Baran *et al.* 2006; Coleman *et al.* 2007; Mendez-Arriaga *et al.* 2009; Yang *et al.* 2008; Lester *et al.* 2104; Sood *et al.* 2015; Lamba *et al.* 2015; Horovitz *et al.* 2016; Méndez-Medrano *et al.* 2016; Luster *et al.* 2017; Yuan *et al.* 2019), ozonation (Balcioglu and Otker, 2003; Huber *et al.* 2003; Tunay *et al.* 2004; Hua *et al.* 2006; Vieno *et al.* 2007; Dantas *et al.* 2008), photolysis (Hassanzadeh-Khayyat *et al.* 2011), O_3/UV (Alaton *et al.* 2002; Irmak *et al.* 2005), UV/H_2O_2 (Rosario-Ortiz *et al.* 2010), O_3/H_2O_2 (Zwiener and Frimmel, 2000; Andreozzi *et al.* 2003; Shemer *et al.* 2006; Pereira *et al.* 2007), electrolysis (Hirose *et al.* 2005; Pauwels *et al.* 2006; Murugananthan *et al.* 2007), sonolysis (Hartmann *et al.* 2008; Sanchez-Prado *et al.* 2008) and Fenton and photo-Fenton (Ravina *et al.* 2002; Shemer *et al.* 2006; Gonzalez *et al.* 2007; Luca *et al.* 2013). In addition to this, several hybrid AOPs have been utilized for the treatment of pharmaceuticals in wastewater including sono-Fenton process (Adityosulindro *et al.* 2017), sonolysis and UV/H_2O_2 photolysis (Kormann *et al.* 1991; Ghafoori *et al.* 2015), US/O_3 (Naddeo *et al.* 2015) and sono-photo Fenton and sono-bi-photocatalysis with TiO_2 and Fe^{2+} (Mendez-Arriaga *et al.* 2009). Applications of AOPs for wastewater treatment in particular types of AOPs to pharmaceuticals degradation is extensively reviewed (Mantzavinos and Psillakis, 2004; Gogate and Pandit, 2004; Comninellis *et al.* 2008; Klavarioti *et al.* 2009; Deegan *et al.* 2011; Wang and Xu, 2012;

Gadipelly *et al.* 2014; Oturan and Aaron, 2014; Wang and Wang, 2016; Kanakaraju *et al.* 2018). The reviewed literature indicated that most of the studies in the context of pharmaceutical contaminant treatment are subjected to heterogeneous photocatalysis and ozonation, while very less attention is paid towards other AOPs like sonolysis, electrolysis, Fenton's oxidation and the emerging technology like ionizing radiations (Klavarioti *et al.* 2009).

Table 2.1 Results of different AOPs utilized for the treatment of selected model compounds

S.No	Pharmaceuticals	Treatment employed	Optimized conditions	Treatment time and degradation efficiency	Reference
1.	Amoxicillin (100 µM)	UV/H_2O_2 processes	10 mM H_2O_2 under UV-C light	99% degradation in 20 min	Jung et al. 2012
2.	Amoxicillin (25 mg L^{-1})	Ozonation (O_3) and Ultrasound (US)irradiation	575 kHz ultrasound frequency at pH 10 and 0.18 mg L^{-1} O_3 gas at pH 7	> 99% degradation in 90 min with US and 99% degradation in 10 min with O_3	Kıdak & Doğan, 2018
3.	Amoxicillin (50 mg L^{-1})	Photo-Fenton process using potassium ferrioxalate complex (FeO_x)	0.05 mM of FeO_x, 120 mg L^{-1} H_2O_2 and pH 2.5	99% degradation in 5 min	Trovo et al. 2011
4.	Amoxicillin (10 mg L^{-1})	UV-A/ TiO_2 photocatalysis	250 mg L^{-1} Degussa P25 TiO_2 and pH 5	100% degradation in 25 min	Dimitrakopoulou et al. 2012
5.	Amoxicillin (0.1 mM)	Photocatalytic ozonation (O_3 + UV/Vis + TiO_2)	Natural pH, 50 g O_3 Nm^3 and 0.5 g L^{-1} of TiO_2	>99% degradation in 5 min	Moreira et al. 2012
6.	Ofloxacin (10 mg L^{-1})	UV/H_2O_2 process	pH 3, 0.27 g L^{-1} H_2O_2 and UV-254 nm	97% degradation in 30 min	Lin et al. 2016
7.	Ofloxacin (15 mg L^{-1})	Ozonation	O_3 output of 0.70 g h^{-1}, 290 mL min^{-1} flow rate and pH 7	Complete degradation	Tay and Madehi, 2015
8.	Ofloxacin (22 mg L^{-1})	Ozonation	O_3 dosage of 58 mg L^{-1}	Complete degradation	Carbajo et al 2015
9.	Ofloxacin (10 mg L^{-1})	Sonophotocatalytic	0.14 mM H_2O_2, 1 g L^{-1} TiO_2, pH 6 and 8.4 W cm^{-2} power intensity of US	96% degradation in 25 min	Hapeshi et al. 2013
10.	Ofloxacin (10 mg L^{-1})	TiO_2 photocatalysis	pH 3, 250 mg L^{-1} TiO_2 and 0.07 mM	97% degradation in 120 min	Hapeshi et al. 2010

			H_2O_2		
11.	Ofloxacin (25 mg L^{-1})	Bi_2O_3/TiO_2 photocatalysis	pH 7 and 0.5 g L^{-1} catalyst dose in solar light	92% degradation in 120 min	Sood et al. 2016
12.	Ofloxacin (25 mg L^{-1})	Bi–Ni co-doped TiO_2 photocatalysis	pH 3 and 1.5 g L^{-1} catalyst dose in solar light	86% degradation in 6 h	Bhatia et al. 2016a
13.	Ornidazole (20 mg L^{-1})	Y^{3+} doped $Bi_5Nb_3O_{15}$ Photocatalysts	pH 5.60 and catalyst dose of 2 g L^{-1}	95% degradation in 180 min	Zhao et al. 2012

Among the various classes of pharmaceuticals, antibiotics are considered to be most important class of pharmaceuticals in medicine today. Among antibiotics, amoxicillin (AMX), ofloxacin (OFX) and ornidazole (ORZ) are widely used antibiotics of considerable environmental significance due to their higher consumption rate; thus they are frequently detected extensively in the environmental samples. In this respect, several AOPs have been explored to degrade AMX in aqueous medium, including UV/H_2O_2 (Jung *et al.* 2012), ozonation (Kıdak and Doğan, 2018), photo-Fenton (Trovo *et al.* 2011), photocatalysis (Dimitrakopoulou *et al.* 2012; Kockler *et al.* 2012) and photocatalytic ozonation (Moreira *et al.* 2015). For OFX treatment in aqueous phase, successful applications of AOPs including photolysis (Wammer *et al.* 2013), UV/H_2O_2 (Lin *et al.* 2016), ozonation (Tay and Madehi, 2015; Carbajo *et al.* 2015), sono-photocatalytic (Hapeshi *et al.* 2013), heterogeneous photocatalysis (Hapeshi *et al.* 2010; Dong *et al.* 2015; Vasquez *et al.* 2013; Sood *et al.* 2016; Bhatia *et al.* 2016a) and Fenton oxidation (De la Cruz *et al.* 2012) has been explored. As far as ORZ is concerned, very limited studies have been reported till date for its degradation despite of its potential threat to the environment and mankind (Singh *et al.* 2003; Sukhdev and Shubha, 2009; Zhao *et al.* 2012). Table 2.1 represnts the results of different AOPs utilized for the treatment of selected model compounds. Nevertheless, these AOPs limit their practical applications due to the production of toxic by-products, dependence on the surface properties of the photocatalyst and cost aspects.

Treatment of real wastewater from pharmaceutical manufacturing unit has received extensive attention and numerous studies dealing with synthetic (Balcioglu and Otker, 2003; Tunay *et al.* 2004; Arslan-Alaton and Caglayan, 2006) or actual (Arslan-Alaton *et al.* 2004; Cokgor *et al.* 2004; Gadipelly *et al.* 2014) effluents have been reported.

2.3.1 Applications of Fenton's oxidation for pharmaceuticals wastewater

As discussed above, both Fenton and photo-assisted Fenton treatments have been utilized in the degradation of pharmaceutical compounds in wastewater. Due to the cost and

economic concerns related to the use of UV light in photo-Fenton processes, several solar induced photo-Fenton has been established for the effective treatment of several pharmaceuticals such as analgesic, antibiotics, anti-inflammatory and antineoplastic drugs (Klamerth *et al.* 2010; Trovo *et al.* 2011; Sirtori *et al.* 2011; Alalm *et al.* 2015) and various other pollutants (Theruvathu *et al.* 2001; Garg and Prasad, 2016; Sandhwar and Prasad, 2017). Although the Fenton based treatment is not energy intensive process when compared to other AOPs like O_3, UV and US, however, it requires acidic pH (3-4) conditions (Malato *et al.* 2002) and generate iron sludge as $Fe(OH)_3$ at higher pH, thus requiring additional treatment stage. In order to prevent the accumulation and precipitation of soluble iron, increasing replacement of homogeneous Fenton/photo-Fenton process has been practiced using heterogeneous catalysts like iron bearing minerals or naturally occurring iron oxides which can be easily removed and recovered from the reaction process at the end of the treatment and, will eventually reduce the overall cost of the treatment (Pouran *et al.* 2014). Comprehensive studies of heterogeneous Fenton-like systems in recalcitrant organic compound treatment have been performed in the presence of various iron containing zeolites (Brites-Nóbrega *et al.* 2014; Tedla *et al.* 2015), iron pillared clays (Tireli *et al.* 2015), iron bearing minerals (Matta *et al.* 2008; Lee *et al.* 2009; Magalhães *et al.* 2007) and iron oxides like pyrite (Chee *et al.* 2011; Che and Lee, 2011; Khataee *et al.* 2016; Barhoumi *et al.* 2016), hematite (Chan *et al.* 2015), magnetite (Yang *et al.* 2008; Xue *et al.* 2009; Usman *et al.* 2012; Ursachi *et al.* 2012), bentonite (Gupta *et al.* 2015) and geothite (de la Plata *et al.* 2010; Guimaraes *et al.* 2009; Molina *et al.* 2012).

For instance, Trovo *et al.* (2011) reported the efficiency of two iron species, $FeSO_4$ and ferrioxalate complex in solar simulator based photo-Fenton degradation of amoxicillin. Results revealed the complete degradation of amoxicillin in the presence of the ferrioxalate complex within 5 min, while 15 min were required with $FeSO_4$ in the presence of 120 mg L^{-1} H_2O_2. The removal of the antibiotic Norfloxacin (NFX) was studied by de Souza Santos *et al.* (2015) using Fenton's oxidation, direct photolysis (UV) and UV/H_2O_2 processes and the results revealed that use of direct photolysis was ineffective in the removal of the NFX when compared to Fenton oxidation and UV/H_2O_2 process. Study conducted by Cavalcante *et al.* (2013) investigated the degradation of the antineoplastic drug Mitoxantrone (MTX) by photo-Fenton (with potassium ferrioxalate—FeO_x, Fe^{3+} and Fe^{2+}—as iron sources), Fenton, solar photo-Fenton, UV/H_2O_2 and the results revealed that photo-Fenton processes employing FeO_x and Fe^{3+}, and UV/H_2O_2 lead to effective mineralization of MTX, with 77, 82, and 90 % of TOC removal in 135 min, respectively. Machulak *et al.* (2015) analyzed 13 illicit

pharmaceuticals drugs in WWTP influent as well as effluent and determined their degradation efficiency via Fenton process (Fe^{2+} and H_2O_2), a modified Fenton process using waste iron shavings from machining processes as metallic iron source ($Fe^0/H_2O_2/H_2SO_4$).

The physical and chemical properties of catalyst are greatly influenced by their composition, size and morphology (Xu *et al.* 2015). These Fenton-like systems may include both homogeneous and heterogeneous reactions as described by a modified Haber-Weiss mechanism (Kitajima *et al.* 1978). Certain advantages of using iron oxides or naturally occurring iron sources in Fenton and photo-Fenton-like processes includes low cost, low toxicity, easy recovery after treatment, high stability and durability in aqueous solution, high corrosion resistivity, wider pHs range applications and probability of simultaneous homogenous as well as heterogeneous reactions in aqueous system (Pouran *et al.* 2014; Li *et al.* 2015). Moreover, the deposition of iron oxide particles onto the surface of unique support layer like graphene oxide (GO) is desirable due to high surface area, thus allowing high availability of reactant pollutants towards the active sites, which are able to reduce the limitations of mass transfer in heterogeneous catalysis (Tan *et al.* 2013; Zubir *et al.* 2014; Soltani *et al.* 2016). GO has drawn more attention because of its easy availability in bulk quantities, willingness for functioning by chemical reaction, high biocompatibility and good dispersion in water (Chen *et al.* 2008; Zhu *et al.* 2010). However, literature studied revealed that available reports on the use of heterogeneous catalyst in Fenton-like process are mostly confined to the synthesis of iron oxides without any structure modifications, and limited research is being carried out on using naturally occurring minerals or morphological dependent iron oxides in the Fenton-like treatment of recalcitrant pharmaceutical compounds in wastewater.

Although several studies related to Fenton and photo-Fenton treatment has been reported for the degradation of pharmaceuticals compounds in synthetic wastewater, but limited attention is paid toward the treatment of real effluents coming from the pharmaceutical manufacturing industry. For instance, about 95% COD removal was achieved in a pharmaceutical wastewater of COD ~12000 mg L^{-1} containing paracetamol and chloramphenicol (Badawy *et al.* 2009) by Fenton process using $FeSO_4 \cdot 7H_2O$ salt. In study conducted by Monteagudo *et al.* (2013), solar photo-Fenton treatment of pharmaceutical wastewater was carried out in compound parabolic collector (CPC) reactor consisting of pharmaceutical wastewater using a ferrioxalate as iron oxide under optimal conditions, and almost 84% mineralization efficiency was achieved in 115 min. Although homogeneous photo-Fenton treatment of pharmaceutical wastewater has been regarded as one of the

suitable method amongst AOPs, however, its treatment efficiency is influenced by COD:H_2O_2:Fe^{2+} ratio and the pH range of 2.5–4 in the presence of light source (Gogate and Pandit, 2004; Shemer *et al.* 2006). Sirtori *et al.* 2009 employed solar photo-Fenton process (SPF) coupled with biological treatment to treat pharmaceutical wastewater and achieved 95% of COD removal, of which 33% was achieved by the SPF and 62% by the biological treatment. Tekin *et al.* 2006 obtained overall 98% COD removal for a coupled Fenton pre-treatment and aerobic sequential batch reactor (SBR) for pharmaceutical wastewater. Although, Fenton and photo-Fenton treatment suffer a main drawback due to pH dependency and generation of sludge, but optimization of the oxidant and catalyst concentrations relative to the effluent's organic load and adopting proper handling, disposal and treatment of sludge may contribute to suitability of process to treat highly polluted effluents from pharmaceuticals industries. Often biodegradability index (BOD_5/COD) ratio is increased by 3-5 times making degradation of the organic wastes in the subsequent biological treatment easy. It can be presumed that the Fenton's oxidation alone can diminish COD of wastewater by about 50% and only when it is combined with traditional biological systems like aerobic degradation, the COD removal efficiency can ascend to more than 90%. Thus, Fenton's processes can be applied as a pre-treatment method to convert and mineralize the toxic as well as non-biodegradable matter of pharmaceutical wastewater into non-toxic and biodegradable, and thus make wastewater susceptible to be treated by subsequent biological treatment (San Sebastian Martinez *et al.* 2003; Kajitvichyanukul and Suntronvipart, 2006; Sirtori *et al.* 2009).

2.3.2 Applications of ionizing radiation for pharmaceuticals wastewater

In comparison to other AOPs, the use of ionizing radiations *viz.* gamma and E-beam radiations offers several advantages as explained in Section 1.4.2. It is noteworthy that wastewater treatment efficiency by radiation or other advanced oxidation processes (generating $HO^{\bullet}$ radicals) is expected to decrease due to scavenging of $HO^{\bullet}$ radicals by the insoluble suspended solids. However, the high energy radiation technology is not easily perturbed or scattered by insoluble suspended solids, where UV radiation with low energy can be attenuated (Cantwell and Hofmann, 2011). Therefore, radiation technology could play a prominent role in near future in pilot as well as commercial scale to treat real pharmaceutical effluent.

Various researchers have demonstrated that use of gamma radiolysis for environmental remediation of organic contaminants like Prednisolone (Bosela *et al.* 2010), Naphthalene (Chu *et al.* 2016), Cyclohexanebutyric acid (Jia *et al.* 2015), herbicides like

Monuron (Kovács *et al.* 2015), Atrazine (Khan *et al.* 2015), Diuron (Kovács *et al.* 2015a), Cyanuric acid (Varghese *et al.* 2007), insecticide, Acephate (Yang *et al.* 2015), non-ionic surfactant, nonylphenol polyethoxylates (Iqbal and Bhatti, 2015), Azo-dyes (Paul *et al.* 2010; 2011), pharmaceutical drugs like Chlorfenvinphos and Diclofenac (Trojanowicz *et al.* 2012), Diclofenac, Carbamazepine, Ibuprofen, and Bisphenol (Bojanowska-Czajka *et al.* 2015), Primidone (Liu *et al.* 2015), Carbamazepine (Wang and Wang, 2017); Ciprofloxacin (Sayed *et al.* 2015), Sulfamethoxazole (Kim *et al.* 2017) and wastewater (Meeroff *et al.* 2004; Bhuiyan *et al.* 2016; Trojanowicz *et al.* 2017). Study focused on the degradation of anti-inflammatory drug Ibuprofen (IBP) by gamma irradiation was performed by Zheng *et al.* (2011) and results showed complete degradation of IBP occurred at an absorbed dose of 1.1 kGy. Degradation of Nitroimidazoles in wastewater using gamma radiations showed significant decrease in concentration of dissolved organic carbon (DOC) with increase in absorbed dose (Sánchez-Polo *et al.* 2009). Natural waters and wastewaters constitute complex aqueous mediums containing inorganic ions (for example,Cl^-,NO_2^-, NO_3^-, CO_3^{2-}, HCO_3^-, SO_4^{2-} etc.) and various organic solvents that affect the degradation efficiency of pharmaceuticals using irradiation process. Various gamma-induced degradation studies on pharmaceuticals has been performed containing several inorganic and organic radical scavengers (Zheng *et al.* 2011; Ocampo-Perez *et al.* 2011; Guo *et al.* 2012a; Abdel *et al.* 2013; Liu *et al.* 2015; Guo *et al.* 2015; Huang *et al.* 2016). For instance, Guo *et al.* (2015) investigated the radiolytic removal of Ciprofloxacin (CIP) under different conditions and different anions and additives, such as NO_2^-, NO_3^-, CO_3^{2-}, humic acid, 2-propanol, methanol and tert-butanol which showed that low initial concentration and acidic condition were favourable for radiolytic degradation of CIP and degradation was inhibited with the addition of anions and additives.

The sensitivity of pharmaceutical drugs to gamma radiation and E-beam has been investigated by Slegers and Tilquin, (2005) and Slegers and Tilquin, (2006), wherein the aqueous solution showed significant degradation of the drug due to presence of $HO^{\bullet}$, $H^{\bullet}$ and e_{aq}^-. The main difference between gamma irradiation chamber and E-beam accelerator is the dose rate. To get the same absorbed dose, gamma irradiation takes several minutes to hours, whereas E-beam with high dose rate needs only few seconds. Slegers and Tilquin, (2006) found that the degradation rate of β-blocker Metoprolol Tartrate in aqueous solution was significantly higher with E-beam with the generation of less radiolytic intermediates when compared to gamma irradiation. Singh *et al.* (2010) investigated the sterilization of antibiotics

Cefixime in solid state by employing gamma and E-beam irradiation and results revealed 7.20 and 7.07% weight of the chemical lost by E-beam and gamma irradiation, respectively at an absorbed dose of 25 kGy, while the G-value was higher for gamma irradiation (0.107) when compared to E-beam (0.077). Further, the addition of a catalyst and oxidants prior to irradiation treatment improved the degradation efficiency (Chmielewski, 2011; Trojanowicz *et al.* 2017; Capodaglio, 2018). Liu *et al.* (2015) determined the efficacy of E-beam irradiation for degradation of the antiepileptic drug Primidone (PMD) in aqueous solution and complete degradation was achieved at an absorbed dose of 2.0 kGy. Study investigated by Cho *et al.* (2015) showed the potential use of E-beam irradiation as an alternative process in complete degradation of Chloramphenicol (CAP) in aqueous solution. The efficacy of the irradiation treatment is not only based on the efficiency of the degradation but also generate degradation products which are lesser toxic than the parent compound. Degradation of Aflatoxin in aqueous medium was investigated in E-beam at various initial concentrations and the results indicated that the mutagenicity and cytotoxicity of E-beam treated samples decreased significantly when compared with that of untreated samples (Liu *et al.* 2016). Illés *et al.* (2013) observed the changes in toxicity of gamma radiolytic degradation of Ibuprofen (IBP) in aqueous solution using zooplankton tests *Daphnia magna* and luminescent bacteria namely, *V. fischeri*. Results exhibited that the toxicity of the IBP irradiated solution augmented initially and then reduced with prolonged irradiation. Similar results were encountered in the degradation of Clofibric acid (Csay *et al.* 2014); Sulfamethoxazole (Sági *et al.* 2014), Pentachlorophenol (Xue and Wang, 2008) and Ketoprofen (Illés *et al.* 2012) in aqueous solution by gamma irradiation. The irradiation process does not introduce any probability of subsequent secondary contamination, as no content of residual radiation stay in the treated solution as well as the gamma and E-beam irradiation treatment will not induce any radioactivity in the aqueous solution. The radicals in fact revert back to the original water state in the order of few milliseconds, if they do not react instantly with pollutant compounds, and thus there is no possibility of residues or radioactivity left in the water.

Due to strong oxidative properties of hydroxyl radicals, generated in large amount in water radiolysis, the AOP with application of ionizing radiation can be applied in decomposition of bio-recalcitrant compounds. Combination of AOPs with ionizing radiation has been employed for degradation of pharmaceutical compounds such as β-blockers (Song *et al.* 2008), Nitroimidazoles (Sánchez-Polo *et al.* 2009), Tetracycline (Cho, 2010) and various antidepressant pharmaceuticals (Kimura *et al.* 2012; Liu *et al.* 2011). In addition, certain oxidants like hydrogen peroxide (H_2O_2), potassium persulfate ($K_2S_2O_8$) or ozone (O_3) in

combination with the ionizing irradiation treatment may further improve the degradation of organic pollutants (Emmi *et al.* 2008; Trojanowicz *et al.* 2008; Zheng *et al.* 2011; Liu and Wang, 2013; Chu *et al*. 2015). Several studies have demonstrated that a certain dosage of H_2O_2 could accelerate the generation of $HO^{\bullet}$ radicals during irradiation treatment. However, when the H_2O_2 is used in excess, it might competes with the target pollutants for the reactive $HO^{\bullet}$, leading to a reduction of the degradation efficiency (Ocampo-Pérez *et al.* 2011). Bhuiyan *et al.* (2016) investigated the influence of H_2O_2 on decolorization and degradation of textile wastewater during gamma radiolysis. The removal efficiency of 100μM Iopromide (IPM) using E-beam (Kwon *et al.* 2012) revealed 90% degradation of IPM at a dose of 20.0 kGy, and the E-beam/ H_2O_2 process increased the degradation efficiency by the generation of additional $HO^{\bullet}$. Liu and Wang, (2013) reported that the TOC removal efficiency increased significantly from 5% by gamma irradiation alone to 48% with 30 mg L^{-1} H_2O_2 addition for degrading sulfamethazine in aqueous solution.

In comparison to gamma radiation, the E-beam technology is used in the most varied application areas, from enhancement of industrial productions (production of new films, cable insulators, packaging, lubricants and medical hydrogels; process of adhesives and surface coatings, sterilization of disposable medical devices and pharmaceuticals), to food safety and distribution (irradiation of vegetables and fruits, fish and chilled meats, and irradiation of agricultural seeds for enhanced conservation), to contaminated soils treatment and flue gas emissions (IAEA, 2008). Lee *et al.* 2012 successfully demonstrated a mobile ionizing radiation (E-beam) accelerator constructed by the Korean Atomic Energy Research Institute (KAERI) on synthetic solution of antibiotics and endocrine disruptors mixed with real wastewater. Significant role of radiation technology on improving the treatment efficiency of sewage, paper mill and textile dye effluent has been examined (Paul *et al.* 2010; 2011; Guin *et al.* 2014). Considering the potential applications of E-beam technology, first full scale E-beam installation has been demonstrated in Daegu, South Korea to treat 10,000 m^3 day^{-1} of textile wastewater signifying the process is a cost effective technology when compared to conventional treatments. High energy E-beam radiation-based pilots as well as commercial sludge treatment plants have been successfully installed in India, USA, New Mexico, Argentina, Korea and Germany (IAEA, 2007 and 2008). In addition, the E-beam technology has proved to be competent approach for simultaneous disinfection of water during the degradation process (Maruthi *et al.* 2011). The E-beam irradiation unit required only one time installation and nullifies the use of any additional chemicals for the treatment which further strengthen the practical application of E-beam irradiation as a cost-effective,

clean and productive technology for water and wastewater treatments. Therefore, radiation technology could also play a prominent role in near future for commercial scale treatment of pharmaceutical effluent in common effluent treatment plants (CETPs).

2.4 Integration of ionizing radiations with biological treatment

It is obvious that several AOPs have proven their effectiveness in the degradation of pharmaceutical pollutants, however most of these processes are usually considered as expensive. To overcome this short-coming, the integrated approach of AOPs coupled with existing conventional water and wastewater treatment technologies has been recommended to be cost efficient and also to improve the overall degradation efficiency (Oller *et al.* 2011; Schröder *et al.* 2016). The concept of integrating AOPs as a pre-treatment stage prior to biological treatment could enhance biodegradability and reduce toxicity has been fetching considerable attention (Comninellis *et al.* 2008). In an application of coagulation treatment prior to gamma-irradiation of textile industry wastewater, improved reduction of COD and TOC were obtained (Perkowski and Kos, 1988). Balcıoğlu and Ötker, (2003) revealed the potential use of ozonation as a pre-treatment process to enhance the biodegradability of antibiotics in wastewater but incompetence in achieving complete mineralization. The treatment employing ionizing radiations has significantly improved the biodegradability of various polluted wastewater streams (Han *et al.* 2012; Rawat and Sarma, 2013). Duarte *et al.* 2002 studied the combined E-beam and biological treatment for the remediation of refractory organic pollutants present in the wastewater samples of WWTPs and reported 99% removal of organic contaminants found in the effluent of industrial receiver unit (IRU) and coarse bar screen (CBS) using 20 kGy of irradiation dose. The enhancement in the biological degradability (BOD_5/COD) from 0 to 0.16 of Sulfamethoxazole (SMX) by gamma radiation in aqueous solution was investigated by Sagi *et al.* (2016) indicating a conversion of a non-biodegradable compound, SMX to biologically treatable compounds. Recent study by Kim *et al.* 2015 showed that the biodegradability of antibiotic compounds *viz.* Sulfamethoxazole (SMX), Lincomycin (LMC) and Tetracycline (TCN) enhanced after gamma irradiation treatment and followed the trend of TCN (36%) > SMX (28%) > LMC (18%). Chu and Wang, (2016) studied gamma radiolytic degradation of a chlorinated aromatic compound, 3-chloro-4-hydroxybenzoic acid (CHBA) in biological treated effluent and the results revealed 99% removal efficiency of CHBA at neutral pH. Study by Iqbal *et al.* (2015) examined the gamma irradiation treatment of textile effluents for reducing cytotoxicity to about 79, 49 and 39% in the case of brine shrimp, sheep and human red blood cells (RBC), respectively and

mutagenicity was not detected after the treatment. Study conducted on the real textile and dyeing wastewater by He *et al.* (2015) revealed that biodegradability enhanced to 224% by E-beam irradiation. Sun *et al.* (2016) investigated the coupled AOPs and membrane bioreactors (MBR) with E-beam radiation for the treatment of textile wastewater containing polyvinyl alcohol (PVA) and results revealed 31 ± 7% COD removal using coupled treatment process. Thill *et al.* (2016) employed hybrid approaches including biodegradation, E-beam and zero-valent nano iron AOPs individually and in sequence for the detoxification of recalcitrant metalworking industrial wastewater. Sequential treatment lead to overall COD removal of more than 90% indicating that E-beam pre-treatment facilitated more effective post bio-treatment. Wang and Wang, (2016) suggested that combination of irradiation and biological treatment could increase the degradation of triclosan containing wastewater in comparison to single biological treatment process. Shin *et al.* 2002 studied the application of E-beam technology to pulp and paper mill effluent, in conjunction with conventional treatments like coagulation, flocculation, and biological and ozonation, and results displayed enhanced COD removal of the effluent, depending on configuration of the tertiary treatment. In cases, where onsite treatment of polluted groundwater or wastewater or transported of wastewater to some stationary installed WWTP is economically unfeasible and excessively hazardous, mobile-type E-beam accelerator has been assembled and working for the successful treatment of limited wastewater (Cooper *et al.* 2002; Kim *et al*. 2017).

When considering the widely utilized conventional treatment technologies or any other emerging technologies for the treatment of wastewater, one of the most significant aspects for their practical applicability is their cost-effectiveness. Although, several attempts have been made in assessing different types of costs for radiolytic treatment of water and wastewater, however, the overall cost of E-beam plant including fixed costs of depreciation and interest, operational costs, the variable costs of electricity, maintenance, labour, etc. is the matter of concern for scientific community (Han *et al.* 2012). In this respect, an estimate of the comprehensive actual operation cost, including depreciation and interest investment associated with E-beam plant, resulted in about 0.3 USD m^{-3} of treated wastewater (Kuk *et al.* 2011). E-beam processing of wastewater has been reflected as a cost effective process when compared to ozonation and UV based treatment for the control of *E. coli* at flows greater than 5,000 m^3 day^{-1} with required irradiation dose as low as 0.2 kGy (Han *et al.* 2008). A recent study showed that complete mineralization of dioxins could be attained water by E-beam process at a cost of 0. 17 USD m^{-3} of treated water (Kimura *et al.* 2012). Shin *et al.* (2002) compared the overall cost of E-beam treatment of pulp and paper mill wastewater with other

existing traditional technologies and estimated that E-beam cost (1.03 USD m^{-3}) was lower than those of the other employed technologies, namely, reverse osmosis (1.67 USD m^{-3}), use of activated carbon as secondary coagulation (1.22 USD m^{-3}) and evaporation (3.0 USD m^{-3}). Thus, utilization of E-beam technology to treat the real wastewater could be a promising and competent technology at industrial scale when compared to other available AOPs or traditional technologies. However, due to large initial investment associated with the E-beam plant, it is difficult for a single pharmaceutical manufacturing unit to prefer this technology. Therefore, it could be simultaneously established with a CETP for the treatment of pharmaceuticals effluents discharged from clusters of pharmaceutical manufacturing unit at a particular location.

Literature studies have revealed that use of ionizing irradiation is cost-effective method in treatment of wide range of toxic and recalcitrant compounds in different aqueous solution, but the initial investment cost associated with radiolytic processes is the subject of concern. The degradation of pharmaceuticals in aqueous phase could be retarded and enhanced in the presence of certain amount of scavengers and oxidants, respectively. Moreover, biological treatments are considered better options for the post-treatment of readily degradable wastewater. Practically, treatment at source may be a realistic option in pharmaceuticals manufacturing units where effluents of high organic load are generated. Therefore, development of the integrated processes of ionizing irradiation with conventional biological treatment would be cost-effective for the complete detoxification and degradation of real wastewater; thereby reducing the overall cost of the treatment at industrial scale.

2. 5 Research gaps

AOPs have been widely explored for the degradation of several persistent organic pollutants as supplemental technologies to conventional techniques for the treatment of wastewaters from industrial and municipal sectors. From the detailed literature, it is evident that the use of ionizing radiation is clean, effective and fast method to degrade the wide variety of organic contaminants in comparison to other AOPs. Despite the increasing attention paid towards the radiolytic treatment, following gaps are identified which are of concern owing to their potential use in wastewater treatment technology:

- Pharmaceuticals are also detected in drug manufacturing effluents and in hospital wastes. Unlike in WWTPs and drinking water plants, concentrations of these pharmaceuticals are relatively high ranging from few mg L^{-1} to several g L^{-1}. Thus, water matrix has to be considered as an industrial effluent for the treatment purpose and the most appropriate treatment technique needs to be explored for such effluents.

- Due to toxicity, high TDS and COD pharmaceutical effluents cannot be disposed off, for which evaporation technique are currently being adopted at individual level which require space as well as high investment.
- Most of the units have their own existing ETPs based on biological, chemical adsorption and membrane separation processes, in addition to multiple effect evaporators (MEE), still operation of individual waste water treatment to meet statuary standard is an extremely tedious job with insurmountable problems.
- Most of the ETPs in India are ineffective in degrading the persistent pharmaceuticals and thereby, the released pharmaceuticals have been found to be in greater concentrations in the different water bodies when compared to other countries.
- Use of UV lights and catalysts in order to generate $HO^{\bullet}$ radicals for the oxidative degradation of organic pollutants makes the process cost intensive in addition to limitations of the recovery of catalyst. Moreover, the requirements of UV light for longer treatment time increase the cost of treatment.
- The majority of the studies related to pharmaceuticals are oriented towards the commercial available or lab-synthesized catalyst which further makes the process cost intensive.
- As an effective alternative, there is a growing interest in the utilization of gamma radiations for the mineralization in addition to sterilization. However, the radiolysis of pharmaceutical contaminants has not extensively been studied.
- Literature lacked knowledge on fate and intermediates or transformed products formed during gamma/E-beam irradiation treatment of persistent pharmaceutical compounds, which might play pivotal role in understanding the degradation mechanism as well as the toxicity potential of these compounds and its intermediates. Many pharmaceuticals and related products such as antibiotics needs high dose of radiations for mineralization and toxicity reduction.
- Very few studies are available that reports the combine information of physicochemical, toxicity and biodegradability analysis to study the viability of the combined Fenton and biological treatment on simulated wastewater, rather than real pharmaceutical wastewater.
- Many researchers have proposed that gamma and E-beam induced radiolytic treatment of water and wastewater can persuade both oxidation and reduction

reaction, without any requirement of additional chemicals, however, the radiolysis of persistent pollutants in aqueous environment has been limited to few reports only.

- The majority of reported studies on pharmaceuticals degradation using ionizing irradiation have been orientated towards the performance of treatment and investigating the effects of different operational parameters in pure water solution rather than real pharmaceutical effluent.
- Research on the toxicity assessment of persistent pharmaceutical compounds and their degradation by-products/ intermediates with ionizing radiations treatment has not been explored to the desired extent.
- High concentrations of pharmaceuticals were used in majority of studies for the easy detection of these compounds, which could only reflect some situations such as the treatment of industrial pharmaceutical effluent and are far from the real situation in water matrix.
- Most of the studies related to ionizing radiations are subjected towards textile and pulp and paper wastewater, rather than implying the feasibility of irradiation process in the treatment of real pharmaceutical industry effluents.
- The examination of the efficiency of the use of gamma and E-beam irradiation for the degradation of persistent pollutants in aqueous solutions and the possibility of increase in the efficiency of the hyphenated processes with simultaneous use of coagulation/ oxidants needs to be further explored.
- Coupling of radiolytic treatment with conventional biological treatment needs to be further examined for real pharmaceutical effluents.
- From a practical viewpoint, studies on the disinfection and decontamination of the real pharmaceutical effluents by ionizing irradiations should be paid more attention and the transformed by-products/ intermediates are of concern due to their potential stability and toxicity.

2.6 Objectives of the study

Keeping in view the encouraging findings in the literature studies, the present study was planned to optimize the process parameters for the degradation of pharmaceutical industry effluents and model compounds by independent γ radiation, electron beam and Fenton/Photo-Fenton treatment (using synthesized shape-dependent hematite, GO-FeS_2 nanocomposite and naturally available red soil); simultaneous use of oxidant in the presence

of γ radiation and electron beam for achieving enhanced degradation efficiencies as well as rate; and integration of ionizing irradiation processes with aerobic biological treatment to achieve enhanced degradation of industrial effluents.

Chapter 3.0 Materials and Methods

This chapter includes the chemicals, reagents and other auxiliary inputs required for the AOP based irradiation treatment of model compounds and real pharmaceutical wastewater. The experimental methodologies employed in the ionizing radiation and biological treatments have been illustrated. Further the details of reactors used for AOP and biological treatment has been discussed.

3.1 Materials

In order to carry out irradiation based treatment of model compounds and real pharmaceutical wastewater, various chemicals and reagents has been used. The details of wastewater collected for AOPs, irradiation and biological treatment has been discussed.

3.1.1 Model compounds and chemicals

Ornidazole (≥99%) and Ofloxacin (≥99%) were purchased from Sigma-Aldrich. Amoxicillin trihydrate (≥98.0%) was procured from TCI Chemicals Pvt. Ltd., India. HPLC grade Methanol (≥99.9%), HPLC grade Acetonitrile (≥99.9%), tert-butanol (*t*-BuOH) (≥99.5%) were purchased from Sigma- Aldrich. 30% (w/v) Hydrogen peroxide, phosphoric acid (88%), 2-propanol (≥99.8 %), ferric chloride hexahydrate (>99%), ferric nitrate nonahydrate (>98.5%), 1, 10-phenonthralein monohydrate (≥99.5%) and nitrilotriacetate (>98%) were purchased from Merck and used as such. Sodium hydroxide (>99%), hydrochloric acid (37%), hydroxyl ammonium chloride (≥98.0%), ferric chloride (>99%), ammonium acetate (≥98.0%), acetic acid (≥96.0%), sulphuric acid (≥98.0%), sodium nitrate (>99%), calcium hydroxide (95%), aluminium sulphate (98%), ammonium sulphate (99%), sodium sulphate (99%), sodium sulphite (98%), potassium phosphate (99%) and sodium dihydrogen phosphate (>99%) were purchased from SD Fine Chemicals Pvt. Ltd. Sodium carbonate (>99%), sodium nitrite and thiourea was purchased from TCI Chemicals Pvt. Ltd., India. Muller Hinton Agar (MHA) media was acquired from HiMedia Laboratories Pvt. Ltd., India. Ultrapure water was used throughout the study and obtained using a Milli-QTM system (Millipore).

3.1.2 Wastewater and sludge collection

The wastewater used in this study was collected on the basis of grab sampling at three different locations of effluent treatment plant (ETP) of bulk pharmaceutical manufacturing industry in Derabassi, (Punjab) India. The activated sludge used for the biological treatment of wastewater was acquired from the aeration tank of ETP of representative pharmaceutical manufacturing unit.

High strength wastewater (HSW) and low strength wastewater (LSW) was obtained from the respective tanks of the ETP of industry and the sampling point along with the layout of ETP is displayed as Fig. 3.1. Effluent coming from plant has been segregated in two streams one is high strength and second is low strength wastewater. HSW goes into oil and grease tank, where oil and grease is removed. Then its goes into equalization tank 1 for pH correction. Effluent is then transferred to flash mixture after maintaining pH 8-8.5 for chemical treatment. In flash mixing tank, wastewater is treated by alum and polyelectrolyte. Chemically treated effluent then goes into tube settler 1 for settling and its overflows goes in feed tank of multi effect evaporator (MEE) plant. From MEE plant, effluent goes in calandria evaporator where effluent is evaporated through steam with temperature of 60 to 85 °C. Vapour is separated in vapour separator and is cool by cooling tower. Condensate of MEE plant goes into condensate tank and slurry goes into centrifuge. The mixed liquor from condensate is treated again through equalization tank no. 1 and cake is incinerated in incinerator plant. Condensate from condensate tank is mixed with LSW in equalization tank 2 after cooling. LSW with condensate of MEE in equalization tank 2 is transferred in aeration tank for biological treatment. Urea and diammonium phosphate are added in aeration tank as source of nutrients for microorganisms and required air is supplied with help of root blower. After biological treatment in aeration tank, effluent goes in the tube settler 2 for settling. Settled sludge is goes into filter press and cake is send to Nimbua Greenfield Punjab Limited (NGPL), India for landfill after drying under sunlight. NGPL is the nodal Treatment Storage Disposal Facility (TSDF) authorized by Punjab Pollution Control Board (PPCB) for disposal of hazardous industrial waste generated in Punjab.

Overflow of tube settler 2 goes into sump tank and then it passes through pressure sand filter and activated carbon filter tank for color and TSS removal. Finally, the treated effluent is collected in the treated water tank. Treated water is being reuse in MEE cooling tower, utility cooling tower and garden.

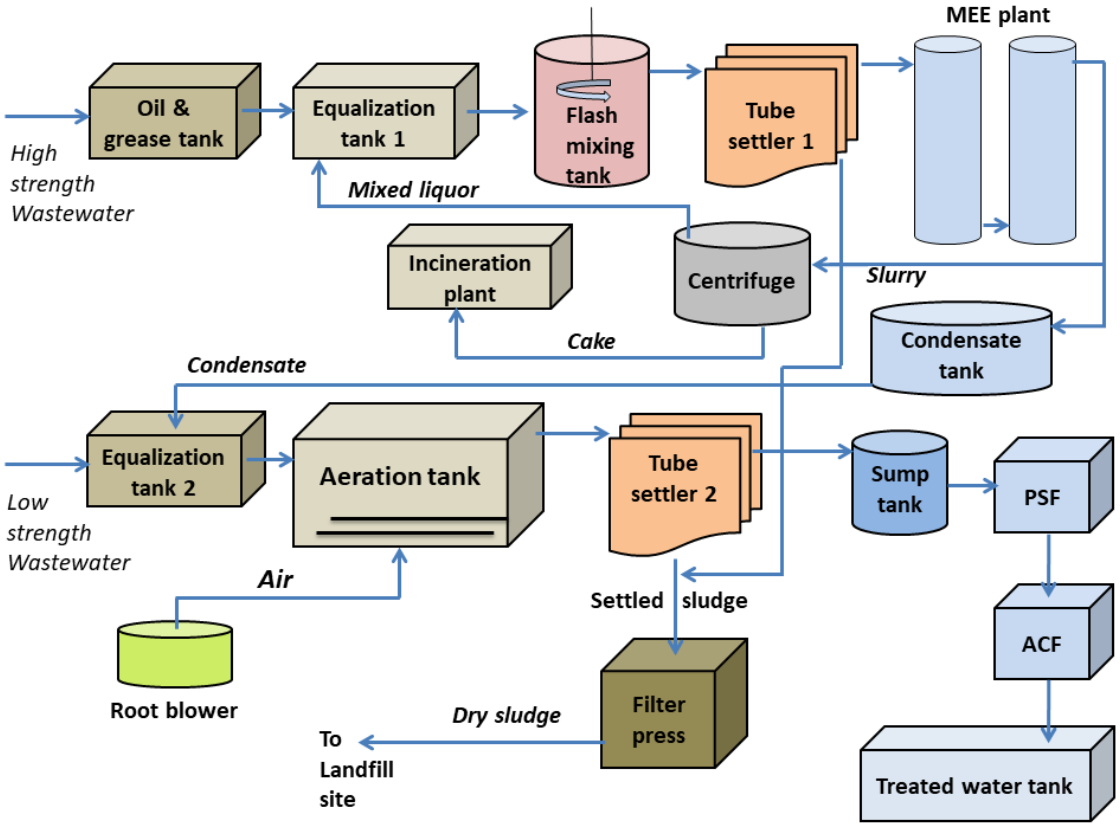

Fig. 3.1 ETP layout of representative industry (MEE: Multiple Effect Evaporator; PSF: Pressure Sand Filter; ACF: Activated Carbon Filter)

3.2 Instruments and reactors

Various instruments and reactors involved in AOPs, irradiation and biological based treatment of model compounds and real pharmaceutical wastewater are summarized as follows:

3.2.1 UV reactor chamber

The UV based rectangular chamber was made up of cast iron sheets equipped with UV-A (Philips, 6 tubes each 36 W, 365 nm λ_{max} and 1.6 W m^{-2} intensity) and UV-B (Philips, 6 tubes each 20 W, 311 nm λ_{max} and 2.3 W m^{-2} intensity) (Fig. 3.2). The tubes were interchanged as per the requirement of treatment process. The intensity of light was measured using radiometer (Eppley, USA).

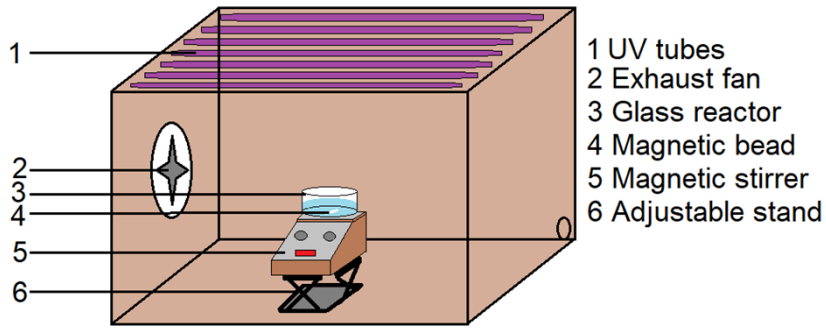

Fig. 3.2 Schematic representation of UV tubes chamber

3.2.2 Continuous baffled reactor

Continuous scale experiments were performed in a baffled reactor made up of polycarbonate (PCB) sheet with the dimensions 92.5 × 49 × 4 cm consisting of six baffles which were incorporated to increase the retention time in the reactor (Fig. 3.3). Inlet and outlet valves were kept at a height of 1 cm from the bottom surface in order to prevent the outflow of soil from the reactor with the aqueous solution. The total volume of the reactor is 16.5 L and total filled volume was 4.14 L.

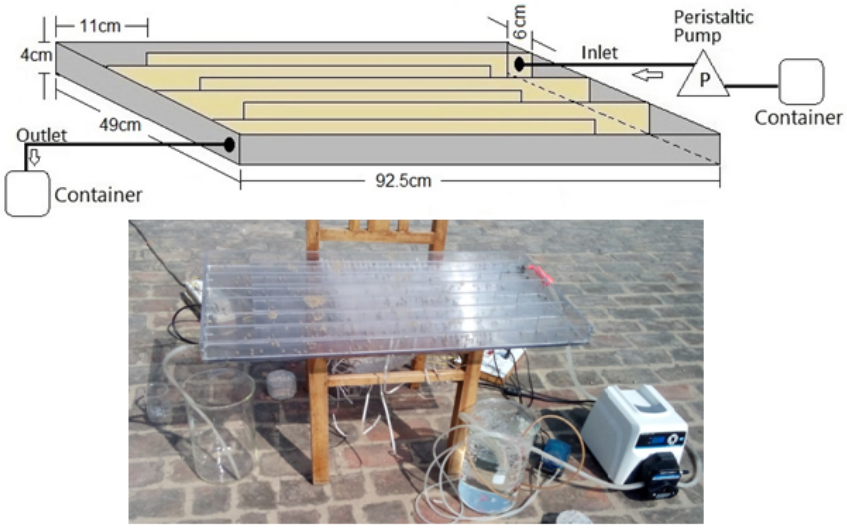

Fig. 3.3 Schematic representation of continuous baffled reactor

3.2.3 Gamma chamber

Gamma irradiation treatment was carried out using GC-5000 gamma chamber at Radiation Technology and Development Division, Bhabha Atomic Research Centre, Mumbai. Gamma chamber was having cobalt-60 (^{60}Co) as a source of gamma radiation. Fricke dosimetry was used to determine its dose rate [$G(Fe^{3+})$ = 1.61 μm J^{-1}] during the irradiation treatment. Fig 3.4 shows the representation of gamma chamber.

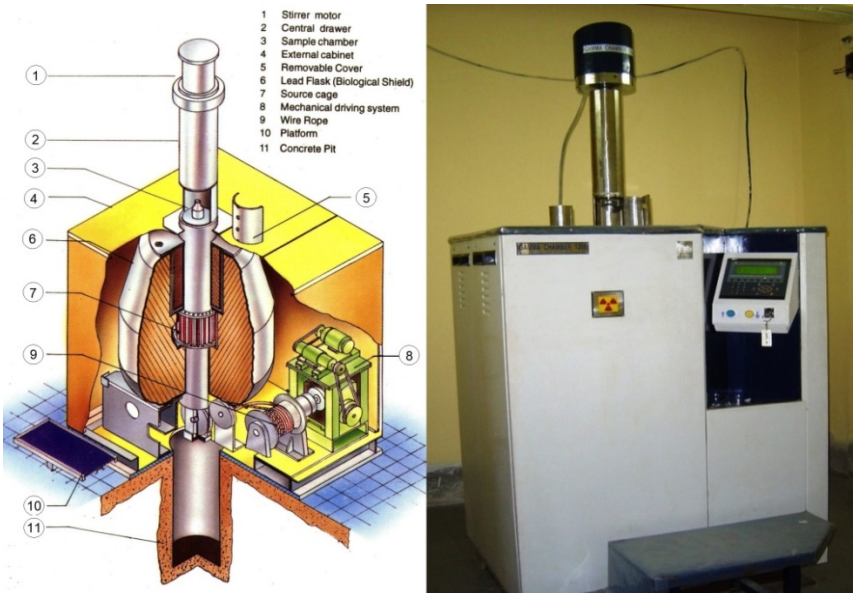

Fig. 3.4 Schematic representation of gamma chamber (*Source:* BARC, Mumbai)

3.2.4 Electron beam accelerator

High energy electron beam induced treatment of wastewater was performed under 4.5 MeV beam energy, 0.156 mA average beam current and 4 Hz pulse frequency using linear electron beam accelerator unit (ILU-6) from Budker Institute of Nuclear Physics, Russia. The E-beam experiments were performed at ILU-EBA facility lab of Electron Beam Processing Section, Board of Radiation and Isotope Technology (BRIT), Navi Mumbai (Fig. 3.5). The E-beam has maximum dose rate of 10 kGy sec^{-1} and penetration depth of 25 mm in unit density.

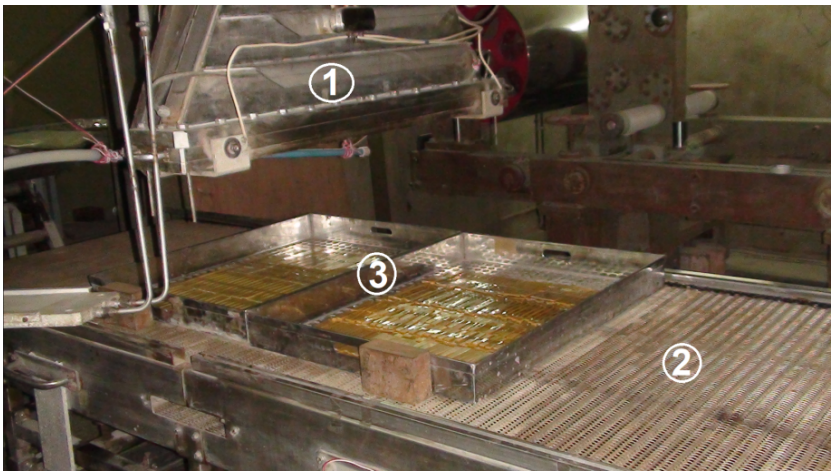

Fig. 3.5 View of electron beam accelerator unit at BRIT, Navi Mumbai [1: Electron exit window; 2: Conveyor: 3: Stainless steel tray] (*Source:* BARC, Mumbai)

3.2.5 Biological reactor

Aerobic biodegradation of pharmaceutical wastewater was performed in batch and continuous mode using batch reactor system and activated sludge process (ASP) reactor.

Batch reactor system consists of wide mouth glass bench reactor ($13 \times 7\ cm$) equipped with air supply, mixing and temperature controlled incubator (Fig. 3.6).

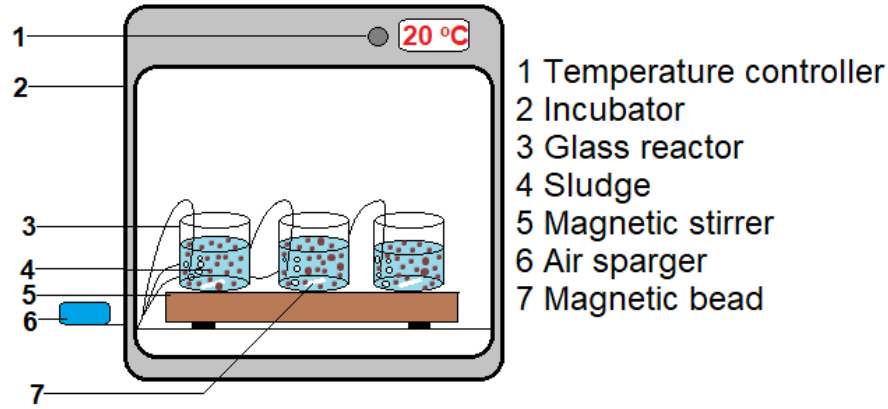

Fig. 3.6 Schematic layout of batch mode biological reactor

Aerobic degradation of wastewater was performed in laboratory scale stainless steel fabricated activated sludge process (ASP) unit as shown in Fig. 3.7. The reactor consists of aeration tank of 9 L capacity and settling chamber of 2 L capacity. The sludge recirculation provision was made to maintain the MLSS in the reactor. Air sparger was utilized to provide submerged aeration to the mixed liquor in the aeration tank. Also, 3 L capacity of treated water tank was set up to collect the treated wastewater from the draining system of settling chamber's overflow.

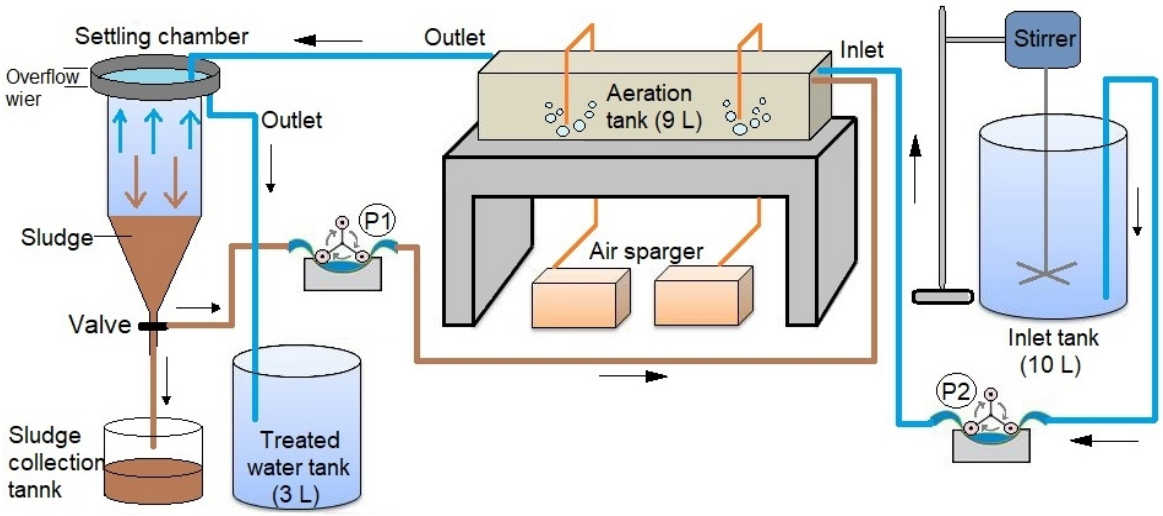

Fig. 3.7 Schematic diagram of experimental setup for activated sludge treatment of wastewater. P1: Peristaltic pump for sludge recirculation; P2: Peristaltic pump for influent of wastewater

3.3 Methods

In order to study the AOP based treatment of model compounds and pharmaceutical wastewater, independent gamma irradiation, E-beam irradiation and Fenton's treatment was employed for degradation studies. Effect of various operational parameters was evaluated during each treatment processes, whereas $FeSO_4.7H_2O$ was used during Fenton's treatment of real pharmaceutical wastewater. Besides, real pharmaceutical wastewater was subjected to coupled treatment of AOPs and biological degradation to achieve the enhanced treatment efficiency. Gamma, E-beam and biological treatment of real pharmaceutical wastewater was performed in Gamma chamber, E-beam accelerator and ASP reactor, respectively.

3.3.1 Synthesis of hematite

Hematite particles (α-Fe_2O_3) with three different shapes i.e., Spherical (S-α-Fe_2O_3), Cubical (C-α-Fe_2O_3) and Rod (R-α-Fe_2O_3) were synthesized using sol- gel procedures as reported (Demarchis *et al.* 2015). For synthesis of all the three shapes, 6 M of 45 mL NaOH was slowly added to 2 M of 50 mL $FeCl_3$ under constant stirring and different shape additives were added under varying treatment options. For synthesizing S-α-Fe_2O_3, 6 mL nitrilotriacetate (0.3 M) was added drop wise to the obtained solution and kept for an additional stirring of 15 min. The resultant gel was transferred to tightly closed bottle and placed in oven at 90 °C for 60 h.

For the synthesis of C-α-Fe_2O_3, the obtained solution of NaOH and $FeCl_3$ was further stirred for 15 min and then kept at 90 °C for 6 h to allow the conversion of $Fe(OH)_3$ gel to β-FeOOH (akaganeite) precipitate. Afterwards, the solution was centrifuged to pellet down the akaganeite precipitates and washing was done twice with 0.5 M $NaNO_3$. Stock suspension of akaganeite was prepared in 200 mL of deionized water by ultra-sonication. 100 mL of this suspension was added to 6 mL HCl (1 M) and 44 mL deionized water. The final suspension was stirred for 10 min with drop wise addition of 0.3 M NaCl and transferred to tightly closed bottle which was kept overnight at 100 °C to obtain C-α-Fe_2O_3. For the R-α-Fe_2O_3 synthesis, the prepared solution of NaOH and $FeCl_3$ was transferred to tightly closed bottle and placed in oven at 60 °C for 60 h.

Final washing of all the synthesized hematite particles was performed using ultrapure water, 1 M NH_3 and again by ultrapure water. Finally, drying of the particles was carried out in hot air oven at 70 ºC.

3.3.2 Collection of red soil

Soil, a natural resource, is present in abundant amount on the earth's crust. Among various types, red soil represents the third largest soil group of India covering an area of

about 3.5 x 10^5 hectare (10.6% of the total geographical area of the country). Red color of the soil is attributed to its high content of iron oxides; however, it is poor in phosphate, nitrogen and organic matter (Bhattacharya *et al*. 2008). Due to the existence of high contents of iron oxides, the use of environmentally friendly and economical applications of soil is of substantial interest in photo-Fenton like processes. Red soil was obtained from Warangal region in Tamil Nadu, India and washed thrice with ultra-pure water.

3.3.3 Synthesis of graphene oxide-pyrite nanocomposite

GO was synthesized from graphite flakes using modified Hummers method (Marcano *et al.* 2010). The schematic process of GO synthesis from graphite flakes has been shown in Figure 3.8.

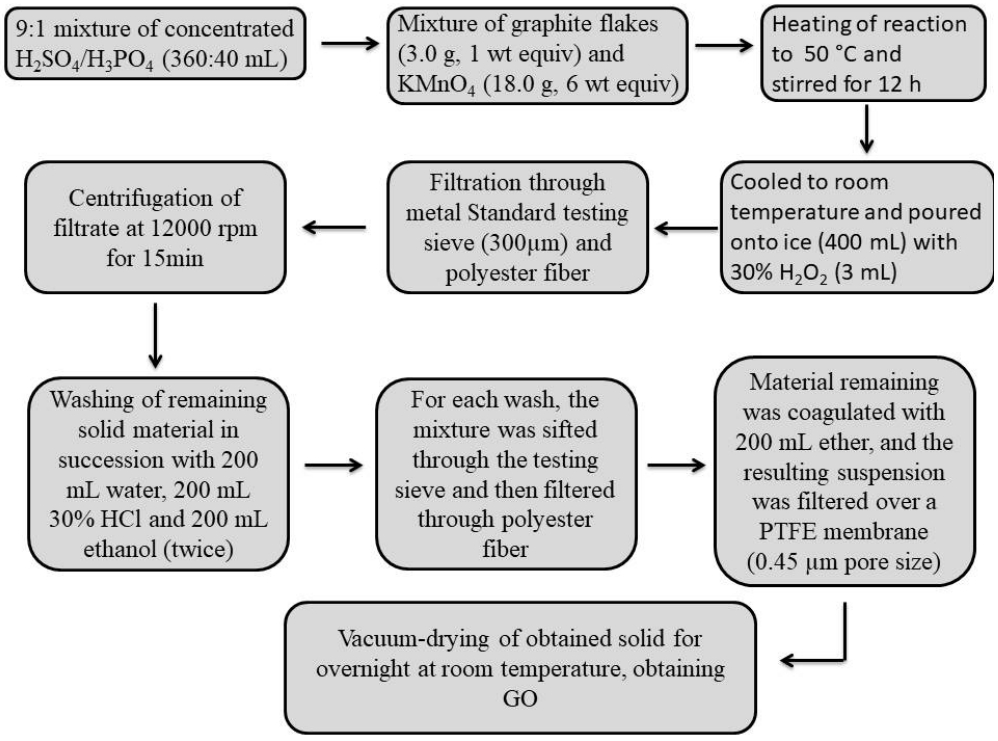

Fig. 3.8 Synthesis procedure of graphene oxide

The GO-FeS_2 nanostructure composite was synthesized using a simple one-pot hydrothermal procedure (Chen *et al.* 2018). The weight ratio of FeS_2 and GO in GO-FeS_2 in nanocomposite was maintained to be 4:3. The schematic process of GO-FeS_2 synthesis has been shown in Figure 3.9. Bare FeS_2 was also synthesized using the same protocol without the addition of GO in the precursors.

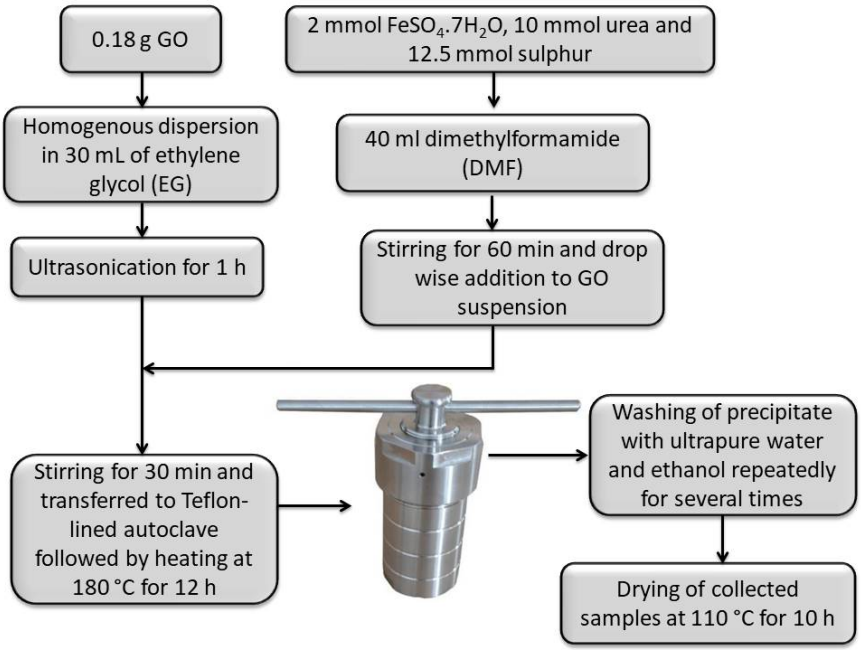

Fig. 3.9 Synthesis procedure of graphene oxide-pyrite (GO-FeS_2) nanocomposite

3.3.4 Characterization hematite, GO-pyrite and red soil

The crystalline phases and composition of the synthesized hematite, GO-pyrite and soil particles were determined by X-Ray Diffraction (XRD, Philips X-Ray diffractometer, Cu Kα radiation, λ=0.154 nm, 45 kV, 40 mA) with a PW3050/60 XPERT-PRO diffractometer. Diffraction peaks were identified by applying Match 3.3.0 build 88 (Crystal Impact, Germany) processing software. To examine the morphology and chemical composition of hematite and soil particles, scanning electron microscopy-Energy dispersive spectroscopy (SEM-EDS) (JEOL-JSM-6510LV instrument, Japan) operating at 20 kV was done. Structural analysis of hematite and GO-FeS_2 was also performed using High-resolution Transmission electron microscopy (HR-TEM) using TECNAI- G2T20ST (200 kV). For determining specific surface area of hematite, soil and GO-FeS_2, Brunauer- Emmett- Teller (BET) by N_2 adsorption analyzer (NOVA2000e, USA) was used.

3.4 Mode of experiments for model compounds

For the independent Fenton, gamma and E-beam irradiation treatment, aqueous solutions of model compounds, such as ORZ, OFX and AMX were prepared. All the model compound solutions were prepared by adding the required concentration of model compound in volumetric flask (1000 mL) followed by constant mixing at 300 rpm for 12 h, so as to obtain homogeneous solutions of model compounds. The aqueous solutions of model compounds were subjected to independent Fenton, gamma and E-beam irradiation treatment.

3.4.1 Photo-Fenton treatment of model compounds

The model compound (ORZ) was subjected to photo-Fenton treatment using synthesized hematite particles. Both the model compounds (ORZ and OFX) were subjected to photo-Fenton treatment using synthesized soil particles, independently. AMX and OFX were subjected to photo-Fenton treatment using synthesized GO-FeS_2 nanocomposite, independently

3.4.1.1 Batch experiments for photo-Fenton oxidation using hematite

The synthesized hematite particles were used as an iron source in the photo-Fenton degradation of ORZ (initial concentration of 0.22 mM). The entire batch of experiments were conducted in a glass reactor ($150 \times 75\, mm$) filled with 150 mL of ORZ solution under UV/solar irradiations. The solution pH was adjusted using 1 M HCL and 1 M NaOH. For adsorption-desorption isotherm studies, 150 ml of ORZ solution was treated with C-α-Fe_2O_3 particles (0.13 g L^{-1}) in dark with continuous stirring for 30 min. For photo-Fenton experiments, C-α-Fe_2O_3 concentration (0.03-0.2 g L^{-1}), H_2O_2 dosage (3-20 mM) and pH (2-7) were varied and assessed for its efficacy in the degradation of ORZ solution under solar irradiation for 3 h. After regular interval of 30 min, 5 ml aliquots was withdrawn and syringe filtered using PTFE Millex-LCR syringe filters (pore size 0.45 μm). Each experiment was performed in triplicate to check the reproducibility of results. UV-based treatment was performed in UV-tubes chamber (Fig. 3.2). Solar Experiments were performed in the month of May-July, 2016 in between 11:00 A.M. to 3:00 P.M at the roof top of Thapar Institute of Engineering and Technology, Patiala. The intensity of solar radiations was 930 ±48 W m^{-2} measured using pyranometer (Apogee, MP-100). In summer, about 20–30% of the total daily amount of UV radiation is received between 11:00 and 13:00 as reported earlier (Diffey, 1991).

3.4.1.2 Batch experiments for photo-Fenton oxidation using soil particles

Experiments were executed in batch mode for assessing the viability of soil as an iron source for photo-Fenton-like degradation of ORZ (0.09 mM) and OFX (0.05 mM) individually. Batch experiments were performed in a glass reactor (150 mm diameter, 75 mm height) with 150 mL of model compound's solution, under sunlight having an average intensity of 941 ±40 W m^{-2}. pH was adjusted using 1 M HCl. Prior to reaction, the aqueous solutions of both the compounds were magnetically stirred in the presence of soil in dark for 30 min to establish an adsorption-desorption isotherm. The reaction was initiated by the addition of H_2O_2 in aqueous solutions illuminated under solar light. Parametric optimization for ORZ and OFX was carried out by varying soil dose (0.006-0.073 g L^{-1}), H_2O_2

concentration (0.7-5.0 mM) and pH (2-7). Further, the optimized experiments were conducted in UV-tubes chamber (Fig. 3.2) under UV-A and UV-B radiations for examining their effect on degradation efficiency. After regular time intervals, 5 mL of sample was withdrawn from the reaction chamber into the test tubes containing 1 mL ethanol to quench the Fenton reaction by raising the pH (8.0-9.0), which was stored for its subsequent determination of ORZ and OFX residual concentrations. Soil particles were separated using syringe filters (pore size 0.45 μm). Leached iron concentration and total organic carbon (TOC) was examined for the optimized conditions.

The formation of hydroxyl radicals ($HO^{\bullet}$) during the treatment process was analyzed using fluorescence method with terephthalic acid (TA) as a probe molecule which readily reacts with $HO^{\bullet}$ to produce fluorescent compound 2-hydroxyterephthalic acid (HTA) which have fluorescence signal at 425 nm (Ishibashi *et al.* 2000). In a typical process, optimized quantity of soil and H_2O_2 were added in 150 mL of 0.5 mM TA solution and 5 mM NaOH, and exposed to UV-A, UV-B and solar irradiations. The fluorescent intensity at 425 nm was measured using a fluorescent spectrophotometer (LS 45, Perkin Elmer, USA).

3.4.1.3 Continuous experiments for photo-Fenton oxidation using soil particles

Continuous scale experiments for photo-Fenton treatment of ORZ (0.09 mM) and OFX (0.05 mM) were performed in a baffled reactor as shown in Fig. 3.3. Aqueous solution of model compounds was continuously fed into the reactor with a constant flow rate of 30 mL min^{-1} using peristaltic pump (Cole Parmer, Masterflex L/S® Model-7720062, L/S 36 tubing). The retention time of the aqueous solution in the reactor was 150 min. 5 L aqueous solution of both the model compounds at pH 3 was treated individually. Soil was either used as a thin layer of about ≈0.2-0.3 mm spread on the bottom surface of the reactor or in the form of small soil bead. The beads with an average diameter ≈60 mm were prepared using soil: cement (1:1) followed by drying at 80 °C. The reactions in both the modes were initiated after the addition of H_2O_2 in the storage container attached to inlet of the reactor. For analysis, aliquot sample was withdrawn from the outlet of the reactor after 150 min for ORZ and OFX independently. For assessing the reusability potential, soil beads were separated from the reactor after completion of each run and then, washed with ultrapure water followed by drying for 2 h at 80 °C and were reused for the next run with fresh pharmaceuticals solution.

3.4.1.4 Batch experiments for photo-Fenton oxidation using GO-FeS_2

Experiments were executed in batch mode for assessing the viability of GO-FeS_2 as an iron source for photo-Fenton-like degradation of AMX (0.1 mM) and OFX (0.1 mM)

individually. Batch experiments were carried out in a 30 mL glass vial loaded with 20 mL of model compound's solution, under sunlight having an average intensity of 880 ±50 W m^{-2}. pH was adjusted using 1 M HCl. Prior to reaction, the aqueous solutions of both the compounds were magnetically stirred in the presence of soil in dark for 60 min to establish an adsorption-desorption isotherm. The reaction was initiated by the addition of H_2O_2 in aqueous solutions illuminated under solar light. The degradation of model compounds was assessed under preliminary optimized conditions of 10 mM H_2O_2, 1 g L^{-1} GO-FeS_2 at pH 5. After regular time intervals, aliquot of sample was withdrawn from the reaction tubes for its subsequent determination of AMX and OFX residual concentrations. GO-FeS_2 particles were separated using hydrophilic syringe filters (pore size 0.45 μm).

The formation of HO• during the treatment process was analyzed using fluorescence method as discussed in Section 3.4.1.2. During the treatment process, the rate of H_2O_2 decomposition was analyzed spectrophotometrically using potassium titanium (IV) oxalate method as reported by Sellers (1980).

3.4.2 Gamma irradiation treatment of model compounds

Aqueous solutions of model compounds (OFX, AMX and ORZ) were permitted to attain state of equilibrium under room temperature and atmospheric pressure prior to radiation exposure and were tightly closed in order to prevent the introduction of air. Irradiation studies were performed in a GC-5000 gamma chamber as shown in Fig. 3.4. The dose rate of gamma chamber was found to be 0.75 kGy h^{-1} in case of OFX and ORZ degradation study, whereas in case of AMX, dose rate of 10.9 kGy h^{-1} was determined using Fricke dosimetry [$G(Fe^{3+})$=1.61 μmol J^{-1}]. Radiation experiments were performed in a 30 mL air-tight borosilicate glass vials loaded with 20 mL of model compound's solution. The absorbed doses were controlled at 0, 0.25, 0.5, 0.75, 1.0, 1.5, 2.0 and 3.0 kGy for OFX and ORZ by adjusting the radiation time. The absorbed doses were controlled at 0, 2.5, 5, 7.5, 10, 12.5 and 15.0 kGy for AMX. The pH effect was studied by adjusting initial pH of the solution using 1 M HCl and 1 M NaOH. Various additives such as NO_3^-, NO_2^-, CO_3^{2-}, HCO_3^-, SO_4^{2-}, SO_3^{2-}, thiourea, *t*-BuOH (tert-Butanol), propanol and H_2O_2 were added to aqueous solution of model compounds in order to examine their effect on degradation efficiency of model compounds. The glass container with solutions was placed inside a closed lead-shielded gamma source with the aid of an electronically controlled motorized stage ensuring the safety of the operator. The irradiation with gamma energy was carried out

in non-contact mode. It does not induce radioactivity to the model compounds composed of low atomic number elements like C, H, N and O, hence do not promote any health hazards (Spinks and Woods, 1990). After gamma radiolysis of model compounds solution at a specified dose (the irradiation time was calculated with the quotient of specified dose and dose rate), the irradiated samples were preserved in refrigerator at 4 °C until further analysis.

3.4.3 E-beam irradiation treatment of model compounds

Electron beam-induced treatment of model compounds (OFX, AMX and ORZ) was performed under linear electron beam accelerator unit (ILU-6) as shown in Fig. 3.5. Irradiation experiments were performed in 25 mL borosilicate glass petri-dishes loaded with 15 mL of model compound solution and 1 kGy min^{-1} of dose rate was employed with conveyor speed of 3 cm s^{-1} for OFX and ORZ degradation study. For the degradation study of AMX, dose rate was fixed to be 2.5 kGy min^{-1}. The samples were placed at an approximate distance of 40 cm from the irradiation window, and were given dose ranging from 0.5 to 3.0 kGy at room temperature ($30 \pm 2°C$). All the experiments were conducted parallel and in triplicates to examine the consistency of results. The influence of various parameters including initial concentration of model compound, solution pH and additives for instance, as NO_3^-, NO_2^-, CO_3^{2-}, HCO_3^-, SO_4^{2-}, SO_3^{2-}, thiourea, *t*-BuOH, propanol and H_2O_2 were added to model compound solutions to analyze their impact on the degradation efficiency. The irradiated samples were kept in refrigerator at 4 °C till further analysis.

3.4.4 G-value and dose constants calculations

The degradation efficacy of model compounds (AMX, OFX and ORZ) using irradiation based treatment can be quantitatively described by radiation chemical yield (G-value) values and is presented by Eq. 3.1 (Woods and Pikaev, 1994).

$$G - value = \frac{R\,(6.023 \times 10^{23})}{\mathrm{D}\,(6.24 \times 10^{16})} \tag{3.1}$$

Where, R is the change in the concentration of model compound (M); 6.023×10^{23} is Avogadro's number; D is absorbed dose (Gy); and 6.24×10^{16} is the conversion factor from Gy to 100 eV L^{-1}. The dose constants *(k)* were used to evaluate the absorbed doses required for 50% ($D_{0.5}$) and 90% ($D_{0.9}$) degradation of model compounds as shown by Eqs. (3.2) and (3.3).

$$\mathrm{D}_{0.5} = \frac{\ln 2}{k} \tag{3.2}$$

$$\mathrm{D}_{0.9} = \frac{\ln 10}{k} \tag{3.3}$$

The dose constant, k, was evaluated from the slope of the plot of natural logarithm (ln) of the model compound concentration (mM) versus absorbed dose (Gy) as presented in Eq. 3.4

$$\ln\left(\frac{C}{C_o}\right) = -kD \tag{3.4}$$

Where, C is the concentration of model compound at different absorbed doses, D and C_o is the initial concentration of model compound.

3.5 Mode of experiments for real pharmaceutical wastewater

LSW and HSW samples were subjected to independent Fenton's oxidation, gamma irradiation and E-beam irradiation treatment. For the collected wastewater samples, Fenton applications like dark Fenton and photo-Fenton were evaluated for the treatment of real pharmaceutical wastewater.

3.5.1 Pre-coagulant treatment of wastewater

Due to high solids content of wastewater, the pre-treatment treatment of LSW and HSW was performed using different types of chemical coagulants including calcium hydroxide ($Ca(OH)_2$), ferric chloride ($FeCl_3$) and aluminium sulphate ($Al_2(SO_4)_3$. For both the LSW and HSW, optimization of coagulant dosage, pH and contact time was done to reduce the organic load of wastewater prior to irradiation treatment.

3.5.2 Applications of gamma irradiation for pharmaceutical wastewater treatment

Irradiation of coagulant treated LSW and HSW was carried as pre- and post-treatment to biological process. Irradiation experiments were performed in a gamma chamber (GC-5000) having ^{60}Co as a source of gamma radiation and 10.9 kGy h^{-1}dose rate. LSW and HSW samples were irradiated in 30 mL borosilicate glass bottles containing 20 mL of sample volume. All the bottles were tightly closed in order to avert the introduction of air. Wastewater samples were allowed to reach the equilibrium state under atmospheric pressure and room temperature prior to irradiation exposure. Both LSW and HSW were given irradiation dose in the range of 2.5 to 100 kGy. The effect of various factors like pH, type of oxidant including H_2O_2 and $K_2S_2O_8$ were optimized for LSW and HSW independently. After irradiation treatment of samples at a particular dose, the irradiated samples of wastewater were refrigerated at 4 °C till further analysis. The coagulant treated wastewater samples were also irradiated with 500 mL volume under the obtained optimized conditions which were utilized for post-biological treatment in batch reactor as shown in Fig. 3.6.

3.5.3 Applications of E-beam irradiation for pharmaceutical wastewater treatment

E-beam irradiation treatment to coagulant treated LSW and HSW were given under

linear electron beam accelerator unit (ILU-6) as represented in Fig. 3.5. Experiments were conducted in 25 mL glass petri-plates laden with 15 mL of wastewater samples and 25 kGy min^{-1} of dose rate. The wastewater samples were placed beneath the irradiation window at an approximate distance of 40 cm and were given dose ranging from 2.5 to 100 kGy at room temperature (30 ± 2 °C). The influence of parameters like pH of wastewater, irradiation dose and addition of oxidants like $K_2S_2O_8$ and H_2O_2 were examined to analyze their impact on the degradation of organic matter of wastewater samples. All the LSW and HSW samples were irradiated parallel by placing the petri-plates in stainless steel tray. After accumulation of particular irradiation dose, petri-dishes were removed from the tray and irradiated samples were syringe filtered (0.22 μm) for COD, TOC and toxicity analysis. Under the optimized conditions of E-beam treatment of LSW and HSW, 20 L of each wastewater samples were placed in a stainless steel tray of dimensions $80 \times 60 \times 2\ cm$ and given irradiation dose. The irradiated samples of LSW and HSW were given post-biological treatment using activated sludge process in ASP reactor as shown in Fig. 3.7.

3.5.4 Applications of Fenton technologies for pharmaceutical wastewater treatment

Dark-Fenton (DF) and photo-Fenton (PF) oxidation studies were conducted in batch experiment with 250 mL volume of wastewater samples in a glass reactor (150 × 75 mm) equipped with magnetic stirrer at constant agitation speed of 200 rpm. All the dark-Fenton experiments were performed by covering the glass reactor with aluminum foil in order to stop light penetration and photo-Fenton experiments were conducted in the month of May to July, 2018 under solar irradiations with an average intensity of 900 ±75 W m^{-2} as measured by pyranometer (MP-100, Apogee Instruments, Inc. USA). At the beginning of all the DF and PF experiments, the wastewater samples were directly added to the glass reactor, and initial sample was withdrawn after 20 min of homogenization. pH adjustment was done using H_2SO_4 and NaOH solutions. Afterwards, iron source was added and samples were homogenized for 20 min. Finally, initial dose of H_2O_2 was added to initiate the reaction. The study evaluates the operational parameters involved in the operation of DF and PF processes such as iron concentration, H_2O_2 dosage and pH. All these parameters were optimized for LSW and HSW independently.

Aliquot of samples were withdrawn during DF and PF treatment at regular interval and were immediately analyzed. For neutralization of treated solutions, NaOH solution was added to stop the oxidation reaction (pH 12.0) followed by filtration to remove the formed ferric hydroxide sludge. Finally, samples were boiled for 10 min to eliminate the excess of H_2O_2 and were analyzed for COD, TOC and toxicity assessment.

3.6 Biological treatment

The LSW and HSW were given biological treatment using aerobic activated sludge obtained from the aeration tank of ETP of pharmaceutical manufacturing industry. Biological treatment was employed as pre- and post-treatment to gamma irradiated samples of LSW and HSW, whereas biological treatment was employed as a post-treatment to Fenton/photo-Fenton and E-beam treated samples of LSW and HSW.

3.6.1 Biological treatment in batch mode

The biodegradation of LSW and HSW samples were conducted in batch mode experiments using the aerobic activated sludge collected from the aeration tank of ETP of pharmaceutical manufacturing unit. The activated sludge was aerated for two days in order to remove the residual compounds and subsequently washed three times with phosphate buffer (pH 7.0) prior to biodegradation process. Afterwards, sludge was acclimatized for 25 days. The sludge was continuously fed with air to maintain dissolved oxygen (DO) concentration of 2.0-3.0 mg L^{-1}. Sludge was considered to be acclimatized when the concentration of mixed liquor suspended solids (MLSS) maintained constant concentration of 3200 ± 110 mg L^{-1}. Gamma irradiated and non-irradiated samples of wastewater were kept for biodegradation treatment in 300 mL wide mouth glass reactor with 200 mL of sample at 200 rpm with the provision of air supply using air pumps as shown in Fig. 3.6. The pH of pre-coagulant treated and gamma irradiated samples was adjusted in the range of 7.0-8.0 prior to biodegradation treatment. The levels of nutrient were maintained to be COD:N:P at 100:5:1, respectively prior to biological treatment (Metcalf and Eddy, 1995; Raj and Anjaneyulu, 2005). Both LSW and HSW samples were subjected to biodegradation at different concentrations of activated sludge at temperature conditions (20 °C, 27 °C and 30 °C) prior to irradiation treatment. Post-biological degradation experiments were conducted on gamma-irradiated samples of LSW and HSW. During biodegradation process, each bottle was covered with aluminium foil in order to avert the photo-oxidation. At regular intervals, 3 mL of sample was withdrawn and centrifuged for 15 min to separate the sludge. The supernatant was syringe filtered (0.22 μm) and kept at 4 °C till COD, TOC and toxicity analysis.

LSW and HSW samples treated with Fenton applications were subjected to subsequent biological degradation with the aerobic activated sludge in batch mode experiments as shown in Fig. 3.6. All the wastewater samples were kept for biological treatment in 300 mL wide mouth glass bottle with 200 mL volume of sample. Both the pre-treated LSW and HSW with different Fenton applications were subjected to post-biodegradation using different concentrations of activated sludge at different temperature

conditions (20 °C, 27 °C and 37 °C). At regular intervals, 3 mL sample was withdrawn and subsequently centrifuged for 15 min to separate the sludge. The supernatant was syringe filtered (0.22 μm) and analyzed for COD, TOC and cytotoxicity evaluation.

3.6.2 Biological treatment using continuous mode

The potential for activated sludge process treatment of wastewater samples was evaluated by feeding diluted or raw wastewater samples of LSW and HSW, which were pre-treated by E-beam irradiation. The reactor was inoculated by the activated sludge obtained from the aeration tank of ETP of industry from where wastewater was collected. The sludge was transferred to the reactor and was retained in it, allowing the build-up of mixed liquor suspended solids (MLSS) concentration. Before start-up of the reactor, gradual introduction was applied for the acclimatization of activated sludge to the pharmaceutical wastewater. The initial 500 mg L^{-1} COD load wastewater was taken for the acclimatization of sludge in a continuous reactor. The acclimatization of sludge was done for 25 days. The reactor was continuously fed with air to maintain 2.0-3.0 mg L^{-1} dissolved oxygen (DO) concentration. The pH and nutrients amount were maintained in the range of 7.0-8.0 and COD:N:P ratio at 100:5:1, respectively. The experiments were carried out by gradually increasing the COD at 500 mg L^{-1} rate for every 5 days till the COD value reaches 2000 mg L^{-1}. The reactor was monitored on daily basis for the outlet COD and MLSS concentration to understand the activity of reactor. The rate of substrate utilization during the acclimatization period was analyzed in the terms of COD uptake. The ratio of COD uptake increased from 1 to 20 days of reactor operation at a rate of 100 ± 25 mg day^{-1}. The COD uptake of reactor reached 2000 mg day^{-1} on 20^{th} day and observed to be constant thereafter. The variation in MLSS concentration during the reactor operation was also assessed. The initial MLSS concentration was 1000 mg L^{-1} and till 20^{th} day it gradually reaches the value 3000 mg L^{-1}. When the MLSS concentration maintained a constant value of 3500 ± 120 mg L^{-1}, the biomass was considered to be acclimatized. On complete acclimatization of wastewater to sludge, the reactor was fed with wastewater with an initial COD load of 1000 and 4000 mg L^{-1} for LSW and HSW, respectively, in separate experiments.

3.7 Analytical techniques

The concentrations of model compounds *viz*. AMX, ORZ and OFX were measured using UV-visible Spectrophotometer (UV-2450, Shimadzu, Japan) with λ_{max} at 272, 310 and 288 nm, respectively. Degradation of model compounds was also confirmed by HPLC system equipped with C_{18} reversed- phase column (Enable C18G (250 x 4.6mm; 5μm)) and diode array detector SPD-M20A. For ORZ, elution was performed using a mixture of water:

acetonitrile (60:40, v/v) as mobile phase with column temperature 30 °C, flow rate of 1 mL min^{-1} and detected at 310 nm. OFX was eluted out using phosphate buffer: acetonitrile (20: 80, v/v) and detected at 288 nm. A fixed volume injection loop was used to inject 20 µL of sample for every determination. In order to validate the stability of the system, linear standard calibration curves with four or five point were plotted regularly during the analysis period. pH of the reaction was monitored regularly by Hach, SensION™ and Cyber Scan PCD 650 multi-parameter analyzer. Leaching of total soluble iron in the Fenton treatment of model compounds was detected and monitored simultaneously in the solution with spectrophotometric 1, 10- phenanthroline method (APHA, Method 3500-Fe B). The intensity of solar radiations was measured using Pyranometer (Apogee, MP-100).

LC-QTOF-MS system (Waters® Micromass Q-TOF micro™ Mass Spectrometer) was employed to identify the radiolytic degradation products of ORZ and OFX. The system was equipped with C_{18G} reverse-phase column (Unisol YVR) and separation module (Waters Alliance 2795). Conditions of mobile phase were used as utilized in the analysis of ORZ and OFX in HPLC system. 25 µL sample injection volume was used. Electrospray ionization (ESI) source in positive mode was utilized for the ESI-MS analysis. For mass spectrometer, the parameters were kept as follows: Desolvation gas 550 LPH, source temperature 110 °C, desolvation temperature 300 °C, collision energy 4 eV, capillary Voltage 3000 V and sheath gas, nitrogen and argon at 30 LPH flow rate with respective supply pressure of 6-7 bar and 5-6 bar, respectively. Acquisition of mass spectrum was performed over the range of 60-440 m/z.

The COD analysis of wastewater samples was performed using Merck® Spectroquant kits and closed reflux colorimetric method (APHA, Method 5220C). All the samples containing H_2O_2 were boiled for 10 min to remove its interference prior to COD analysis. The 5-days biological oxygen demand (BOD_5) was measured using OxiTop® Single Measuring System (WTW Weilheim, Germany). The chemical analysis of other parameters including pH, total dissolved solids (TDS), total suspended solids (TSS), mixed liquor volatile suspended solids (MLVSS), mixed liquor suspended solids (MLSS), total Kjeldahl nitrogen (TKN) and concentrations of chlorides, sulphates, phosphates, nitrates and nitrites was performed using standard methods (APHA, 1998). Total organic carbon (TOC) analyzer was used to study the mineralization of model compounds and real wastewater samples (Multi N/C 2100 BU, Analytic Jena AG Corporation, Germany) procured in BRNS sponsored project (No. 35/14/48/BRNS-2014).

3.8 Toxicity assessment

Cytotoxicity potential of treated solutions was examined through Standard Kirby-Bauer (disk diffusion method) against clinical isolates of three microbes: *E. coli, B. subtilis* and *P. aeruginosa*. *E. coli* is considered to be major constituent of the intestinal micro-biota of humans and animals (Teophilo *et al.* 2002; Soleimani *et al*. 2013). Due to its fast growing ability, low-cost and extensive group of accessible genetic tools, it is extensively used microbial population platform (Planson *et al.* 2012). *P. aeruginosa* is a broad group of free-living gram-negative bacteria that are ubiquitous in the aquatic environments such as rivers, lakes and sea. *P. aeruginosa* have ability to persist in deionized or distilled water (Warburton *et al.* 1994). *B. subtilis* is commonly found in the upper layers of the soil and in putrefactive organisms (Chen *et al.* 2008).

The detailed procedure for toxicity assessment is as follows: the microbes were cultured aerobically using McFarland standards followed by overnight incubation at 37 $\pm$ 2 ºC in an incubator (New Brunswick™ Innova® 42 Shaker, Eppendorf, Germany). The MHA plates were prepared and the activated bacterial suspension was spread evenly on the surface of plates using sterile cotton swab. The inoculated plates were allowed to dry for 10-15 min before the formation of 5mm well on the agar surface with sterile cork borer. After the addition of 50 µL of control and its irradiated samples in the wells, the prepared plates were incubated at 37 $\pm$ 2 ºC for 24-48 h in an incubator. After incubation, the diameter of the zone of inhibition on each plate was determined at the point of marked inhibition rate of microbial activity and measured in millimeters. Cytotoxic activities were assessed by the comparison of zone of inhibition on the plates.

Chapter 4.0 Results and Discussions

This chapter deals with the results of treatment technology employed to treat the aqueous solution of model compounds and pharmaceutical wastewaters. In broad, study covered the applications of AOPs such as Fenton technologies and ionizing radiations like gamma irradiation and high energy electron beam (E-beam) irradiation for the treatment of model compounds (AMX, ORZ and OFX) and raw pharmaceutical wastewater of low and high organic load. The influence of various experimental parameters on the degradation efficiency was optimized for all the treatment processes. The studies of model compounds and raw wastewater were assessed as hyphenated process in the presence of various oxidants to achieve the enhanced degradation efficiency. Lastly, Fenton and ionizing radiations based treatment was coupled to biological treatment for assessing the effectiveness of combined process to treat the real industrial wastewater. Toxicity and cost analysis of irradiation based treatments of model compounds and pharmaceutical wastewater has been discussed.

4.1 Photo-Fenton treatment of model compound using hematite particles

Hematite particles (α-Fe_2O_3) with three different shapes i.e., Spherical (S-α-Fe_2O_3), Cubical (C-α-Fe_2O_3) and Rod (R-α-Fe_2O_3) were synthesized using sol- gel procedures and were characterized by SEM-EDS, TEM, XRD, BET surface area and pore volume.

4.1.1 Characterization of hematite (α-Fe_2O_3) particles

The XRD pattern of the annealed catalysts with three different morphologies is shown in Fig 4.1. As can be seen from the measured pattern of XRD, all the diffraction peaks are consistent with the values of Joint Committee on Powder Diffraction Standards (JCPDS No. 33-0664). The well-defined appearance of the diffraction peaks confirmed the actual presence of α-Fe_2O_3 and well-crystallinity of the synthesized catalysts. The peaks (104) and (110) maintains its sharp height in C-Fe_2O_3 (Fig, 4.1), indicating its better crystal development from morphological transformation as compared to S-Fe_2O_3 and R-Fe_2O_3.

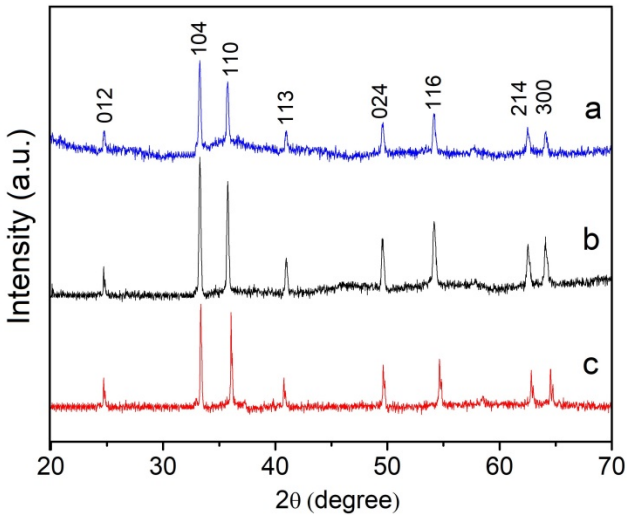

Fig. 4.1 XRD patterns of the α-Fe_2O_3 with different shapes: (a) R-α-Fe_2O_3 (b) C-α-Fe_2O_3 and (c) S-α-Fe_2O_3

The SEM images (Fig 4.2) revealed that the synthesized particles possess rods (a), cubical (b) and spherical (c) shaped morphology and their respective elemental information is provided in Table 4.1. EDS analysis revealed the presence of only Fe and O in the synthesized microstructure which shows that the prepared material is clean without any contamination indicating improved synthesis of α-Fe_2O_3. TEM images of the synthesized rods (d), cubical (e) and spherical (f) shaped morphology further confirmed the shapes of α-Fe_2O_3. The typical average dimensions of synthesized R-α-Fe_2O_3 (g) are 1.46 µm in length and 0.3 µm in width; while C-α-Fe_2O_3 (h) and S-α-Fe_2O_3 (i) has average diameter of 1.26 µm and 0.8 µm, respectively.

Table 4.1 EDS analysis of synthesized α-Fe_2O_3

Element	**Weight (%)**		
	C-α-Fe_2O_3	R-α-Fe_2O_3	S-α-Fe_2O_3
Fe	65.58	65.36	65.27
O	34.42	34.64	34.73
Totals	100.00	100.00	100.00

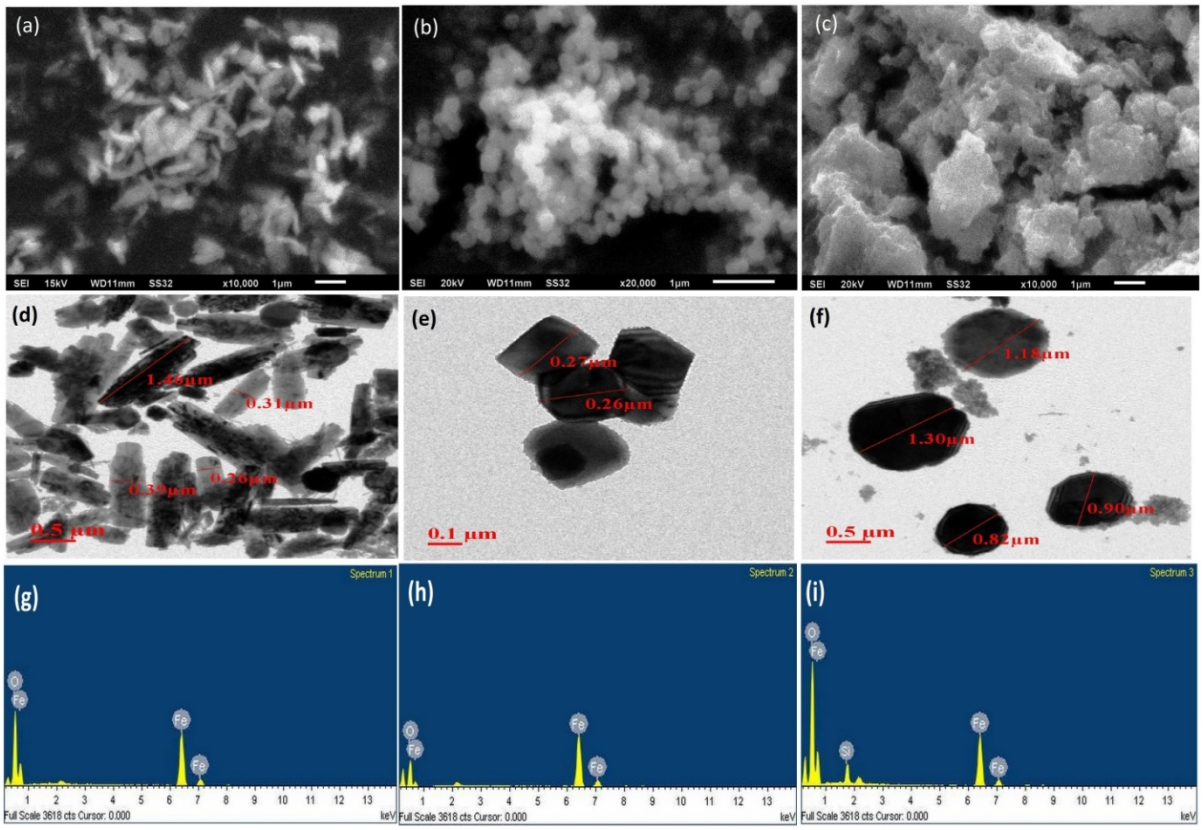

Fig. 4.2 SEM (a: Rod-shaped α-Fe_2O_3; b: Cubical-shaped α-Fe_2O_3; c: Spherical-shaped α-Fe_2O_3), TEM (d: Rod-shaped α-Fe_2O_3; e: Cubical-shaped α-Fe_2O_3; f: Spherical-shaped α-Fe_2O_3) and EDS (g: Rod-shaped α-Fe_2O_3; h: Cubical-shaped α-Fe_2O_3; i: Spherical-shaped α-Fe_2O_3) analysis of α-Fe_2O_3 microstructures

Table 4.2 BET surface area and porosity details of the synthesized catalyst

α-Fe_2O_3	**Surface Area (m^2 g^{-1})**	**Total pore volume (cm^3 g^{-1})**
R-α-Fe_2O_3	99.85	0.0483
C-α-Fe_2O_3	123.46	0.1013
S-α-Fe_2O_3	54.39	0.0446

In order to determine the surface area and pore volume, the synthesized α-Fe_2O_3 particles were characterized by nitrogen adsorption- desorption measurements. The surface area and corresponding porosities of synthesized hematite are presented in Table 4.2. C-α-Fe_2O_3 was found to possess high surface area value of 123.5 m^2 g^{-1}. Previous findings also documented high surface area of synthesized hematite particles due to the aggregation of particles in the solid phase, which is likely to lose in the aqueous solution (Demarchis *et al.* 2015).

4.1.2 Catalytic activity of the α-Fe_2O_3

Preliminary experiments were conducted to assess the efficacy of synthesized C-α-Fe_2O_3 in the Fenton system (H_2O_2 + C-α-Fe_2O_3) and degradation efficacy of ORZ was observed to be insignificant (11%) indicating that dissolved Fe^{3+} species are more reactive than the surface bound Fe^{3+} species on C-α-Fe_2O_3 towards H_2O_2 (Huang *et al.* 2013). Further, it may be due to the high affinity of ORZ for water which limits its adsorption on the catalyst surface. Degradation of ORZ using H_2O_2 alone under light source was found to be negligible which may be due to the limited absorption of irradiations by H_2O_2 (Finlayson-Pitts, 1999). In the case of light irradiation alone, insignificant (13%) degradation was observed. Therefore, in order to achieve significant degradation, contemporary presence of H_2O_2, α-Fe_2O_3 and irradiation was required. ORZ solution (0.22 mM) was subjected to treatment with C-α-Fe_2O_3 in the presence of H_2O_2 under solar irradiations to evaluate the effect of operating parameters *viz.* catalyst dose, H_2O_2 concentration, pH, etc. on the degradation efficacy of ORZ.

4.1.3 Effect of variation of C- α-Fe_2O_3 dose

To evaluate the surface effect on the catalytic properties of α-Fe_2O_3 particles, the photo-Fenton degradation of ORZ was conducted with varying C- α-Fe_2O_3 dose. ORZ (0.22 mM) solution was irradiated in UV/solar light for 180 min in the existence of 10 mM H_2O_2 at pH 3 with variation in the dose of C-α-Fe_2O_3 from 0.03 to 0.2 g L^{-1}. Degradation efficacy was found to increase up to 0.13 g L^{-1} and thereafter, decrease in the degradation efficiency was observed (Fig 4.3a). The low degradation efficiency at lower hematite dose may be due to the less production of $HO^{\bullet}$ radicals and their availability for the oxidative reactions. Inhibition in the degradation efficiency beyond 0.13 g L^{-1} dose of α-Fe_2O_3 may be due to the agglomeration of α-Fe_2O_3 (Xu and Wang, 2011) and the hydroxyl radical scavenging effect (Eq. 4.1) (Xu and Wang, 2012).

$$HO^{\cdot} + Fe^{2+} \rightarrow HO^{-} + Fe^{3+} \qquad (4.1)$$

4.1.4 Effect of H_2O_2 concentration

H_2O_2 acts as a precursor for the production of hydroxyl radical in the reaction with ferrous ion (Fe^{2+}) according to the Haber-Weiss mechanism (Xu and Wang, 2012). Also, it can react with Fe^{3+} for regenerating Fe^{2+} which can take part in the Fenton reaction. In order to optimize the dosage, H_2O_2 was varied in the range 3- 20 mM with C-α-Fe_2O_3 dose of 0.13 g L^{-1} at pH 3 for the degradation of ORZ. Fig 4.3b shows 10 mM H_2O_2 concentration leads to the degradation efficiency of 98% in 180 min of solar exposure. As seen, ORZ removal

increased with increasing amount of H_2O_2 till 10 mM, due to the improved oxidation potential of Fenton process with increasing amount of HO• in the solution obtained by increasing decomposition of H_2O_2. However, beyond 10 mM dose, degradation efficacy decreased which may be due to the consumption of reactive HO• by H_2O_2 and resultant generation of •OOH which are less reactive (Eq. 4.2) (Wang *et al.* 2015). Also if H_2O_2 is present in excess amount, it reacts with ferric ions to produce Fe(III)-hydroperoxy which leads to reduction in the number of ferrous ions required for Fenton process (Sun *et al.* 2007a; Guimarães *et al.* 2014).

$$H_2O_2 + HO^{\cdot} \rightarrow HOO^{\cdot} + H_2O \qquad (4.2)$$

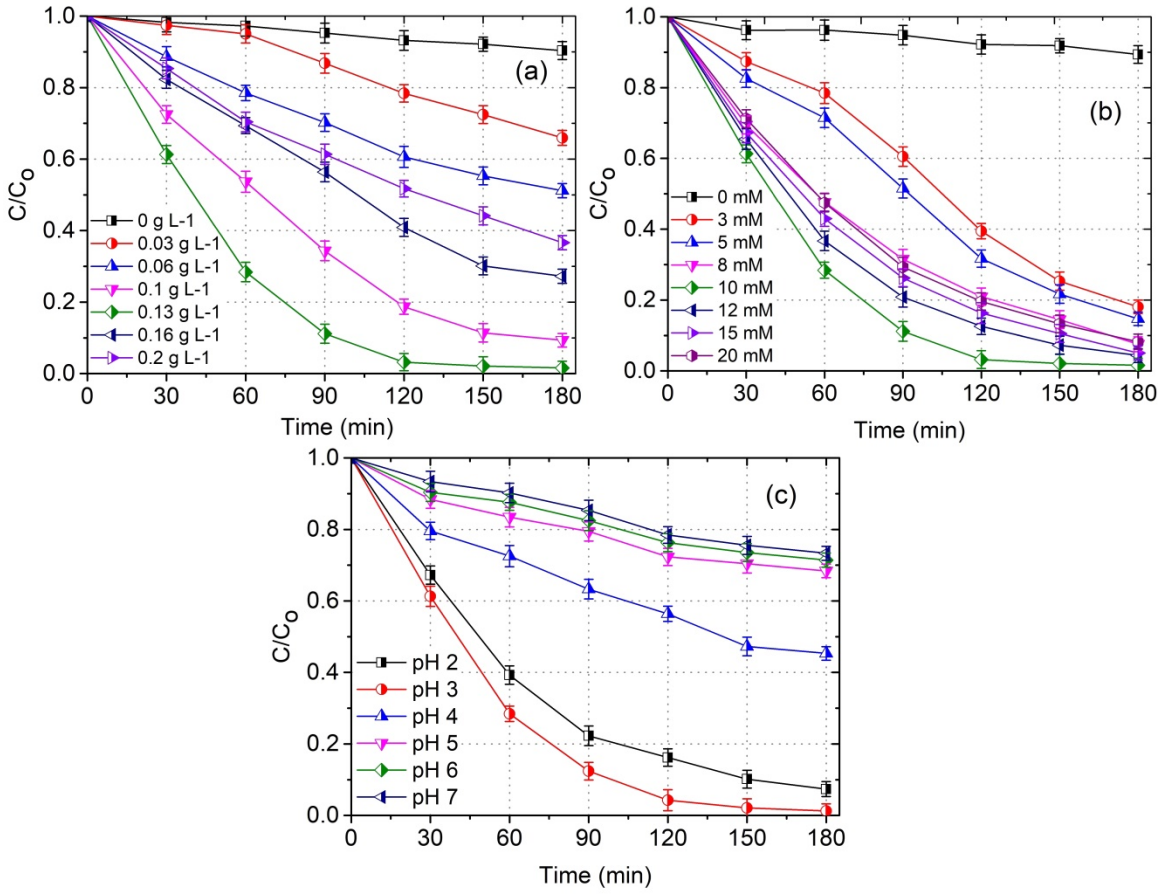

Fig. 4.3 Factorial effects of heterogeneous photo- Fenton reaction on ORZ degradation: (a) C-α-Fe_2O_3 dosage, (b) H_2O_2 dosage, and (c) pH

4.1.5 Effect of pH

In Fenton's process, pH of the solution plays a vital role by controlling the production rate of HO• and Fe^{2+} concentration. Generally, Fenton reaction is fast under acidic conditions

so, pH of the aqueous solution was varied from 2 to 7 with 0.13 g L^{-1} of C-α-Fe_2O_3, H_2O_2 concentration of 10 mM for the degradation of ORZ. The results in Fig 4.3c clearly indicate that the pH significantly influences ORZ degradation and maximum degradation efficiency was found at pH 3. At pH 2, lesser degradation rates might be due to the stability of H_2O_2 by solvation of a proton and forming an oxonium ion (Eq. 4.3). An oxonium ion turns H_2O_2 electrophilic while improving its stability and substantially reducing its reactivity with ferrous ions. The slight reduction in the removal efficiency might also be due to scavenging of $HO^{\bullet}$ by H^+ ions (Reaction 4.4) (Muruganandham and Swaminathan, 2004). When pH was increased from 3 to 7, decreasing trend in the degradation efficiency was observed. The probable reason behind this might be the lower ability to catalyse hydrogen peroxide due to FeO^{2+} production which is less reactive than $HO^{\bullet}$ (Saritha *et al.* 2007). Moreover, at pH 3, there is slow reduction of Fe^{3+} ions (Eq 4.7) accounting due to the fact that $FeOH^{2+}$ prevailing at pH 3 is the Fe^{3+} ions which undergoes the easiest reduction to Fe^{2+} (Eq. 4.5) which is lesser important reaction because the Eq. 4.6 is the key source of Fe^{2+} (Sedlak and Hoigné, 1993).

$$H_2O_2 + H^+ \rightarrow H_3O_2^+ \quad (4.3)$$

$$HO^{\cdot} + H^+ + e^- \rightarrow H_2O \quad (4.4)$$

$$FeOH^{2+} + H_2O_2 \rightarrow Fe^{2+} + O_2 + H_2O \quad (4.5)$$

$$Fe^{3+} - OH_{surf} + hv \rightarrow Fe_{aq}^{2+} + HO^{\cdot} \quad (4.6)$$

$$Fe_{aq}^{2+} + H_2O_2 \rightarrow \left[\left(Fe^{3+} + HO^-\right)\right] + HO^{\cdot} \quad (4.7)$$

4.1.6 Leaching of iron

It is important to know the concentration of dissolved Fe during the photo-Fenton process since α-Fe_2O_3 would act as an iron source that would be activated when irradiated so that Fenton process can take place in the solution. At acidic pH, the dissolved Fe species mainly occurred as Fe_{aq}^{3+} in all samples due to the presence of H_2O_2. Dissolved Fe concentration in the solution was investigated during the photo-Fenton oxidation of ORZ at optimized conditions (0.13 g L^{-1} α-Fe_2O_3, 10 mM H_2O_2 and pH 3). In case of C-α-Fe_2O_3 (Fig 4.4), the concentration of Fe in aqueous solution increased and attained a peak value of about 0.7 µg mL^{-1} after 60 min with almost 70% removal of ORZ and then Fe concentration decreased to about 0.4 µg mL^{-1} after 180 min. However, in case of R-α-Fe_2O_3 and S-α-Fe_2O_3, 0.4 µg mL^{-1} of Fe was found in the solution after 60 min. The amount of Fe leached in the solution was observed to be in the order of C-α-Fe_2O_3 > R-α-Fe_2O_3> S-α-Fe_2O_3. The higher

leaching of Fe in C-α-Fe_2O_3 may have contributed to higher degradation of ORZ in the aqueous solution, when compared to R-α-Fe_2O_3 and S-α-Fe_2O_3. Moreover, considering the BET surface area of the synthesized samples, the observed differences may be due to the aggregation of the catalyst samples in the solid phase, which are likely to disperse in aqueous medium (Demarchis *et al.* 2015). Fig. 4.5 depicts the schematic representation of heterogeneous photo-Fenton degradation process occurring through hematite particles.

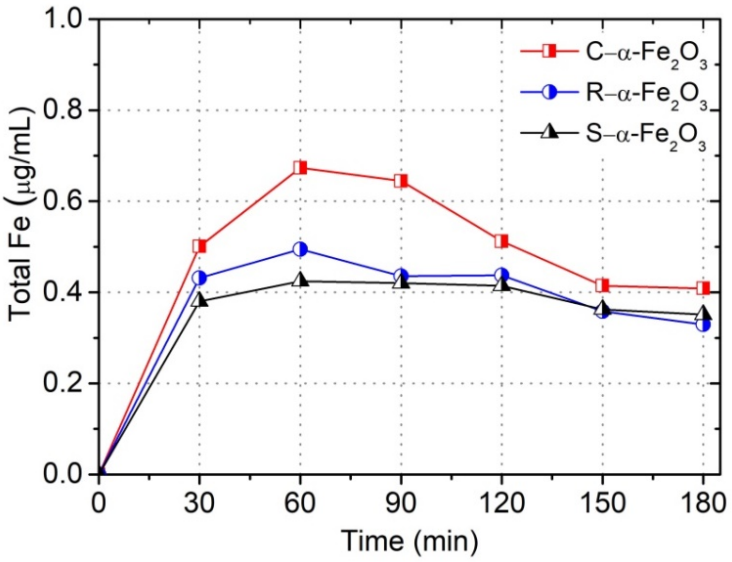

Fig 4.4 Time trend of total dissolved Fe upon solar irradiation

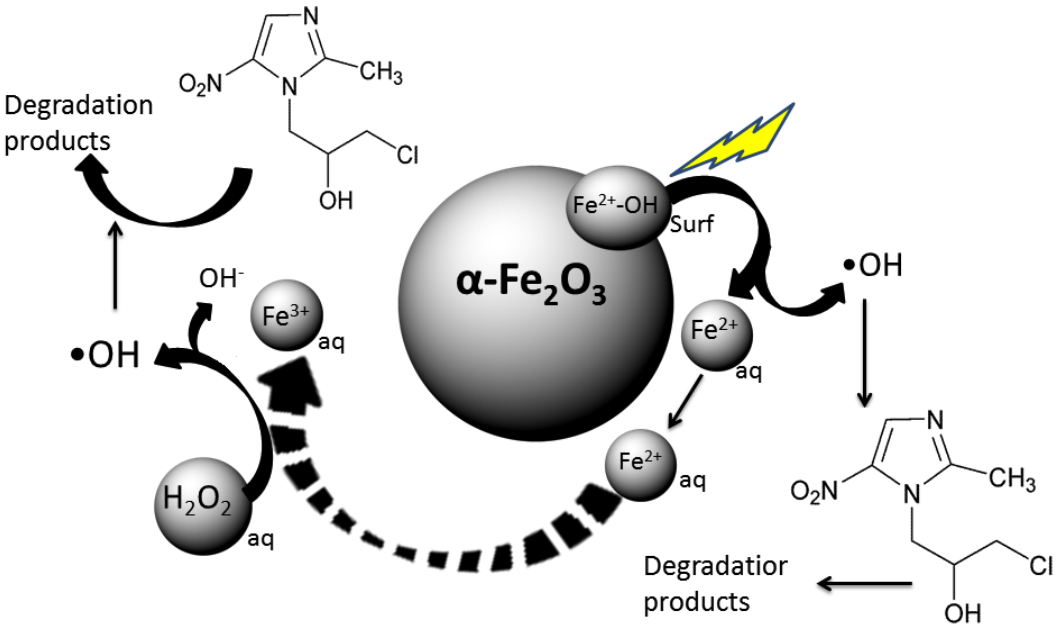

Fig. 4.5 Schematic diagram depicting the degradation process using hematite particles

4.1.7 Comparison of α-Fe_2O_3 activity

Activity of various synthesized α-Fe_2O_3 particles were assessed in the degradation of ORZ at optimized conditions (0.13 g L^{-1} α-Fe_2O_3 , 10 mM H_2O_2, pH 3) under UV/ solar irradiations. Fig 4.6 shows the comparative activity of R-α-Fe_2O_3, C-α-Fe_2O_3, and S-α-Fe_2O_3 under UV and solar irradiations. For the degradation of ORZ, the order of removal rates under same conditions was: C-α-Fe_2O_3 (98%)> R-α-Fe_2O_3 (96%)> S-α-Fe_2O_3 (92%) under sunlight and C-α-Fe_2O_3 (51%)> R-α-Fe_2O_3 (42%)> S-α-Fe_2O_3 (31%) under UV irradiations. This enhanced catalytic performance of C-α-Fe_2O_3 might be due to uniform composition of the catalyst, thereby increasing relative mass transfer rates between the catalyst and aqueous solution. All the three α-Fe_2O_3 were found to be more active in the degradation of ORZ under solar irradiations when compared to UV exposure which may be attributed to the fact that α-Fe_2O_3 absorbs light up to 600 nm and solar photons promote the photo-reduction of hydroxylated form of Fe^{3+} [Fe^{3+} -OH] to ferrous ions, thus giving rise to more hydroxyl radicals in the aqueous solution (Cornell and Schwertmann, 2003).

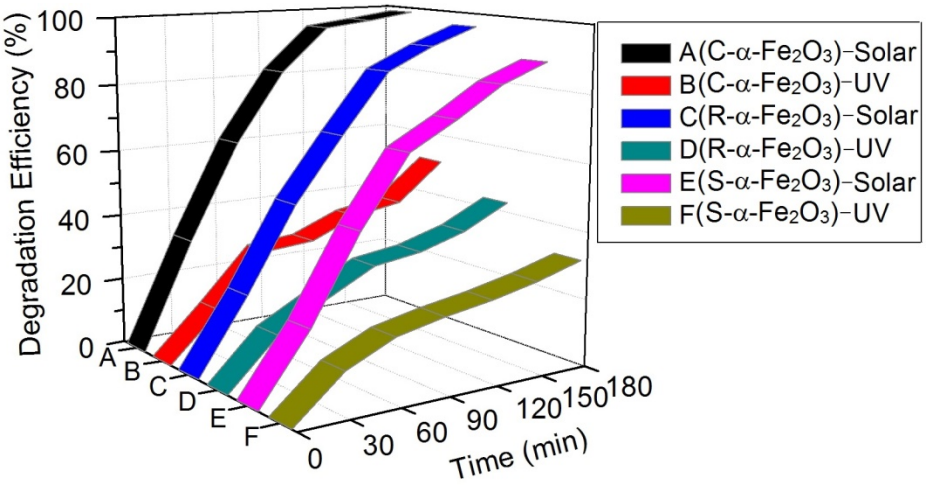

Fig. 4.6 Activity comparison of different α-Fe_2O_3 under solar and UV irradiations

4.1.8 HPLC and mineralization study

HPLC study was conducted to establish the degradation of ORZ. Fig 4.7 illustrates the recorded HPLC profile at 310 nm under UV/solar light corresponding to the initial ORZ solution (0.22 mM) and after 180 min of treatment time. Strong peak of ORZ standard was observed at the retention time (RT) of 5.2 min. After 180 min of treatment time, the peak almost disappeared with all the synthesized α-Fe_2O_3 particles under the solar optimized condition with detection of additional peak at RT of 2.1 min along with the appearance of some small peaks indicating the formation of some intermediate/by-products. The decrease in

the peak area with increasing treatment time indicates the successful removal of model compound under the solar-assisted Fenton experiment. Whereas, HPLC chromatograms for experiments conducted under UV radiations showed less degradation even after 180 min of treatment.

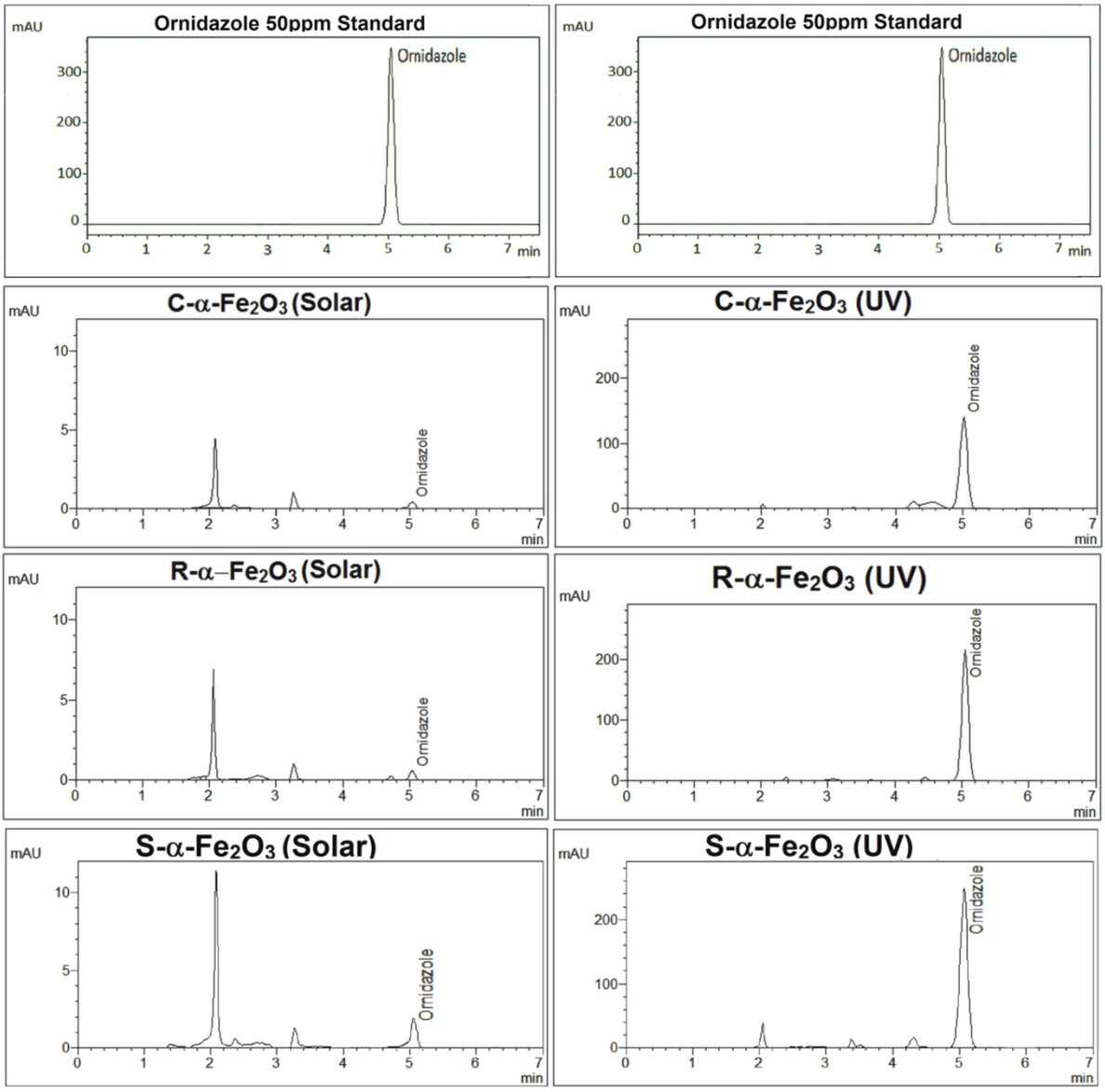

Fig. 4.7 HPLC of initial and treated samples using different α-Fe_2O_3 under solar/UV irradiations

Total organic carbon (TOC) (Fig 4.8) was assessed to evaluate the mineralization of the model compound under UV/ solar irradiations. Although the degradation of ORZ under solar-induced Fenton experiment was about 98% but only 59% TOC removal was achieved after 180 min using C-α-Fe_2O_3 indicating the presence of complex organic molecules that resist mineralization. For ORZ degradation, the order of mineralization rates was: C-α-Fe_2O_3

(59%)> R-α-Fe_2O_3 (54%)> S-α-Fe_2O_3 (29%) under sunlight and C-α-Fe_2O_3 (33%)> R-α-Fe_2O_3 (30%)> S-α-Fe_2O_3 (17%) under UV irradiations. It is well known fact that the extent of mineralization in photo- Fenton system depends upon the ratio of H_2O_2/pollutant whereas in the present study very less fraction of H_2O_2 (10mM) was used which can be the possible reason behind the lesser mineralization of model compound. So, it can be concluded that photo-Fenton process is necessary to initiate the bulk compound degradation, while the oxidant is required for the mineralization of the smaller fragments (Cornell and Schwertmann, 2003).

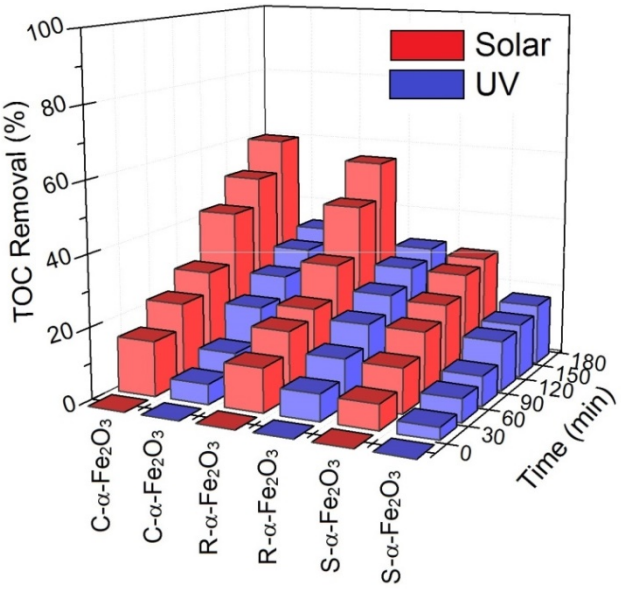

Fig 4.8 Time dependent TOC removal of ORZ using synthesized catalyst under solar and UV irradiations

4.2 Photo-Fenton treatment of model compounds using soil particles

Soil collected from Warangal region of India and due to the presence of high contents of iron oxides, the use of environmentally friendly and economical applications of soil is of considerable interest in photo-Fenton like processes.

4.2.1 Characterization of Soil

Fig. 4.9a and 4.9b shows the SEM images of soil particle and EDS pattern is exhibited in Table 4.3. It can be seen from the figures that the soil has irregular morphology. EDS analysis revealed the major components of soil were Fe, Al, Si, K, C, Mg and Ca. As heavy metals were not detected so, potential risk of their leaching into the aqueous solution is not plausible. Presence of considerable amount of iron (37.13 wt. %) in soil ensures the proceeding of photo-Fenton-like treatment in the presence of H_2O_2 and sunlight. Fig. 4.10

shows the XRD diffractogram depicting the crystalline iron oxides detection peaks and indicated presence of hematite (26.15°, 39.68°, 54.87°, 56.86° and 63.76°), magnetite (34.56°, 50.25°, 51.02° and 67.70°), goethite (21.40° and 51.14°), pyrite (60.01°), wustite (42.18° and 75.49°) and existence of graphite carbon-3R at 26.6° (JCPDS 26-1079) as identified by Match 3.3.0 processing software. BET analysis revealed that surface area and pore size of soil were 30.03 m^2 g^{-1} and 0.0333 cm^3 g^{-1}, respectively.

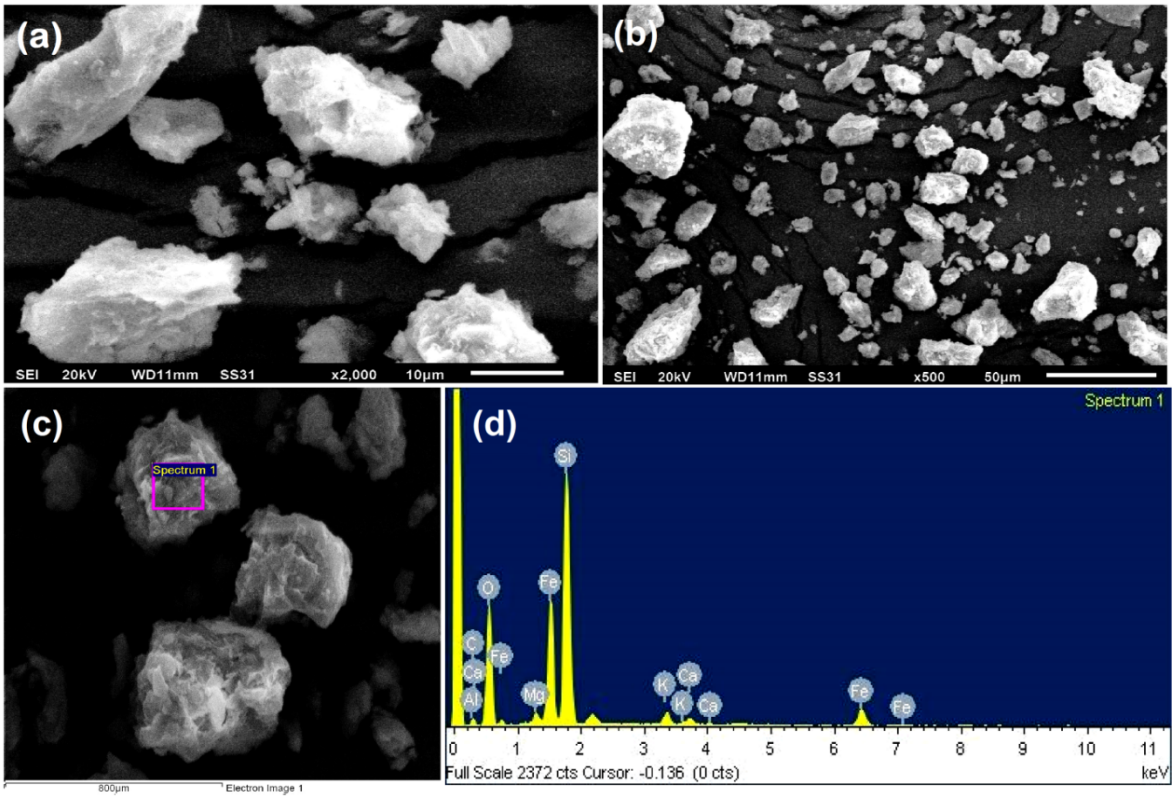

Fig. 4.9 SEM micrograph (a & b) and EDS pattern of soil (c & d)

Table 4.3 EDS analysis of soil

Element	C	O	Mg	Al	Si	K	Ca	Fe	Totals
Weight (%)	1.78	34.84	0.92	0.57	22.26	1.65	0.85	37.13	100.00

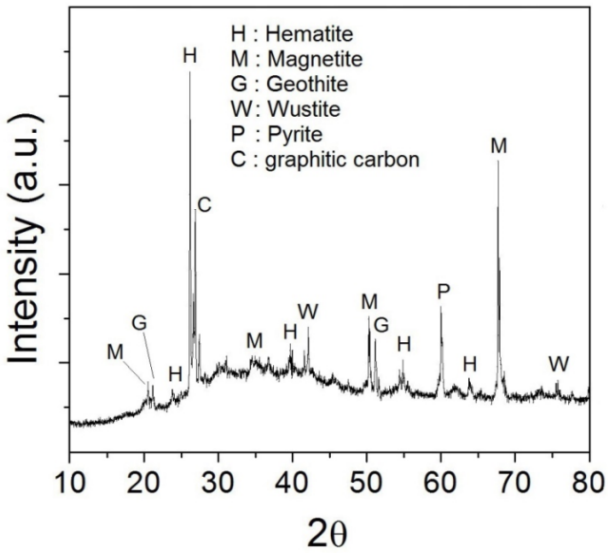

Fig. 4.10 XRD pattern of soil

4.2.2 Degradation of model compounds under batch mode

Preliminary experiments were performed in order to compare the degradation efficiency ORZ and OFX under various conditions. Small amount of ORZ and OFX removal (3-5%) was observed by soil in dark which could be ascribed primarily to the surface adsorption of soil. Results even showed insignificant removal of both the compounds in the presence of either H_2O_2, or sunlight, alone after 60 min. However, both the compounds were degraded effectively in the presence of soil and H_2O_2 under UV/sunlight (Fig. 4.11). After 60 min reaction time, 61 and 55% degradation efficiency of ORZ and OFX, respectively was achieved in the presence of soil/H_2O_2/sunlight, and 41 and 39% degradation efficiency in the presence of soil/H_2O_2/UVA. Thus, preliminary experiments confirmed that solar photo-Fenton-Like treatment employing soil and H_2O_2 was most efficient in degrading the model compounds.

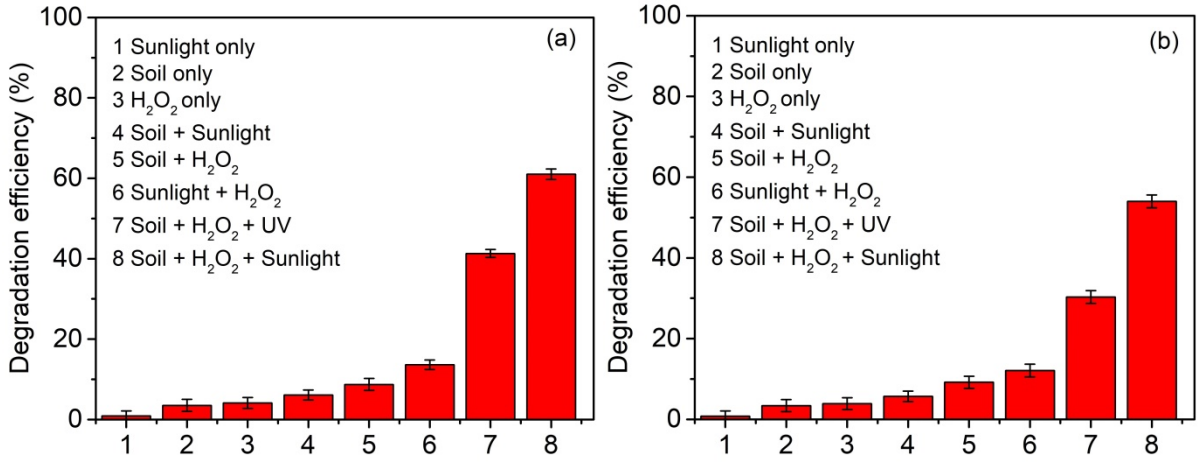

Fig. 4.11 Preliminary experimental results of (a) ORZ (b) OFX

4.2.2.1 Effect of experimental conditions

For Fenton process, initial pH of the solution is an important factor. At acidic pH, dissolution of iron species in the aqueous solution increases, reflecting the oxidative power of photo-Fenton-like reaction (Teixeria *et al.* 2015). Moreover, $[Fe(OH)(H_2O)_5]^{2+}$ is the main iron species at pH 3, having the advantage of very large light absorption coefficient and high yield of $HO^{\bullet}$ production (Benkelberg and Warneck, 1995). At alkaline pH, degradation rate might reduce due to the blockage of decomposition of H_2O_2 catalysed by ferrous ions due to the formation of ferric hydroxo complexes and also Fe^{3+} precipitates as $Fe(OH)_3$ at higher pH (Safarzadeh-Amiri *et al.* 1996; Kavitha and Palanivelu, 2004). On the basis of preliminary study, the concentration of soil was varied from 0.006 to 0.073 g L^{-1} for degrading aqueous solution of ORZ and OFX, with H_2O_2 concentration of 1 mM, at pH 3. At pH 3, $[Fe^{3+}]$ are the main iron species having the advantage of very large light absorption coefficient and high yield for $HO^{\bullet}$ production as cited by the previous study (Benkelberg and Warneck, 1995). 97% ORZ removal (Fig. 4.12a) was attained with 0.033 g L^{-1} soil, while 93% OFX removal was achieved (Fig. 4.12d) with 0.020 g L^{-1} soil dose in 180 min. Soil was observed to facilitate the degradation of both compounds in the presence of H_2O_2 and sunlight. The probable reason might be the availability of unsaturated surface active sites and amount of pollutant adsorbed on soil increased with increasing concentration of soil (Watts and Dilly, 1996). Moreover, more $HO^{\bullet}$ radicals are produced with increase of $[Fe^{2+}]$ which increases with increasing amount of soil due to the leaching of total iron species $[FeT_{soluble}]$ in the solution. However, increase in the dosage beyond a limit did not lead to considerable increase in the removal rates which may be ascribed to the production of excess $[Fe^{2+}]$ ions, due to the photo reduction of $[Fe^{3+}]$ ions in the solution, that competes for the $HO^{\bullet}$ thereby, acting as $HO^{\bullet}$ scavenger and decreasing availability of $HO^{\bullet}$ (Tang and Chen, 1996).

Removal of ORZ (Fig. 4.12b) and OFX (Fig. 4.12e) was assessed at various initial concentrations of H_2O_2 (0.7 to 5.0 mM) as a function of time. 97% ORZ removal with 1 mM concentration of H_2O_2 (0.033 g L^{-1} soil and pH 3) and 95% OFX removal was observed with 2 mM H_2O_2 (0.020 g L^{-1} soil and pH 3) after 180 min. H_2O_2 was found to be efficient in the degradation of model compounds when used in conjunction with soil under sunlight. The degradation rate increased when the H_2O_2 dose was increased in both cases, probably due to increased generation of $HO^{\bullet}$ and increase in the fraction of light for photodecomposition of H_2O_2 (Sun *et al.* 2007). Further, when the concentration was increased beyond a certain value, the degradation rates were slightly reduced which may be because of the scavenging

effect of $HO^{\bullet}$ due to the formation of hydroperoxide radicals ($HO_2^{\bullet}$) (Wu *et al.* 2006). Generally, the concentration of H_2O_2 is directly related to the amount of $HO^{\bullet}$ produced in the photo-Fenton reaction system (Li *et al.* 2015; Du *et al.* 2016). Fig. 4.13 shows increase in the $HO^{\bullet}$ generation at initial stage of reaction and thereafter, slower $HO^{\bullet}$ generation with extended durations was observed, which may be attributed to the rapid decomposition of H_2O_2 in the initial phase when compared to the later phase of reaction.

Since, H_2O_2 decompose to give oxygen and water in basic solution, thereby loses its oxidation ability. So, pH was varied in acidic range from 2 to 7 for assessing the degradation of both the model compounds. Fig. 4.12c and Fig. 4.12f shows achievement of 95% ORZ degradation (0.033 g L^{-1} Soil and 1 mM H_2O_2) and 92% OFX (0.013 g L^{-1} Soil and 2 mM H_2O_2) degradation after 180 min at pH 3. High degradation rates of ORZ and OFX were observed at low pH values and a decreasing degradation trend was observed with increasing pH values because at an acidic pH, minerals in soil get ionized and the formed [Fe^{2+}] ions reacts with H_2O_2 producing $HO^{\bullet}$ (Lee *et al.* 2009).

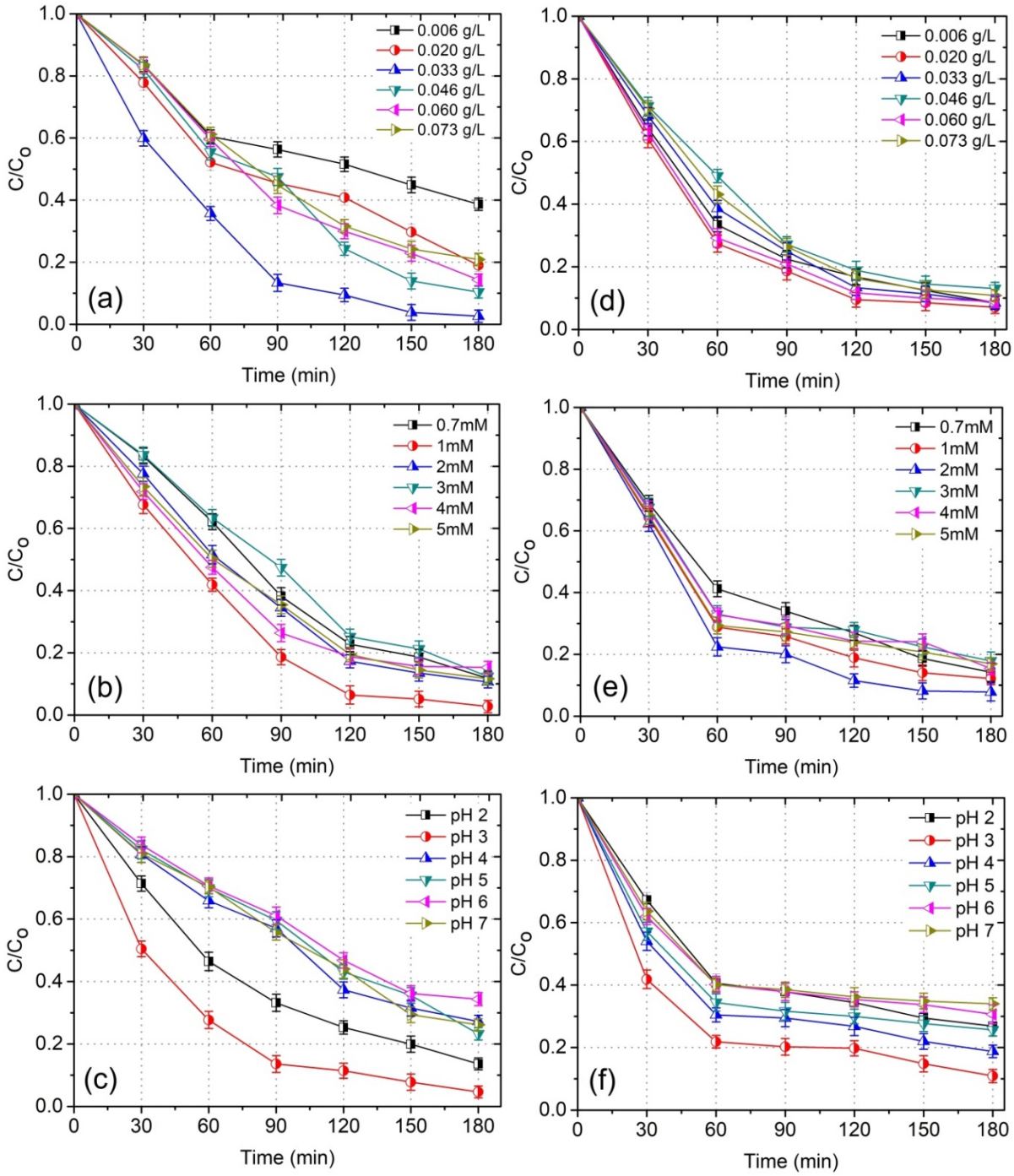

Fig. 4.12 Variation of process parameters (a) soil dosage (1 mM H_2O_2, pH 3) , (b) H_2O_2 (0.033 g L^{-1} soil, pH 3) and (c) pH (0.033 g L^{-1} soil, 1 mM H_2O_2), for the degradation of 150 mL ORZ solution and (d) soil dosage (1 mM H_2O_2, pH 3) (e) H_2O_2 (0.020 g L^{-1} soil, pH 3) and (f) pH (0.020 g L^{-1} soil, 2 mM H_2O_2), for the degradation of 150 mL OFX solution

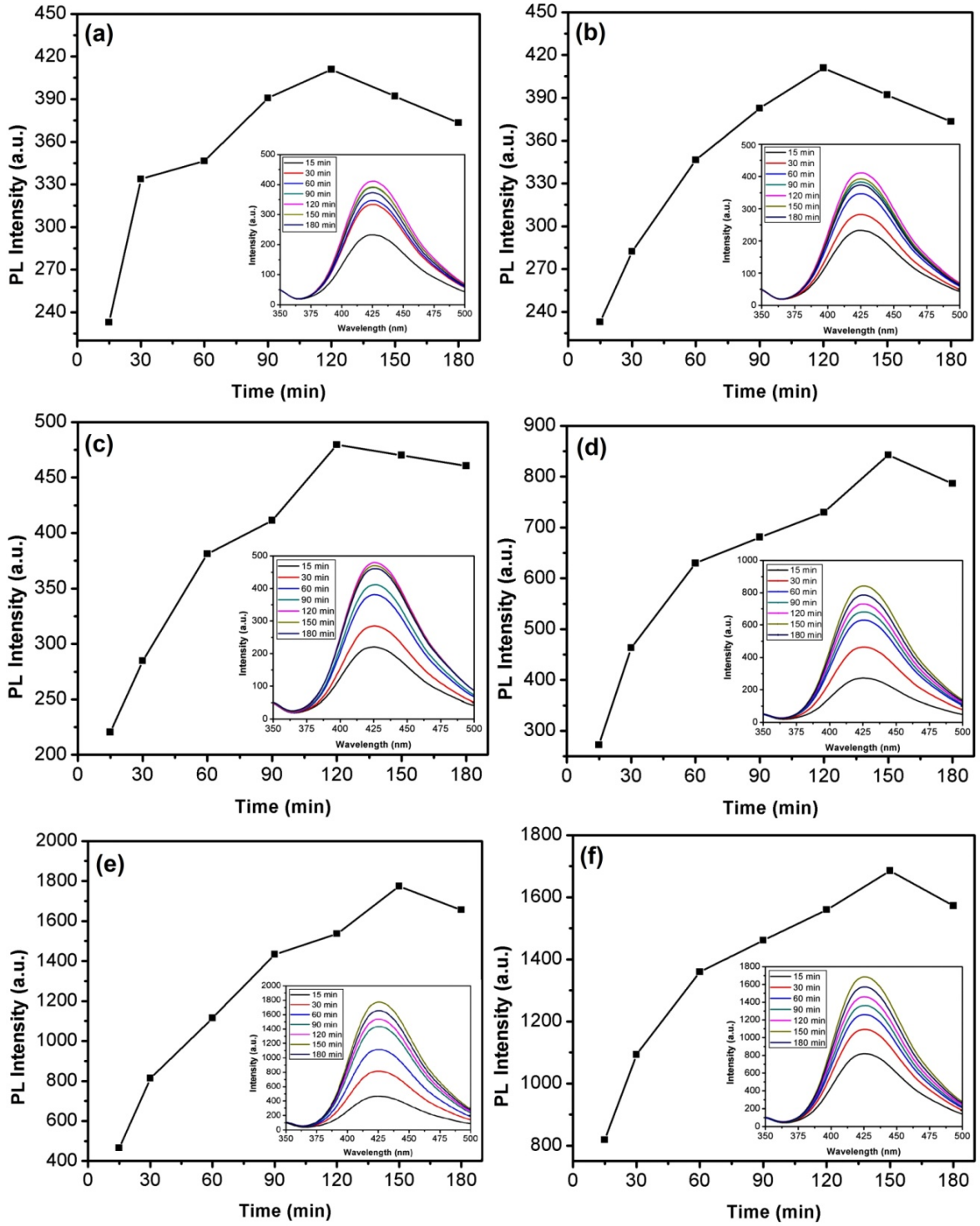

Fig. 4.13 PL spectrum for HO• determination (a) ORZ under UV-A, (b) OFX under UV-A, (c) ORZ under UV-B, (d) OFX under UV-B, (e) ORZ under solar and (f) OFX under solar. [ORZ 0.09 mM and OFX 0.05 mM; 150 mL solution volume]

Although degradation of model compounds was effective with soil mediated photo-Fenton-like reaction, but the mineralization studies revealed 47 and 50% reduction of TOC in

case of ORZ and OFX, respectively under the batch experiment after 180 min (Table 4.4). The reason for this behaviour may be the low concentration of H_2O_2 which would have resulted only in the degradation of the pollutant rather than its complete mineralization as also documented in previous study (Liu *et al.* 2015).

Table 4.4 TOC removal vs. Reaction time in solar-induced batch mode [For ORZ, 0.033 g L^{-1} soil dosage, 1 mM H_2O_2, pH 3, 150 mL solution volume; For OFX, 0.020 g L^{-1} soil dosage, 2 mM H_2O_2, pH 3, 150 mL solution volume]

Time (min)	ORZ	OFX
0	0	0
30	18.23	22.60
60	31.42	33.00
90	35.31	39.48
120	40.12	43.61
150	44.27	46.04
180	47.15	50.30

4.2.2.2 Influence of leached iron

More acidic the pH, more will be the dissolution of iron species in the aqueous solution reflecting the oxidative power of photo-Fenton like reaction (Teixeira *et al.* 2015). Thus, pH of solution in batch experiments (Fig. 4.14) was monitored after every 30 min of reaction time and was found to remain in between pH~3.05 to 3.2. This interesting pH buffer-like property of soil can be ascribed to the oxidation of surface-bound iron and subsequent release of iron species into the solution, which are in agreement to previously employed various other oxides of iron (Demarchis *et al.* 2015; Liu *et al.* 2015; Mameri *et al.* 2016).

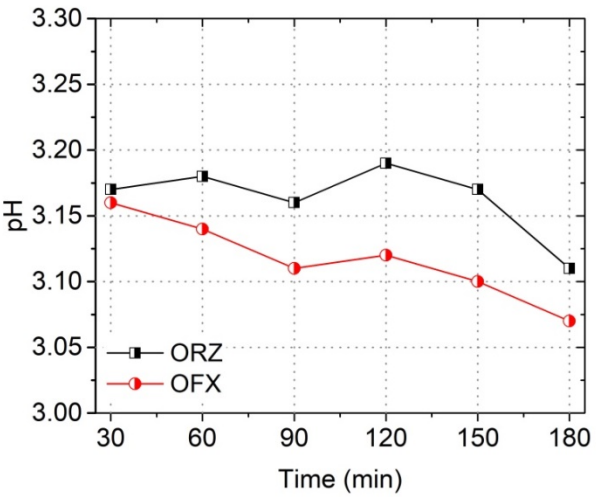

Fig. 4.14 pH profile of ORZ and OFX degradation with time in solar-induced batch mode [For ORZ, 0.033 g L^{-1} soil dosage, 1 mM H_2O_2, pH 3, 150 mL solution volume; For OFX, 0.020 g L^{-1} soil dosage, 2 mM H_2O_2, pH 3, 150 mL solution volume]

Moreover, to assess the homogeneity and heterogeneity of the degradation process, concentration of Fe species were investigated at regular intervals in a batch photo-Fenton like experiment for the optimized sets of ORZ and OFX degradation. Fig. 4.15a and 4.15b depicts that the concentration of [$FeT_{soluble}$] increases in both the solutions during the batch experiment in first 60 min and then remains unaltered throughout the remaining time period. The observed trend of [$FeT_{soluble}$] was most likely due to the gradual oxidation of surface Fe-pharmaceutical complex by H_2O_2 which resulted in the release of [Fe^{3+}] into the aqueous solution. Formation of $HO^{\bullet}$ can take place on the soil surface due to the presence of various iron oxides (as discussed in section 4.2.1) and also in the aqueous solution due to inter-conversion of [Fe^{2+}] and [Fe^{3+}] suggesting the simultaneous occurrence of homogeneous and heterogeneous reactions (Fig. 4.16). These results showed that initially more [Fe^{3+}] were observed in the aqueous solution than [Fe^{2+}] which might be due to the presence of large number of ferric species (hematite, magnetite, goethite, wustite and pyrite) on the soil surface and then a part of [Fe^{3+}] was converted to [Fe^{2+}] by hydrogen peroxide.

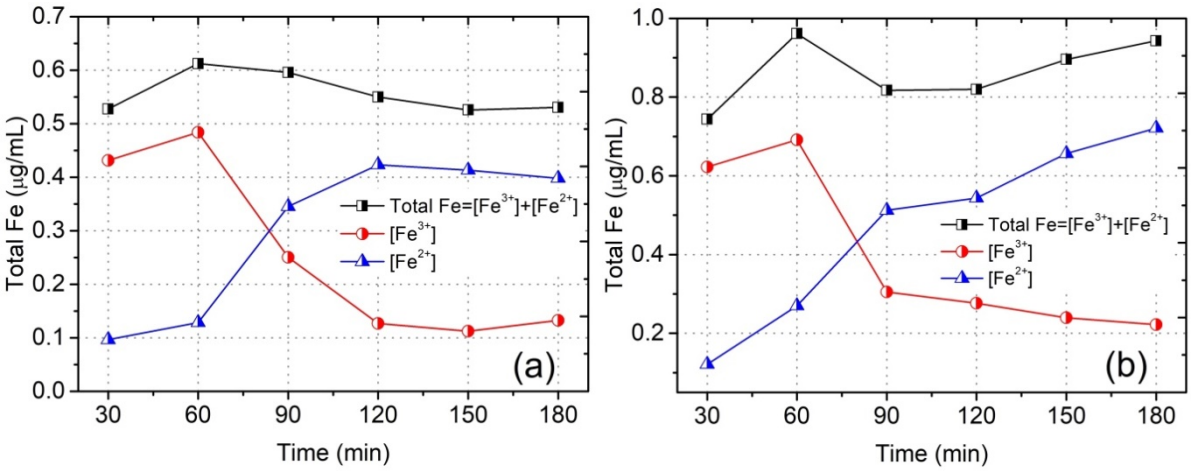

Fig. 4.15 Leaching of iron in solar-induced batch degradation of (a) ORZ (0.033 g L^{-1} soil, 1 mM H_2O_2 and pH 3) and (b) OFX (0.020 g L^{-1} soil, 2 mM H_2O_2 and pH 3)

The existence time of maximum concentration of [$FeT_{soluble}$] is close to the highest degradation rate of ORZ and OFX as shown in Fig. 4.12c and 4.12f, and after that degradation remains almost constant. In order to assess the effectiveness of simultaneous occurrence of homogeneous and heterogeneous process for the removal of pharmaceuticals, homogeneous ferric ions [Fe^{3+}] were used as a catalyst instead of soil under batch optimized conditions. The removal efficiency was found to be only 11.3 and 9.5% in 60 min for ORZ and OFX respectively, which was far less than (74 and 77% removal efficiency in 60 min for ORZ and OFX respectively from Fig. 4.12c and 4.12f) that of heterogeneous photo Fenton-like process using soil.

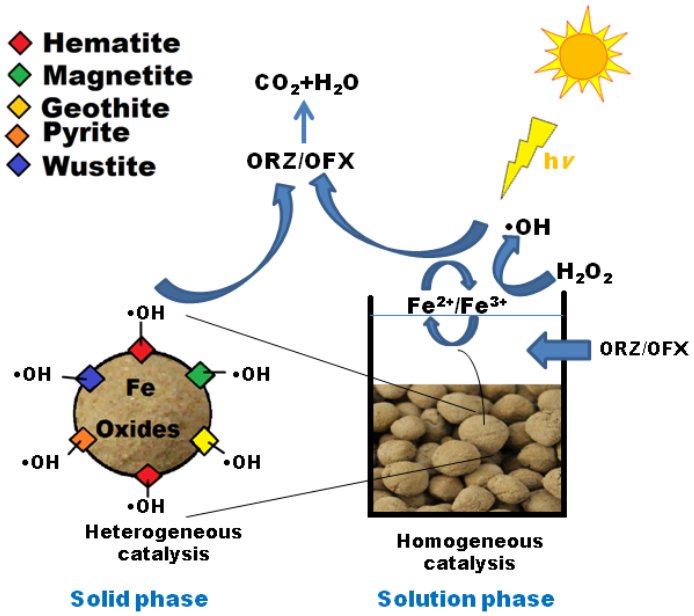

Fig. 4.16 Schematic diagram depicting the occurrence of simultaneous homogeneous and heterogeneous reactions

4.2.2.3 Effect of different irradiation sources

To compare the efficiency of degradation process under discrete irradiation sources, batch experiments were performed under optimized condition for ORZ degradation (0.033 g L^{-1} Soil and 1 mM H_2O_2) and OFX (0.013 g L^{-1} Soil and 2 mM H_2O_2) in the presence of either of UV-A or UV-B or solar irradiations and then statistically analysed using ANOVA (Analysis of Variance) single factor hypothesis. In general, if P-value is less than 0.01, the design model is considered to be significant and can be used as statistical predictive model. For ORZ, the very small P-value of 6.17×10^{-7} and high F-value of 547.56 indicates that the model was statistically significant and valid (Table. 4.5). Similar trend was observed for OFX with P-Value of 5.67×10^{-9} and F-value of 1678.81 (Table. 4.6). To further compare the mean difference among the irradiation sources, Tukey multiple comparison test was performed for both the compound independently. Results of statistical analysis using Tukey test shows that the mean difference among the irradiation sources was significant with R-squared value of 0.9946 and 0.9982 for ORZ and OFX, respectively. The degradation of ORZ and OFX was in the order: Solar > UV-B > UV-A (Fig. 4.17). Enhanced activity in solar light might be attributed to the fact that solar photons support the reduction of ferric to ferrous ions, promoting the generation of more $HO^{\bullet}$ as evident from Fig. 4.13 (Cornell and Schwertmann, 2003; Kavitha and Palanivelu, 2004).

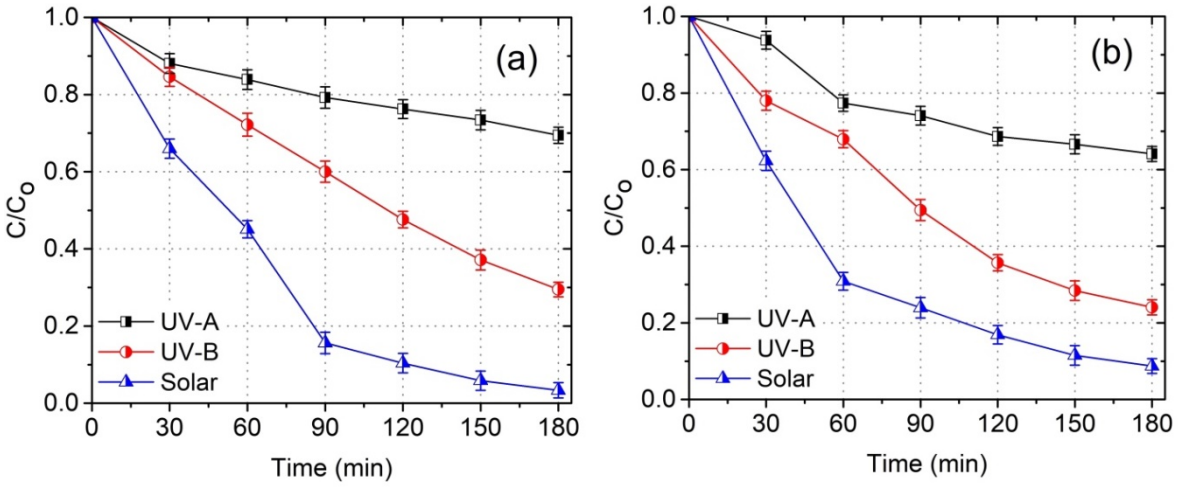

Fig. 4.17 Degradation profile with time under different irradiation sources (a) ORZ [0.033 g L^{-1} soil dosage, 1 mM H_2O_2, pH 3, 150 mL solution volume] (b) OFX [0.020 g L^{-1} soil dosage, 2 mM H_2O_2, pH 3, 150 mL solution volume]

Table 4.5 Statistical analyses (ANOVA and Tukey's) on different irradiation sources for the degradation of ORZ

SUMMARY				
Groups	*Count*	*Sum*	*Average*	*Variance*
UV-A	3	91.0287	30.3429	11.4513
UV-B	3	211.124	70.37480	5.39899
Solar	3	289.5522	96.51741	1.40776

ANOVA						
Source of Variation	***SS***	***df***	***MS***	***F***	***P-value***	***F crit***
Between Groups	6665.0548	2	3332.527	547.5682	1.617E-07	5.14325
Within Groups	36.516294	6	6.086049			
Total	6701.5711	8				

Tukey's Multiple Comparison Test	Mean Diff.	Q	Significant? P < 0.05?	95% confidence interval of diff
UV-A vs UV-B	-40.03	28.11	Yes	-46.21 to -33.85
UV-A vs Solar	-66.17	46.46	Yes	-72.35 to -59.99
UV-B vs Solar	-26.14	18.35	Yes	-32.32 to -19.96

Table 4.6 Statistical analyses (ANOVA and Tukey's) on different irradiation sources for the degradation of OFX

SUMMARY				
Groups	*Count*	*Sum*	*Average*	*Variance*
UV-A	3	129.1156	43.0385	2.8984
UV-B	3	253.8095	84.6031	0.8576
Solar	3	280	93.3333	0.1156

ANOVA						
Source of Variation	***SS***	***df***	***MS***	***F***	***P-value***	***F crit***
Between Groups	4333.39915	2	2166.699	1678.8123	5.675E-09	5.1432
Within Groups	7.743687044	6	1.290614			
Total	4341.142837	8				

Tukey's Multiple Comparison Test	Mean Diff.	q	Significant? P < 0.05?	95% confidance interval of diff
UV-A vs UV-B	-41.56	63.37	Yes	-44.41 to -38.72
UV-A vs Solar	-50.29	76.68	Yes	-53.14 to -47.45
UV-B vs Solar	-8.730	13.31	Yes	-11.58 to -5.884

4.2.3 Degradation of model compounds under continuous mode

Feasibility of soil was tested for the degradation of pharmaceuticals in a continuous baffled reactor, using soil in the form of either thin layer or beads. Retention time of 150 min was provided with 30 mL min^{-1} flow rate. Soil was spread uniformly over the surface of reactor as a thin layer with thickness of ≈0.2-0.3 mm. H_2O_2 concentration was kept same as in batch experiments by adding 0.5 and 1.0 mL H_2O_2 in 5 L aqueous solution of ORZ and OFX, respectively. Degradation efficiency of 84 and 79% was achieved in single pass in time span of 150 min in case of ORZ and OFX, respectively. Fig. 4.18 shows the degradation profile of model compounds in continuous experiment using soil beads with 71 and 68% degradation of ORZ and OFX, respectively in 150 min. Although the reaction conditions were same for both the continuous mode, but the degradation of pharmaceuticals was higher when soil was spread as thin layer when compared to soil beads. Probable reason could be the large surface area of soil in contact with the pollutant due to small size of soil particles. Moreover, in case of soil beads, reaction occurs at solid-liquid interface and overall rate may be limited due to poor mass transport of pollutants to the soil surface (Chong *et al.* 2010).

For the field applications of solar photo-Fenton-like process, the catalyst stability is of considerable interest. In this regard, the activity of soil beads against the pharmaceuticals degradation was monitored for subsequent runs. The soil beads were effectively reused for

four times with ≈13% reduction in degradation efficiency for both the pharmaceuticals (Fig. 4.18). After four runs, the reduction in degradation efficiency might be due to the loss of active phase leaching, accumulation of intermediates and surface deposition (Daud and Hameed, 2010).

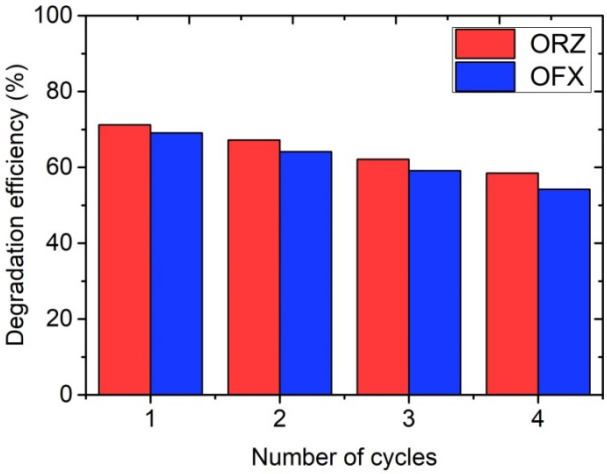

Fig. 4.18 Degradation and reusability in continuous immobilized mode [For ORZ, 0.033 g L^{-1} soil dosage, 1 mM H_2O_2, pH 3, 5 L solution volume; For ORZ, 0.020 g L^{-1} soil dosage, 2 mM H_2O_2, pH 3, 5 L solution volume]

4.2.4 HPLC and mineralization study

Figure 4.19 shows the HPLC chromatograms of batch and continuous experiments with of ORZ and OFX at 310 and 288 nm, respectively. At retention time (RT) of 5.3 min and 16 min, strong peaks of ORZ and OFX were observed. Sharp decrease in the peak area was observed in both batch and continuous mode with increasing treatment time indicating the efficient degradation of both the compounds. Appearance of other small peaks in the HPLC profile shows the formation of intermediates/by-products. Moreover, more sharp peaks of intermediates were observed in batch and continuous experiments of OFX when compared to ORZ degradation.

Total organic carbon (TOC) studies were carried out to assess the extent of mineralization of aqueous ORZ and OFX treated solution in continuous mode. 30 and 36% mineralization of ORZ and OFX was achieved using soil in the form of thin layer whereas, 27 and 33% of mineralization was achieved after 150 min when soil beads were used. Less mineralization was observed in continuous experiment when compared to batch, which are likely due to the formation of more concentrated intermediates as shown in HPLC results (Fig. 4.19). Probable reason for lesser mineralization in continuous experiments might be due

to poor contact, lesser penetration of light and poor mass transfer between soil and the aqueous solution.

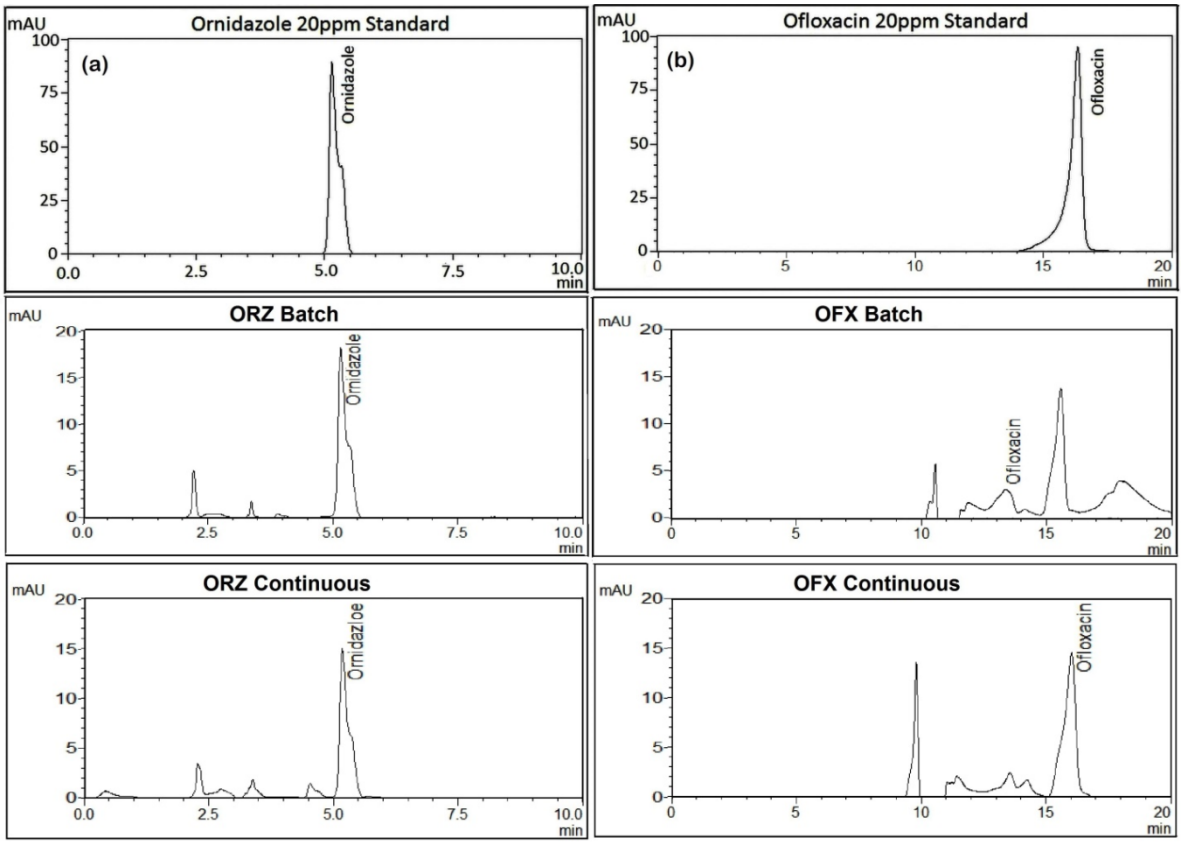

Fig 4.19 HPLC chromatograms of ORZ (Batch: 0.033 g L^{-1} soil, 1 mM H_2O_2, pH 3, 150 mL ORZ solution; Continuous: 0.033 g L^{-1} soil, 1 mM H_2O_2, pH 3, 5 L ORZ solution) and OFX (Batch: 0.020 g L^{-1} soil, 2 mM H_2O_2, pH 3, 150 mL OFX solution; Continuous: 0.020 g L^{-1} soil, 2 mM H_2O_2, pH 3, 5 L OFX solution)

4.2.5 Toxicity assessment

For assessing the toxic nature of formed intermediates, acute toxicity of the batch treated solution was scrutinized by bio-assay method (IS: 6582-2001- Standard) as acknowledged by Central Pollution Control Board, India. This method is based on minimum amount of wastewater dilution required to achieve no mortality for zebra fish. The results from this test demonstrate 100% survival after 96 h exposure time, indicating the absence of acute toxicity in treated water of both model compounds.

4.3 Photo-Fenton treatment of model compounds using GO-pyrite nanocomposite

Graphene oxide-pyrite (GO-pyrite) nanocomposite were synthesized using a simple one-pot hydrothermal process were utilized in photo-Fenton based degradation of model compounds *viz.* AMX and OFX.

4.3.1 Characterization of GO-pyrite nanocomposite

Fig. 4.20 shows the HR-TEM images of GO-FeS_2 nanocomposite and EDS pattern is presented in Table 4.7. Fig. 4.20a shows the image of irregular shaped FeS_2 particles made up of many nanoparticles aggregated with one another and Fig. 4.20 b, c and d shows the images of GO-FeS_2 nanocomposite. HR-TEM images clearly indicate the highly dispersive nature of synthesized FeS_2 nanoparticles on the surface of graphene oxide. With the addition of GO, the number of nanoparticles forming on the surface of GO increased tremendously while the size of nanoparticles decreased to ≈50 nm (Fig. 4.20d) from the size of ≈200 nm. One of the possible reason could be that the surface active sites increased with the addition of GO, leading to higher number of nucleation sites (Golsheikh *et al.* 2013).

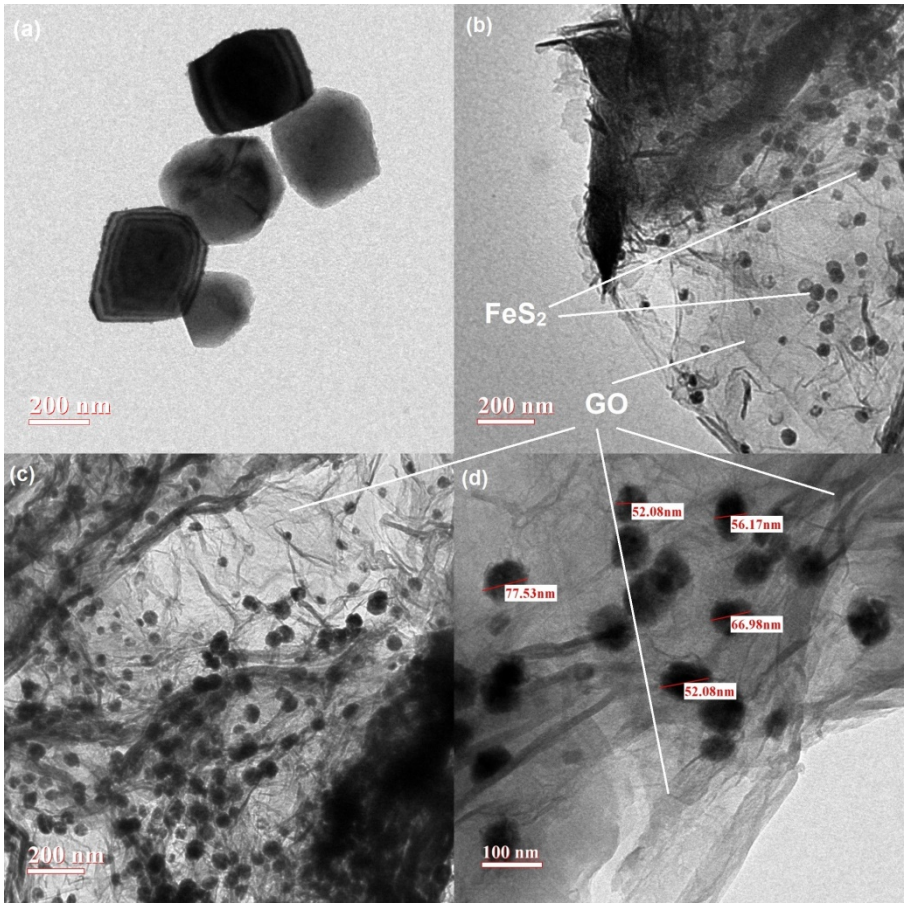

Fig. 4.20 HR-TEM analysis of (a) FeS_2 (b, c & d) GO-FeS_2 nanocomposite

Furthermore, the phase purity and composition of FeS_2 and GO-FeS_2 were analysed by XRD (Fig. 4.21). It can be observed that all detection peaks are confined to pure cubic phase of FeS_2, which match well with the standard (JCPDS No. 43-1340). The XRD pattern of the GO-FeS_2 displays the same detection peaks as pure FeS_2 except for $2\theta = 26°$, which can be assigned to diffraction by the (002) planes of the graphite-like structure of graphene

oxides. EDS analysis (Table 4.7) revealed the presence of only C, O, Fe and S in the synthesized nanocomposite which shows that the prepared material is clean without any contamination indicating improved synthesis of GO-FeS_2. BET analysis revealed that surface area of synthesized FeS_2 and GO-FeS_2 was 7.93 m^2 g^{-1} and 26.82 m^2 g^{-1}, respectively.

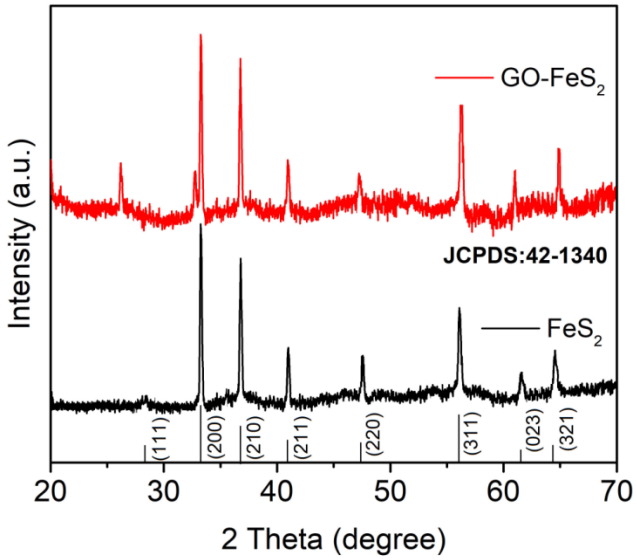

Fig. 4.21 XRD patterns of FeS_2 and GO-FeS_2 nanocomposite

Table 4.7 EDS analysis of synthesized GO-FeS_2 nanocomposite

Element	C	O	Fe	S
Weight %	70.20	24.94	3.91	0.95

4.3.2 Catalytic activity of GO-FeS_2 in photo-treatment of model compounds

Solar-induced photo-Fenton experiments were performed in order to compare the degradation efficiency AMX (0.1 mM) and OFX (0.1 mM) under various conditions. Negligible degradation of AMX and OFX degradation was observed by GO-FeS_2 in dark which could be ascribed primarily to the surface adsorption of nanocomposite. Results even showed insignificant removal of both the compounds in the presence of solar light, FeS_2 or GO-FeS_2 + H_2O_2 in dark, alone after 180 min (Fig. 4.22). After 180 min reaction time, 42.6 and 67.9% degradation efficiency of AMX and OFX, respectively was achieved in the presence of GO-FeS_2 under solar light. However, with the addition of H_2O_2 in GO-FeS_2 + solar light, the degradation of OFX (Fig. 4.22a) and AMX (Fig. 4.22b) were found to be 97.5 and 80.9% with 10 mM H_2O_2, 1 g L^{-1} GO-FeS_2 at pH 5. Thus, experiments confirmed that solar photo-Fenton-Like treatment employing GO-FeS_2 and H_2O_2 was most efficient in degrading the model compounds.

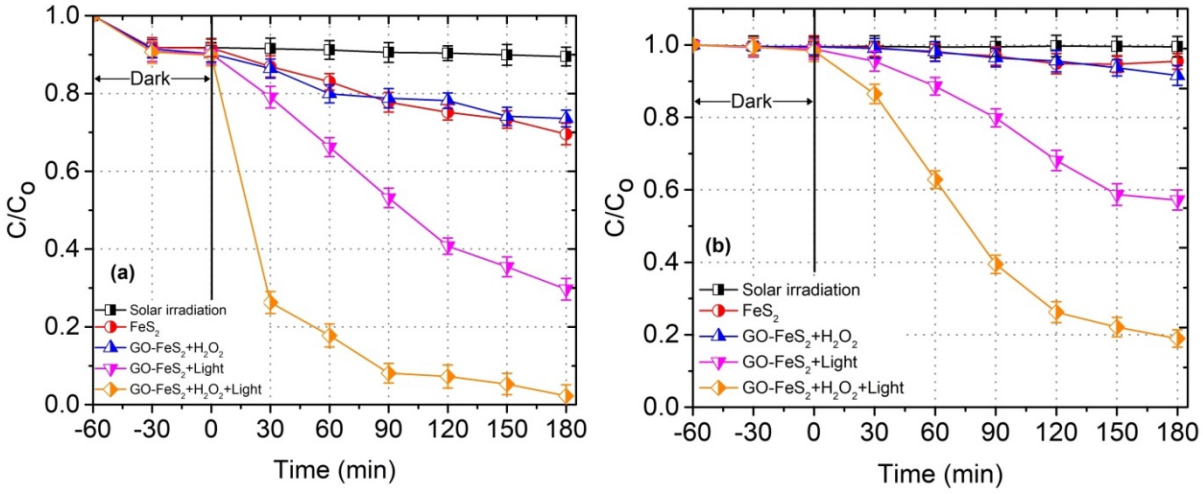

Fig. 4.22 Degradation profile of (a) OFX and (b) AMX using synthesized GO-FeS_2 nanocomposite

Results indicate that FeS_2 have the lowest efficiency for AMX and OFX when compared to GO-FeS_2 and GO-FeS_2 + H_2O_2. GO-FeS_2 possesses the most remarkable dispersibility as well as AMX and OFX degradation efficiency in the photo-Fenton treatment process. Two factors are considered to be responsible for the enhanced degradation of OFX and AMX in the solar photo-Fenton process. Firstly, the $HO^{\bullet}$ which are the dominant oxidizing species accounting for the degradation of organic pollutants in FeS_2 based Fenton process, were produced via reduction of H_2O_2 by Fe^{2+} dissolved from FeS_2 under aerobic condition (Che *et al.* 2011). Secondly, the GO-FeS_2 mediated degradation of model compounds stayed in a high rate in slight acidic to neutral mediums (pH 4.0–7.0). It has been reported that pH declined in FeS_2 suspension and reach the point of acidic equilibrium during the oxidation by releasing hydrogen and Fe^{2+}, providing an suitable pH conditions for the subsequent Fenton process. Furthermore, the existence of H_2O_2 extremely exacerbated pH decreasing, since the kinetics of FeS_2 dissolution by H_2O_2 is considerably faster than that by molecular oxygen in suspensions (McKibben and Barnes, 1986; Liu *et al.* 2015a) which accounts for the higher degradation efficiency of AMX and OFX under weak acidic to neutral conditions (pH 4.0 to pH 7.0). Additionally, the abundant hydroxyl groups (–OH) and carboxyl groups (–COOH) on the surface of GO also provided an acidic interface for the existence of Fenton's reaction (Ren *et al.* 2014).

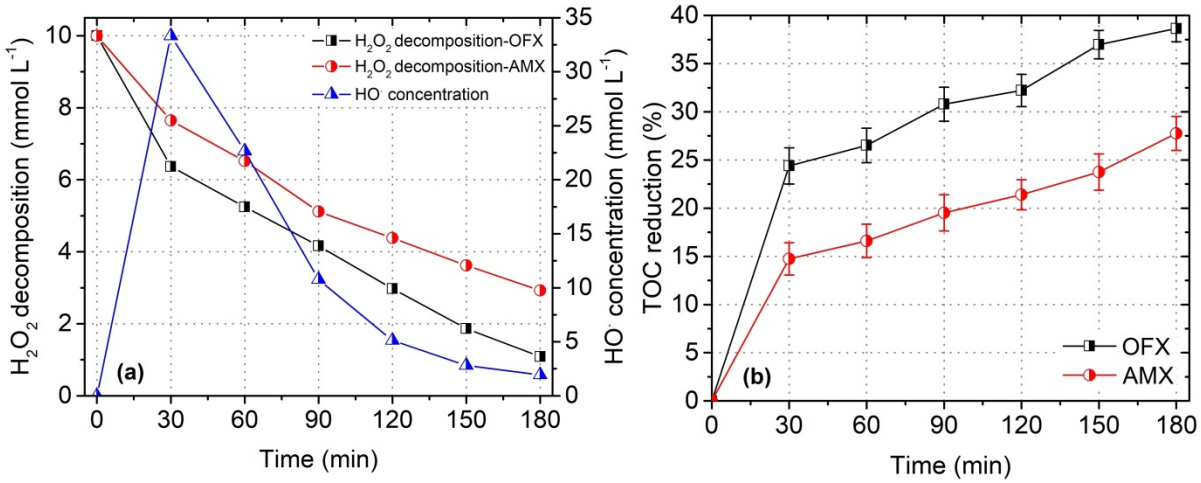

Fig. 4.23 (a) Profile of H_2O_2 decomposition and HO• concentration in GO-FeS_2 photo-Fenton treatment (b) TOC profile of AMX and OFX in GO-FeS_2 photo-Fenton treatment

The presence of H_2O_2 in the removal of AMX and OFX was precursor of HO•. Because H_2O_2 itself is not an efficient oxidizer of AMX and OFX, HO• generated from H_2O_2 are the actual oxidant in the GO-FeS_2 based photo-Fenton treatment. Fig. 23a represents the results of H_2O_2 decomposition in the GO-FeS_2 based photo-Fenton treatment of AMX and OFX. Fig. 23a also represents the results of HO• concentration produced in GO-FeS_2 based photo-Fenton treatment of OFX. Results clearly indicate that H_2O_2 was decomposed leading to simultaneous generation of HO• in the presence of GO-FeS_2 during reaction. With initial H_2O_2 concentration of 10 mM in photo-Fenton oxidation of OFX and AMX, the residual H_2O_2 concentration was found to be 1.09 and 2.9 mM for OFX and AMX, respectively after the reaction. The study revealed that highly dispersive nature of FeS_2 on GO possesses a relatively high oxidative capacity for degrading AMX and OFX in H_2O_2 solution, providing a good alternative for the treatment of organic contaminants in aqueous solution.

The treatment efficiency not only depends on the potency of degradation of model compound but also on the extent of mineralization of the compound and intermediates generated. Thus, the TOC removal of the treated aqueous solutions of OFX and AMX was assessed (Fig. 4.23b), and 38.6 and 27.7% TOC removal was found for OFX and AMX, respectively. However, organic by-products formed during photo-Fenton degradation of model compounds are expected to exhibit remaining TOC in the solutions despite almost complete degradation of parent compounds.

4.4 Gamma irradiation treatment of model compounds

All the model compounds (AMX, OFX and ORZ) were independently treated using gamma irradiation under different experimental conditions. Degradation efficiency, degradation mechanism, toxicity and cost analysis were evaluated for the treatment process.

4.4.1 Gamma radiolytic degradation of model compounds

Gamma radiolytic degradation of the organic pollutants in aqueous solution is initiated by the reaction with the major reactive radicals ($HO^{\bullet}$, e_{aq}^{-} and $H^{\bullet}$) produced during the gamma radiolysis of water as earlier mentioned in Chapter 1.0 (Eq. 1.10). Among these, hydroxyl radicals ($HO^{\bullet}$) are efficient oxidizing species which are produced with higher G-value (0.28) and are able to achieve favourable goals in removal of organic pollutants (Getoff, 1995; Le Caër, 2011). The degradation extent of AMX, OFX and ORZ was investigated under different absorbed doses at various initial concentrations of AMX and OFX ranging from 0.05 to 0.2 mM and for ORZ, 0.11 to 0.45 mM. The degradation of model compounds was found to be negligible under control experiment carried out at room temperature in absence of gamma radiation. The ratio of model compound concentration after and before radiolysis (C/C_o) was plotted as a function of absorbed doses as shown in Fig. 4.24. It was observed that low-concentration of model compound could be effectively degraded during gamma radiation under the experimental conditions though the degradation extent was increased with increasing absorbed doses at all concentrations. The degradation extents (%) of OFX were achieved as 99.6, 95.6, 87 and 80.6% for the initial OFX concentrations of 0.05, 0.1, 0.15 and 0.2 mM, respectively at an absorbed dose of 3.0 kGy. The degradation extents (%) of ORZ were achieved as 99.2, 99.0, 95.8 and 92.8% for the initial ORZ concentrations of 0.11, 0.22, 0.31 and 0.45 mM, respectively at an absorbed dose of 3.0 kGy. The (%) degradation extents of AMX were achieved as 98.9, 92.7, 73.2 and 51.5% for the initial AMX concentrations of 0.05, 0.1, 0.15 and 0.2 mM, respectively at an absorbed dose of 15.0 kGy. Higher concentration of model compound could increase the probability of radical reactions with the parent compound and thus increased the extent of radiation induced degradation (C_o-C) at a particular absorbed dose, though the calculated C/C_o ratio were decreased with the increase in C_o of model compound.

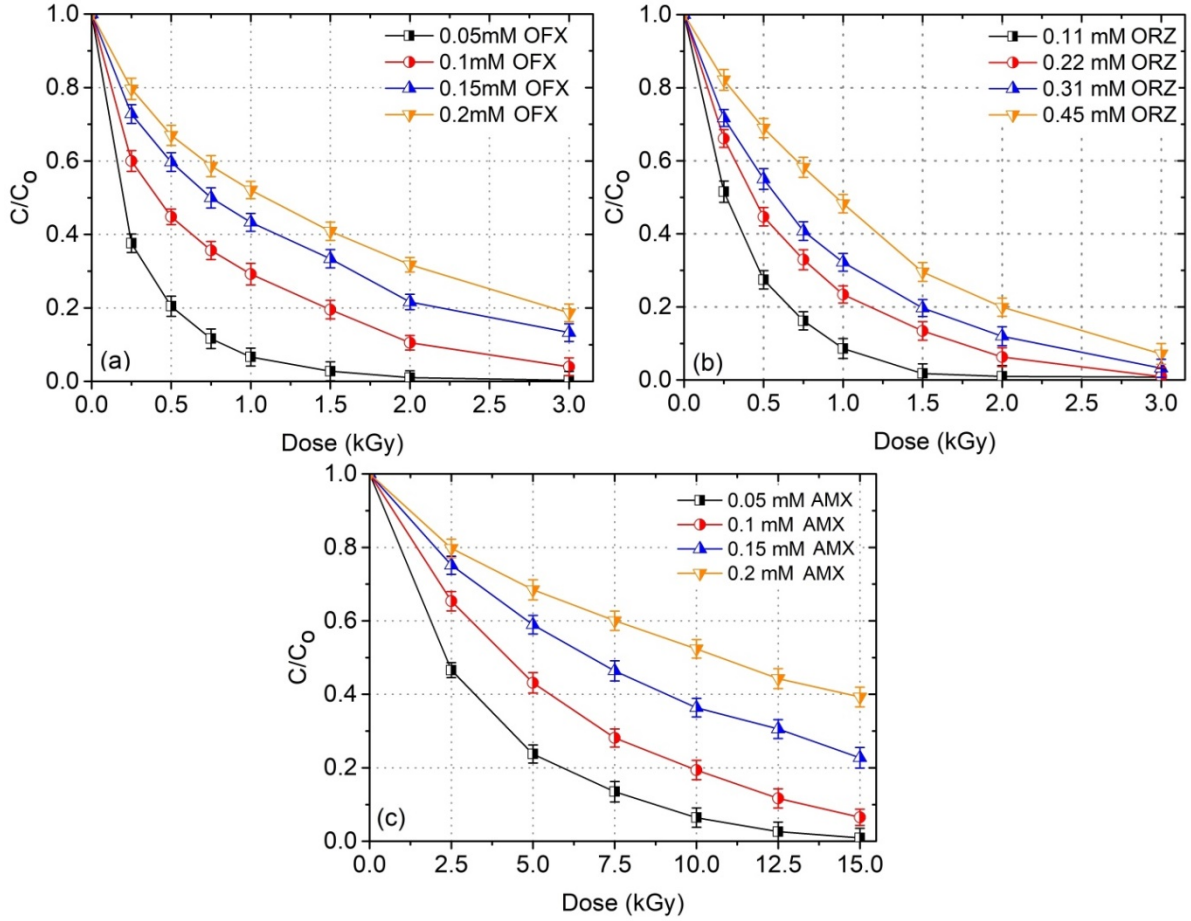

Fig. 4.24 (a) Change in concentration (C/C_o) of OFX as a function of absorbed dose (b) Change in concentration (C/C_o) of ORZ as a function of absorbed dose (c) Change in concentration (C/C_o) of AMX as a function of absorbed dose

From Fig. 4.25, it was evident that concentration of model compounds was decreased exponentially with the increase in absorbed dose. This is represented by Eq. 3.4 (Chapter 3.0), which is in agreement with the pseudo first-order-rate kinetics. Moreover, *k*-value at different initial concentrations of model compounds was obtained from the slope of the plot (with moderately higher correlation coefficients (R^2)) as shown in the Fig. 4.25. The corresponding dose constants values for OFX, ORZ and AMX are shown in Table 4.8, 4.9 and 4.10, respectively. With increase in initial OFX concentrations from 0.05 to 0.2 mM, the *k*-values were found to decrease from 2.36 to 0.61 kGy^{-1}, respectively. With increase in initial ORZ concentrations from 0.05 to 0.2 mM, the *k*-values were found to decrease from 2.340 to 0.806 kGy^{-1}, respectively. With increase in initial AMX concentrations from 0.05 to 0.2 mM, the *k*-values were found to decrease from 0.293 to 0.065 kGy^{-1}, respectively. The decrease in *k*-value with increased initial concentration of model compounds was resulted due to simultaneous competition reactions of model compounds and their degradation intermediates

with the radiolytically generated reactive radicals (Magureanu *et al.* 2010; Guo *et al.* 2012; Huang *et al.* 2016). The dose constant, *k*, was taken into account to determine the dose required to bring about 50% ($D_{0.50}$ values) and 90% ($D_{0.90}$ values) degradation of model compounds as calculated by Eqs. 3.2 and 3.3 and the results obtained for OFX, ORZ and AMX are shown in Table 4.8, 4.9 and 4.10, respectively. These results can be attributed to the fact that, at low initial concentration of model compound, lower absorbed dose was required to achieve 50 and 90% degradation efficiencies of model compound with correspondingly high dose constant and vice-versa. The *k*-value could be affected by the several experimental conditions such as, solution pH, chemical structure of organic contaminant, initial concentration of organic contaminant, and the characteristics of solvent and/or additive used. Therefore, the degradation rate of OFX, ORZ and AMX at different initial concentrations could be well-fitted to Eq. 3.4 to calculate dose constants.

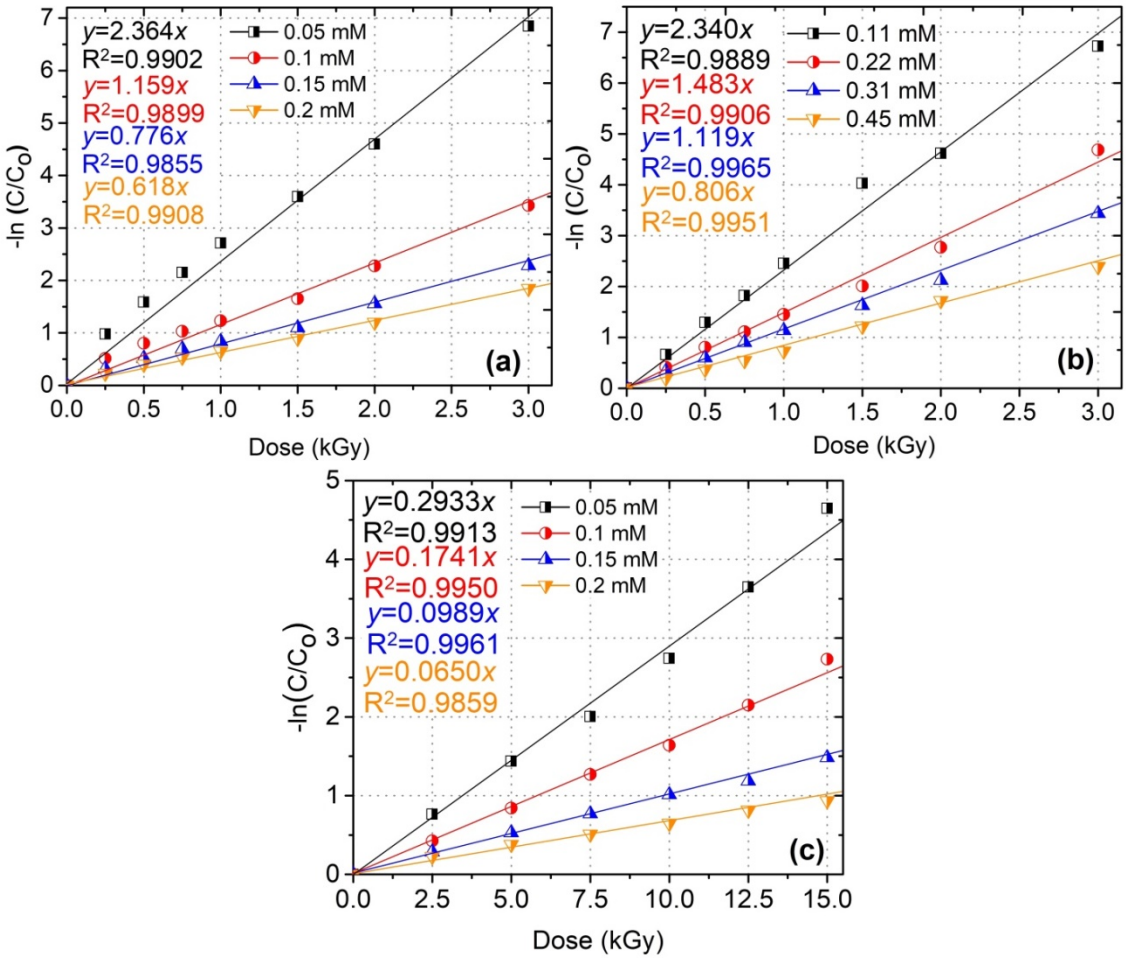

Fig. 4.25 (a) Pseudo first-order kinetics of OFX degradation as a function of absorbed dose (b) Pseudo-first-order kinetics of ORZ degradation as a function of absorbed dose (c) Pseudo-first-order kinetics of AMX degradation as a function of absorbed dose

The efficacy of gamma radiolytic degradation of model compounds was compared between G-value and degradation extents (%) as depicted in Fig. 4.26. Results revealed a decrease in G-values and an increase in degradation extents of model compounds with the increasing absorbed doses. The (G(-OFX)) values for the radiolytic degradation of OFX were calculated to be 0.68 and 0.30 for an absorbed doses of 1.0 and 3.0 kGy, respectively. The (G(-ORZ)) values for the radiolytic degradation of ORZ were calculated to be 1.68 and 0.72 for an absorbed doses of 1.0 and 3.0 kGy, respectively. The (G-(AMX)) values were calculated to be 0.08 and 0.06 for absorbed doses of 10.0 kGy and 15.0 kGy, respectively. The probable reason for the decrease in G-values with the increase in absorbed doses presumably could be the increase in probability of competition reactions between the model compound and its degraded products for reacting with the reactive radical species produced during water radiolysis (Basfar *et al.* 2005; Sánchez-Polo *et al.* 2009). Moreover, radical-radical recombination reaction during radiolysis also leads to a decrease in G-values with doses (Liu *et al.* 2011). The increase in G-values with higher initial concentration of model compound also revealed that the reactive radical species had a greater possibility to react with model compound causing higher degradation extents. However, the total concentration of reactive radical species increased in solution with increase in accumulated absorbed dose and consequently, the degradation extent of model compound was also increased at each dose. Therefore, it showed overall higher degradation extents of OFX, ORZ and AMZ with increasing absorbed dose.

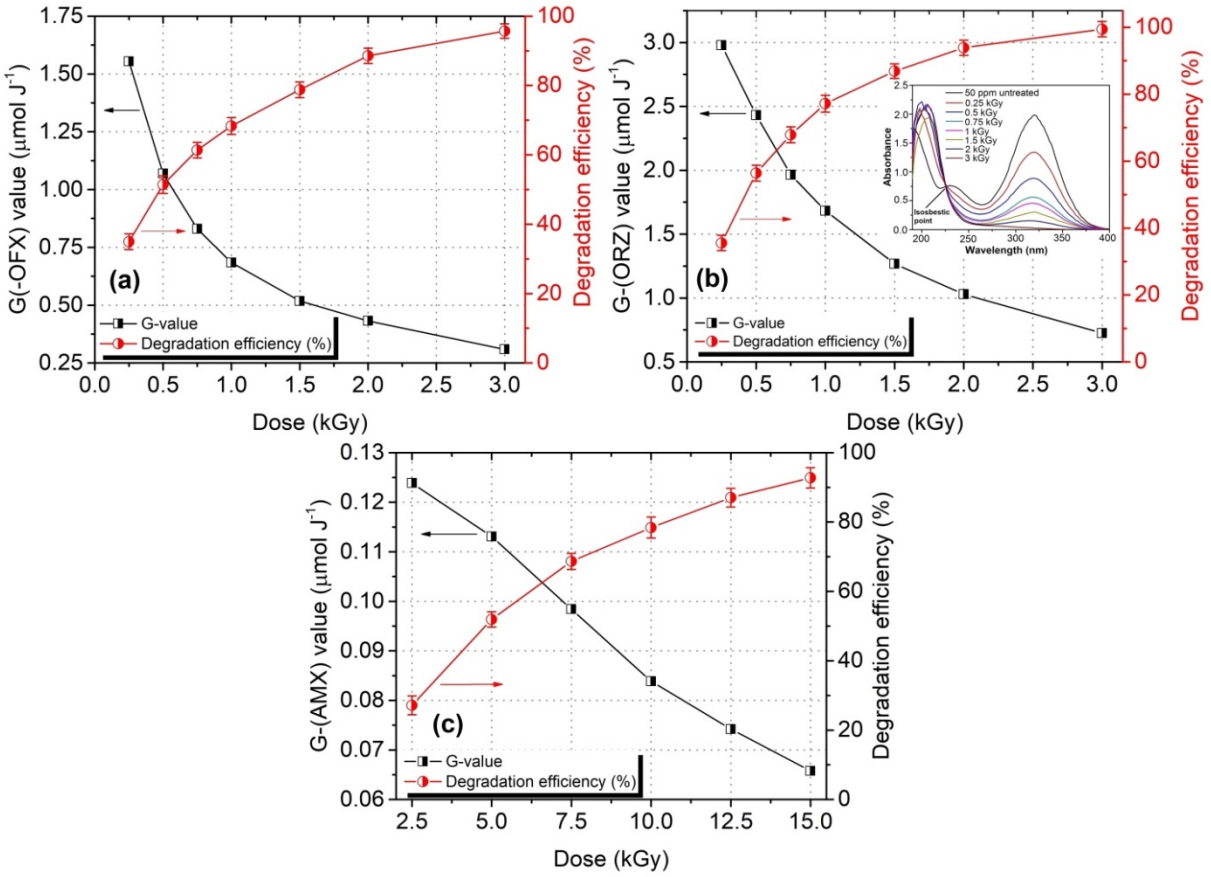

Fig. 4.26 (a) G-(OFX) and degradation efficiency (%) of OFX using gamma radiation with $[OFX]_o$=0.1 mM and pH 6.5 (b) G-(ORZ) and degradation efficiency (%) of ORZ using gamma radiation with $[ORZ]_o$=0.22 mM and pH 6.5 (c) G-(AMX) and degradation efficiency (%) of AMX using gamma radiation with $[AMX]_o$=0.1 mM

The inset of Fig. 4.26b shows the pattern of absorption spectra of irradiated ORZ solutions. The intensities in the characteristic absorption peaks of ORZ at 320 nm and 232 nm were decreased with increase in the doses owing to the removal of the compound. The increases in the absorption of ORZ with increase in absorbed dose in the wavelength range of 190–230 nm also signifies the generation of reaction by-products or intermediates as evidence from the inset of Fig. 4.26b (Chu and Wang, 2016; Huang *et al.* 2016). Further, the appearance of isosbestic point at 246 nm indicates the generation and accumulation of intermediates during the radiolytic degradation of ORZ (Tian *et al.* 2009; el mehdi Benacherine *et al.* 2017). However, an enhancement in the increase in total amount of reactive radicals in solution with increase in accumulated absorbed dose leads to increase the overall degradation extent of ORZ at each dose.

Table 4.8 Data from gamma radiolytic experiments of ofloxacin: Influence of initial concentration, pH and various additives. [(G-(OFX)) values calculated for 1.0 kGy absorbed dose using Eq. 3.1]

Exp.	$[OFX]_o$ (mM)	pH	$[Na_2CO_3]$ (mM)	[*t*-BuOH] (M)	$[H_2O_2]$ (mM)	(G-(OFX))	*k* (kGy^{-1})	$D_{0.5}$ (kGy)	$D_{0.9}$ (kGy)
1	0.05	6.5	0.00	0.00	0.00	0.481	2.364	0.293	0.974
2	0.10	6.5	0.00	0.00	0.00	0.684	1.159	0.598	1.986
3	0.15	6.5	0.00	0.00	0.00	1.755	0.776	0.893	2.967
4	0.20	6.5	0.00	0.00	0.00	1.971	0.618	1.121	3.725
5	0.10	3.0	0.00	0.00	0.00	0.903	1.160	0.597	1.984
6	0.10	6.5	0.00	0.00	0.00	0.829	0.853	0.812	2.699
7	0.10	11.0	0.00	0.00	0.00	0.862	0.743	0.932	3.099
8	0.10	6.5	0.05	0.00	0.00	0.708	0.545	1.272	4.227
9	0.10	6.5	0.10	0.00	0.00	0.668	0.486	1.425	4.733
10	0.10	6.5	0.00	0.05	0.00	0.404	0.174	3.983	13.23
11	0.10	6.5	0.00	0.10	0.00	0.390	0.160	4.332	14.39
12	0.10	6.5	0.00	0.50	0.00	0.281	0.106	6.539	21.72
13	0.10	6.5	0.00	0.00	0.25	0.908	1.040	0.666	2.214
14	0.10	6.5	0.00	0.00	0.50	0.943	1.357	0.510	1.696
15	0.10	6.5	0.00	0.00	10.0	0.914	1.122	0.617	2.052
16	0.10	6.5	0.00	0.00	20.0	0.846	0.783	0.885	2.940

Table 4.9 Data from gamma radiolytic experiments of ORZ: Influence of initial concentration, pH and various additives. [*G*-value calculated for 1 kGy dose using the Eq. 3.1]

Exp.	$[ORZ]_o$ (mM)	pH	$[Na_2CO_3]$ (M)	[*t*-BuOH] (M)	$[H_2O_2]$ (mM)	G-value	*k* (kGy^{-1})	$D_{0.5}$ (kGy)	$D_{0.9}$ (kGy)
1	0.11	6.5	0	0	0	1.004	2.340	0.296	0.983
2	0.22	6.5	0	0	0	1.683	1.483	0.467	1.552
3	0.31	6.5	0	0	0	2.237	1.119	0.619	2.057
4	0.45	6.5	0	0	0	2.273	0.806	0.859	2.856
5	0.22	3	0	0	0	1.724	1.631	0.424	1.411
6	0.22	6.5	0	0	0	1.627	1.260	0.547	1.818
7	0.22	11	0	0	0	1.464	0.995	0.696	2.314
8	0.22	6.5	0.05	0	0	1.190	0.650	1.066	3.542

9	0.22	6.5	0.1	0	0	0.990	0.482	1.438	4.777
10	0.22	6.5	0	0.05	0	0.345	0.186	3.726	12.37
11	0.22	6.5	0	0.1	0	0.215	0.123	5.635	18.72
12	0.22	6.5	0	0	0.5	1.884	1.970	0.351	1.168
13	0.22	6.5	0	0	5	2.009	2.234	0.310	1.030
14	0.22	6.5	0	0	10	1.987	1.730	0.400	1.330
15	0.22	6.5	0	0	20	1.852	1.528	0.453	1.506

Table 4.10 Data from gamma radiolytic experiments of AMX: Influence of initial concentration, pH and various additives. [*G*-value calculated for 2.5 kGy dose using the Eq. 3.1]

Exp.	$[AMX]_o$ (mM)	pH	Additives (M)	$[H_2O_2]$ (mM)	G-value	*K* (kGy^{-1})	$D_{0.5}$ (kGy)	$D_{0.9}$ (kGy)
1	0.05	6.5	0	0	0.190	0.2933	2.363	7.850
2	0.10	6.5	0	0	0.356	0.1741	3.981	13.22
3	0.15	6.5	0	0	0.422	0.0989	7.008	23.28
4	0.2	6.5	0	0	0.526	0.065	10.66	35.42
5	0.10	3	0	0	0.364	0.2003	3.460	11.49
6	0.10	6.5	0	0	0.355	0.1708	4.058	13.48
7	0.10	11	0	0	0.344	0.1562	4.437	14.74
8	0.10	6.5	NO_3^-	0	0.327	0.1279	5.419	18.00
9	0.10	6.5	NO_2^-	0	0.050	0.0266	26.05	86.56
10	0.10	6.5	CO_3^{2-}	0	0.202	0.0574	12.07	40.11
11	0.10	6.5	HCO_3^-	0	0.276	0.0908	7.633	25.35
12	0.10	6.5	SO_4^{2-}	0	0.348	0.155	4.471	14.85
13	0.10	6.5	SO_3^{2-}	0	0.106	0.0389	17.81	59.19
14	0.10	6.5	Thiourea	0	0.031	0.0203	34.14	113.4
15	0.10	6.5	Propanol	0	0.088	0.0329	21.0	69.98
16	0.10	6.5	0	0.5	0.362	0.1906	3.636	12.08
17	0.10	6.5	0	2.5	0.375	0.2368	2.927	9.723
18	0.10	6.5	0	5	0.339	0.1537	4.509	14.98
19	0.10	6.5	0	10	0.315	0.1258	5.509	18.30
20	0.10	6.5	0	25	0.296	0.1071	6.471	21.49

4.4.2 Effect of solution pH on gamma radiolytic degradation of model compounds

Figure 4.27a, 4.27b and 4.27c represents the influence of solution pH on gamma radiolytic degradation of OFX, ORZ and AMX, respectively. It was found that the degradation efficiency of model compounds was higher in the acidic medium when compared to alkaline and neutral medium. At an absorbed dose of 1.0 kGy, 75, 68 and 60% degradations of OFX were achieved at a pH of 3.0, 6.5 and 11.0, respectively with the corresponding *k*-values of 1.160, 0.853 and 0.743 kGy^{-1}, respectively (Table 4.8, experiments 5–7). With 1.0 kGy of an absorbed dose, ORZ degradation efficiency was found to be 75, 70.1, and 66.3% at the pH of 3, 6.5, and 11, respectively with the corresponding *k*-values of 1.631, 1.260, and 0.995 kGy^{-1}, respectively (Table 4.9, experiments 5–7). In case of AMX, degradation efficiency was found to be 82.4, 77.5 and 74.9% at the pH of 3, 6.5, and 11, respectively with the corresponding *k*-values of 0.200, 0.170 and 0.156 kGy^{-1}, respectively at an absorbed dose of 10.0 kGy (Table 4.10, experiments 5–7).

The degradation rate of pollutant during gamma radiolysis explicitly depends upon the existing radical species (Guo *et al.* 2015; Liu *et al.* 2015). It is understood that pH of the solution influences the yield of key reactive species during water radiolysis and hence affects the degradation efficiency of model compounds. Under acidic conditions, e_{aq}^- generated during gamma radiolysis of water are expected to produce $H^{\bullet}$ radical on the reaction with H^+ (Eq. 4.8) (Guo *et al.* 2012). The decreased e_{aq}^- concentration restrained its reaction with $HO^{\bullet}$, thereby increasing the concentration of $HO^{\bullet}$ in the solution. Under alkaline condition, $HO^{\bullet}$ readily reacts with OH^- (Eq. 4.9), thus decreasing the $HO^{\bullet}$ concentration in the solution (Liu *et al.* 2015). The pKa of ORZ was reported as 2.4 and thus ORZ was expected to in its molecular form in the studied pH range (Salo *et al.* 2003). Thus, $HO^{\bullet}$ is expected to initiate the degradation of ORZ via formation of ORZ epoxide. It degrades into 2-methyl-5-nitroimidazole through subsequent cleavage of epoxide ring followed by demethylation (Zhao *et al.* 2012). Overall reaction increases the degradation efficiency of ORZ. The increased degradation efficiency of model compounds in acidic solution and decreased efficiency in alkaline solution demonstrated that $HO^{\bullet}$ is a main radical specie affecting the gamma radiolytic degradation of OFX, ORZ and AMX. Similar trend in results were also observed in the published reports (Liu *et al.* 2015; Sayed *et al.* 2016; Chu *et al.* 2016).

$$e_{aq}^- + H^+ \rightarrow H^{\cdot} \; [k = 2.3 \times 10^{10} \text{ L mol}^{-1}\text{S}^{-1}] \quad (4.8)$$

$$OH^- + HO^{\cdot} \rightarrow O^- + H_2O \; [k = 1.3 \times 10^{10} \text{ L mol}^{-1}\text{S}^{-1}] \quad (4.9)$$

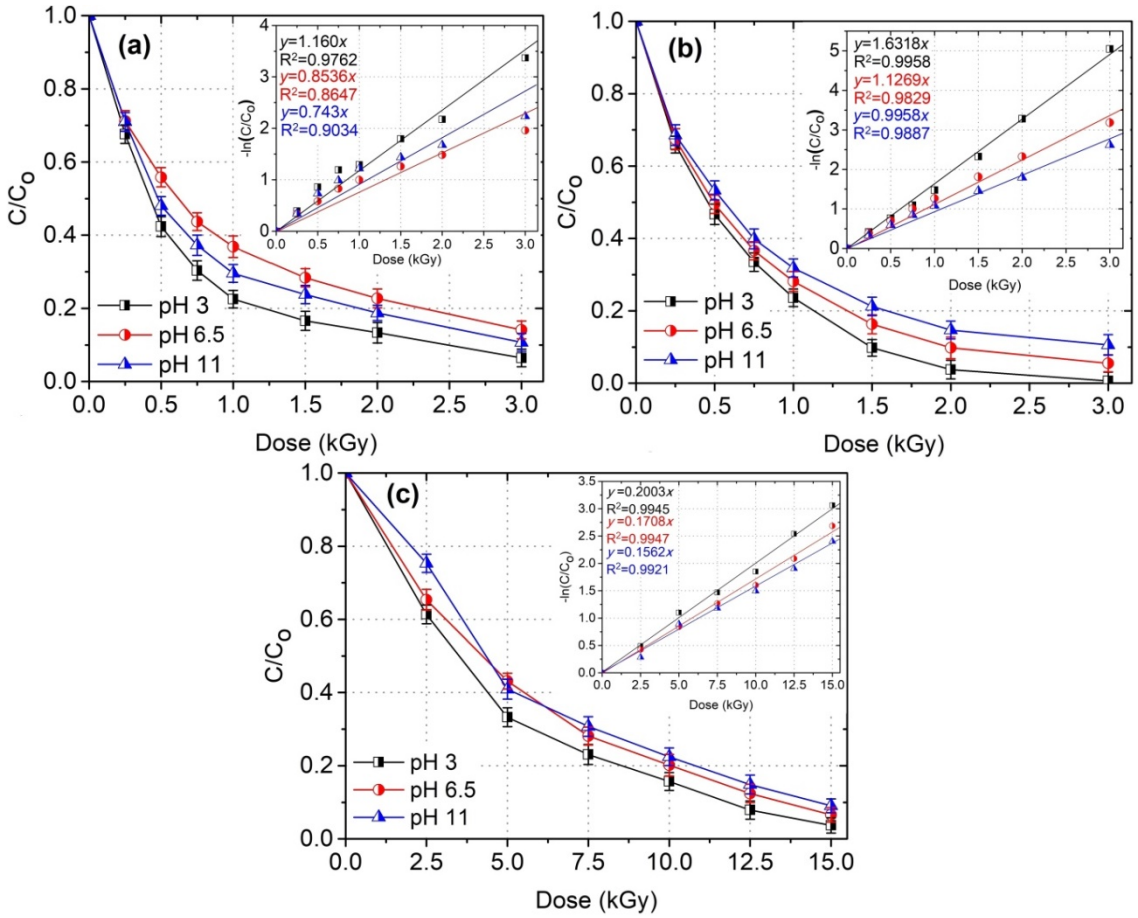

Fig. 4.27 Effect of pH on gamma radiolytic degradation of (a) OFX (b) ORZ and (c) AMX

The removal rates of OFX, ORZ and AMX at different initial pH were well fitted with the Eq. 3.4 and the corresponding *k*-values are listed in Table 4.8, 4.9 and 4.10, experiments 5-7. It can be seen that aqueous solution of model compounds with higher pH resulted in lower *k*-value, which is analogous to the change in removal rate of model compounds with solution pH under gamma radiolysis.

4.4.3 Effect of additives on gamma radiolytic degradation of model compounds

Natural water and wastewater are considered to be complex matrices that consist of many organic and inorganic species which may retard the extent of gamma-induced radiolytic degradation of model compounds by competing with the reactive radical species produced during gamma radiolysis. Therefore, to assess their impact on the degradation extent of model compounds, the radiolytic degradation efficiency of OFX and ORZ was monitored in presence of different concentrations of CO_3^{2-} and tert-butanol (*t*-BuOH) at pH 6.5, whereas for AMX, the radiolytic degradation efficiency was monitored in the presence of NO_3^-, NO_2^-

, CO_3^{2-}, HCO_3^-, SO_4^{2-}, SO_3^{2-}, thiourea and propanol at pH 6.5.

It can be observed from Fig. 4.28 that at a given absorbed dose, degradation efficiency of OFX and ORZ in the solution was higher without the additives when compared to those in the presence of additives, CO_3^{2-} and *t*-BuOH. 95.6% OFX degradation was achieved in the aqueous solution at an absorbed dose of 3.0 kGy, while 68.7 and 38.0% OFX degradation efficiencies were obtained in the presence of 0.1 M CO_3^{2-} and *t*-BuOH, respectively. On the other hand, 99.4% ORZ degradation was achieved in the aqueous solution at an absorbed dose of 3.0 kGy, while 68 and 34.5% ORZ degradation efficiencies were obtained in the presence of 0.1 M CO_3^{2-} and t-BuOH, respectively.

It can be seen from Fig. 4.29 that at a given absorbed dose, degradation efficiency of AMX in the solution was higher without the additives when compared to those in the presence of additives. 92.7% AMX degradation was achieved in the aqueous solution at an absorbed dose of 15.0 kGy, while 85.7, 18.7, 55.5, 73.3, 90.7, 32.3, 14.1 and 28.0% degradation efficiencies were obtained in the presence of 0.1 M NO_3^-, NO_2^-, CO_3^{2-}, HCO_3^-, SO_4^{2-}, SO_3^{2-}, thiourea and propanol, respectively.

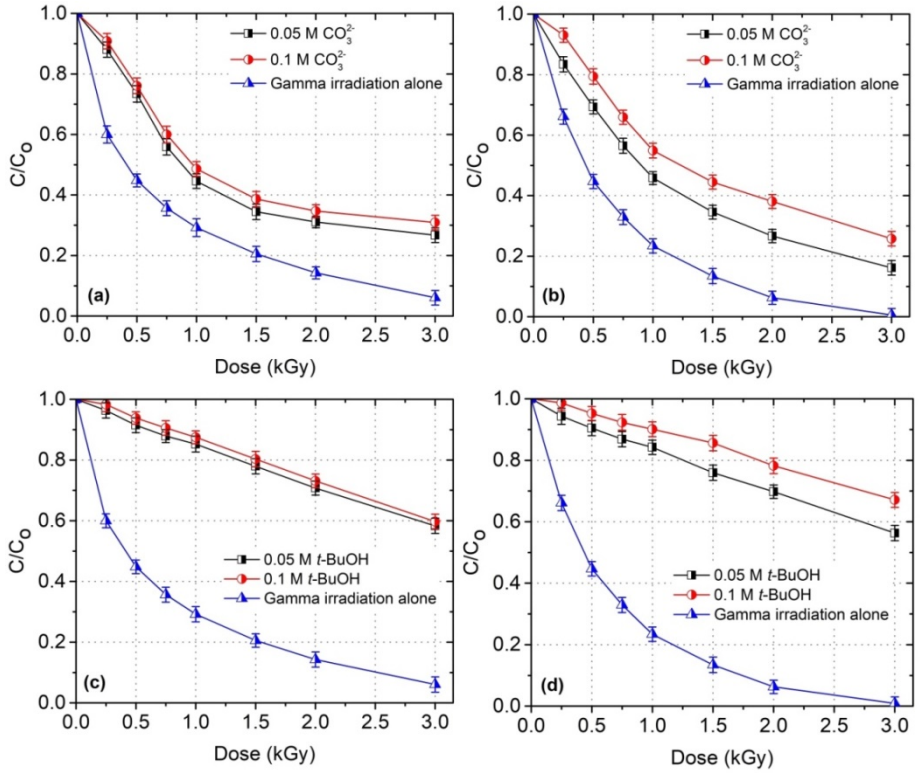

Fig. 4.28 Effect of CO_2^{3-} on gamma radiolytic degradation of (a) OFX and (b) ORZ; Effect of *t*-BuOH on gamma radiolytic degradation of (c) OFX and (d) ORZ [$(OFX)_o$ =0.1 mM; pH = 6.5] [$(ORZ)_o$ =0.22 mM; pH = 6.5]

The role of HO• in the degradation of model compounds (ORZ and OFX) under gamma radiolysis was also confirmed by adding *t*-BuOH as an organic additive (Fig. 4.28). Results achieved for OFX and ORZ with the addition of different concentration of additives are given in Table 4.8 and 4.9, respectively. This can be ascribed due to the scavenging effect of CO_3^{2-} and *t*-BuOH for the radical species such as HO•, e_{aq}^-, and H• as shown by Eqs 4.10-4.18. Table 4.8 and 4.9 exhibited that the pseudo first-order reaction dose constants (k) for radiolytic degradation of OFX and ORZ were decreased with increase in the concentration of CO_3^{2-} (*experiments* 8-9) and *t*-BuOH (*experiments* 10-11) in the aqueous solution. Moreover, the k values of OFX in the presence of 0.1 M CO_3^{2-} and *t*-BuOH were found to be 0.486 and 0.160 kGy^{-1}, respectively which was lower than 1.159 kGy^{-1} in the solution without the additives. On the other hand, the k-values of ORZ in the presence of 0.1 M CO_3^{2-} and *t*-BuOH were found to be 0.482 and 0.123 kGy^{-1}, respectively which was lower than 1.483 kGy^{-1} in the solution without the additives. Hence, the k value decreased with the addition of CO_3^{2-} and *t*-BuOH in the aqueous solution. It was also observed from the Table 4.8 and 4.9 that the G-value was calculated to be higher in presence of CO_3^{2-} compared to in presence of *t*-BuOH.

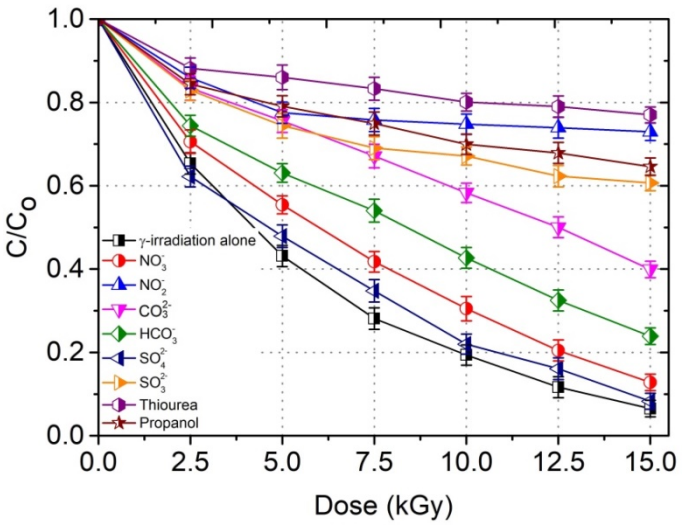

Fig. 4.29 Effect of additives on radiolytic degradation of AMX [$(AMX)_o$ =0.1 mM; pH = 6.5]

The preferential scavenging of HO• radicals by CO_3^{2-} ions lead to the generation of carbonate radical anion ($^{\bullet}CO_3^-$) (Eq. 4.10). Although, the CO_3^{2-} ions can directly react with e_{aq}^-, but at a much lower reaction rates (Eq. 4.11). It may be pointed out that the equilibrium state (Eq. (4.12)) is established in the aqueous solution with a pK_a value of 10.33,

accordingly, at working pH (which is < 10), the given equilibrium shifts to the left with a prevalence of HCO_3^- ions (Eq. (4.13), (4.14) and (4.15) (Buxton *et al.* 1988). HCO_3^- reacts with $HO^\bullet$, $H^\bullet$ and e_{aq}^- according to Eqs. 4.13 to 4.15. On the other hand, the $^\bullet CO_3^-$ radical produced in the reaction (4.10), (4.13) and (4.15) has a redox potential of 1.78 V at neutral pH, which have ability to slowly oxidize model compounds (Huie *et al.* 1991; Hu and Wang, 2007).

$$CO_3^{2-} + HO^\cdot \rightarrow OH^- + {}^\bullet CO_3^- \; [k = 3.9 \times 10^8 \text{ L mol}^{-1}\text{S}^{-1}] \quad (4.10)$$

$$CO_3^{2-} + e_{aq}^- \rightarrow CO_3^{3-} \; [k = 3.5 \times 10^5 \text{ L mol}^{-1}\text{S}^{-1}] \quad (4.11)$$

$$HCO_3^- \rightleftharpoons CO_3^{2-} + H^+ \quad (4.12)$$

$$HCO_3^- + HO^\cdot \rightarrow {}^\bullet CO_3^- + H_2O \; [k = 8.5 \times 10^6 \text{ L mol}^{-1}\text{S}^{-1}] \quad (4.13)$$

$$HCO_3^- + e_{aq}^- \rightarrow HCO_3^{2-} \; [k = 6.0 \times 10^5 \text{ L mol}^{-1}\text{S}^{-1}] \quad (4.14)$$

$$HCO_3^- + H^\cdot \rightarrow {}^\bullet CO_3^- + H_2 \; [k = 4.0 \times 10^4 \text{ L mol}^{-1}\text{S}^{-1}] \quad (4.15)$$

Results in Fig. 28 also demonstrated that the degradation efficiency of OFX and ORZ with the addition of *t*-BuOH was lower than that without *t*-BuOH. *t*-BuOH could react with reactive species, which are summarized as Eqs. (4.16-4.18).

$$HO^\bullet + C(CH_3)_3OH \rightarrow {}^\bullet CH_2C(CH_3)_2OH + H_2O \quad [k = 6.1 \times 10^8 \text{ L mol}^{-1}\text{S}^{-1}] \quad (4.16)$$

$$H^\bullet + C(CH_3)_3OH \rightarrow H_2 + CH_2OH \; [k = 1.7 \times 10^5 \text{ L mol}^{-1}\text{S}^{-1}] \quad (4.17)$$

$$e_{aq}^- + C(CH_3)_3OH \rightarrow H^+ + CH_3C(CH_3)_2O^- \; [k = 4.1 \times 10^5 \text{ L mol}^{-1}\text{S}^{-1}] \quad (4.18)$$

t-BuOH reacts with $HO^\bullet$ radicals with moderately high rate constant (Eq. 4.16) (Basfar *et al.* 2005) and form inert radical $^\bullet CH_2C(CH_3)_2OH$. Compared to that between CO_3^{2-} and $HO^\bullet$, the higher rate constant between *t*-BuOH and $HO^\bullet$ results in less $HO^\bullet$ radical available to react with OFX and ORZ (Eq. (4.10) and (4.16). The lower degradation of OFX and ORZ with *t*-BuOH than that with CO_3^{2-} suggests that $HO^\bullet$ radical plays a dominant role in removal of model compounds from the aqueous solution. Thus, two additives exhibit different radical reaction patterns (Eq. (4.10)-(4.18)), which explain the difference found in the extent of degradation of model compounds.

The results in Fig. 4.29 showed that degradation of AMX increased with increasing dose but the degradation was found to be lower in the presence of NO_2^- and NO_3^- ions. The addition of NO_2^- caused a large decrease in AMX degradation, whereas NO_3^- addition had a

slight effect on AMX degradation under different doses. NO_3^- is an efficient scavenger of e_{aq}^- (Eq. 4.19). Although, NO_3^- do not react directly with HO•, but at high concentration NO_3^- may decrease the concentration of HO• indirectly via NO_2^- formation according to Eqs. (4.19-4.21) (Velo Gala *et al.* 2013). The insignificant decrease in *k*-value at 0.1 M NO_3^- ion concentration indicated that the addition of 0.1 M NO_3^- had not substantially affected the AMX degradation as shown in Table 4.10 (*experiment* 8). NO_2^- is considered as inhibitors of HO•, e_{aq}^- and H• (Eqs. (4.22-4.25)) (Ocampo-Pérez *et al.* 2011). The transient products, NO_2 and NO_2^{2-}, have low oxidizing capability when compared to HO• radical and are reluctant to degrade AMX when compared to HO• (Shin *et al.* 2002; Velo Gala *et al.* 2013). Thus, the *k*-value showed significant decrease with the addition of 0.1 M NO_2^- (Table 4.10, *experiment* 9) and this effect was more pronounced as compared to NO_3^- ion. According to Table 4.10 (*experiment* 8 and 9), the *k*-values of AMX radiolysis in the presence of NO_2^- and NO_3^- were 0.026 and 0.127 kGy^{-1}, respectively which were lower than 0.174 kGy^{-1} (Table 4.10, *experiment* 2) in solution without ions.

$$e_{aq}^- + NO_3^- \rightarrow NO_3^{2-} \quad [k = 9.7 \times 10^9 \text{ L mol}^{-1}\text{S}^{-1}] \tag{4.19}$$

$$NO_3^{2-} + H_2O \rightarrow NO_2^{\cdot} + 2OH^- \quad [k = 5.5 \times 10^4 \text{ L mol}^{-1}\text{S}^{-1}] \tag{4.20}$$

$$NO_2^{\cdot} + H_2O \rightarrow NO_3^- + NO_2^- + 2H^+ \quad [k = 6.5 \times 10^7 \text{ L mol}^{-1}\text{S}^{-1}] \tag{4.21}$$

$$NO_2^- + HO^{\cdot} \rightarrow NO_2^{\cdot} + OH^- \quad [k = 5.0 \times 10^9 \text{ L mol}^{-1}\text{S}^{-1}] \tag{4.22}$$

$$NO_2^{\cdot} + HO^{\cdot} \rightarrow HNO_3 \quad [k = 1.0 \times 10^{10} \text{ L mol}^{-1}\text{S}^{-1}] \tag{4.23}$$

$$NO_2^- + H^{\cdot} \rightarrow NO + OH^- \quad [k = 7.2 \times 10^8 \text{ L mol}^{-1}\text{S}^{-1}] \tag{4.24}$$

$$e_{aq}^- + NO_2^- \rightarrow NO_2^{\cdot 2-} \quad [k = 3.5 \times 10^9 \text{ L mol}^{-1}\text{S}^{-1}] \tag{4.25}$$

It can be seen from the Eqs. 4.26-4.28 that SO_4^{2-} ion have low or no reactivity towards HO•, e_{aq}^- and H•, respectively (Khan *et al.* 2015; Liu *et al.* 2015). Therefore, addition of SO_4^{2-} ions in the solution had not substantially affected the degradation efficiency of AMX when compared to the other additives. On the other hand, SO_3^{2-} significantly decreased the degradation of AMX which might be due to the reason that SO_3^{2-} can act as a scavenger of HO• with a high rate constant (Eq. 4.29) (Liu *et al.* 2015). According to Table 4.10 (*experiment* 12 and 13), the *k*-values of AMX radiolysis in the presence of SO_4^{2-} and SO_3^{2-}

were 0.155 and 0.038 kGy^{-1}, respectively which were lower than 0.174 kGy^{-1} (Table 4.10, *experiment* 2) in solution without ions.

$$SO_4^{2-} + e_{aq}^- \rightarrow SO_4^{3-} \quad [k < 1.0 \times 10^6 \text{ L mol}^{-1}\text{S}^{-1}] \tag{4.26}$$

$$SO_4^{2-} + H^{\cdot} \rightarrow \text{No reaction reported} \tag{4.27}$$

$$SO_4^{2-} + HO^{\cdot} \rightarrow \text{No reaction reported} \tag{4.28}$$

$$SO_3^{2-} + e_{aq}^- \rightarrow .SO_3^- + HO^- \quad [k = 5.5 \times 10^9 \text{ L mol}^{-1}\text{S}^{-1}] \tag{4.29}$$

In order to make clear the comparative contribution of $HO^{\bullet}$, $H^{\bullet}$ and e_{aq}^- on AMX radiolysis, the degradation was studied in the presence of different concentrations of 0.1 M propanol and thiourea. 28.0 and 14.1% degradations were observed with 0.1 M propanol and thiourea, respectively at 15.0 kGy dose and the results are shown in Table 4.10 (*experiments* 14-15). It was observed that in the presence of these scavengers, the degradation efficiencies were diminished. The obvious decrease of AMX degradation can be ascribed to the loss of reactive species. Propanol can react with $HO^{\bullet}$ and $H^{\bullet}$, which are summarized as Eqs. (4.30-4.31) (Khan *et al.* 2015):

$$HO^{\cdot} + (CH_3)_2CHOH \rightarrow (CH_3)_2{}^{\bullet}COH + H_2O \quad [k = 1.9 \times 10^9 \text{ L mol}^{-1}\text{S}^{-1}] \tag{4.30}$$

$$H^{\cdot} + (CH_3)_2CHOH \rightarrow (CH_3)_2{}^{\bullet}COH + H_2 \quad [k = 7.4 \times 10^7 \text{ L mol}^{-1}\text{S}^{-1}] \tag{4.31}$$

On the other hand, thiourea is an active scavenger of all the primary reactive species (Eqs. 4.32-4.34) generated during water radiolysis ($HO^{\bullet}$, e_{aq}^- and $H^{\bullet}$) (Basfar *et al.* 2005; Sánchez-Polo *et al.* 2009).

$$HO^{\cdot} + H_2NCSNH_2 \rightarrow \text{unknwon products} \quad [k = 3.9 \times 10^9 \text{ L mol}^{-1}\text{S}^{-1}] \tag{4.32}$$

$$H^{\cdot} + H_2NCSNH_2 \rightarrow \text{unknwon products} \quad [k = 6 \times 10^9 \text{ L mol}^{-1}\text{S}^{-1}] \tag{4.33}$$

$$e_{aq}^- + H_2NCSNH_2 \rightarrow \text{unknwon products} \quad [k = 2.9 \times 10^9 \text{ L mol}^{-1}\text{S}^{-1}] \tag{4.34}$$

The negative impact on the AMX degradation in the presence of certain additives was found in the following decreasing order: thiourea > NO_2^- > propanol > SO_3^{2-} > CO_3^{2-} > HCO_3^- > NO_3^- > SO_4^{2-}. The degradation of model compounds can happen through the oxidation pathways by the reaction with oxidizing $HO^{\bullet}$ radicals. That is why, when the

parallel competitive reaction paths of HO• were opened up in the presence of scavengers (NO_2^-, SO_3^{2-}, propanol and thiourea) the extent of degradation (C/C_0) significantly decreased due to the lack of extent of reaction between model compounds and HO•.

4.4.4 Effect of oxidant on gamma radiolytic degradation of model compounds

Production of HO• radicals increase in the presence of strong oxidant like, H_2O_2 and subsequently G-value of HO• may increase Eq. (4.35) (values in the bracket indicates the G-value in μmol J^{-1}) (Le Caër, 2011). However, higher concentration of H_2O_2 may inhibit HO• generation, therefore it needs to be optimized (Woods and Pikaev, 1994). Figure 4.30 depicts the effect of H_2O_2 on the degradation of OFX and ORZ by gamma radiolysis and the corresponding results obtained are shown in Table 4.8 (experiments 13–16) and Table 4.9 (experiments 12–15). Fig. 4.31 show the results of gamma radiolytic degradation of AMX in the presence of H_2O_2 and the corresponding results obtained are shown in Table 4.10 (experiments 16–20).

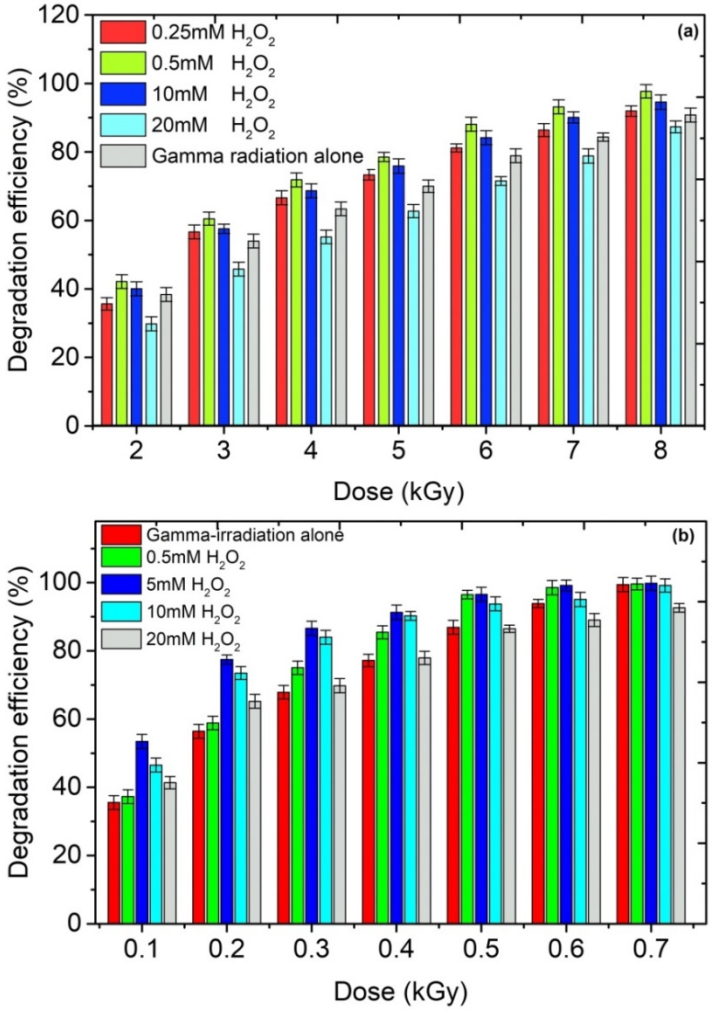

Fig. 4.30 Effect of H_2O_2 on gamma radiolytic degradation of (a) OFX and (b) ORZ

The results exhibited that the addition of concentration of 5 mM H_2O_2 favoured OFX degradation with *k*-values of 1.357 kGy^{-1}, respectively versus the *k*-value (1.159 kGy^{-1}) obtained without the addition of H_2O_2 at pH 6.5 (Table 4.8, experiment 2). The results showed that the addition of concentration of 0.5 and 5 mM H_2O_2 favoured ORZ degradation with k values of 1.970 and 2.234 kGy^{-1}, respectively versus the k value (1.483 kGy^{-1}) obtained without the addition of H_2O_2 at pH 6.5 (Table 4.9, experiment 2). In case of AMX, addition of concentration of 0.5 and 2.5 mM H_2O_2 favoured AMX degradation with k values of 0.190 and 0.236 kGy^{-1}, respectively versus the *k*-value (0.174 kGy^{-1}) obtained without the addition of H_2O_2 at pH 6.5 (Table 4.10, experiment 2).

This can be explained by the fact that the rapid reaction of H_2O_2 with e_{aq}^- (Eq. 4.36) and $H^{\bullet}$ (Eq. 4.37) enhances the $HO^{\bullet}$ radical concentration in the aqueous solution and thus helped to enhance the degradation efficiency of model compounds (Buxton *et al.* 1988).

$$H_2O_2 - \gg 2HO^{\cdot}[0.28 + 0.28 = 0.56] \quad (4.35)$$

$$H_2O_2 + e_{aq}^- \rightarrow HO^{\cdot} + OH^- [k = 1.1 \times 10^{10}\ L\ mol^{-1}s^{-1}] \quad (4.36)$$

$$H_2O_2 + H^{\cdot} \rightarrow HO^{\cdot} + H_2O\ [k = 9.0 \times 10^{7}\ L\ mol^{-1}s^{-1}] \quad (4.37)$$

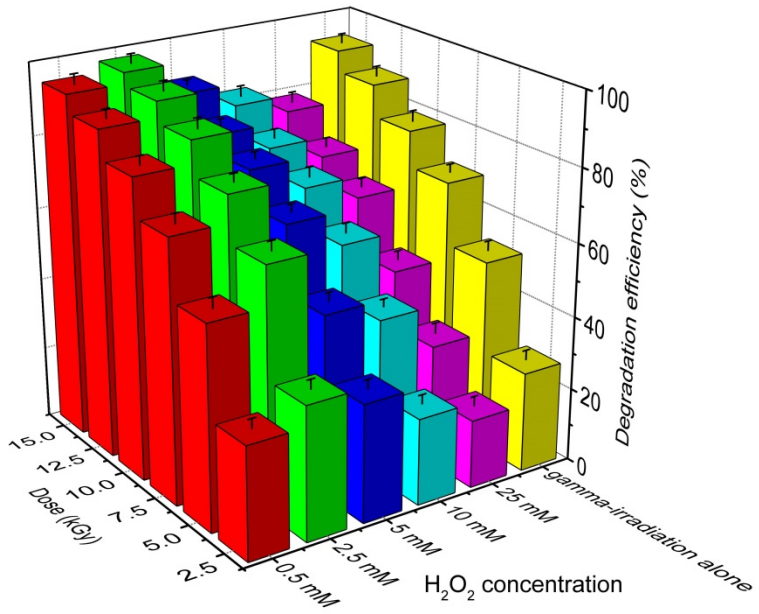

Fig. 4.31 Effect of H_2O_2 on gamma radiolytic degradation of AMX

However, *k*-values reduced with initial H_2O_2 concentration of 10 mM for OFX and ORZ, and 5 mM for AMX. It indicates that reactions (4.38) and (4.39) predominantly occur

at this H_2O_2 concentration, generating less reactive peroxyl radical species compared to HO• radical (Buxton *et al.* 1988). Moreover, the formed peroxyl radical species facilitates the recombination reaction with HO• radical (Eq. (4.39)) resulting a decrease in the *k* value.

$$HO^{\cdot} + H_2O_2 \rightarrow HO_2^{\cdot} + H_2O \; [k = 2.7 \times 10^7 \text{ L mol}^{-1}\text{s}^{-1}] \quad (4.38)$$

$$HO^{\cdot} + HO_2^{\cdot} \rightarrow H_2O + O_2 \; [k = 6.0 \times 10^9 \text{ L mol}^{-1}\text{s}^{-1}] \quad (4.39)$$

Accordingly, optimal concentration of H_2O_2 in the gamma radiolytic degradation of OFX, ORZ and AMX were found to be 0.5, 5 and 2.5 mM, respectively under the given experimental conditions. These results are consistent with the above section assuming that HO• radical is the primary species accountable for model compounds degradation.

4.4.5 Effect of oxidant on mineralization efficiency of model compounds

The radiolysis treatment efficiency not only depends on the potency of radiolytic degradation of model compound but also on the extent of mineralization of the compound and intermediates generated. Thus, the TOC removal of the irradiated aqueous solutions of OFX, ORZ and AMX at different doses was assessed to evaluate the effect of H_2O_2 on the extent of mineralization of OFX (Fig. 4.32a), ORZ (Fig. 4.32b) and AMX (Fig. 4.32c), respectively. The removal of TOC for OFX and ORZ were found to be ~29.6 and 35% at an absorbed dose of 3.0 kGy in absence of H_2O_2, whereas for AMX, the TOC removal was 39.8% at an absorbed dose of 15.0 kGy in the absence of H_2O_2. As depicted in Fig. 4.32a, when compared to gamma irradiation alone, the TOC removal of OFX increased to 33% with 0.25 mM H_2O_2 addition and to 36.1% with addition of 0.5 mM H_2O_2. In case of ORZ, when compared to gamma irradiation alone, the TOC removal of ORZ increased to 38.4% with 5 mM H_2O_2 addition and to 44% with addition of 10 mM H_2O_2. In case of AMX, when compared to gamma irradiation alone, the TOC removal of AMX increased to 47.8% with 2.5 mM H_2O_2 addition. For gamma irradiation/H_2O_2 process, rather enhanced TOC removals were observed indicating that the presence of H_2O_2 had more obvious effect on mineralization of model compounds than on its degradation. For example, it can be seen from Figs. 4.32b, with the initial H_2O_2 concentration of 0.5, 5, 10, and 20 mM, the degradation efficiency of ORZ was found to be 99.5, 99.7, 99.1, and 92.6% respectively, whereas the TOC removal efficiency was found to be 34.9, 38.4, 44.0, and 57%, respectively. The concentration of HO• increases during radiolysis in presence of H_2O_2 due to the conversion of the reducing species, e_{aq}^- and H•, into HO• (Eqs. 4.36 and 4.37). The generated HO•, reacts non-selectively with model compounds, its degradation intermediates and eventually leads to

the enhanced mineralization. However, at an absorbed dose of 3.0 kGy (in case of OFX and ORZ) and 15.0 kGy (in case of AMX), organic by-products formed during degradation are expected to exhibit remaining TOC in the solutions despite almost complete degradation of model compounds. The enhancement of TOC reduction in the gamma/H_2O_2 process indirectly supports the mechanistic interpretation of the enhanced degradation due to the supplementary $HO^{\bullet}$ production in the gamma/H_2O_2 process. Similar results were also documented in the decomposition of chlorophenols (Hu and Wang, 2007), sulfamethazine (Liu and Wang, 2013), nitrophenol (Yu *et al.* 2010), and dyes (Wang *et al.* 2006) under irradiations.

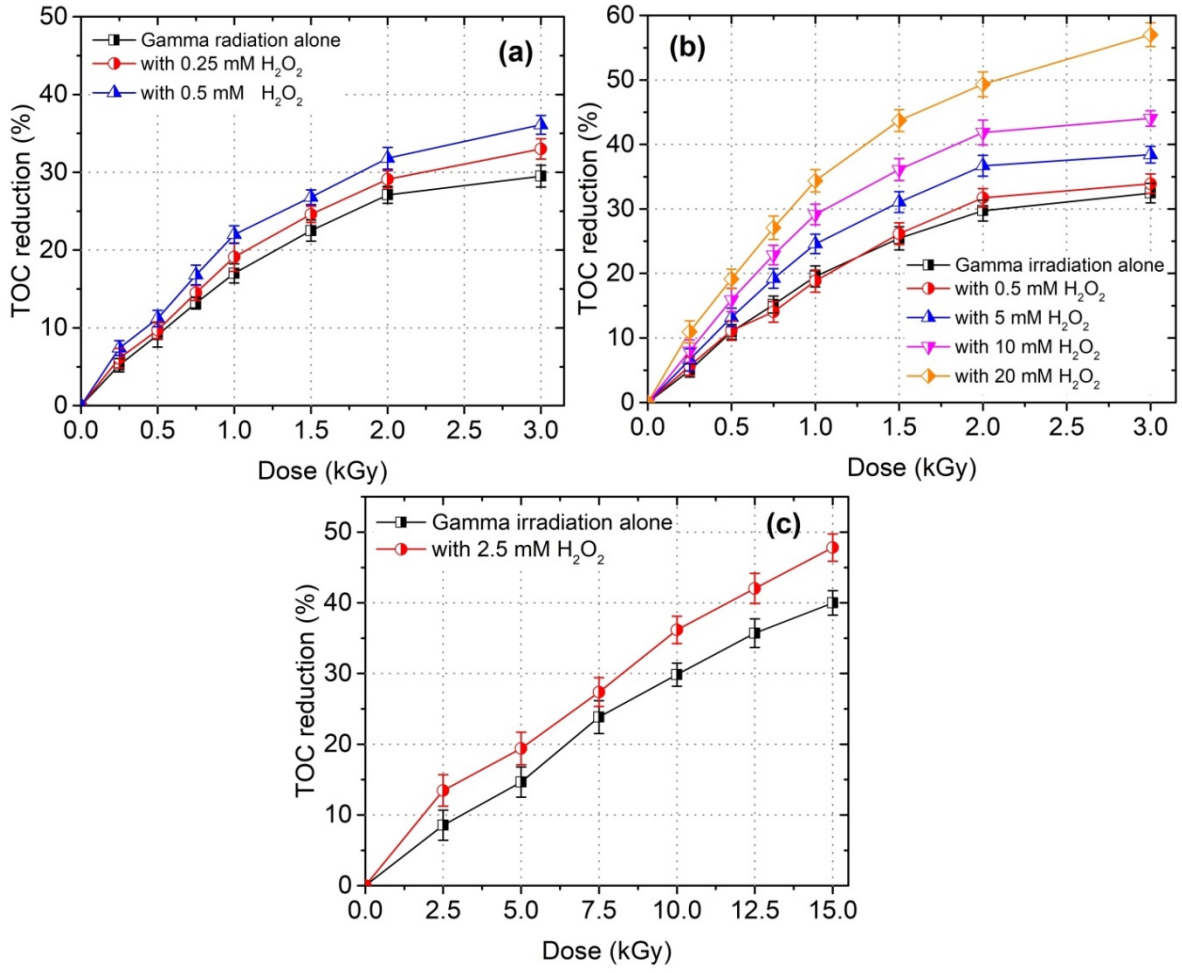

Fig. 4.32 Effect of absorbed dose and initial H_2O_2 concentration on TOC reduction of (a) OFX (b) ORZ and (c) AMX

4.4.6 LC-MS analysis of gamma irradiated solutions of OFX

Different AOP methods intended at contaminant oxidation results in different transformed products. Although with certain similarities, degradation pathways of OFX in these approaches differ from each other (Michael *et al.* 2010; Vasquez *et al*. 2013; Pi *et al.*

2014). This section is focused on the degradation pathways of OFX as well as the identification of the intermediate/degradation products formed in gamma radiolytic degradation of OFX. Fig. 4.33a and 4.33b shows the TIC chromatograms and ESI mass spectrum recorded with positive mode for 0.1 mM OFX solution irradiated with 1.0 and 2.0 kGy absorbed doses, respectively (where about 68% and 88% degradation of OFX occurs). Based on the data of LC-QTOF-MS analysis, the possible transformation pathways of OFX under gamma radiolysis can be inferred in Fig. 4.34.

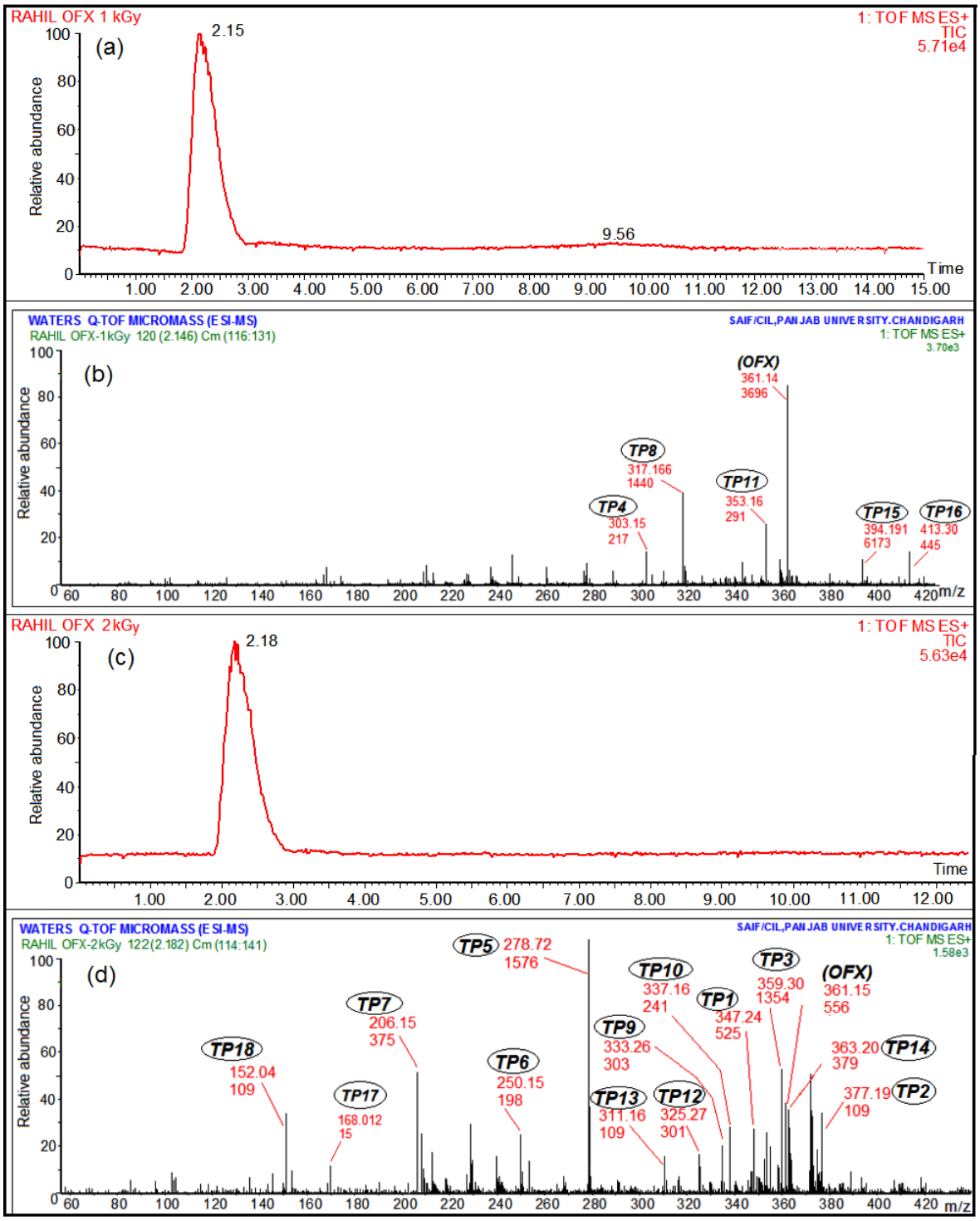

Fig. 4.33 (a) & (b) Total ion current chromatograms and ESI mass spectra recorded for aqueous solution of irradiated OFX at 1.0 kGy (c) & (d) Total ion current chromatograms and ESI mass spectra recorded for aqueous solution of irradiated OFX at 2.0 kGy

Overall, as many as 18 transformed products (TPs) were tentatively identified, with their peak intensity being greater than 10%, thus allowing the precise identification of TPs.

Based on the *m/z* values obtained through LC-QTOF-MS and the results of previous studies on OFX oxidation, quite a few degradation pathways are proposed, in which decarboxylation, hydroxylation, piperazinyl dealkylation, oxidation of hydroxyl group and cleavage of OFX molecule are described as main transformation mechanisms (Hapeshi *et al.* 2010; Vasquez *et al.* 2013). Several intermediates were identified in this study, the formations of which were attributed to transformation at the piperazinyl substituents. **TP1** (*m/z* 348) might be formed by dimethylation of piperazinyl ring. Formation of **TP2** (*m/z* 378) could be ascribed to hydroxylation at the piperazinyl ring, as identically obtained in the degradation of ciprofloxacin in the earlier report (De Witte *et al.* 2008). **TP2** could be considered as the promoter for the formation of **TP3** (*m/z* 360) by dehydration on **TP2**. Further oxidation at piperazinyl substituents of OFX molecule might lead to the formation of **TP4** (*m/z* 304) and **TP5** (*m/z* 279). More specifically, **TP4** could be formed due to the opening of *N*-piperazine ring and **TP5** formation could be ascribed to the oxidation of the piperazine side chain till this intermediate could be reduced to an amino group. In correspondence with the oxidation of the *N*-piperazine ring, **TP6** (*m/z* 251) might be formed from **TP5** after losing a carbonyl moiety. Subsequent oxidation treatment arising from the loss of CO_2 from **TP6** could lead to the formation of **TP7** (*m/z* 207).

TP 8-10 represents the major intermediates which might be formed due to the cleavage of OFX molecule at quinolone moiety under gamma radiolysis. **TP8** with *m/z* 318 analogous of OFX formed after the subsequent oxidation due to decarboxylation, as is in agreement with the reported study (Vasquez *et al.* 2013). Attack at the quinolone moiety of OFX could result into the formation of carbon-centered ring radical, leading to the identification of **TP9** (*m/z* 334), as identically obtained from the oxidation of enrofloxacin in the earlier report (Karl *et al.* 2006). **TP10** (*m/z* 338) might have formed from **TP9** after the cleavage of the double-bonded side chain on the C-ring structure of OFX molecule with a keto group.

A by-product with *m/z* 354 was identified and labelled as **TP11**, which usually formed via attack of $HO^{\bullet}$ on heterocyclic ring-D. **TP11** could be considered as the promoter to form **TP12** (*m/z* 326) and **TP13** (*m/z* 312). **TP 12** was formed via cleavage of C-C bond and loss of the hydroxyl group form the heterocyclic ring-C of **TP11**. Removal of the methyl group attached to the N of heterocyclic ring-C of **TP12** would give **TP13** at *m/z* 312. Furthermore, the breakdown of the heterocyclic ring-C of OFX molecule would generate **TP14** (*m/z* 364) having keto acid group, not reported so far in previous studies.

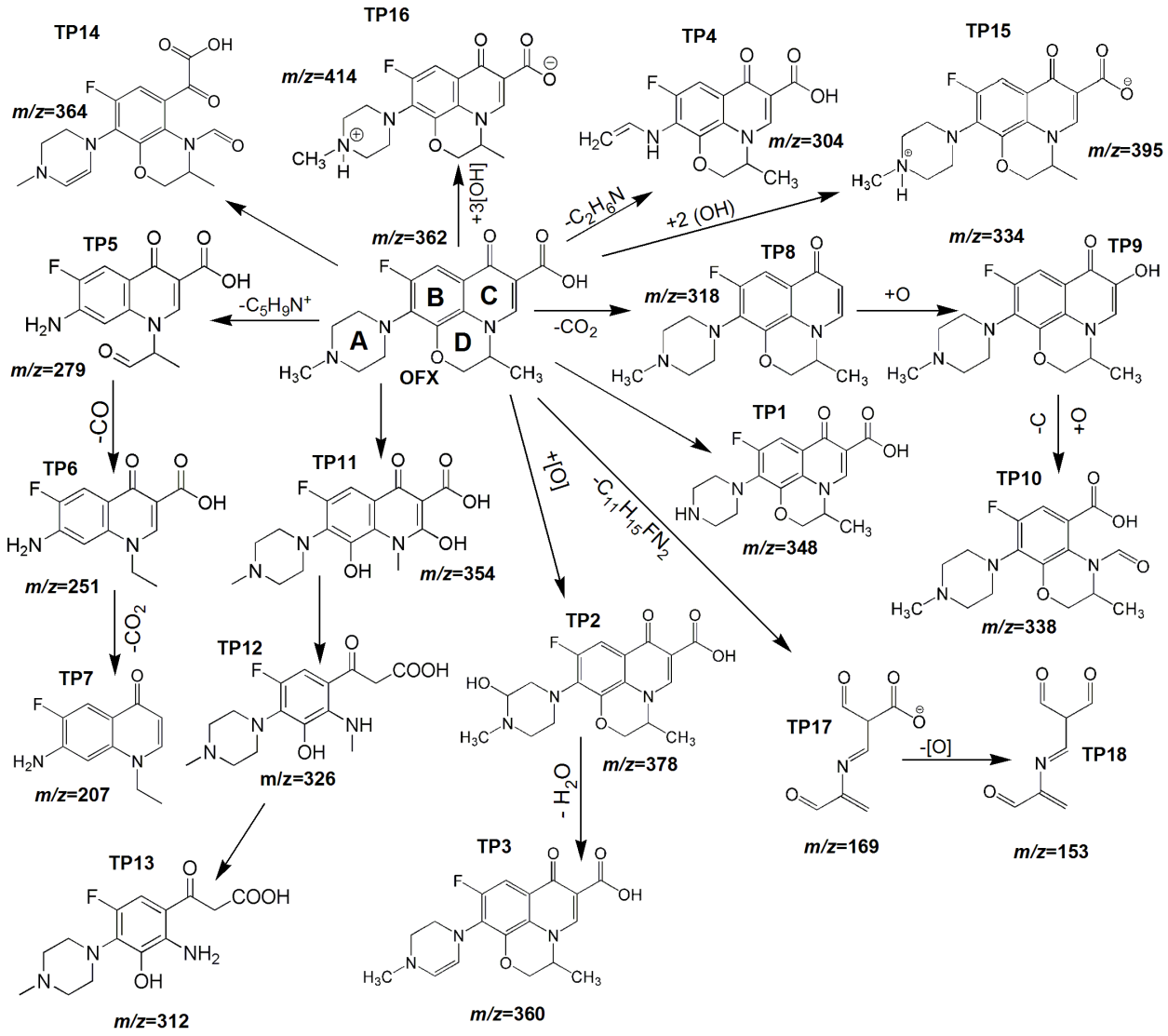

Fig. 4.34 Proposed transformation pathways of gamma radiolytic degradation of OFX

As HO• radicals could not able to show a high extent of selectivity to numerous functional groups, some isobaric compounds might have formed. Subsequent HO• radical attack on OFX could lead to the formation of bi-hydroxylated (**TP15**, *m/z* 395) and tri-hydroxylated (**TP16**, *m/z* 414) transformed products, such as 2-OH-OFX and 3-OH-OFX, respectively. Additionally, cleavage products **TP17** (*m/z* 169) and **TP18** (*m/z* 153) were identified that remained until the end of experiment. **TP17** might have formed after the loss of $C_{11}H_{15}FN_2$ and again oxygen atom removal from **TP17** would generate **TP18**. As shown, these cleavage compounds have a heterocyclic amine ring, which remained intact. These TPs (**TP17 and TP18**) were identified in greater abundance in gamma radiation-induced treatment of OFX at an absorbed dose of 2.0 kGy.

It can be observed that fluorine was present in most of the identified TPs (Fig. 4.34),

and its presence would result in conflict with most of the earlier studies on effective release of fluorine with the assistance of HO• radical for the degradation of fluorinated quinolone antibiotics (De Witte *et al.* 2009; Liang and Su, 2009).

4.4.7 LC-MS analysis of gamma irradiated solutions of ORZ

Gaussian 03 Software (Frisch *et al.* 2003) at density functional theory with B3LYP/6-31G(d) level was considered to optimize the geometry structure of ORZ molecule, which might be used to evaluate the charge distribution of the ORZ molecule through Gaussian calculations. Fig 4.35 shows the result of charge distribution of ORZ obtained by Gaussian calculation. It was found that C[16] had the highest negative charge (− 0.574). Therefore, the strong electrophilic species HO• radicals can attack to C[16] atom. As a result, the bond Cl[19]– C[16] becomes most susceptible to be cleaved to form new intermediates as also evidenced from product analysis studies in the subsequent section. Thus, we can presume that the gamma-radiolytic degradation of ORZ is mainly attributed to HO• oxidation. In addition, O[14] (− 0.507) possess the second higher negative charge, which shows that HO• radical can also attack O[14]. Similarly, the bonds of C[21]–H[24], C[12]–C[9],N[1]–C[20], and N[9]–C[8] may be possibly broken due to negative charges. Based on the prediction of Gaussian calculations, we can propose the possible cleavage of bonds of O[14]–C[12], H[24]–C[21], N[9]–C[8], C[20]–N[1], C[9]–C[12], and C[16]–Cl[19] under gamma radiolysis and subsequent formation of some new products.

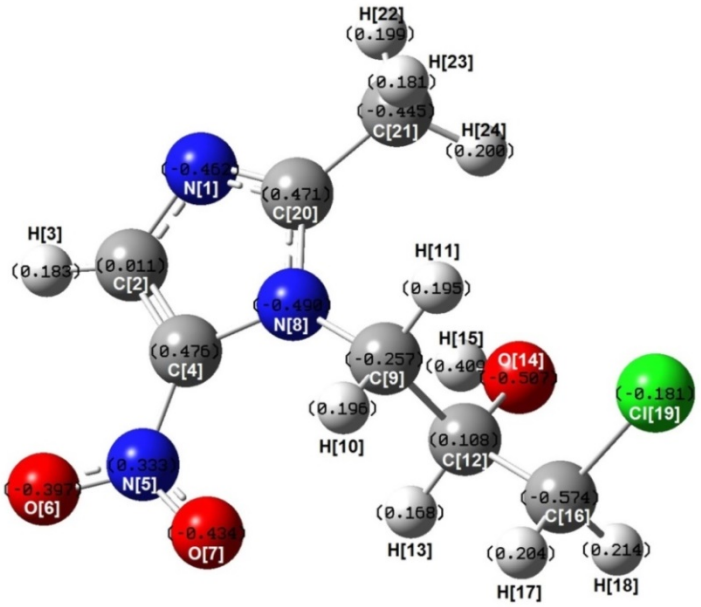

Fig. 4.35 ORZ molecule structure and its charge distribution

To confirm the formation of intermediates/products from the gamma radiolytic degradation of ORZ, the reaction by-products of irradiated solutions were analyzed by LCQTOF-MS. The radiolytic degradation products of 0.22 mM ORZ at an absorbed dose of 2.0 kGy were identified using LC-QTOF-MS. Six major decomposition by-products were identified, and their retention time as well as molecular structure is listed in Table 4.9. Based on the obtained results, the removal pathways of gamma-induced radiolytic degradation of ORZ can be inferred in Fig. 4.36. In one instance, HO• radicals can react with ORZ to generate intermediate A (ornidazole epoxide), which represents one of the oxidative degradation products of ORZ as discussed in previous studies (Zhao *et al.* 2012; Salo *et al.* 2003). The obtained intermediate is in consistent with the results of Gaussian calculations. The second instance may be the direct degradation of ORZ under gamma radiolysis. Further, breaking of C[9]–C[12] bond in ornidazole epoxide generates intermediate C (1,2-dimethyl-5-nitroimidazole), which further generates intermediate D (2-methyl-5- nitroimidazole) by demethylation of intermediate C (Salo *et al.* 2003). In addition, the intermediate D may also be generated by breaking of N[8]–C[9] bond in intermediate A (ornidazole epoxide). Further, intermediate B (ornidazole glycol) can be generated from ORZ by hydrolytic halogenation of aliphatic halomethyl Cl[19]. In addition to this, intermediate B is expected to be formed from intermediate A by the attack of HO• radicals (Salo *et al.* 2003). Combining with the optimization results of ORZ molecule, B was cleaved, leading to D and to a moiety corresponding to the hydroxylated aliphatic chain, itself being oxidized to E and F.

Based on the intermediate B, the products of E and F could be generated during the gamma radiolysis due to the instability of O[14]– C[12], N[8]–C[9], C[21]–H[24], and N[1]–C[20] bonds. Therefore, we could attribute the main degradation mechanism of ORZ during gamma radiolysis to HO• radicals oxidation and the direct degradation of ORZ molecule. In addition, results of LC-QTOF/MS and the Gaussian calculations are able to predict the ORZ degradation mechanism.

Table 4.11 Intermediate compounds during gamma-radiolytic degradation of ORZ

Compound	Retention Time (min)	Observed m/z [M+H]	Calculated m/z $[M+H]^+$	Elemental composition	Proposed structure $[M+H]^+$
ORZ	5.35	221.0019	219.0381	$C_7H_{10}ClN_3O_3$	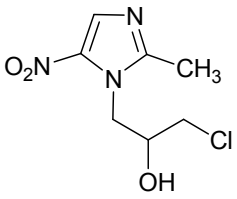
A	5.12	184.0030	184.06439	$C_7H_9N_3O_3$	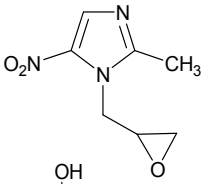
B	5.18	201.0030	201.07496	$C_7H_{11}N_3O_4$	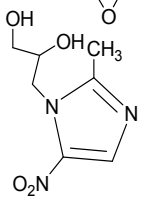
C	2.46	142.0294	142.05385	$C_5H_7N_3O_2$	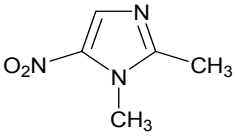
D	3.32	128.0560	128.03818	$C_4H_5N_3O_2$	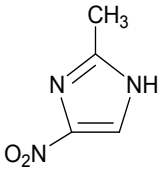
E	5.12-5.18	104.0521	104.01096	$C_3H_4O_4$	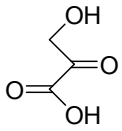
F	5.12-5.18	104.0521	104.01096	$C_3H_4O_4$	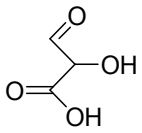

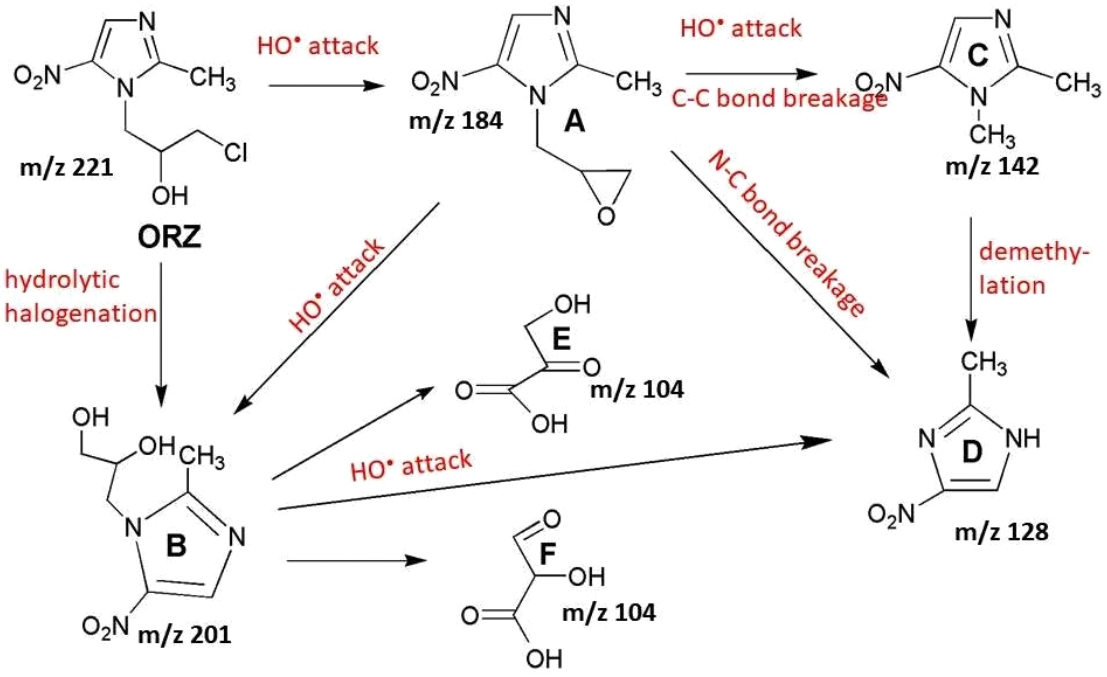

Fig. 4.36 The main degradation pathways of ORZ during gamma radiolysis

4.4.8 Toxicity analysis of gamma irradiated solutions of model compounds

Assessment of changes in the toxicity of irradiated solutions is an important parameter in order to investigate the efficacy of degradation process. Thus, cytotoxicity of un-irradiated and irradiated aqueous OFX solutions at 2.0 and 3.0 kGy of absorbed dose were evaluated. Toxicity analysis was performed through agar well diffusion assay against *E. coli* taking pure solution of OFX (0.1 mM) as control. Unlike the un-irradiated OFX solution, no zone of inhibition was observed in the irradiated solutions and thus indicating that irradiated OFX solutions did not acquire any toxicity as shown in Fig. 4.37.

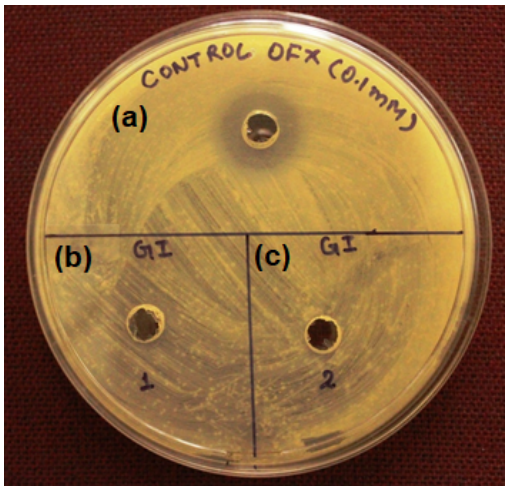

Fig. 4.37 Cytotoxicity activity of aqueous solutions of OFX under gamma radiation (a) before irradiation (b) after 2.0 kGy absorbed dose and (c) after 3.0 kGy absorbed dose

The toxicity potential of ORZ and its irradiated solutions (at different absorbed dose) was studied against clinical isolates of three microbes: *E. coli, B. subtilis, and P. aeruginosa*. The results indicate that the irradiated as well as un-irradiated ORZ solution (i.e., 0.22 mM ORZ concentration) did not showed any toxicity against any of the microbes (Fig. 4.38). Thus, it can be concluded that the parent compound (ORZ) as well as the intermediates produced during gamma radiolytic degradation of ORZ are non-toxic to the studied microbes. However, as discussed in the "Mineralization study" Section 4.3.5, the TOC of the solution significantly decreased upon gamma irradiation and this is important for the availability of dissolved oxygen in water.

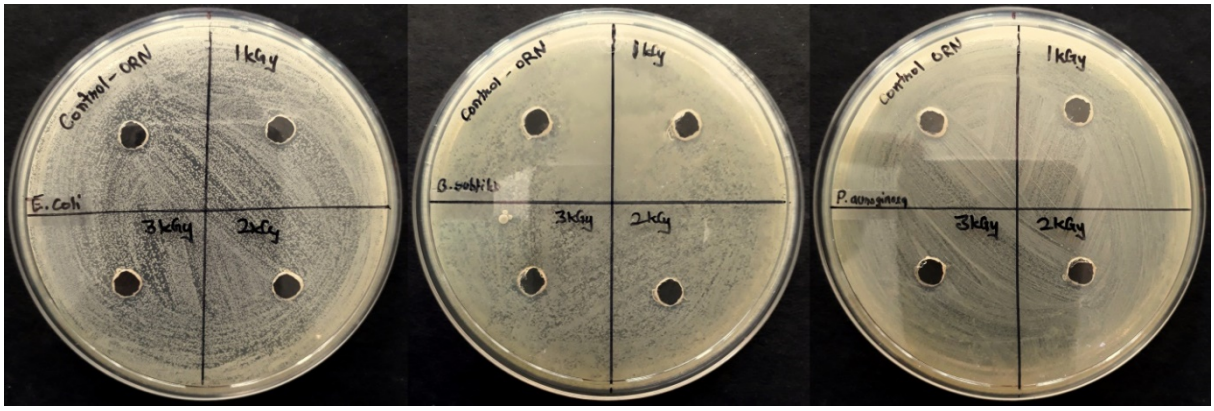

Fig. 4.38 Inhibition rate of activity of ORZ solutions before and after gamma irradiation against (a) *B. subtilis (b) P. aeruginosa (c) E. coli*

The toxicity potential of AMX and its irradiated solutions (at different absorbed dose) was also studied against clinical isolates of *E. coli, B. subtilis, and P. aeruginosa*. The results indicate that unlike the un-irradiated AMX solution, no zone of inhibition was observed in the irradiated solutions and thus indicating that irradiated AMX solutions did not acquire any toxicity after gamma irradiation treatment as shown in Fig. 4.39. Thus, it can be concluded that the intermediates/by-products produced during gamma radiolytic degradation of AMX are non-toxic to the studied microbes.

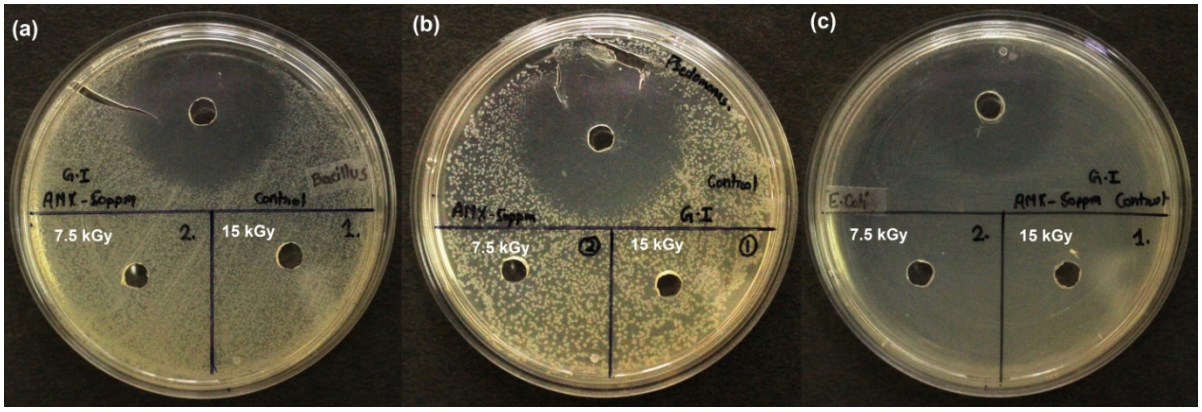

Fig. 4.39 Inhibition rate of activity of AMX solutions before and after gamma irradiation against (a) *B. subtilis (b) P. aeruginosa (c) E. coli*

4.4.9 Cost analysis of gamma irradiated treatment of model compounds

The efficiency of gamma radiolysis for the treatment of model compounds was evaluated in terms of cost of energy consumed. Since gamma irradiations do not involve electrical energy, the cost of energy could be calculated by accounting for five effective half-lives of ^{60}Co source using the given Eq. 4.40.

$$ATC = R \times I \times t/(t_{1/2} \times v \times 365 \times 24) \times (1000/v) \quad (4.40)$$

where ATC is the average treatment cost in INR m^{-3}, I is the initial activity of ^{60}Co source in Curie (Ci), R is the price of ^{60}Co source/Ci, t is the time of treatment in hours, $t_{1/2}$ is the half-life of ^{60}Co source in hours, and v is the maximum volume capacity of the gamma chamber (in L) that can be treated in time (t). In my study, total volume capacity of the gamma chamber was 5 L with the initial activity of ^{60}Co source to be 10,000 Ci and involving a cost of INR 70 Ci^{-1}. The cost involved during gamma radiolysis was calculated based on the 90% degradation efficiency of 0.1 mM OFX and 0.22 mM ORZ at an absorbed dose of 3.0 kGy. For AMX, cost involved was calculated based on the 90% degradation efficiency of 0.1 mM AMX at an absorbed dose of 15.0 kGy; so assumption of any other auxiliary chemical or reagent was neglected. The results obtained are presented in Table 4.12. The total cost of gamma radiolysis of OFX, ORZ and AMX was found to be 32.3, 39.6 and 17.3 INR m^{-3}.

Table 4.12 Cost involved during gamma radiolysis of model compounds

Model compound	Average treatment time (hr) of compound	Total ATC (INR m^{-3})	Total ATC (USD m^{-3})
ORZ	2.33*	32.3	0.45
OFX	2.86*	39.6	0.56
AMX	1.25**	17.3	0.24

*Guided by the working dose rate during experimentations for OFX and ORZ i.e. 0.75 kGy h^{-1}

**Guided by the working dose rate during experimentations for AMX i.e. 10.9 kGy h^{-1}

4.5 E-beam irradiation treatment of model compounds

After gamma radiolytic treatment of model compounds, all the model compounds (OFX, ORZ and AMX) were independently treated using electron beam (E-beam) irradiation under different experimental conditions. Degradation efficiency, degradation mechanism, toxicity and cost analysis were evaluated for the treatment process.

4.5.1 E-beam radiolytic degradation of model compounds

The E-Beam induced radiolytic degradation of OFX and AMX was investigated with four different initial concentrations of 0.05, 0.1, 0.15 and 0.2 mM, whereas E-Beam induced radiolytic degradation of ORZ was investigated with different initial ORZ concentrations of 0.11, 0.22, 0.31 and 0.45 mM. As exhibited in Fig. 4.40, OFX, ORZ and AMX with low concentration could be efficiently degraded at a given dose. At 3.0 kGy dose, 99 and 94% of OFX degradations were accomplished at initial concentrations of 0.05 and 0.1 mM, respectively, and 99.5 and 96.6% of ORZ degradations at initial concentrations of 0.11 and 0.22 mM. At 15.0 kGy dose, 95 and 88.4% of AMX degradations were accomplished at initial concentrations of 0.05 and 0.1 mM, respectively implying that E-Beam irradiation could be an extremely effective approach for OFX, ORZ and AMX degradation. Herein, the OFX, ORZ and AMX concentration decreased exponentially with increased dose which could be well described by *pseudo first-order* reaction kinetics model Eq. (3.4). The values of dose constant, *k*, could be calculated from Eq. (4.41), a modified version of Eq. (3.4), from the linear least-squares fit of the obtained experimental results.

$$\ln C = lnC_o - kD \tag{4.41}$$

Based on the data in Fig. 4.40, a linear relationship was found between -ln(C/C_o) and dose as presented in inset of Figures. It indicates that E-beam induced radiolysis of model compounds at different initial concentrations followed *pseudo first-order* kinetics model and the calculated corresponding parameters (radiation chemical yields, (G-values) and *k* values) were compared in Table 4.13 (OFX), Table 4.14 (ORZ) and Table 4.15 (AMX). The obtained *k* value was utilized to determine doses needed to achieve 50% ($D_{0.50}$) and 90% ($D_{0.90}$) degradation of OFX, ORZ and AMX using Eqs. (3.2) and (3.3).

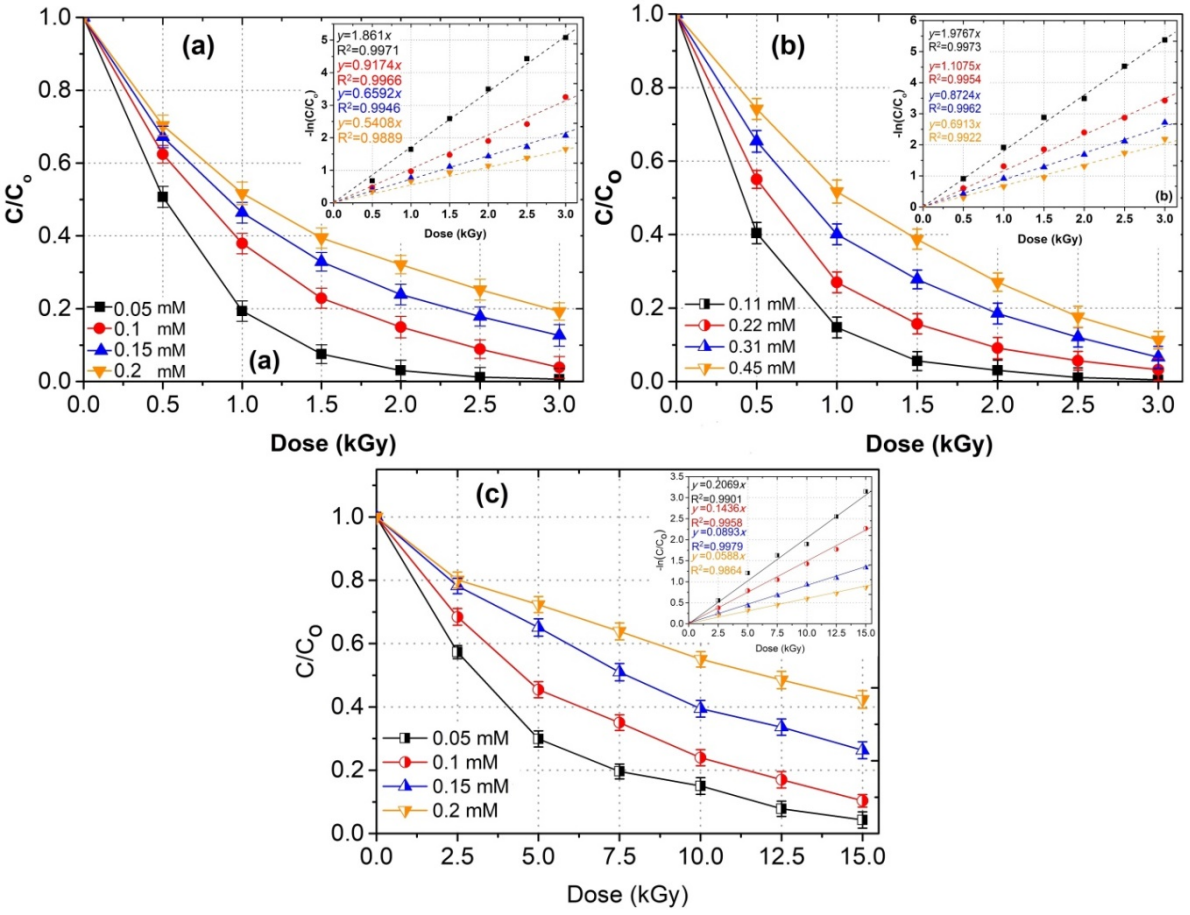

Fig. 4.40 (a) Concentration change of OFX as a function of dose [Inset: Degradation kinetics study of OFX] (b) Concentration change of ORZ as a function of dose [Inset: Degradation kinetics study of ORZ] and (c) Concentration change of AMX as a function of dose [Inset: Degradation kinetics study of AMX]

It was found that the *k*-values decreased from 1.861 to 0.540 kGy^{-1} with the increasing OFX concentration from 0.05 to 0.2 mM, respectively, whereas it decreased from 1.976 kGy^{-1} to 0.691 kGy^{-1} with the increasing ORZ concentration from 0.11 to 0.22 mM, respectively. In case of AMX, *k*-values decreased from 0.206 to 0.058 kGy^{-1} with the increasing AMX concentration from 0.05 to 0.2 mM, respectively. This difference in *k*-values is based on the

assumption that high concentration of model compound increases reaction probability between compound and the radiolytically generated reactive radicals. It results in the accumulation of more number of degradation intermediates which otherwise triggers the simultaneous competition reactions between compound and its intermediates with radiolytically generated reactive radicals at a particular dose. Therefore, at high initial concentration of model compound, higher dose was required to achieve 50 and 90% degradation efficiencies of model compounds with correspondingly low *k*-values (Table 4.12, 4.13 and 4.14) and vice-versa (Magureanu *et al.* 2010; Huang *et al.* 2016). Interestingly, the *k* value of OFX, ORZ and AMX degradation by E-Beam radiation was found to be lower than that obtained by gamma radiolysis of OFX, ORZ and AMX. The dissolved oxygen concentration in the solution depletes with increase in dose. The higher dose rate of E-beam radiation (1 kGy min^{-1}) compared to gamma radiolysis (0.0125 kGy min^{-1}) results in fast depletion of oxygen in the solution, thus requiring higher dose (lower *k* value) to achieve desired degradation of model compounds.

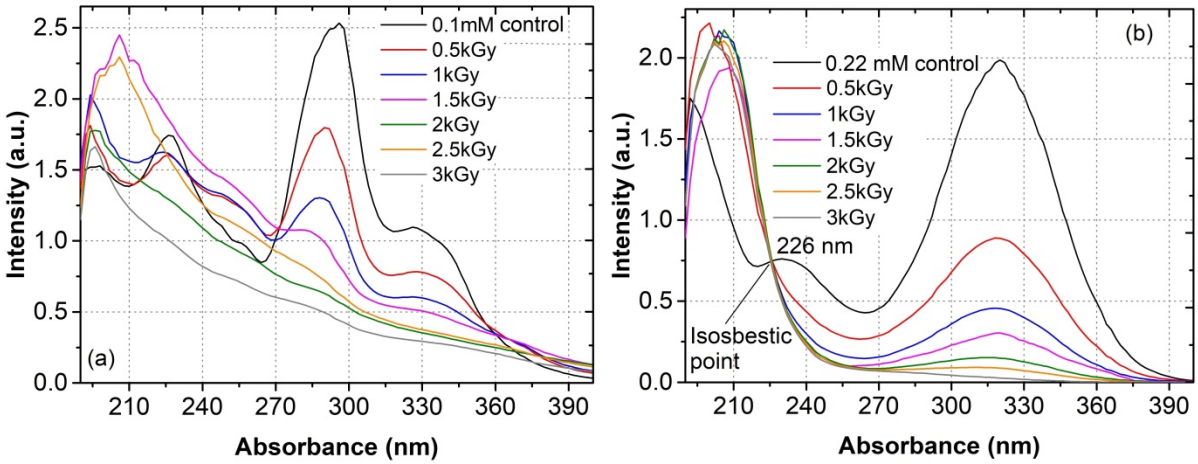

Fig. 4.41 (a) Absorption spectrum of OFX at 190–400 nm after E-beam irradiation treatment (b) Absorption spectrum of ORZ at 190–400 nm after E-beam irradiation treatment

Fig. 4.41a and 4.41b shows the pattern of absorption spectra of OFX and ORZ with different doses. The intensities in the characteristic absorption peaks of OFX at 288 nm decreased with increase in the doses owing to the degradation of OFX. The intensity of absorption peak of ORZ at 320 nm decreased with increasing doses indicating the degradation and break down of parent compound. However, the increased absorption intensity within 190 to 230 nm range also indicates the accumulation of degradation reaction intermediates (Huang *et al.* 2016; Chu *et al.* 2016). The presence of isosbestic point at 226

nm (Fig. 4.41b) signifies the formation and build-up of various by-products during the E-beam irradiation induced degradation of ORZ (el mehdi Benacherine *et al.* 2017).

Generally, the efficacy of irradiation process in degradation study is related to G-value. G-value was calculated for different initial concentrations of model compounds at particular dose and the results are shown in Fig. 4.42. Interestingly, the G-value increased with higher initial concentrations and decreased with increasing dose. This increase in G-value with high initial concentrations of model compounds is expected due to the greater probability for reaction of radiolytically generated reactive radicals with model compound leading to higher degradation (Basfar *et al.* 2005).

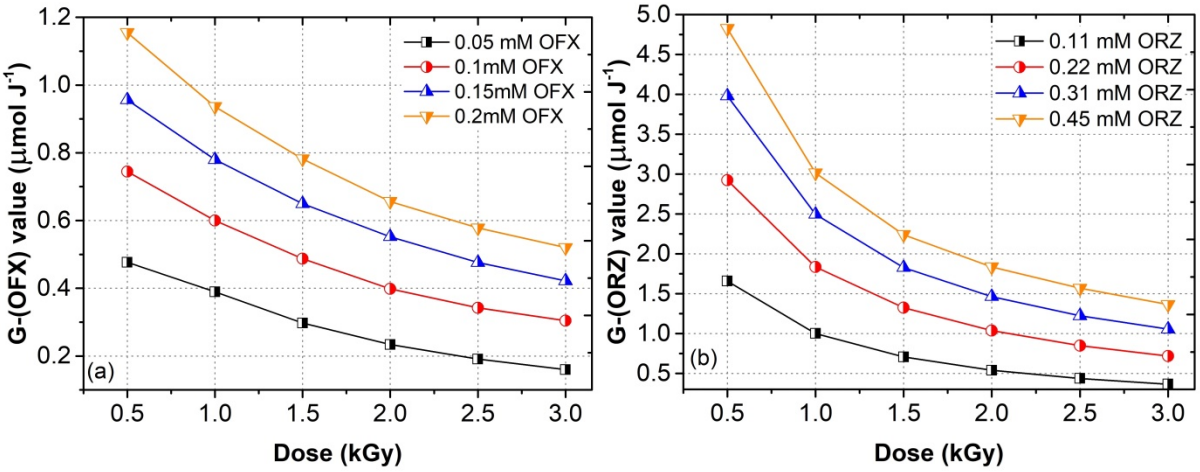

Fig. 4.42 (a) G-values for the degradation of different initial concentration of OFX as a function of dose (b) G-values for the degradation of different initial concentration of ORZ as a function of dose using E-beam irradiation

On the other hand, the competence of E-beam in the degradation of OFX (0.1 mM), ORZ (0.22 mM) and AMX (0.1 mM) was compared between degradation efficiency (%) and G-values (Fig. 4.43). The results revealed that with increasing dose, G-value decreased, though the degradation of compound increased. The decrease in G-value with increase in doses is attributed to the increase in probability of simultaneous competition reactions between parent compound and degraded intermediates of compound for reacting with the radiolytically generated reactive species. Moreover, total reactive radical species concentration increases with accumulated doses and thereby increasing the degradation efficiency of model compounds at each dose (Basfar *et al.* 2005; Sánchez-Polo *et al.* 2009). Initially at very low doses, reactive radicals predominantly react with parent molecules and thus resulting into higher extent of radiation induced degradation. With progress of the reaction, the concentration of degradation intermediates of parent compound increases. It

leads to initiate the parallel competition reactions between parent compound and intermediates with the reactive radicals and thus decreasing the rate of degradation at higher doses.

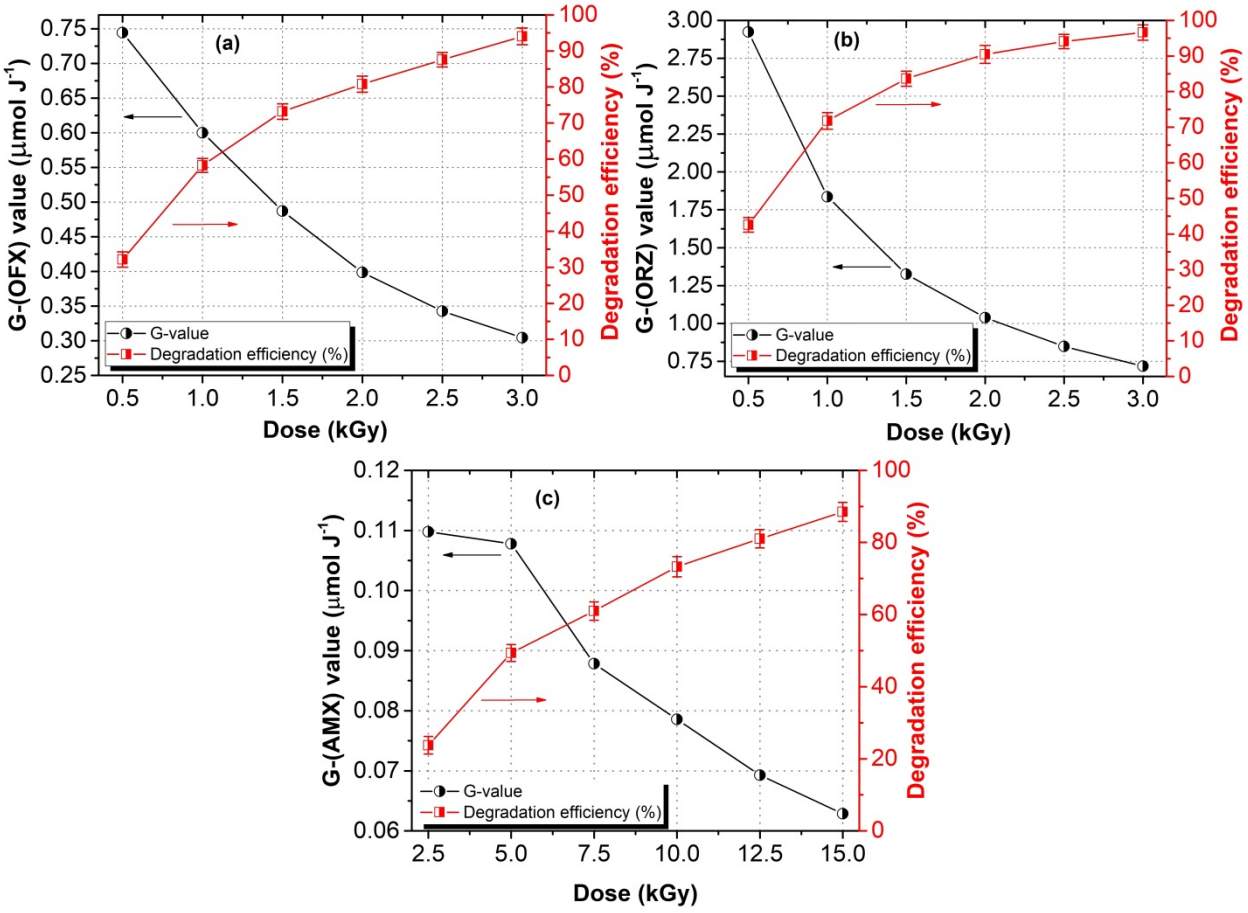

Fig. 4.43 (a) G-values and degradation extent (%) of OFX using E-beam irradiation with $[OFX]_o$=0.1 mM (b) G-values and degradation extent (%) of ORZ using E-beam irradiation with $[ORZ]_o$=0.22 mM (c) G-values and degradation extent (%) of AMX using E-beam irradiation with $[AMX]_o$=0.1 mM

Table 4.13 Experimental data from E-beam induced treatment of OFX: Influence of various parameters. [G-(OFX) calculated for 1.0 kGy dose using Eq. 3.1]

Exp.	Initial [OFX] (mM)	pH	$[NO_2^-$ and $NO_3^-]$ (M)	[Propanol] (M)	[Thiourea] (M)	$[H_2O_2]$ (mM)	G-(OFX) (µmol J^{-1})	k (kGy^{-1})	$D_{0.5}$ (kGy)	$D_{0.9}$ (kGy)
1	0.05	6.5	0	0	0	0	0.389	1.861	0.372	1.237
2	0.1	6.5	0	0	0	0	0.600	0.917	0.755	2.510
3	0.15	6.5	0	0	0	0	0.779	0.659	1.051	3.492
4	0.2	6.5	0	0	0	0	0.936	0.540	1.281	4.257

5	0.1	3	0	0	0	0	0.638	0.949	0.730	2.426
6	0.1	6.5	0	0	0	0	0.603	0.911	0.760	2.526
7	0.1	11	0	0	0	0	0.530	0.703	0.985	3.275
8	0.1	6.5	0.1 NO_2^-	0	0	0	0.320	0.339	2.044	6.792
9	0.1	6.5	0.1 NO_3^-	0	0	0	0.530	0.816	0.849	2.821
10	0.1	6.5	0	0.1	0	0	0.202	0.250	2.772	9.210
11	0.1	6.5	0	0.5	0	0	0.111	0.125	5.545	18.420
12	0.1	6.5	0	0	0.1	0	0.147	0.123	5.635	18.720
13	0.1	6.5	0	0	0.5	0	0.100	0.061	11.36	37.747
14	0.1	6.5	0	0	0	0.5	0.626	0.799	0.867	2.881
15	0.1	6.5	0	0	0	2.5	0.692	0.911	0.760	2.527
16	0.1	6.5	0	0	0	5	0.717	1.034	0.670	2.226
17	0.1	6.5	0	0	0	10	0.688	0.879	0.788	2.619
18	0.1	6.5	0	0	0	20	0.592	0.659	1.051	3.494
19	UW	6.5	0	0	0	0	0.600	0.917	0.755	2.510
20	GW	7.6	0	0	0	0	0.478	0.655	1.058	3.515
21	SW	8.1	0	0	0	0	0.455	0.542	1.278	4.248
22	WW	7.8	0	0	0	0	0.239	0.259	2.349	7.805

Table 4.14 Experimental data from E-beam induced treatment of ORZ: Influence of various parameters. [G-(ORZ) calculated for 1.0 kGy dose using Eq. 3.1]

Exp.	Initial [ORZ] (mM)	pH	[NO_2^- and NO_3^-] (M)	[Propanol] (M)	[Thiourea] (M)	[H_2O_2] (mM)	G-(ORZ) (μmol J^{-1})	k (kGy^{-1})	$D_{0.5}$ (kGy)	$D_{0.9}$ (kGy)
1	0.11	6.5	0	0	0	0	1.000	1.976	0.350	1.164
2	0.22	6.5	0	0	0	0	1.835	1.170	0.592	1.967
3	0.31	6.5	0	0	0	0	2.496	0.872	0.794	2.639
4	0.45	6.5	0	0	0	0	3.013	0.691	1.002	3.330
5	0.22	3	0	0	0	0	1.893	1.490	0.464	1.544
6	0.22	6.5	0	0	0	0	1.822	1.177	0.588	1.954
7	0.22	11	0	0	0	0	1.710	0.881	0.786	2.613
8	0.22	6.5	0.1 NO_2^-	0	0	0	1.078	0.208	3.332	11.07
9	0.22	6.5	0.1 NO_3^-	0	0	0	1.526	0.834	0.831	2.760
10	0.22	6.5	0	0.1	0	0	1.165	0.273	2.532	8.412
11	0.22	6.5	0	0.5	0	0	1.050	0.143	4.816	16.00
12	0.22	6.5	0	0	0.1	0	1.068	0.146	4.724	15.69
13	0.22	6.5	0	0	0.5	0	0.943	0.051	13.38	44.45
14	0.22	6.5	0	0	0	2.5	1.756	1.102	0.628	2.087
15	0.22	6.5	0	0	0	5	1.909	1.230	0.563	1.871

16	0.22	6.5	0	0	0	10	2.016	1.818	0.381	1.266
17	0.22	6.5	0	0	0	20	2.101	0.971	0.713	2.369
18	UW	6.5	0	0	0	0	1.835	1.170	0.592	1.967
19	GW	7.5	0	0	0	0	1.446	0.628	1.103	3.665
20	SW	8.0	0	0	0	0	1.296	0.438	1.579	5.246
21	WW	7.9	0	0	0	0	1.077	0.215	3.211	10.66

Table 4.15 Experimental data from E-beam induced treatment of AMX: Influence of various parameters. [G-(AMX) calculated for 2.5 kGy dose using Eq. 3.1]

Exp.	$[AMX]_o$ (mM)	pH	Additives (M)	$[H_2O_2]$ (mM)	G-(AMX) (μmol J^{-1})	k (kGy^{-1})	$D_{0.5}$ (kGy)	$D_{0.9}$ (kGy)
1	0.05	6.5	0	0	0.183	0.2069	3.350	11.12
2	0.1	6.5	0	0	0.259	0.1463	4.737	15.73
3	0.15	6.5	0	0	0.397	0.0893	7.762	25.78
4	0.2	6.5	0	0	0.498	0.0588	11.78	39.15
5	0.1	3	0	0	0.353	0.1783	3.887	12.91
6	0.1	6.5	0	0	0.336	0.1442	4.806	15.96
7	0.1	11	0	0	0.319	0.1285	5.394	17.91
8	0.1	6.5	NO_3^-	0	0.321	0.1199	5.781	19.20
9	0.1	6.5	NO_2^-	0	0.076	0.0298	23.25	77.26
10	0.1	6.5	CO_3^{2-}	0	0.198	0.0553	12.53	41.63
11	0.1	6.5	HCO_3^-	0	0.295	0.0997	6.952	23.09
12	0.1	6.5	SO_4^{2-}	0	0.334	0.1364	5.081	16.88
13	0.1	6.5	SO_3^{2-}	0	0.085	0.0339	20.44	67.92
14	0.1	6.5	Thiourea	0	0.017	0.0176	39.38	130.8
15	0.1	6.5	Propanol	0	0.067	0.0277	25.02	83.12
16	0.1	6.5	0	0.5	0.341	0.1574	4.407	14.62
17	0.1	6.5	0	2.5	0.363	0.1923	3.604	11.97
18	0.1	6.5	0	5	0.314	0.1251	5.540	18.40
19	0.1	6.5	0	10	0.294	0.1043	6.645	22.07
20	0.1	6.5	0	25	0.261	0.087	7.967	26.46

4.5.2 Effect of solution pH on E-beam radiolytic degradation of model compounds

In order to investigate the impact of initial pH on the E-beam radiolysis of model compounds, solutions of different pH was prepared using 1 M NaOH and 1M HCl solutions. The degradation was evaluated in acidic and alkaline medium (Fig. 4.44) by irradiating aqueous solutions of OFX (initial concentration of 0.1 mM), ORZ (initial concentration of 0.22 mM) and AMX (initial concentration of 0.1 mM) aqueous solutions at pH 3.0, 6.5 and

11.0, respectively. As displayed in Fig. 4.44, degradation of model compounds increased in acidic medium whereas decreased in alkaline/neutral medium, and these findings were in agreement with previously reported studies for the degradation of Sulfadiazine (Guo *et al.* 2012), Primidone (Liu *et al.* 2015) and Norfloxacin (Sayed *et al.* 2016). Results demonstrated that at 3.0 kGy dose, OFX degradation was found to be 95.9, 94.2 and 85.8% at the initial pH of 3.0, 6.5 and 11.0, respectively, whereas ORZ degradation was found to be 99.0, 96.9 and 91.6% at the initial pH of 3.0, 6.5 and 11.0, respectively. In case of AMX, degradation was found to be 92.2, 87.9 and 83.9% at 15.0 kGy dose at the initial pH of 3.0, 6.5 and 11.0, respectively

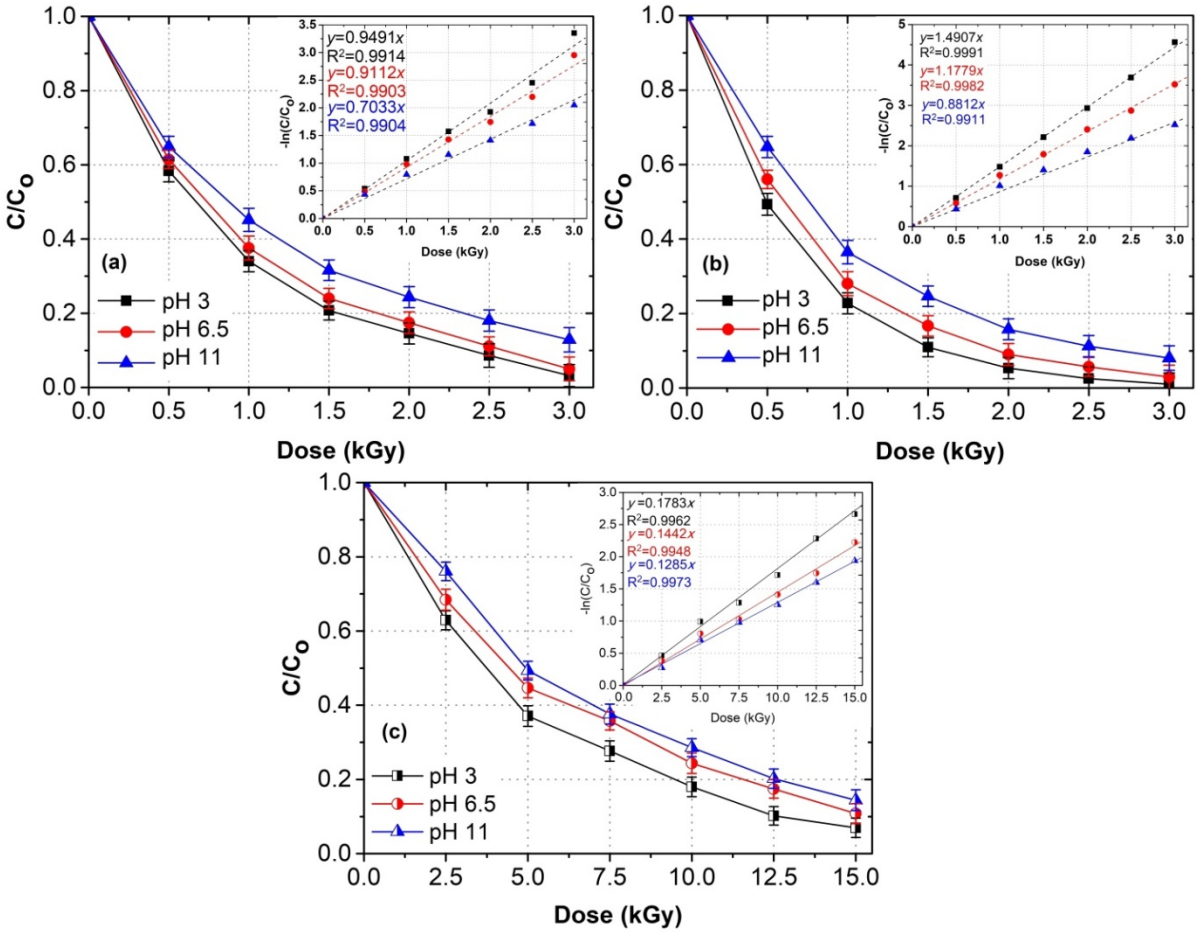

Fig. 4.44 Effect of different pH solutions on (a) OFX and (b) ORZ (c) AMX degradation using E-beam irradiation

The degradation of organic pollutant during the E-beam radiolysis is dependent on the generated reactive radical species during water radiolysis. As already discussed in Section 4.3.2, under acidic medium, e_{aq}^- is easily converted into H$^\bullet$ on reaction with H^+ (Eq. 4.8), thus preventing the recombination of e_{aq}^- and HO$^\bullet$ radicals to form OH^-, allowing HO$^\bullet$ radicals to

be available in the reaction medium to react with model compounds (Basfar *et al.* 2005). However, in alkaline medium (pH 11.0), fraction of H$^{\bullet}$ and HO$^{\bullet}$ react with OH^{-} to produce e_{aq}^{-} and weak oxidative O$^{\bullet-}$ species, respectively (Eq. 4.9), thereby reducing the HO$^{\bullet}$ concentration in the solution (Liu *et al.* 2015). The increased degradation at acidic condition and decreased degradation at alkaline condition demonstrate that the presence of HO$^{\bullet}$ was proved to be effective for the degradation of model compounds during E-beam radiolysis.

OFX, ORZ and AMX degradation at different solution pH also fitted *pseudo first-order* reaction kinetics (Fig. 4.34 (insets)). Table 4.13, 4.14 and 4.15 exhibits the corresponding *k* and G-values (*experiments* 5-7) for OFX, ORZ and AMX, respectively. It can be seen that model compounds solution at alkaline pH lead to smaller *k*-value, which is equivalent to their degradation at studied pH range. From the findings, it can be inferred that HO$^{\bullet}$ played a dominating role in degrading OFX, ORZ and AMX in aqueous medium using E-beam irradiation.

4.5.3 Effect of different additives on E-beam radiolytic degradation of model compounds

The different water matrices including natural waters and wastewaters constitute complex aqueous mediums containing inorganic ions (for example NO_2^-, NO_3^-, SO_3^{2-}, SO_4^{2-}, CO_3^{2-} and HCO_3^-) and various solvents that affect the degradation efficiency of organic compound on competition with the generated reactive species during water radiolysis. To study the effect of various additives, NO_2^- and NO_3^- ions (0.1 M) were added to OFX (0.1 mM) and ORZ solution (0.22 mM) prior to irradiation treatment. To explicate the influence of solvents, 2-propanol and thiourea at different concentrations were added as reference substance to study the degradation of OFX (0.1 mM) and ORZ solution (0.22 mM) during E-beam radiolysis. In case of AMX (0.1 mM), the E-beam radiolytic degradation efficiency was monitored in the presence of NO_3^-, NO_2^-, CO_3^{2-}, HCO_3^-, SO_4^{2-}, SO_3^{2-}, thiourea and propanol at pH 6.5.

The effect of anions NO_2^- and NO_3^- on the E-beam radiolytic degradation of OFX and ORZ is depicted in Fig. 4.45. The results showed that degradation of model compounds increased with increasing dose but the degradation was found to be lower in the presence of NO_2^- and NO_3^- ions. The addition of NO_2^- caused a large decrease in degradation, whereas, NO_3^- addition had a slight effect on degradation under different doses. Table 4.13 and Table 4.14 (*experiment* 8-9) shows the results obtained with the addition of NO_2^- and NO_3^-.

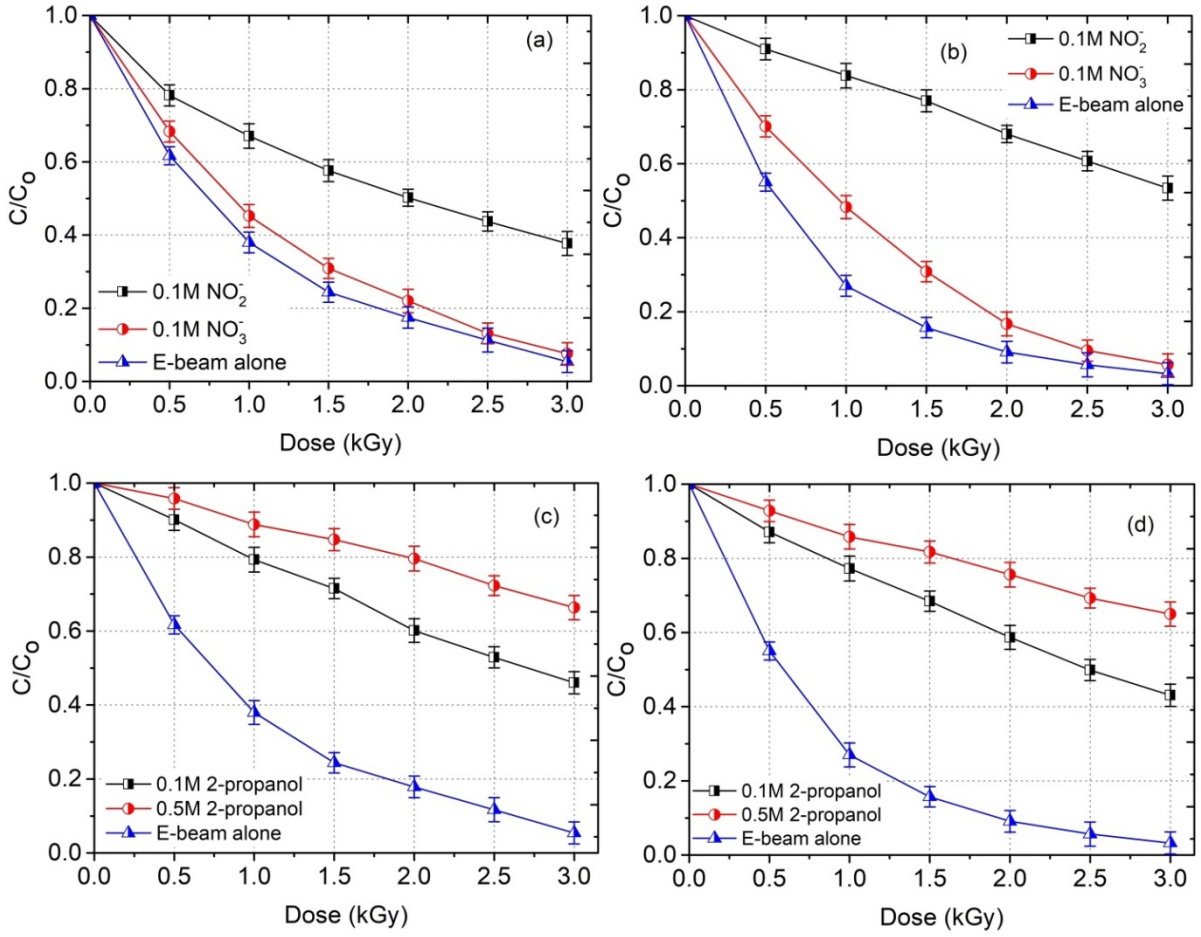

Fig. 4.45 Effect of NO_2^- and NO_3^- on E-beam radiolytic degradation of (a) OFX (b) ORZ; and Effect of 2-propanol on E-beam radiolytic degradation of (c) OFX (d) ORZ

As discussed in Section 4.3.3, NO_3^- is an efficient scavenger of e_{aq}^- and NO_2^- is considered as inhibitors of HO•, e_{aq}^- and H•. Although, NO_3^- do not react directly with HO•, but at high concentration NO_3^- may decrease the concentration of HO• indirectly via NO_2^- formation according to Eqs. (4.19-4.21) (Velo Gala *et al.* 2013). The insignificant decrease in *k*-value at 0.1 M NO_3^- ion concentration indicated that the addition of 0.1 M NO_3^- had not substantially affected the OFX and ORZ degradation under E-beam irradiation as shown in Table 4.13 and 4.14. Thus, the *k*-value showed significant decrease with the addition of 0.1 M NO_2^- and this effect was more pronounced as compared to NO_3^- ion. According to Table 4.13 (*experiment* 8 and 9), the *k* values of OFX radiolysis in the presence of NO_2^- and NO_3^- were 0.339 and 0.816 kGy^{-1}, respectively which were lower than 0.917 kGy^{-1} (*experiment* 2) in solution without ions. According to Table 4.14 (*experiment* 8 and 9), the *k* values of ORZ

radiolysis in the presence of NO_2^- and NO_3^- were 0.208 and 0.834 kGy^{-1}, respectively which were lower than 1.170 kGy^{-1} (*experiment* 2) in solution without ions.

In order to make clear the comparative contribution of $HO^{\bullet}$, $H^{\bullet}$ and e_{aq}^- on OFX and ORZ radiolysis, the degradation was studied in the presence of different concentrations of propanol (Fig. 4.45) and thiourea (Fig. 4.46). 49 and 29% degradations of OFX were observed with 0.1 M propanol and thiourea, respectively at 3.0 kGy dose and the results are shown in Table 4.13 (*experiments* 10-13). 55 and 38% degradations of ORZ were observed with 0.1 M propanol and thiourea, respectively at 3.0 kGy dose and the results are shown in Table 4.14 (*experiments* 10-13). It was observed that in the presence of these scavengers, the degradation efficiencies were diminished. Furthermore, this effect was enhanced when the concentrations of the scavengers was increased, indicating that degradation of OFX and ORZ was inhibited in the presence of propanol and thiourea. The obvious decrease of degradation can be ascribed to the loss of reactive species. Propanol and thiourea can react with $HO^{\bullet}$, e_{aq}^- and $H^{\bullet}$, which are summarized as Eqs. (4.30-4.34) in section 4.3.3 (Khan *et al.* 2015; Basfar *et al.* 2005).

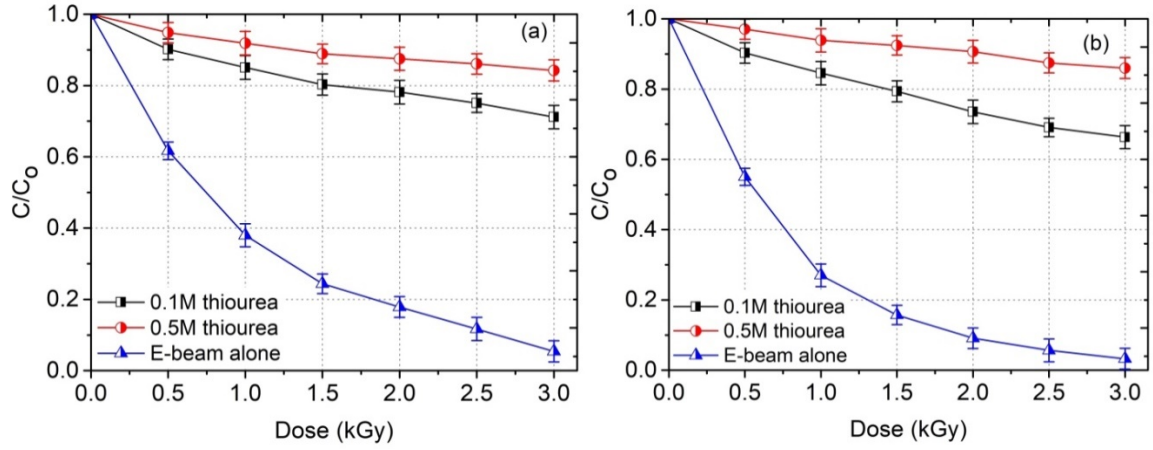

Fig. 4.46 Effect of thiourea on E-beam radiolytic degradation of (a) OFX (b) ORZ

It can be seen from Fig. 4.47 that at a given absorbed dose, degradation efficiency of AMX in the solution was higher without the additives when compared to those in the presence of additives. 88.4% AMX degradation was achieved in the aqueous solution at an absorbed dose of 15.0 kGy, while 84.3, 24.9, 54.6, 78.0, 87.6, 27.2, 10.7 and 22.8% degradation efficiencies were obtained in the presence of 0.1 M NO_3^-, NO_2^-, CO_3^{2-}, HCO_3^-, SO_4^{2-}, SO_3^{2-}, thiourea and propanol, respectively. According to Table 4.15 (*experiment* 8 and 9), the *k*-values of AMX radiolysis in the presence of NO_2^- and NO_3^- were 0.029 and 0.119 kGy^{-1}, respectively which were lower than 0.146 kGy^{-1} (*experiment* 2) in solution

without ions. Similarly, *k*-values of AMX radiolysis in the presence of CO_3^{2-}, HCO_3^-, SO_4^{2-}, SO_3^{2-}, thiourea and propanol were 0.055, 0.097, 0.136, 0.033, 0.017 and 0.027 kGy^{-1}, respectively which were lower than 0.146 kGy^{-1} (*experiment* 2) in solution without ions (Table 4.15). The negative impact on the degradation efficiency of AMX by the added additives was found in the following decreasing order: thiourea > propanol > NO_2^- > SO_3^{2-} > CO_3^{2-} > HCO_3^- > NO_3^- > SO_4^{2-}. The observed decrease of AMX degradation can be ascribed to the loss of reactive species due the reaction of the radiolytically generated reactive species with these additives as explained earlier in Section 4.3.3.

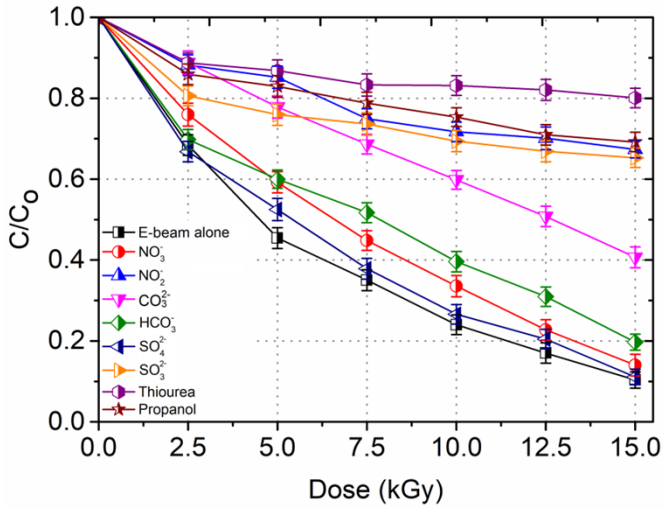

Fig. 4.47 Effect of different additives on E-Beam radiolytic degradation of AMX

The degradation of model compounds can happen through the oxidation pathways by the reaction with oxidizing HO• radicals. That is why, when the parallel competitive reaction paths of HO• were opened up in the presence of scavengers (NO_2^-, 2-propanol and thiourea) the extent of degradation (C/C_0) significantly decreased due to the lack of extent of reaction between parent compound and HO•. On the other hand, the reactions of parent compound with the reducing radical e_{aq}^- does not lead to degradation, but the absorption properties of the product slightly differs from the parent molecule. Thus, the extent of degradation does not differ much, when the parallel competitive reactions of e_{aq}^- starts in the presence of specific scavenger NO_3^-. The yield of other reducing radical H• is lesser (G value = 0.06 µmol J^{-1}) compared to HO• and e_{aq}^-(G value = 0.28 µmol J^{-1}) and thus the degradation of OFX, ORZ and AMX by H• is expected to be lesser compared to other radicals.

4.5.4 Effect of oxidant on E-beam radiolytic degradation of model compounds

Fig. 4.48a depicts the effect of H_2O_2 on the degradation of OFX under E-beam

radiolysis and the corresponding results are shown in Table 4.13 (*experiments,* 14-18). Fig. 4.48b depicts the effect of H_2O_2 on the degradation of AMX under E-Beam radiolysis and the corresponding results are shown in Table 4.15 (*experiments,* 16-20). Fig. 4.48c depicts the effect of H_2O_2 on the degradation of ORZ under E-Beam radiolysis and the corresponding results are shown in Table 4.14 (*experiments,* 14-17). The results indicated that increase of H_2O_2 concentration from 0.5 to 5 mM favoured OFX degradation with increasing *k*-values of 0.799 to 1.034 kGy^{-1}, respectively versus the *k* value (0.917 kGy^{-1}) obtained without the addition of H_2O_2 at pH 6.5 (Table 4.13, *experiment* 2). It can be observed from the Table 4.14 that with the increase of H_2O_2 concentration from 2.5 to 10 mM, ORZ degradation increased with increasing *k*-value from 1.102 to 1.818 kGy^{-1}, respectively against the *k*-value of 1.170 kGy^{-1} (Table 4.14, *experiment 2*) obtained in the absence of H_2O_2 at pH 6.5. In case of AMX, the increase in H_2O_2 concentration from 0.5 to 2.5 mM favoured AMX degradation with increasing *k* values of 0.157 to 0.192 kGy^{-1}, respectively versus the *k*-value (0.146 kGy^{-1}) obtained without the addition of H_2O_2 at pH 6.5 (Table 4.15, *experiment* 2). This is attributed due to the certainty that H_2O_2 rapidly reacts with e_{aq}^- (Eq. 4.36) and $H^\bullet$ (Eq. 4.37), and enhances the $HO^\bullet$ radical concentration in the aqueous solution with increase in H_2O_2 concentration. This helps in better degradation of parent compound and thus requires lower doses and correspondingly attaining higher *k*-values.

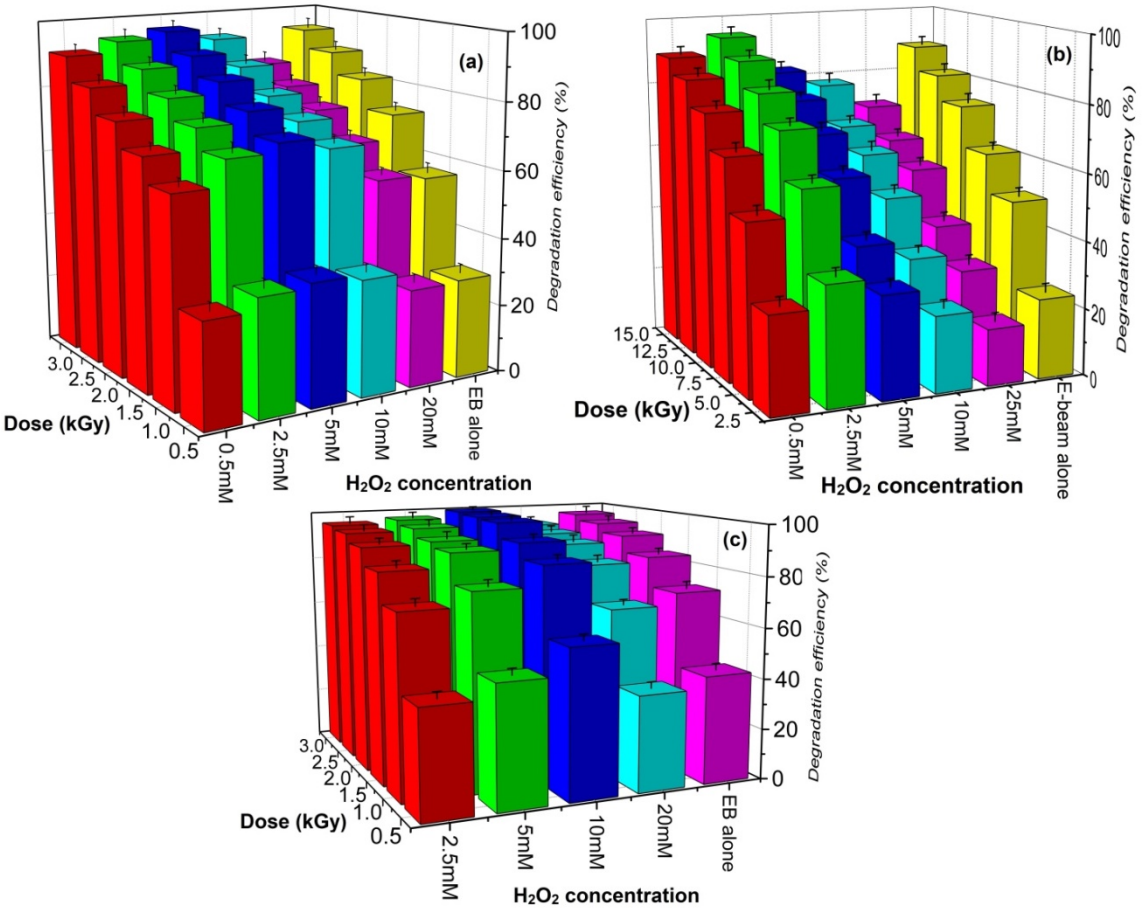

Fig. 4.48 Effect of H_2O_2 concentrations on E-beam radiolytic degradation of (a) OFX (b) AMX and (c) ORZ

However, it was observed that *k* value decreased when H_2O_2 concentration was increased beyond the optimum concentration. It indicated that peroxyl radical species which are generated at this H_2O_2 concentration (Eq. 4.38 and 4.39), are expected to be less reactive compared to $HO^{\bullet}$ radical (Buxton *et al.* 1988). Accordingly, optimal concentration of H_2O_2 was found to be 5, 10 and 2.5 mM in the E-beam radiolytic degradation of OFX, ORZ and AMX, respectively. The results are in accordance with the above section assuming that $HO^{\bullet}$ radical is the primary specie accountable for the OFX, ORZ and AMX degradation.

4.5.5 Effect of oxidant on mineralization efficiency of model compounds

The TOC removal of irradiated aqueous solutions of OFX (Fig. 4.49a), ORZ (Fig. 4.49b) and AMX (Fig. 4.49c) at different doses was assessed to evaluate the influence of H_2O_2 on the extent of mineralization. The removal of TOC was found to be ~28.5% at 3.0 kGy in absence of H_2O_2 for OFX and for ORZ, TOC was found to be ~29.7% in absence of H_2O_2. The removal of TOC was found to be ~47.3% at 15.0 kGy in absence of H_2O_2 for AMX. For E-beam/H_2O_2 process, rather enhanced TOC removal was observed indicating that the presence of H_2O_2 had more pronounced effect on mineralization of parent compound

when compared to degradation. It can be observed from Figs. 4.49a and 4.48a, with initial H_2O_2 concentrations of 0.5, 2.5, 5, 10 and 20 mM, the degradation efficiencies of OFX were found to be 90.6, 94.0, 96.8, 92.6 and 83.1%, respectively; however, TOC removal efficiencies were found to be 33.1, 37.9, 41.5, 45.7 and 52.9%, respectively. In case of ORZ, Figs. 4.49(b) and 4.48(c) depicts that when the initial H_2O_2 concentration was 2.5, 5, 10 and 20 mM, the ORZ degradation was 95.5, 96.9, 99.5 and 92.5%, respectively at 3.0 kGy dose, however, TOC removal efficiency was found to be 33.9, 39.6, 46.8 and 57.8%, respectively. In case of AMX, with initial H_2O_2 concentrations of 2.5 mM, the degradation efficiency of AMX was found to be 94.6%, however, TOC removal efficiency was found to be 56.7%. This trend suggests that concentration of $HO^{\bullet}$ increases in the presence of H_2O_2 and the enhanced concentration of oxidative radicals helps to obtain a higher degree of mineralization with increase in dose and H_2O_2 concentrations. However, organic by-products formed during E-beam induced degradation of model compounds are expected to exhibit remaining TOC in the solutions despite almost complete degradation of parent compounds at a given absorbed dose.

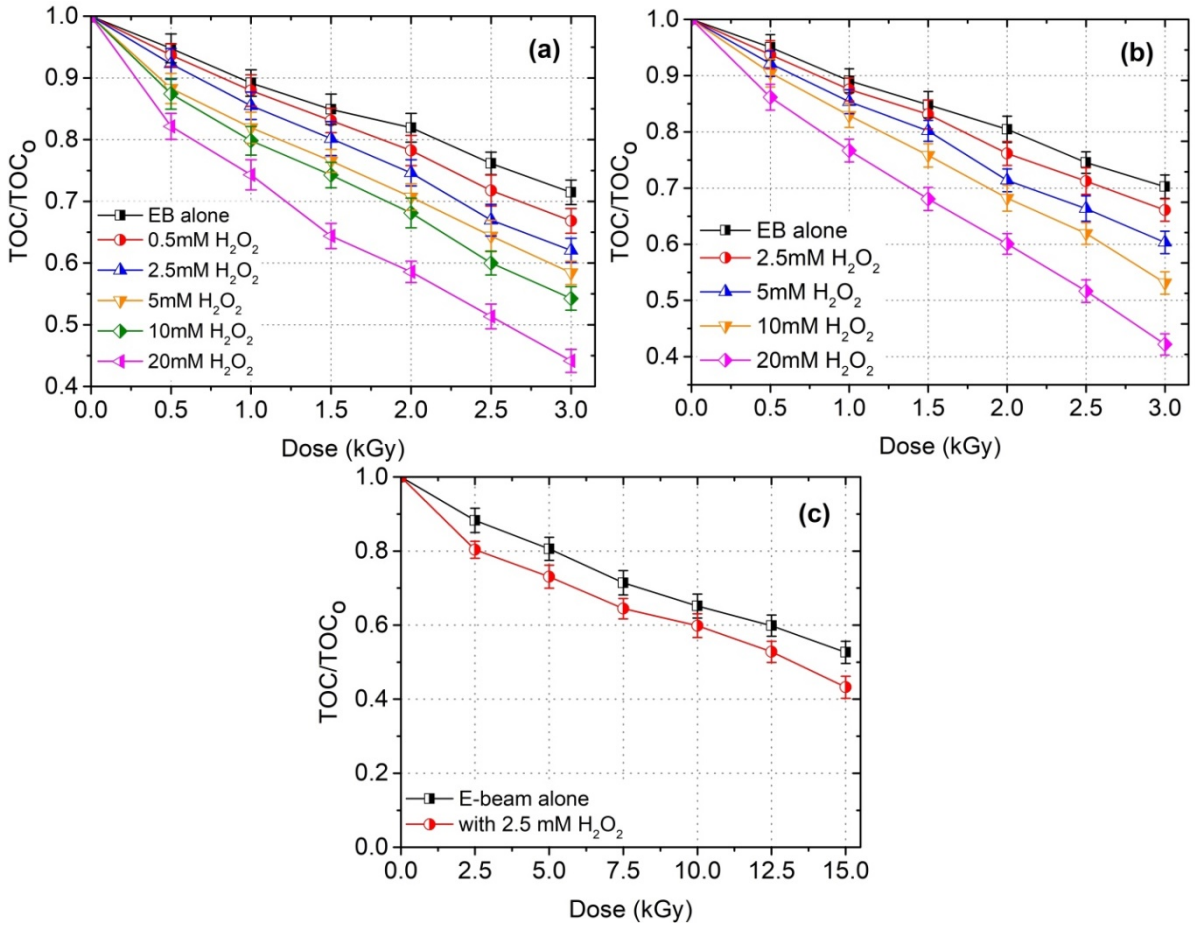

Fig. 4.49 Effect of H_2O_2 concentrations on mineralization efficiency of (a) OFX and (b) ORZ (c) AMX

4.5.6 Influence of water matrices on degradation efficiency of model compounds

The effect of different types of water composition i.e. ultrapure water (UW), surface water (SW), groundwater (GW) and wastewater (WW) was investigated on the degradation of OFX (0.1 mM) and ORZ (0.22 mM) under E-beam radiolysis so as to evaluate the viability of E-beam radiolysis for the OFX and ORZ degradation in real water matrices. Fig. 4.50a and 4.50b show the results of degradation of OFX and ORZ under different water matrices.

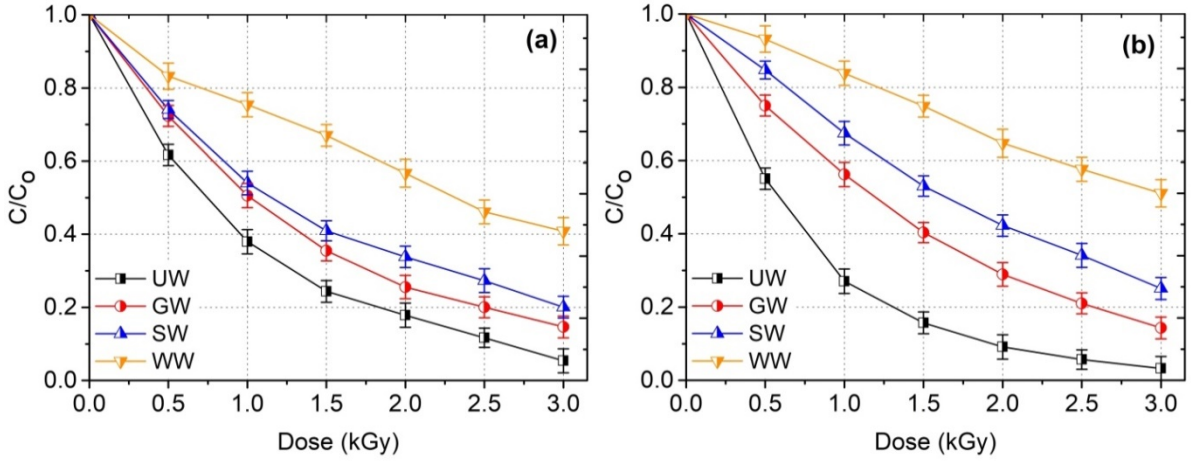

Fig. 4.50 Effect of water matrices on E-beam radiolytic degradation of (a) OFX and (b) ORZ [UW: ultrapure water; SW: surface water; GW: ground water and WW: wastewater]

Results revealed that lower degradation of OFX and ORZ was observed in GW and SW in comparison to UW and considerably much lower degradation was observed in WW. At 3.0 kGy dose, 94% of OFX degradation was achieved in UW in comparison to 83% in GW, 77% in SW and 55% in WW; whereas, 96.6% of ORZ degradation was obtained in UW when compared to 85.0, 73.8 and 46.7% in GW, SW and WW, respectively at irradiation dose of 3.0 kGy. Furthermore, it can be said that the interaction of reactive species ($HO^{\bullet}$, e_{aq}^{-} and $H^{\bullet}$) with the NO_2^-, NO_3^-, HCO_3^- and the dissolved organic matter content in the water matrices result into the reduction of *k* value for UW to GW, SW and WW. Inhibition rates of $HO^{\bullet}$, e_{aq}^{-} and $H^{\bullet}$ for the selected water samples were calculated as function of pH, nitrate, nitrite, alkalinity and organic matter content according to the Eqs. (4.41-4.43).

$$r_{HO^{\bullet}} = k_{H^+}[H^+] + k_{TOC}[TOC] + k_{HCO_3^-}[HCO_3^-] + k_{NO_3^-}[NO_3^-] + k_{NO_2^-}[NO_2^-] \quad (4.41)$$

where $r_{HO\cdot}$ is the HO• inhibition rate (s^{-1}), k_{H^+} =$7.0 \times 10^9\ M^{-1}s^{-1}$; k_{TOC}=$2.0 \times 10^8\ M_c^{-1}s^{-1}$; $k_{HCO_3^-}$=$8.5 \times 10^6\ M^{-1}s^{-1}$; $k_{NO_3^-}$=$5 \times 10^5\ M^{-1}s^{-1}$; $k_{NO_2^-}$=$8.0 \times 10^9\ M^{-1}s^{-1}$, and $[H^+]$, [TOC], $[HCO_3^-]$, $[NO_2^-]$ and $[NO_3^-]$ are the initial concentration of these constituents in the given water samples (Basfar *et al.* 2005; Guo *et al.* 2012). M_c is the molarity of the natural organic matter content, based on the moles of carbon present assuming 12 g C per mole of C.

$$r_{H\cdot}=k_{H^+}[H^+] + k_{TOC}[TOC] + k_{HCO_3^-}[HCO_3^-] + k_{NO_3^-}[NO_3^-] + k_{NO_2^-}[NO_2^-] \quad (4.42)$$

where $r_{H\cdot}$ is the H• inhibition rate (s^{-1}), k_{H^+}=$7.8 \times 10^9\ M^{-1}s^{-1}$; k_{TOC}=$1.7 \times 10^7 M_c^{-1}\ s^{-1}$; $k_{HCO_3^-}$=$4.0 \times 10^4\ M^{-1}s^{-1}$; $k_{NO_3^-}$=$1.4 \times 10^6\ M^{-1}s^{-1}$ and $k_{NO_2^-}$=$7.1 \times 10^8\ M^{-1}s^{-1}$ (Basfar *et al.* 2005).

$$r_{e_{aq}^-}=k_{H^+}[H^+] + k_{TOC}[TOC] + k_{HCO_3^-}[HCO_3^-] + k_{NO_3^-}[NO_3^-] + k_{NO_2^-}[NO_2^-] \quad (4.43)$$

where $r_{e_{aq}^-}$ is the e_{aq}^- inhibition rate(s^{-1}), k_{H^+} =$2.3 \times 10^{10}\ M^{-1}s^{-1}$; k_{TOC}=$1 \times 10^7\ M_c^{-1}s^{-1}$; $k_{HCO_3^-}$=$1 \times 10^6\ M^{-1}s^{-1}$; $k_{NO_3^-}$=$9.7 \times 10^9\ M^{-1}s^{-1}$ and $k_{NO_2^-}$=$4.1 \times 10^9\ M^{-1}$ (Basfar *et al.* 2005; Sayed *et al.* 2016).

Table 4.16 Chemical composition of the selected water matrices and the results of inhibition rates of HO•, e_{aq}^- and H• for E-beam radiolytic degradation of OFX

Water	pH	[TOC] (mg L^{-1})	$[HCO_3^-]$ (mg L^{-1})	$[NO_3^-]$ (mg L^{-1})	$[NO_2^-]$ (mg L^{-1})	$r_{HO\cdot}$ (s^{-1})	$r_{H\cdot}$ (s^{-1})	$r_{e_{aq}^-}$ (s^{-1})	r_{total} (s^{-1})
Ultrapure	6.5	0.0	0.0	0.0	0.0	2.2×10^3	2.4×10^3	7.3×10^3	11.9×10^3
Surface	8.1	10.9	5.7	11.7	7.8	1.5×10^6	1.3×10^5	2.5×10^6	4.1×10^6
Groundwater	7.6	0.0	6.6	4.1	1.8	3.1×10^5	2.8×10^4	8.0×10^5	1.1×10^6
Wastewater	7.8	18.2	8.1	41.2	32.4	5.9×10^6	5.2×10^5	9.3×10^6	1.5×10^7

Table 4.17 Chemical composition of the selected water matrices and the results of inhibition rates of HO•, e_{aq}^- and H• for E-beam radiolytic degradation of ORZ

Water	pH	[TOC] (mg L^{-1})	$[HCO_3^-]$ (mg L^{-1})	$[NO_3^-]$ (mg L^{-1})	$[NO_2^-]$ (mg L^{-1})	$r_{HO\cdot}$ (s^{-1})	$r_{H\cdot}$ (s^{-1})	$r_{e_{aq}^-}$ (s^{-1})	r_{total} (s^{-1})

Ultrapure	6.5	0.0	0.0	0.0	0.0	2.2×10^3	2.4×10^3	7.3×10^3	11.9×10^3
Surface	8.0	11.2	4.8	10.3	7.5	1.4×10^6	1.3×10^5	2.2×10^6	3.9×10^6
Groundwater	7.5	0.0	6.2	3.8	1.9	3.3×10^5	2.9×10^4	7.6×10^5	1.1×10^6
Wastewater	7.9	19.3	7.8	43.7	35.2	6.4×10^6	5.7×10^5	9.9×10^6	1.7×10^7

Table 4.16 and 4.17 lists the chemical composition of the selected water matrices and the results of inhibition rates of $HO^{\bullet}$, e_{aq}^{-} and $H^{\bullet}$. It is evident from the results that total scavenging rates of $HO^{\bullet}$, e_{aq}^{-} and $H^{\bullet}$ were higher in WW when compared to GW, SW and UW. Irrespective of chemical composition of different water systems, E-Beam irradiation was able to degrade OFX and ORZ, and thus validated the feasibility of E-Beam irradiation for treating OFX and ORZ contaminated water.

4.5.7 LC-MS analysis of E-beam irradiated solutions of OFX

Gaussian 03 Software at density functional theory with B3LYP/6-31G level was applied to optimize the geometry structure of OFX, which might be used to evaluate the charge distribution of the OFX molecule through Gaussian calculations. Fig. 4.43 shows the result of charge distribution of OFX obtained by Gaussian calculation. It is found that N[1] and O[4] contain the highest negative charge -0.630 and -0.605 in the oxazinyl substituent and carboxylic substituents of OFX, respectively; therefore, N[1] and O[4] atoms can be attacked by reactive $HO^{\bullet}$ species. As a result, the bonds N[1]-C[12] and O[4]-C[1] are most susceptible for cleavage to form new intermediates. Thus, it can be presumed that the E-beam radiolytic degradation of OFX is mainly attributed to $HO^{\bullet}$ oxidation. In addition, N[2], O[1], N[3], O[2] and O[3] possess the negative charges, which shows that these atoms are also vulnerable to be attacked by $HO^{\bullet}$ radical. Consequently, the bonds of N[1]-C[12], N[1]-C[5], N[2]-C[9], N[2]-C[14], N[2]-C[15], N[3]-C[16], N[3]-C[17], C[1]-O[3], C[1]-O[4], C[5]-C[3], C[11]-O[1], C[12]-C[11], C[13]-C[12] and O[4]-H[1] may be possibly broken due to negative charges. Based on the prediction of Gaussian calculations, it can be proposed that the specified bonds are expected to be destroyed under E-beam irradiation and form some new products subsequently.

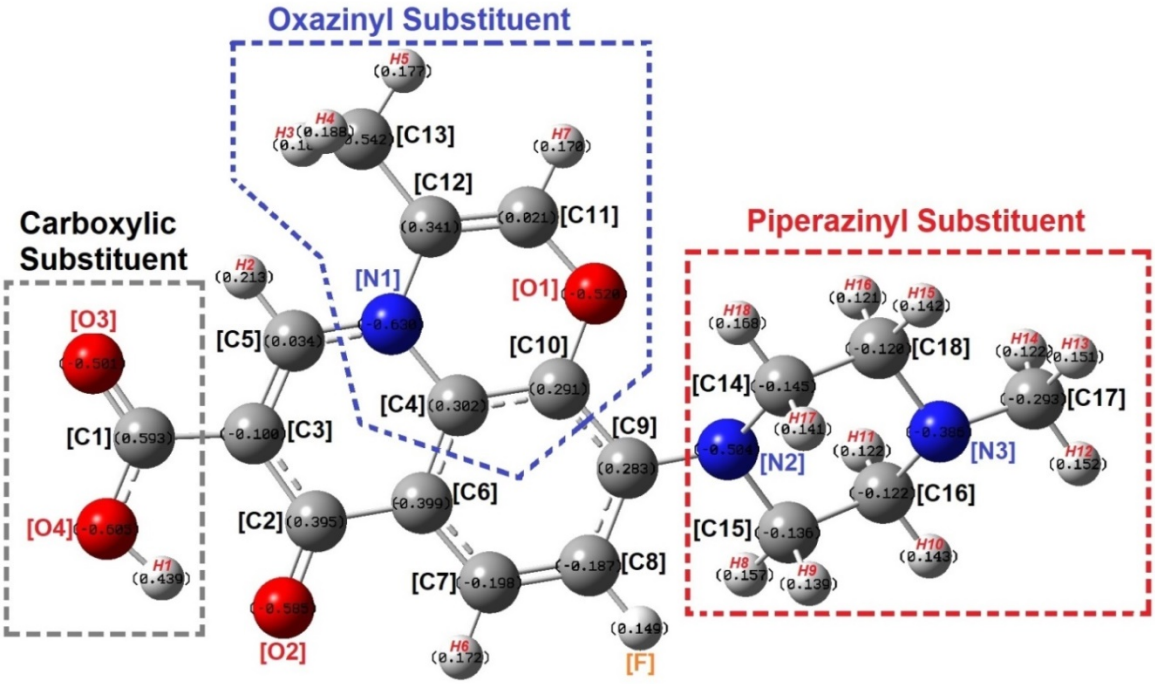

Fig. 4.51 OFX molecule structure and its charge distribution

To confirm the formation of intermediates/by-products from the E-beam induced degradation of OFX, the reaction transformation products of 0.1 mM OFX at dose of 2.0 kGy and 3.0 kGy irradiated solutions were analyzed and identified by LC-QTOF-MS. Fig. 4.52 and 4.53 displays the total ion chromatograms and electrospray ionization mass spectrums recorded for 0.1 mM OFX solution with 2.0 and 3.0 kGy dose. Based on the results, the removal pathways of E-beam induced radiolytic degradation of OFX has been inferred in Fig. 4.54.

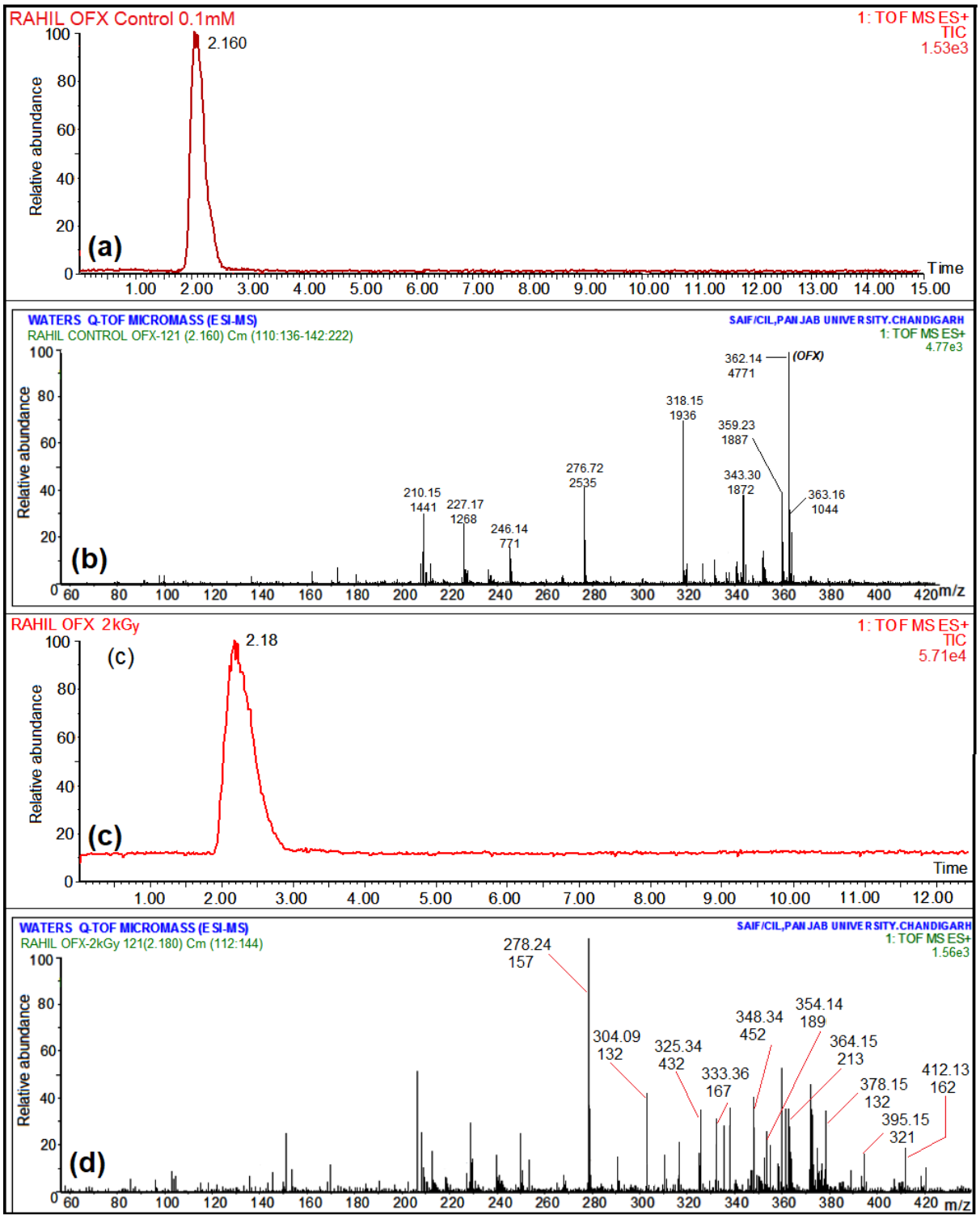

Fig. 4.52 (a) & (b) Total ion current chromatogram and mass spectrum recorded for OFX with initial concentration of 0.1 mM (c) & (d) Total ion current chromatogram and mass spectrum recorded for aqueous solution of OFX E-beam irradiated with 2.0 kGy

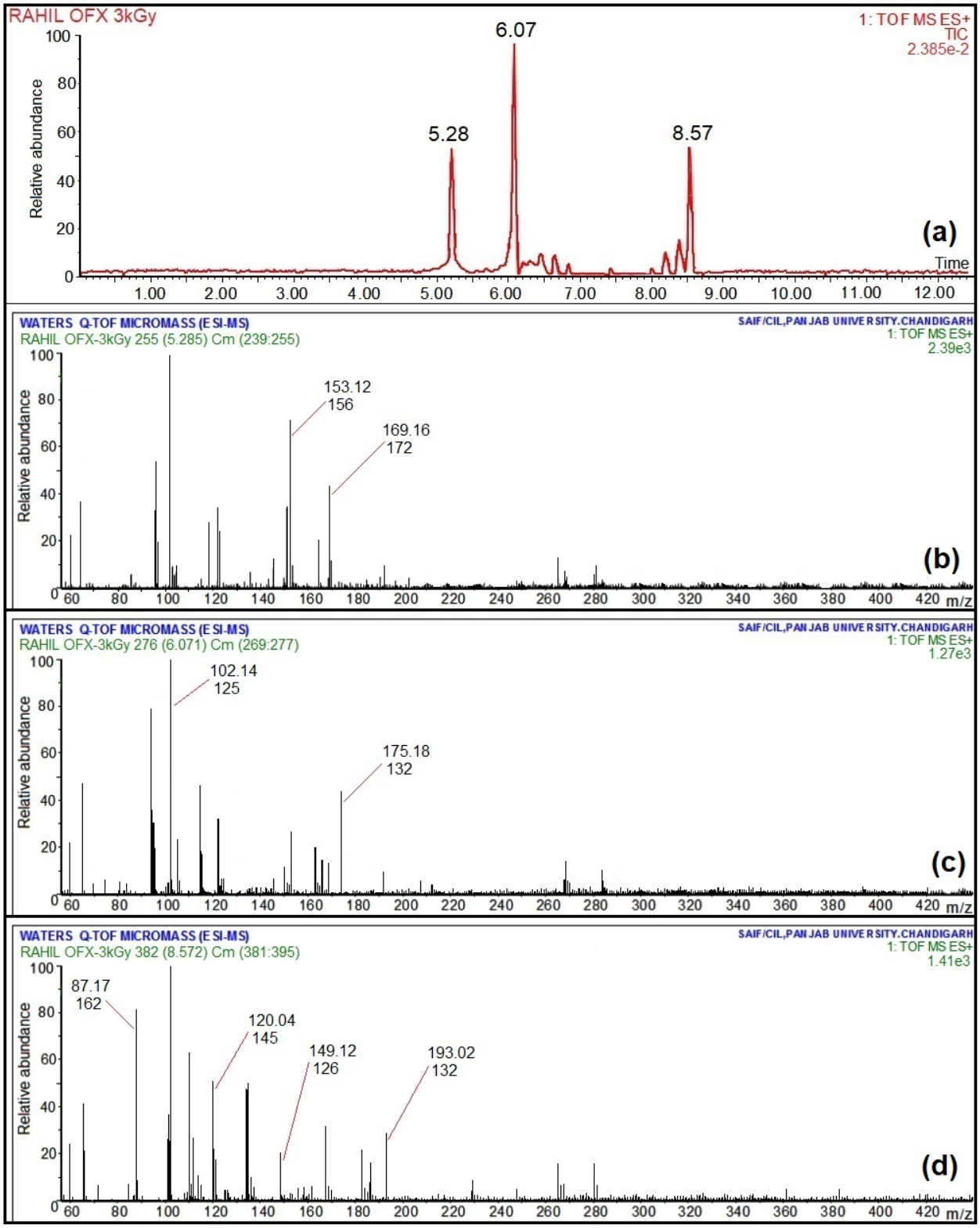

Fig. 4.53 (a) Total ion current chromatogram and (b), (c) & (d) mass spectrum recorded for aqueous solution of OFX E-beam irradiated with 3.0 kGy

Results revealed the identification of twenty one major degradation by-products with their peak intensities exceeding 10%, therefore, leading to the precise identification of OFX

reaction intermediates or OFX transformation products (OTPs). Based on the ESI-MS analysis and the results of earlier reports on OFX oxidation, several removal pathways have been proposed, wherein, hydroxylation, decarboxylation, hydroxyl group oxidation, piperazinyl dealkylation, and direct cleavage of OFX molecule are defined as leading transformation mechanisms (Hapeshi *et al.* 2013; Carbajo *et al.* 2015; Zhu *et al.* 2016; Sturini *et al.* 2017). In one instance, carboxylic moiety of OFX may be attacked by HO• radicals to generate **OTP1** with *m/z* of 318, which represents one of the oxidative degradation product of OFX as showed in previous studies (Calza *et al.* 2008; Vasquez *et al.* 2013; Liu *et al.* 2016a). The obtained product is in consistent with the results of quantum chemical calculations with attack of HO• on carboxylic substituents of OFX i.e. bonds O[4]-C[1] and O[3]-C[1]. Further, the attack on the quinolone moiety of OFX results in the production of transformed product **OTP2** (*m/z* 334) comprising of ring radical with centered-carbon. **OTP3** with *m/z* of 338 can be formed from OTP2 after the cleavage of the C[3]-C[5] bonded side chain of OFX with a keto group. **OTP4** (*m/z* 261) is expected to be formed from the elimination of CO_2/methyliaziridine from the piperazinyl substituent of OTP1 at N[2]-C[14] and N[3]-C[16]. The attack on N[1]-C[12] and O[1]-C[11] bonds in the oxazinyl substituent and the cleavage of N[1]-C[15] bond in piperazinyl substituent of OTP4 lead to the generation of **OTP5** with *m/z* of 193.

The attack of HO• radical on N[3]-C[17] bond leads to the dimethylation of piperazinyl ring of OFX, thus generating **OTP6** (*m/z* 348). OTP6 is considered as one of the intermediates for **OTP7** (*m/z* 278) formation, which can yield OTP7 owing to the total oxidation of the piperazinyl ring to an amino group by the cleavage of N[2]-C[15] and C[17]-N[2] bonds. Further oxidation at piperazinyl substituents at C[14]-N[2] and N[3]-C[16] of OFX molecule leads to the formation of **OTP8** (*m/z* 304). The attack of HO• on oxazinyl moiety of OFX leads to the identification of transformed product **OTP9** with *m/z* 354. **OTP10** (*m/z* 326) is expected to be generated from OTP9 through cleavage of C[3]-C[5] bond by eventually losing hydroxyl group form the carboxylic moiety of OTP9. **OTP11** (*m/z* 364) is by-product containing a keto group deriving from the breakdown of heterocyclic ring attached to carboxylic moiety of OFX molecule.

Due to the high degree of non-selectivity of HO• to different functional groups, it can be hypothesized that certain polyhydroxylated compounds can form. Subsequently, attack of HO• on OFX molecule can form hydroxylated (**OTP12**, *m/z* 378), bi-hydroxylated (**OTP13,** *m/z* 395) and, tri-hydroxylated (**OTP14**, *m/z* 414) transformation products.

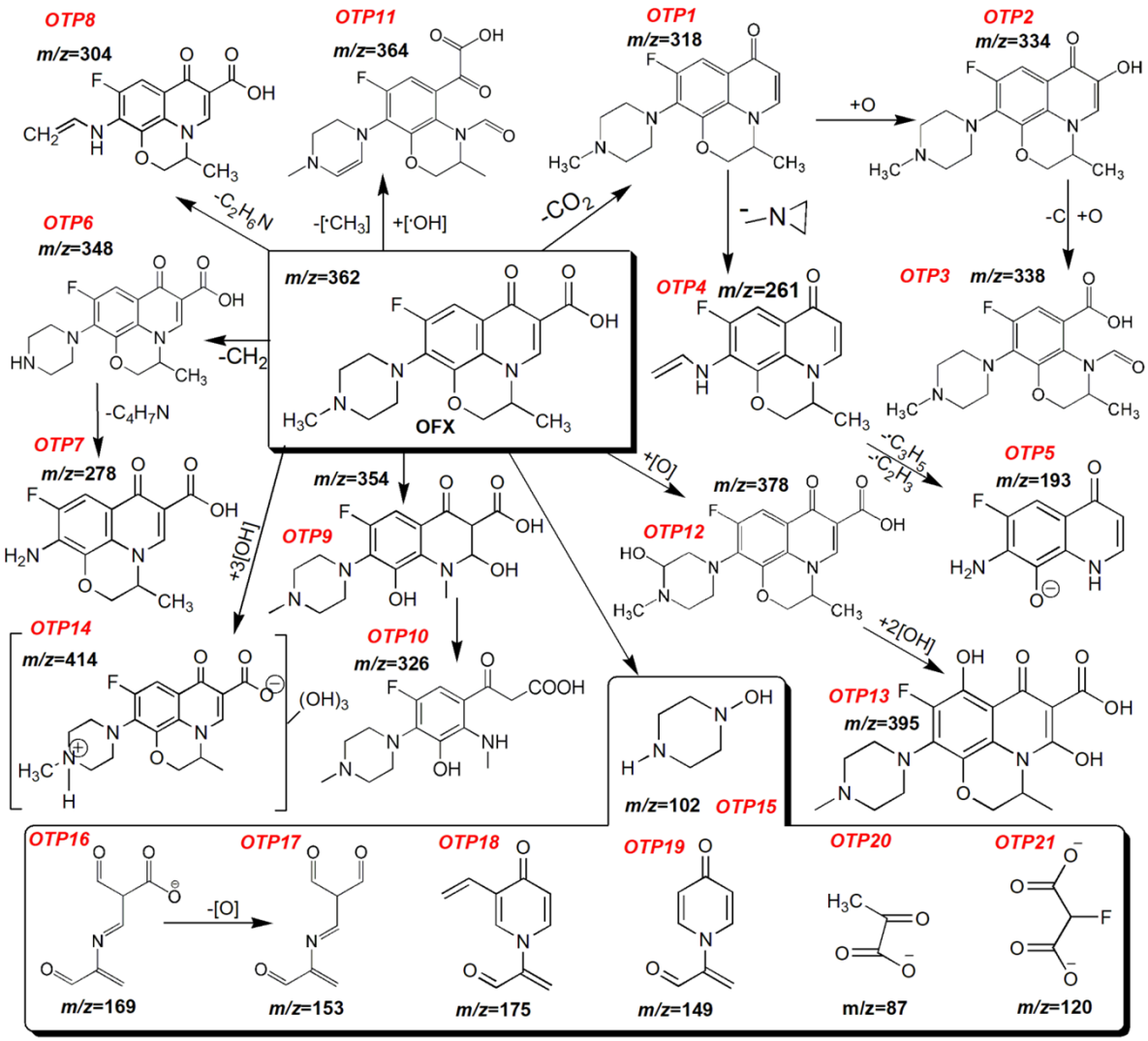

Fig. 4.54 The possible pathways of E-beam induced radiolytic degradation of OFX

Subsequent oxidation of OFX molecule may induce the formation of several cleavage products OTP15-OTP21 and these products were found until the end of experiment. The breakdown of piperazinyl substituent of OFX molecule at N[2]-C[9] may lead to the generation of **OTP15** (*m/z* 102), recognized as *N*-hydroxypiperzaine and this product was identified with higher abundance in E-beam radiolytic treatment of OFX at 3.0 kGy dose (Fig. 4.53). **OTP16** (*m/z* 169) can be formed due to the loss of $C_{11}H_{15}FN_2$ and **OTP17** (*m/z* 153) is presumed to be formed after the oxygen atom removal from OTP16. In addition to this, two hetero-monocyclic products were identified and labeled as **OTP18** (*m/z* 175) and **OTP19** (*m/z* 149), which are supposed to be emerged after the cleavage of OFX molecule at C[7], C[8] and C[10] atoms. As displayed, the cleavage products comprise of heterocyclic amine ring in their structure, which remain intact. Finally, on the exploration of OFX pathway, **OTP20** (*m/z* 87) and **OTP21** (*m/z* 120) were analyzed possibly emerging from the

direct cleavage of OFX and these cleavage products have not been reported earlier. These identified cleavage products existed in greater abundance at the completion of experiments. All OTPs may undergo further oxidation leading to the formation of aliphatic compounds, acids or inorganic ions which are finally converted to CO_2 and H_2O. Therefore, the main degradation mechanism of OFX during E-beam irradiation can be attributed to $HO^{\bullet}$ radicals oxidation and the direct degradation of OFX molecule. In addition, results of LC-QTOF/MS and the Gaussian calculations are able to predict the OFX degradation mechanism.

4.5.8 LC-MS analysis of E-beam irradiated solutions of ORZ

To identify the intermediates/by-products formed during the E-beam induced degradation of ORZ, the reaction products of E-beam irradiated ORZ solution (0.22 mM) at 2.0 kGy and 3.0 kGy dose were analyzed using LC-QTOF-MS. The total ion chromatograms and ESI-MS recorded for ORZ solution with irradiation doses of 2.0 and 3.0 kGy are presented in Fig. 4.55 and 4.56.

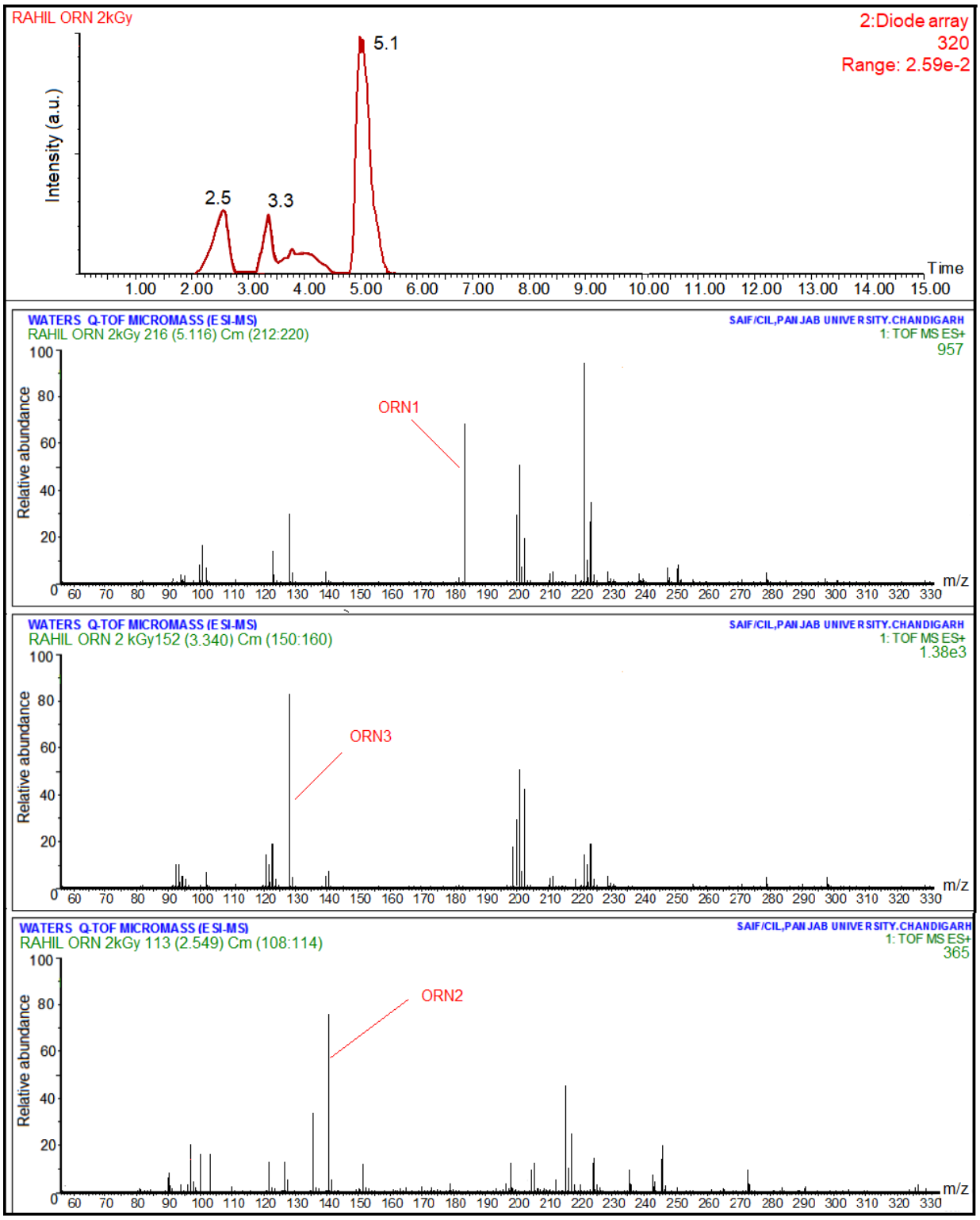

Fig. 4.55 Total ion current chromatogram and mass spectrum recorded for aqueous solution of ORZ (0.22 mM) E-beam irradiated with 2.0 kGy dose

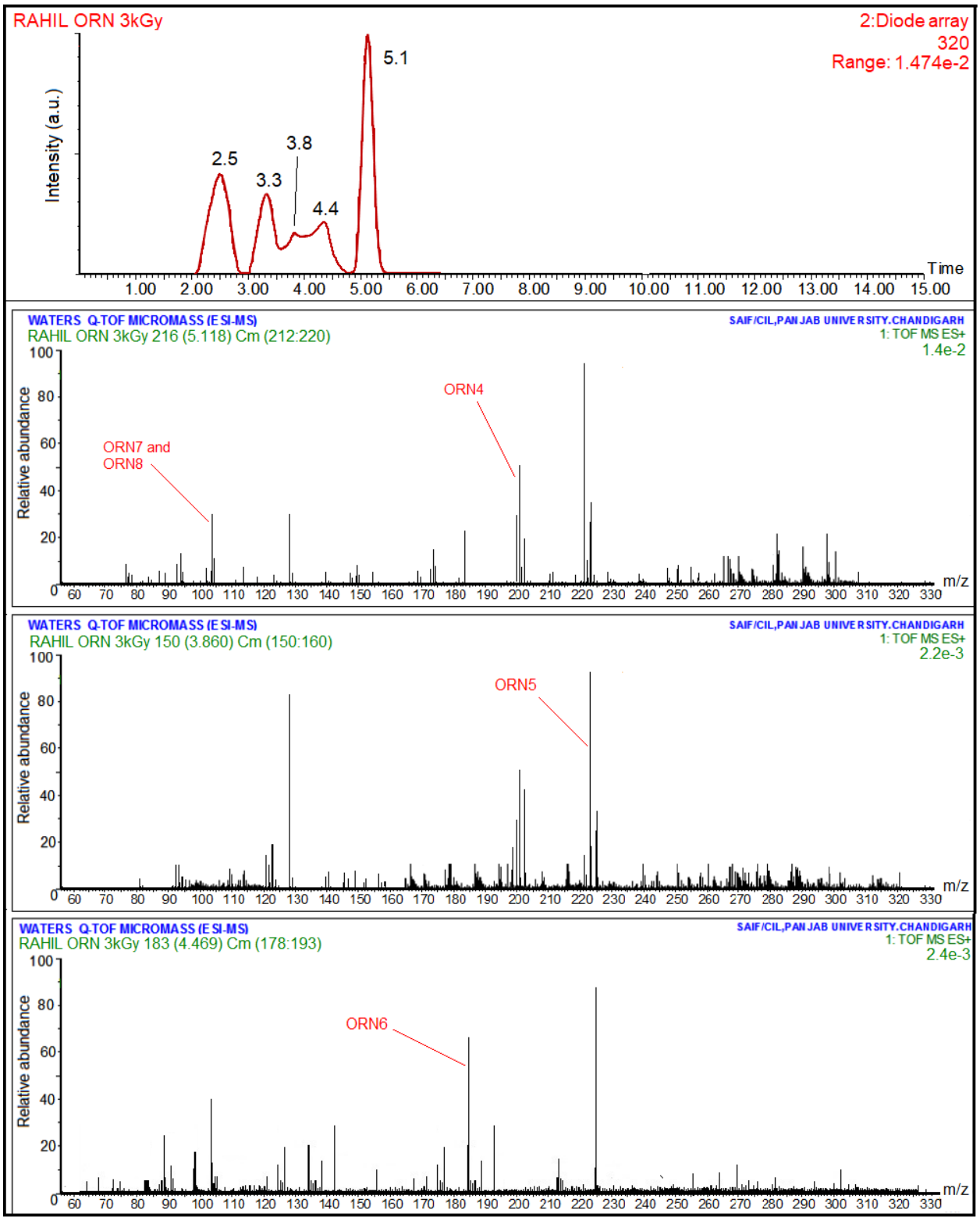

Fig. 4.56 Total ion current chromatogram and mass spectrum recorded for aqueous solution of ORZ (0.22 mM) E-beam irradiated with 3.0 kGy dose

Results displayed the identification of almost eight ORZ degradation products or reaction intermediates with their peak intensity greater than 10%. Based on the results of LC-MS analysis, the possible degradation pathways of ORZ using E-beam irradiation treatment have been inferred in Fig. 4.57. In one instance, the attack of HO$^{\bullet}$ on ornidazole (**ORZ**, t_R=5.27 min) can result in the generation of ornidazole epoxide (ORZ1, *m/z* 184, retention time t_R=5.1 min,). **ORZ1** represents the one of the oxidative degradation products also identified in previous studies (Zhao *et al*. 2012; Salo *et al.* 2003). **ORZ2** (1,2-dimethyl-5-nitroimidazole, *m/z* 142, t_R=2.5 min) can be formed through cleavage of C-C bond in the ORZ1. In addition, the cleavage of bond between C-N in ORZ1 is expected to the generate **ORZ3** (2-methyl-5-nitroimidazole, *m/z* 128, t_R=3.3 min). Furthermore, ORZ3 can be formed through demethylation of ORZ2. The product **ORZ4** (ornidazole glycol, *m/z* 201, t_R=5.1 min) can be generated through the hydrolytic halogenation of aliphatic halomethyl (Cl) in ORZ molecule. ORZ4 might also get formed from ORZ1 by the direct attack of HO$^{\bullet}$ radicals (Salo *et al.* 2003). As an alternative pathway, demethylation and dehydrogenation of ORZ may lead to generate **ORZ5** (1-(3-chloro-2-hydroxyl-1-propene)-2-hydroxyl-5-nitroimidazole, *m/z* 221, t_R=3.8 min) which can further lead to the formation of **ORZ6** (1-(methine-propylene oxide)-2-hydroxyl-5-nitroimidazole, *m/z* 184, t_R=4.4 min). ORZ6 can also be formed through the direct degradation of ORZ by hydrogen chloride cleavage and dehydrogenation. LC-QTOF-MS studies indicated the product ORZ6 has mass 184, equal to that of the ORZ1, though it resolved at different t_R. The initial hypothesis stated that the ORZ6 has a different structure from ORZ1, which appears via well-established photolytic reaction (Tonnesen, 2004). The product ORZ4 can cleave to the hydroxylated chain which can be oxidized to products **ORZ7** (t_R=5.11-5.27 min, *m/z* 104) and **ORZ8** (t_R=5.11-5.27 min, *m/z* 104). The products ORZ7 and ORZ8 can be generated through the direct degradation of ORZ during high energy E-beam induced radiolytic treatment of ORZ.

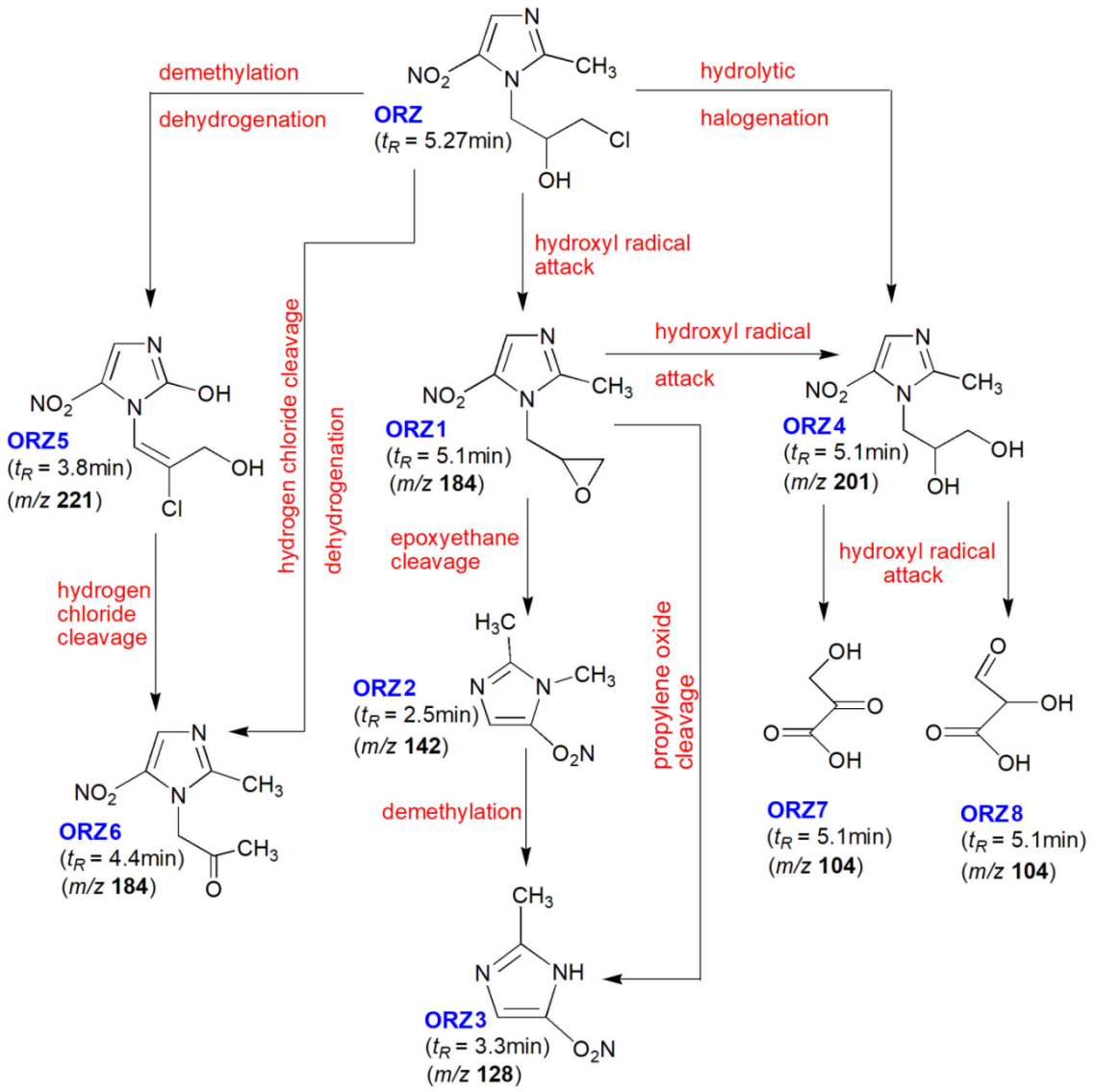

Fig. 4.57 The possible pathways of E-beam induced radiolytic degradation of ORZ

Therefore, the primary degradation mechanism of ORZ using E-beam irradiation treatment could be attributed to the $HO^{\bullet}$ radical species and direct cleavage of ORZ molecules.

4.5.9 Cytotoxicity assessment

The efficacy of the treatment method is not only based on the efficiency of the degradation but also generate degradation products which are lesser toxic than the parent compound. Although, various AOPs have been utilized to degrade OFX, but some investigations have reported that toxicity of OFX treated solutions has been increased, primarily caused by the formation of toxic intermediate and/or by-products (Batt *et al.* 2006; Calza *et al.* 2008; Michael *et al.* 2010; Vasquez *et al*. 2013, Tay and Madehi, 2015; Zhu *et al.*

2016). The photocatalytic treatments leading to the formation of transformed products of OFX have been shown to decrease the antimicrobial activities on the one hand and on the other hand, the genotoxic properties of transformed products was found to be greater than the parent compound (Vasquez *et al.* 2013). The ozonation treatment of OFX might yield transformation products of greater toxicity as compared to OFX (Tay and Madehi, 2015). Study performed by Michael *et al.* (2010) revealed that the toxicity of photocatalytically treated solution of OFX increased slightly using TiO_2, whereas, the toxicity of the solar Fenton treated solution increased dramatically.

The toxicity of un-irradiated (control) and E-Beam irradiated OFX solutions at different absorbed doses (1-3 kGy) were compared through standard Kirby-Bauer (disk diffusion) method against clinical isolates of all three microbes: *E. coli*, *B. subtilis*, and *P. aeruginosa* as depicted in Fig. 4.58. The growth inhibitory zone surrounding the well containing un-irradiated OFX (control) showed its substantial toxicity against all the microbes (Fig. 4.58a-4.58c). On the other hand, absence of such growth inhibitory zone was observed in irradiated OFX solutions at different dose. It indicated that the E-beam induced degradation of OFX did not lead to produce any possible toxic by-products. Thus, E-beam radiolysis is expected to be established as a viable method for the comprehensive and effective treatment of fluoroquinolones antibiotic compounds present in the water and wastewater treatment plants.

The cytotoxicity results obtained for ORZ exhibited that the E-beam treated solutions as well as control ORZ (0.22 mM) solution showed absence of any toxicity against all the studied microorganisms. Therefore, it can be concluded that the parent compound (ORZ) in addition to the degradation intermediates/by-products formed during gamma as well as E-beam induced radiolytic treatment of ORZ are non-toxic to the selected microorganisms.

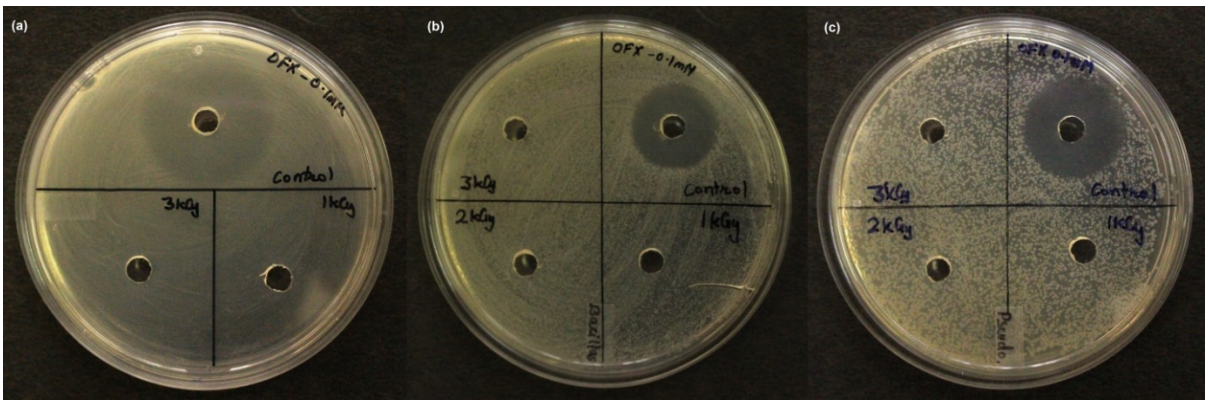

Fig. 4.58 Inhibition rate of activity of OFX solutions before and after E-beam irradiation against (a) *E. coli* (b) *B. subtilis* (c) *P. aeruginosa*

The toxicity potential of AMX and its irradiated solutions (at different absorbed dose) was also studied against clinical isolates of *E. coli, B. subtilis, and P. aeruginosa*. The results indicate that unlike the un-irradiated AMX solution, no zone of inhibition was observed in the E-beam irradiated solutions and thus indicating that irradiated AMX solutions did not acquire any toxicity after E-beam irradiation treatment as shown in Fig. 4.59. Thus, it can be concluded that the intermediates/by-products produced during gamma as well as E-beam radiolytic degradation of AMX are non-toxic to the studied microbes.

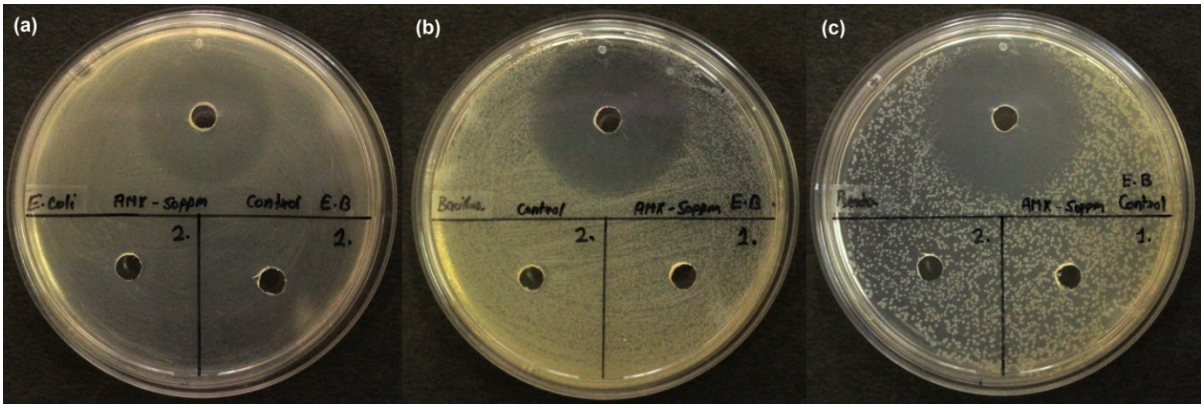

Fig. 4.59 Inhibition rate of activity of AMX solutions before and after E-beam irradiation against (a) *E. coli* (b) *B. subtilis* (c) *P. aeruginosa*

4.5.10 Cost evaluation of treatment process

The cost of electrical energy employed in the E-beam induced radiolytic degradation of OFX, ORZ and AMX was calculated using Eq. 4.44 (Paul *et al.* 2014). The results of cost analysis for E-beam treatment of OFX, ORZ and AMX are explained in Table 4.19, 4.20 and 4.21.

$$EEC = P \times (t/60) \times (1000/v) \quad (4.44)$$

where EEC (in kWh m^{-3}) is the consumption of electrical energy (kWh) to degrade a pollutant in 1 m^3 of volume, t is the time of treatment (min), P is the rated power of the E-beam (kW), and v is the treatment volume of model compound solution (in L). Table 4.18 shows the calculations of power of E-beam and volume of model compounds solution treated.

Under the experimental conditions, the overall cost involved in the degradation of OFX without any additional chemicals was 0.40, 1.07 and 2.15 USD for treating OFX in 1 m^3 of ultrapure water, surface water and wastewater, respectively; whereas, the overall cost involved in the degradation of ORZ without any additional chemicals was 0.40, 1.07 and 2.15

USD for treating ORZ in 1 m^3 of ultrapure water, surface water and wastewater, respectively.

Table 4.18 Calculations of power of E-beam accelerator and volume of model compound solution treated

Power (kW)	P= Energy x I_{avg} = 4.5 MeV x 0.156 mA = 0.702 kW	
Volume of model compound solution (L)	V= 1.3 x 60 x 80 = 6240 cm^3 = 6.25 L	(Dimensions of stainless steel tray)

Table 4.19 The cost of electrical energy involved in E-beam radiolysis of OFX in different water matrices (UW: ultrapure water; SW: surface water; WW: wastewater)

S.No.	Average power employed (kW)	Average treatment time (min) of OFX in different water matrices	Volume of OFX solution treated (L)*	EEC (kWh m^{-3}) consumed	Total EEC (INR m^{-3}) of OFX solution @INR 5/kWh**	Total EEC (US $ m^{-3}) of OFX solution#
1.	0.702	3 (UW)	6.24	5.62	28.1	0.40
2.	0.702	8 (SW)	6.24	15	75	1.05
3.	0.702	16 (WW)	6.24	30	150	2.11

*Directed by the maximum volume capability of the E-beam unit to treat the OFX under the same treatment condition.

**Considering the average cost of Rs 5/kWh for industrial sector (Punjab State Electricity Regulatory Commission, 2017).

#Considering the conversion factor for INR to USD to be 1 USD=71.14 INR

Table 4.20 The cost of electrical energy involved in E-beam radiolysis of ORZ in different water matrices (UW: ultrapure water; SW: surface water; WW: wastewater)

S.No.	Average power employed (kW)	Average treatment time (min) of ORZ in	Volume of ORZ solution treated (L)*	EEC (kWh m^{-3}) consumed	Total EEC (INR m^{-3}) of ORZ solution @INR 5/kWh**	Total EEC (US $ m^{-3}) of ORZ solution

		different water matrices				
1.	0.702	3 (UW)	6.24	5.62	28.1	0.40
2.	0.702	8 (SW)	6.24	15	75	1.07
3.	0.702	16 (WW)	6.24	30	150	2.15

*Directed by the maximum volume capability of the E-beam unit to treat the ORZ under the same treatment condition.

**Considering the average cost of Rs 5/kWh for industrial sector (Punjab State Electricity Regulatory Commission, 2017).

#Considering the conversion factor for INR to USD to be 1 USD=71.14 INR

Table 4.21 The cost of electrical energy involved in E-beam radiolysis of AMX

Average power employed (kW)	Average treatment time (min) of AMX	Volume of AMX solution treated (L)*	EEC (kWh m^{-3}) consumed	Total EEC (INR m^{-3}) of AMX solution @INR 5/kWh**	Total EEC (US \$ m^{-3}) of AMX solution
0.702	16	6.24	30	150	2.11

*Directed by the maximum volume capability of the E-beam unit to treat the AMX under the same treatment condition.

**Considering the average cost of Rs 5/kWh for industrial sector (Punjab State Electricity Regulatory Commission, 2017).

#Considering the conversion factor for INR to USD to be 1 USD=71.14 INR

4.6 Comparison of treatment technologies for degradation of model compounds

All the model compounds (OFX, ORZ and AMX) were treated by independent Fenton, gamma and E-beam irradiation treatment and comparative results of employed treatments are summarized in Table 4.22.

According to Table 4.22, all the treatment technologies applied in the treatment of model compounds were effective in their degradation; however, the use of E-beam irradiation treatment was more effective in degradation of model compounds in term of treatment time. Overall, the use of irradiation based treatment of model compounds has eliminated the use of additional chemicals as well as sludge formation in comparison to photo-Fenton treatment.

Table 4.22 Comparative results of employed treatments for model compounds

S. No.	Treatment	Model compound with initial concentration	Optimized conditions	Degradation efficiency (%)	TOC reduction (%)	Treatment time (min)
1.	Solar photo-Fenton treatment using hematite	ORZ (0.22 mM)	0.13 g L^{-1} cubical-α-Fe_2O_3, 10 mM H_2O_2, pH 3	98%	59%	180
2.	Solar photo-Fenton treatment using soil	ORZ (0.09 mM)	0.033 g L^{-1} soil, 1 mM H_2O_2, pH 3	95%	4.15%	180
		OFX (0.05 mM)	0.020 g L^{-1} soil, 2 mM H_2O_2, pH 3	92%	30%	180
3.	Solar photo-Fenton treatment using GO-FeS_2	AMX (0.1 mM)	1 g L^{-1} GO-FeS_2, 10 mM H_2O_2, pH 5	80%	27.7%	180
		OFX (0.1 mM)	1 g L^{-1} GO-FeS_2, 10 mM H_2O_2, pH 5	97%	38.6%	180
4.	Gamma irradiation treatment	AMX (0.1 mM)	15 kGy absorbed dose	92%	39.8%	82
		ORZ (0.22 mM)	3 kGy absorbed dose	99%	35%	240
		OFX (0.1 mM)	3 kGy absorbed dose	95%	29.6%	240
5.	E-beam irradiation treatment	AMX (0.1 mM)	15 kGy absorbed dose	88%	47.3%	16
		ORZ (0.22 mM)	3 kGy absorbed dose	96%	29.7%	3
		OFX (0.1 mM)	3 kGy absorbed dose	94%	28.5%	3

4.7 Applications of Fenton's technologies for wastewater treatment

After the independent Fenton, gamma and E-beam treatment of model compounds (OFX, ORZ and AMX), the real pharmaceutical wastewater of different organic loads were subjected to independent Fenton, gamma and E-beam treatment and in conjunction with biological treatment. In order to assess the applications of AOPs on real pharmaceutical wastewater treatment, applications of Fenton's treatment such as, dark-Fenton and photo-Fenton were explored for the treatment of collected wastewater samples of low and high strength.

4.7.1 Physicochemical characteristics of wastewaters

The main parameters of industrial low (LSW) and high strength (HSW) pharmaceutical wastewater samples were evaluated and results are summarized in Table 4.23. Biodegradability index (BOD_5/COD) was 0.58 and 0.57 for LSW and HSW, respectively, indicating that raw wastewater was directly amenable to biodegradation. As, the main goal was to achieve maximum degradation of organic matter present in the wastewaters, therefore, both the samples were subjected to independent dark-Fenton (DF) and photo-Fenton (PF) as a pre-treatment technology to achieve the enhanced degradation of organic content of wastewater.

Table 4.23 Physicochemical characteristics of raw low and high strength wastewater

S.No.	Parameter	Raw low strength wastewater	Raw high strength wastewater
		Mean ± S.D.	Mean ± S.D.
1	pH	12.7 ± 0.25	12.8 ± 0.32
2	Color	Light brown	Dark brown
3	Conductivity	6.15	7.25
4	BOD_5	4925 ± 155	21560 ± 160
5	COD	8370 ± 190	37410 ±225
6	BOD_5/COD	0.58 ± 0.05	0.57 ± 0.06
7	TOC	2350 ± 110	8250 ± 145
8	TSS	3780 ± 140	6780 ± 180
9	TDS	14910 ± 175	21340 ± 450
10	TKN	761 ± 85	3010 ± 145
11	Nitrate	12 ± 0.75	18 ± 1.25
12	Nitrite	17 ± 1.86	47 ± 2.10
13	Sulfates	2343 ± 145	3920 ± 250
14	Chloride	1765 ± 105	6230 ± 155
15	Phosphate	< 0.005	0.2 ± 0.03

Note: All the values except pH, color, conductivity and BOD_5/COD are expressed as mg L^{-1}. Units of conductivity is expressed as mS cm^{-1}. All the values are expressed as mean of three values.

4.7.2 Fenton treatment

COD results of LSW and HSW obtained using dark-Fenton's oxidation are illustrated

in Fig. 4.60. For both the samples, effect of pH was studied by varying the pH in the range of 2.0 to 9.0 at a constant loading of H_2O_2 and Fe^{2+}. The constant loading for studying the pH effect was 0.025 M Fe^{2+} and 0.25 M H_2O_2 for LSW, whereas 0.15 M Fe^{2+} and 1 M H_2O_2 was maintained for HSW. The results obtained showed that maximum removal efficiency of COD was achieved at 3.0 pH and reduced COD removal efficiency was obtained at lower and higher pH values for both LSW and HSW. At pH below 3.0, the reaction between H^+ and $HO^{\bullet}$ is significant in comparison to desired oxidation, and H_2O_2 is stabilized as $H_3O_2^+$ at lower pH values (Jamil *et al.* 2011; Ramteke and Gogate, 2016). At higher pH (>3.0), the extent of removal efficiency decreased due to the precipitation of Fe^{3+} ions as $Fe(OH)_3$, thereby preventing the reaction between Fe^{3+} and H_2O_2 to produce $HOO^{\bullet}$ radicals. Moreover, the generation of $HO^{\bullet}$ radical is reduced at higher pH due to catalytic decomposition of H_2O_2 to H_2O and O_2 by $Fe(OH)_3$ (Ramteke and Gogate, 2016). The results obtained are in agreement with the reported literature that confirmed that the optimum pH for Fenton's oxidation ranged between 2.5 to 3.5 which is the important factor in determining the efficacy of Fenton's oxidation (Bautista *et al.* 2007).

The effect of H_2O_2 dosage was investigated at different concentrations ranging from 0.1 to 0.5 M for LSW (Fig. 4.60b) and 0.5 to 1.5 M for HSW (Fig. 4.60e). The initial Fe^{2+} concentration was kept to be 0.025 and 0.15 M for LSW and HSW, respectively. Results indicated that the COD removal extent increased with increase in H_2O_2 dosage from 0.1 to 0.25 M for LSW and from 0.5 to 1 M for HSW. The increase of removal efficiency of COD with increase in H_2O_2 dosage could be ascribed to the fact that the generation of $HO^{\bullet}$ radicals enhanced with the increasing dose of H_2O_2 leading to higher COD removal efficiency. At concentration above the optimum concentration, the reduced COD removal efficiency could be due to the scavenging effect of H_2O_2 at higher dosage of H_2O_2 (Karthikeyan *et al.* 2011). Therefore, no further enhancement in COD removal efficiency was observed at higher dose of H_2O_2 beyond 0.25 and 1 M for LSW and HSW, respectively. The adjustment of optimum H_2O_2 dose is important in Fenton's oxidation as excess H_2O_2 remaining in the solution could induce toxicity to the subsequent biodegradation treatment (Bautista *et al.* 2007; Ramteke and Gogate, 2016).

The effect of Fe^{2+} concentration was investigated by varying the Fe^{2+} concentration from 0.0025 to 0.075 M for LSW (Fig. 4.60a), whereas 0.05 to 0.2 M Fe^{2+} concentration were varied for HSW (Fig. 4.60d). The initial H_2O_2 dosage was optimized to be 0.25 and 1 M for LSW and HSW, respectively. Results indicated that the COD removal extent increased with

increase in Fe^{2+} concentration from 0.0025 to 0.25 M for LSW and from 0.5 to 0.15 M for HSW, and further increase in concentration of Fe^{2+} ions leads to marginal improvement in COD removal efficiency. Fenton treatment is reported to be an efficient method for wastewater treatment and various studies established the importance of increasing Fe^{2+} concentration is more favourable that increasing H_2O_2 dosage (Martinez *et al.* 2003; Karthikeyan *et al.* 2011). However, due to the problem associated with the necessity of additional treatment to remove the iron sludge after the treatment, it is not practical to use higher concentration of Fe^{2+} in reaction system. Thus, optimum dosage of H_2O_2 in Fenton process was established to be 0.25 and 1 M for LSW and HSW, respectively.

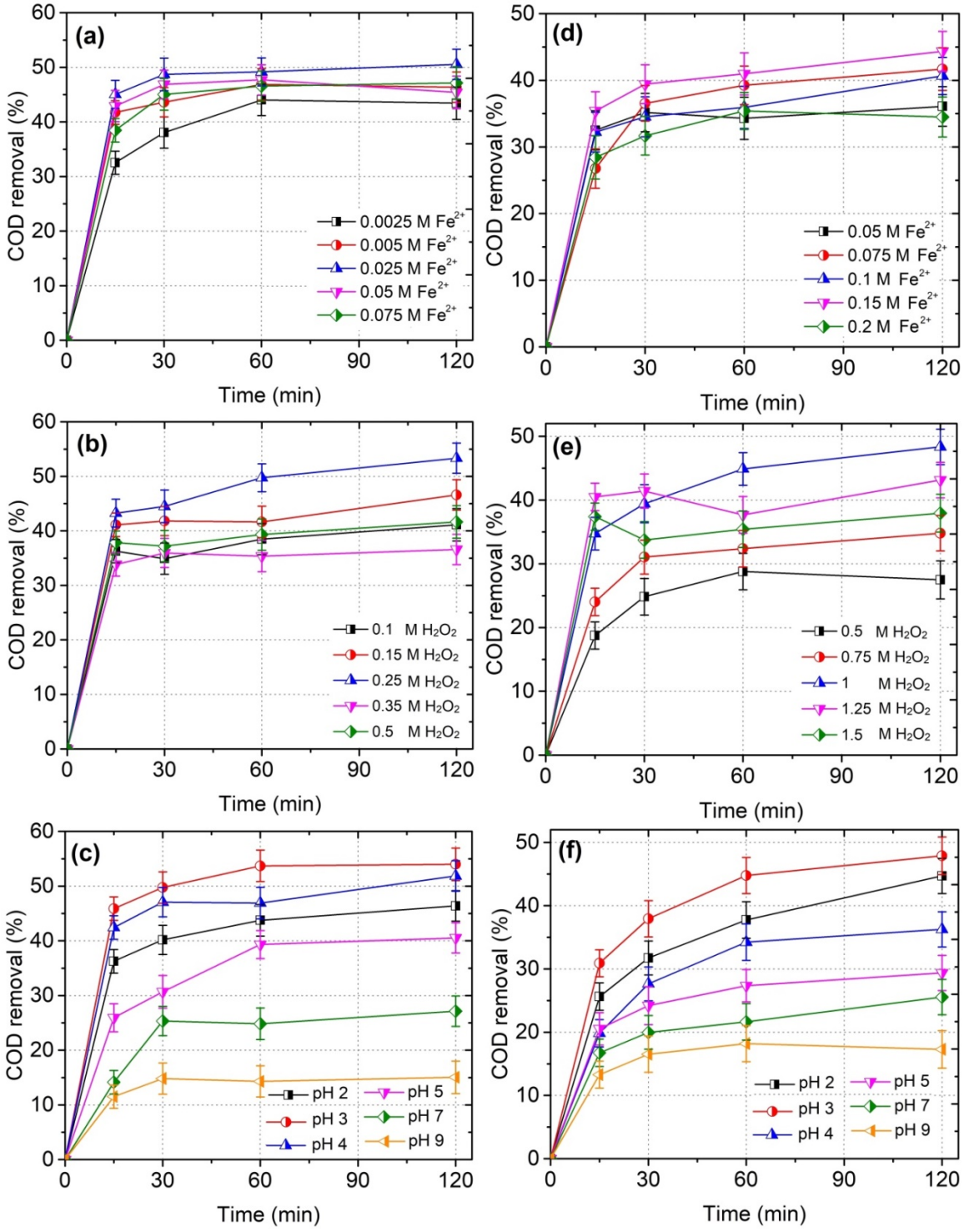

Fig. 4.60 Effect of Fe concentration on COD removal efficiency of (a) LSW and (d) HSW; Effect of H_2O_2 on COD removal efficiency of (b) LSW and (d) HSW; Effect of pH on COD removal efficiency of (c) LSW (f) HSW during dark-Fenton treatment

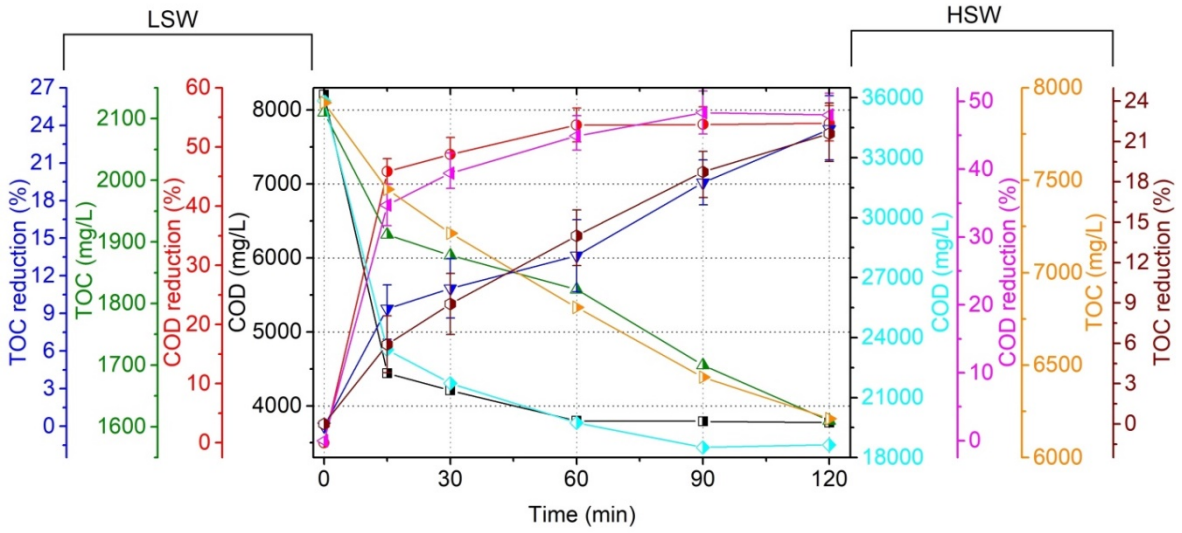

Fig. 4.61 Effect of optimized conditions on COD and TOC removal efficiency of wastewaters during dark-Fenton treatment [LSW: Low strength wastewater with 0.25 M H_2O_2 and 0.025 M Fe^{2+} at pH 3.0; HSW: High strength wastewater with 1 M H_2O_2 and 0.15 M Fe^{2+} at pH 3.0]

Fig. 4.61 depicts the results of COD and TOC removal efficiency obtained under the optimized conditions of LSW and HSW using Fenton treatment. Overall, the results showed that 53.8 and 23.6% of COD and TOC reduction for LSW under the optimized conditions (0.025 M Fe^{2+}, 0.25 M H_2O_2, pH 3.0 and 120 min treatment time); whereas, 47.9 and 21.5% of COD and TOC reduction was obtained for HSW under the optimized conditions (0.15 M Fe^{2+}, 1 M H_2O_2, pH 3.0 and 120 min treatment time). The effect of temperature was not considered in the pre-oxidation processes using Fenton's applications as the influence of temperature was negligible in all preliminary experiments. Although biodegradability index did not improved much for both the wastewater samples even after 120 min of Fenton treatment, however, Fenton treatment could be used as pre-treatment technology to reduce organic load of wastewater to some extent and making wastewater susceptible to post-biological treatment. The application of treatment time can be decided on the basis of requisite changes in biodegradability index and optional design parameters for biodegradation treatment. In fact, according to Symons *et al.* (1960), the BOD_5/COD ratio should be >0.6 for wastewater to be suitable for biological treatment, while BOD_5/COD <0.4 represents non-biodegradable wastewater. In present study, a cutoff biodegradability of 0.6 was used in order to consider the pre-treated wastewater to be able to meet the desired conditions for biological degradation.

4.7.3 Photo-Fenton treatment

Photo-Fenton oxidation was employed to degrade LSW and HSW as illustrated in Fig. 4.62. For both the samples, effect of pH was studied by varying the pH values in the range of 2.0 to 9.0 at a fixed treatment time of 120 min and at a constant loading of H_2O_2 and Fe^{2+}. The constant loading for studying the pH effect was 0.05 mol M Fe^{2+} and 0.25 M H_2O_2 for LSW; whereas, 0.1 M Fe^{2+} and 1 M H_2O_2 was maintained for HSW. The results obtained showed that maximum COD removal efficiency was obtained at pH 3.0 and reduced COD removal efficiency was obtained at lower and higher pH values for both LSW and HSW. The study performed by Kuo and Lo (1999) revealed that more $Fe(OH)^+$ are produced in the pH range of 2-4. The decomposition of H_2O_2 and activity of $Fe(OH)^+$ in Fenton and photo-Fenton process enhances in acidic condition leading to rapid generation $HO^{\bullet}$ radicals. Thus, the initial pH for all the subsequent photo-Fenton experiments of LSW and HSW was kept to be 3.0.

The effect of H_2O_2 dosage was investigated at different concentrations ranging from 0.05 to 0.75 M for LSW and 0.5 to 1.5 M for HSW. The initial Fe^{2+} concentration was kept to be 0.05 and 0.1 M for LSW and HSW, respectively with pH adjustment to 3.0. Results indicated that the extent of COD removal increased with increase in H_2O_2 dosage from 0.05 to 0.25 M for LSW and from 0.5 to 1 M for HSW. Thus, in present work, optimum dosage of H_2O_2 in photo-Fenton process was established to be 0.25 and 1 M for LSW and HSW, respectively. The results revealed that optimum dose of H_2O_2 in photo-Fenton treatment of LSW and HSW were almost same to the dark-Fenton treatment of same wastewater samples.

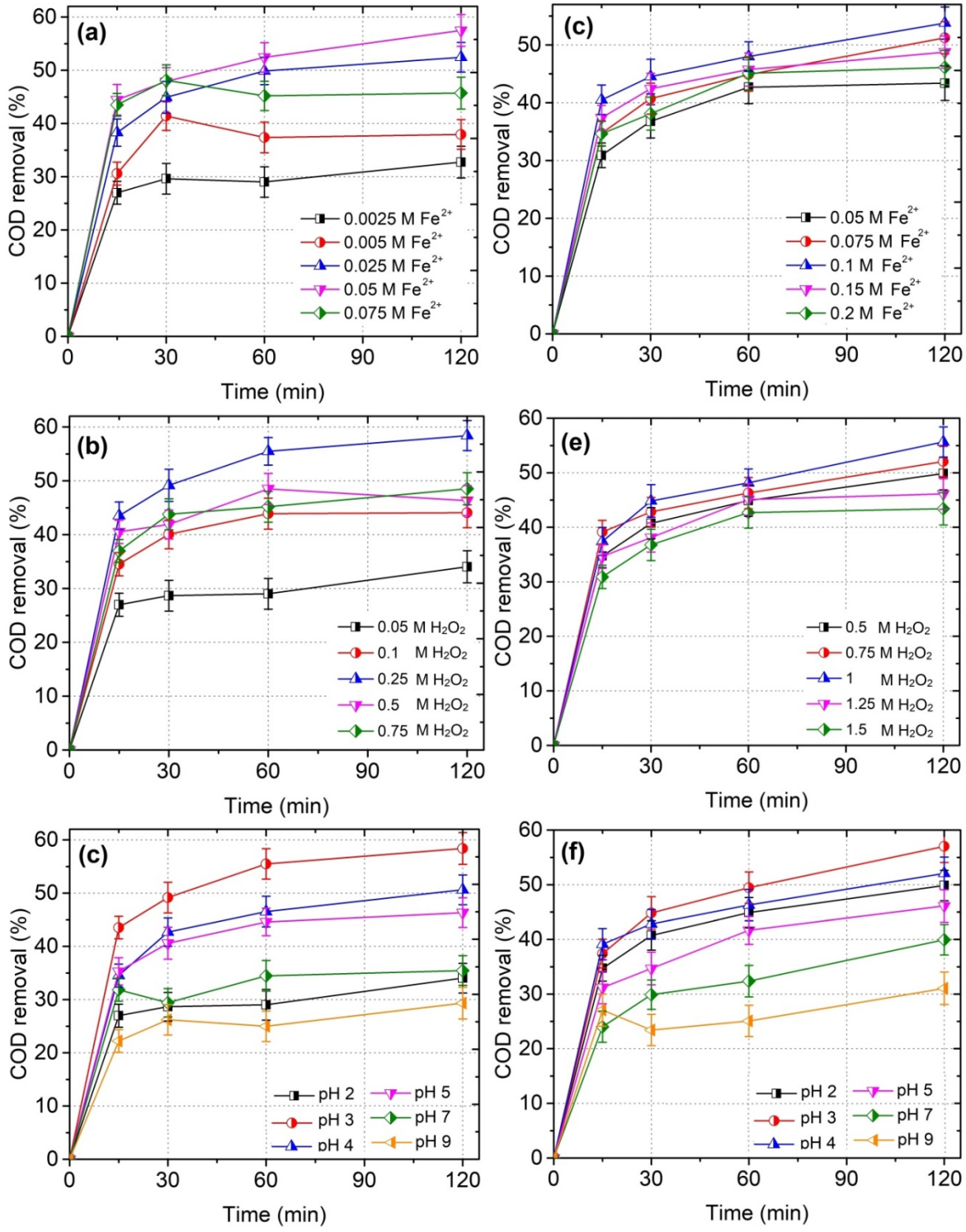

Fig. 4.62 Effect of Fe concentration on COD removal efficiency of (a) LSW and (d) HSW; Effect of H_2O_2 on COD removal efficiency of (b) LSW and (d) HSW; Effect of pH on COD removal efficiency of (c) LSW (f) HSW during photo-Fenton treatment

The effect of Fe^{2+} concentration was investigated by varying the concentration of Fe^{2+} from 0.0025 to 0.075 M for LSW; whereas, 0.05 to 0.2 M Fe^{2+} concentration was varied for

HSW samples. The initial H_2O_2 dosage was kept to be 0.05 and 1 M for LSW and HSW, respectively. The results revealed that the extent of COD removal efficiency increased with Fe^{2+} concentration at a constant H_2O_2 dose for both LSW and HSW samples. Results indicated that the extent of COD removal increased with increase in Fe^{2+} concentration from 0.0025 to 0.05 M for LSW and from 0.5 to 0.1 M for HSW, and further increase in Fe^{2+} concentration leads to marginal improvement in COD removal efficiency. The higher concentration of iron salt may lead to the recombination of $HO^{\bullet}$ radicals with Fe^{2+} (Umar *et al*. 2010). Thus, optimum concentration of Fe^{2+} in photo-Fenton process was found to be 0.05 and 0.1 M for LSW and HSW, respectively.

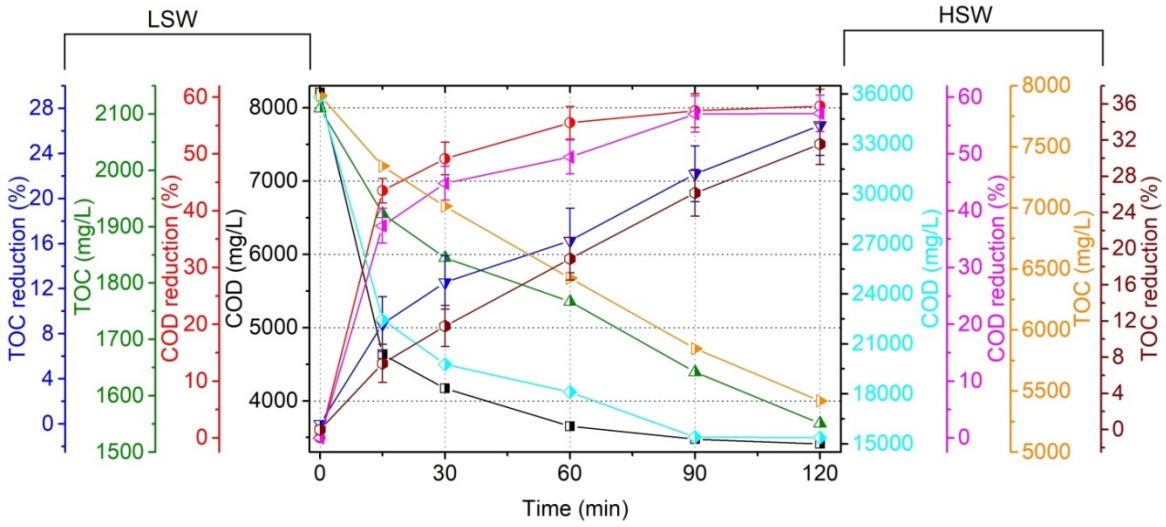

Fig. 4.63 Effect of optimized conditions on COD and TOC removal efficiency of wastewaters during photo-Fenton treatment [LSW: Low strength wastewater with 0.25 M H_2O_2 and 0.05 M Fe^{2+} at pH 3.0; HSW: High strength wastewater with 1 M H_2O_2 and 0.1 M Fe^{2+} at pH 3.0]

Fig. 4.63 represents the COD and TOC removal efficiency obtained under the optimized conditions of LSW and HSW using photo-Fenton treatment. Overall, the results showed that 58.4 and 26.4% of COD and TOC reduction for LSW under the optimized conditions (0.05 M Fe^{2+}, 0.25 M H_2O_2, pH 3.0 and 120 min treatment time); whereas, 57.1 and 31.5% of COD and TOC reduction was obtained for HSW under the optimized conditions (0.1 M Fe^{2+}, 1 M H_2O_2, pH 3.0 and 120 min treatment time). The importance of light irradiation is due to the photochemistry of Fe^{3+} ions which probably produce the hydroxyl complexes, for example $Fe(OH)^{2+}$ and $Fe(OH)_2^{4+}$, which undergo photo-reduction to Fe^{2+} and $HO^{\bullet}$ by absorbing light in UV/visible region (De la Cruz *et al*. 2012). The

treatment efficiency of PF process might also get enhanced due to direct photolysis of compounds in sample, indirect photolysis through interaction with dissolved organic matter in wastewater and photolysis of H_2O_2 to produce additional $HO^{\bullet}$ radicals. The results of biodegradability index obtained using PF treatment of wastewater samples did not improved much; therefore degradation of organic matter present is wastewater is the primary goal of the pre-treatment. The biodegradability index for LSW and HSW after PF treatment was found to be >0.6, thus, it is essential to determine the biodegradability behaviour and toxicity during PF oxidation and afterwards to treat the wastewater samples by subsequent biological degradation to achieve the maximum degradation of organic content of wastewaters.

The interesting issue related to the applications of Fenton's treatment of real pharmaceutical wastewater is the treatment time. It is worthwhile to note that although the sampling of Fenton's treatment (dark-Fenton and photo-Fenton) was done at different times from 0 to 120 min, however, the maximum removal efficiency was achieved within 30 min of reaction and afterwards marginal change in removal efficiency was observed as also documented in previous findings (Umar *et al.* 2010; Kang *et al.* 2002; Martinez *et al.* 2003).

Overall, results of Fenton's treatment indicated that PF oxidation produced better results for both LSW and HSW when compared to DF treatment. However, the overall COD and TOC removal efficiency was not that appreciable in PF treatment and was even significantly lower in case of DF oxidation. Lower reduction of COD could be due to the high dissolved solids content in wastewater samples. TDS content in wastewater is the measure of salinity due to the presence of certain salts, especially carbonates and bicarbonates, sulphates, chlorides, phosphates and certain amount of potassium, calcium, magnesium, manganese and iron which are contributing to high level of TDS. Among the different salts contributing to high dissolved solids in wastewater, carbonates and bicarbonates are considered to be scavenger of $HO^{\bullet}$ radicals, thereby reducing the concentration of $HO^{\bullet}$ radicals to react with organic matter of wastewater (Buxton *et al.* 1998; Mehrvar *et al.* 2001; Guo *et al.* 2012). Additionally, high content of Cl^- ions in wastewater samples had negative effect on the treatment efficiency by inhibiting the generation of $HO^{\bullet}$. The Cl^- ions reacts with $HO^{\bullet}$ radicals generating less reactive species, like dichloride anion radicals ($Cl_2^{-\bullet}$) and chlorine ($Cl^{\bullet}$) atoms (De Laat and Le, 2006). Presence of Cl^- ions is also associated with the formation of Fe^{3+}-chlorocomplexes, simultaneously inhibiting the formation of reactive species i.e., Fe^{3+}-hydroperoxide complexes (Sirtori *et al.* 2009).

It was concluded that the amount of H_2O_2 dosage was not high enough to oxidize all

the organic matter present in the wastewater samples even under the optimal conditions. It is not practical to increase the amount of H_2O_2 in the solution due to the earlier mentioned reason (Section 4.7.2). Moreover, the concentration of iron need to be optimized for Fenton's treatment as the excess iron will precipitate as an iron sludge which will lead to secondary treatment and subsequently increase the cost of the treatment process. Considering the potential application of Fe^{2+} and Fe^{3+} ions as potential coagulants, the Fenton processes employed in the this study have dual function of coagulation as well as oxidation in minimizing the organic load of wastewater prior to biological treatment. Thus, it eliminates the prior coagulation treatment being given as a part of primary treatment before biological treatment in conventional treatment plant.

4.7.4 Biological treatment

The low and high strength wastewaters treated using dark Fenton and photo-Fenton were subjected to aerobic biological degradation with activated sludge obtained from the aeration tank of ETP of pharmaceutical manufacturing unit (Derabassi, Punjab). The pH of pre-treated LSW and HSW was adjusted between 7.0 to 8.0 ± 0.2 using H_2SO_4 and NaOH solutions. As the microbial population is strongly dependent on the temperature and sludge concentration, thus lab-scale experiments were conducted with varied volume of sludge concentrations followed by wastewater addition. For both the LSW and HSW, different concentration of sludge was varied and all beakers were incubated at different temperature conditions of 20, 27 and 37 °C.

Fig. 4.64 and 4.65 shows the results of biological degradation of LSW and HSW pre-treated with Fenton and photo-Fenton, respectively. For LSW, sludge concentration was varied from 5 to 25 % (v/v), whereas 10 to 30 % (v/v) of sludge concentration was maintained for HSW treatment. These results indicated that increase in sludge concentration from 5 to 20 % for LSW and 10 to 25% for HSW led to enhanced COD removal, however further increase in sludge concentration led to reduction in COD removal which might be due to increase in mixed liquor suspended solids (MLSS) that perturbs the biomass to food ratio as well as reduced transfer of oxygen obstructing the survival of microbial community (Metcalf and Eddy, 1995). Moreover, it was observed that both LSW and HSW showed better results at 27 °C which might indicate that this temperature could facilitate the growth and metabolic activity of the microbial community to degrade the biodegradable organic matter present in the wastewater.

In all the figures, results shows the degradation efficiency of biological treated LSW with 20% (v/v) sludge concentration at 27 °C of incubation temperature and 8 days of

treatment and HSW with 25% (v/v) sludge concentration at 27 °C and 8 days of treatment. Fig. 4.64 show the results of biological degradation of LSW and HSW pre-treated with dark-Fenton's oxidation. Results showed that 52.2% COD and 35.4% TOC removal was achieved for LSW, respectively. On the other hand, 37.1% COD and 31.2% TOC removal was achieved for HSW. The insignificant reduction in COD with high strength wastewater could be due to the inhibition of aerobic biotransformation leading to declining activity of the microbial populations in the oxidation of real pharmaceutical wastewater.

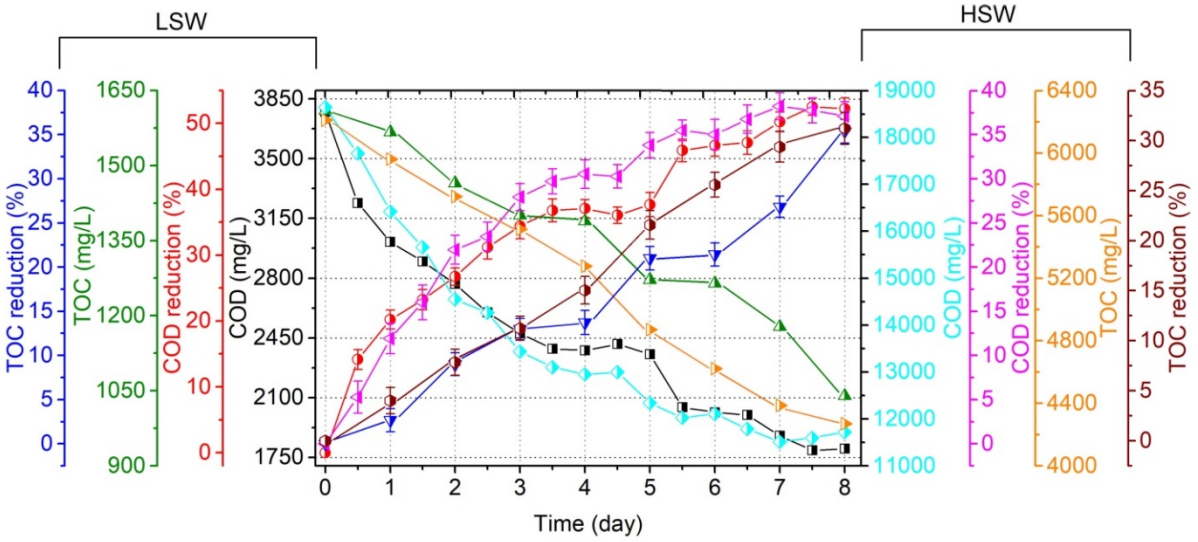

Fig. 4.64 COD and TOC profile using post-biological treatment of LSW and HSW pre-treated with dark-Fenton. [Left axis: Low strength wastewater with 20% (v/v) sludge concentration at 27 °C] and [Right axis: High strength wastewater with 25% (v/v) sludge concentration at 27 °C]

Fig. 4.65 displays the results of biological degradation of LSW and HSW pre-treated with photo-Fenton's oxidation. Results showed that 62.2% COD and 49.2% TOC removal was achieved for LSW; whereas, 55.9% COD and 51.1% TOC removal were achieved for HSW. It was observed that the biodegradation of pre-treated wastewater samples with photo-Fenton oxidation was higher than the wastewater pre-treated with the dark-Fenton. The enhanced COD and TOC removal efficiency could be due to the fact that the pre-treatment of wastewaters with photo-Fenton treatment might have converted the non-biodegradable or recalcitrant organic compounds to the easily biodegradable and simpler molecules which were easily removed by subsequent aerobic biodegradation.

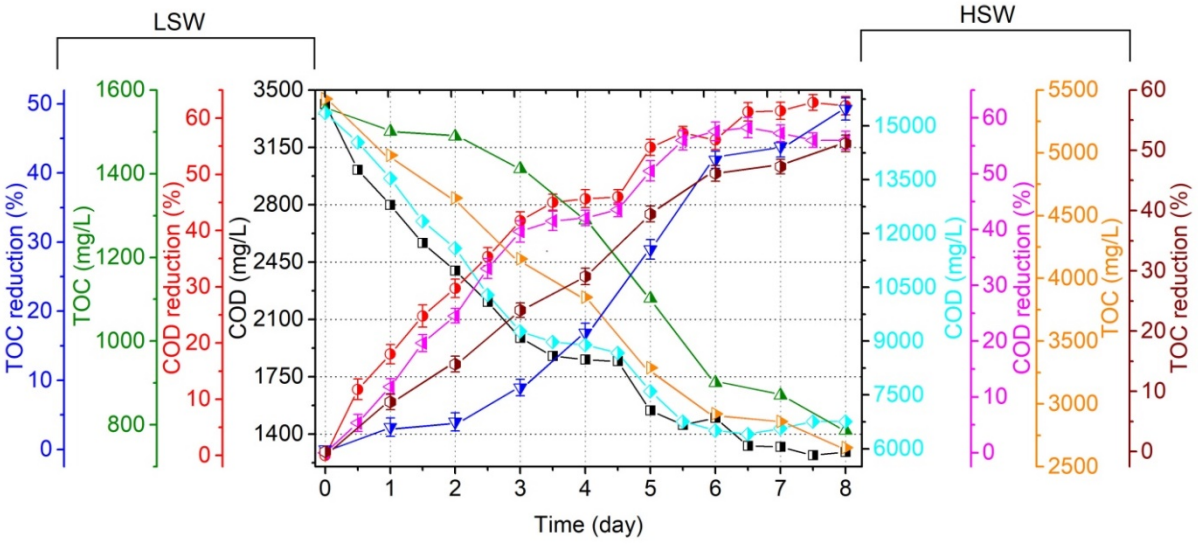

Fig. 4.65 COD and TOC profile using post-biological treatment of LSW and HSW pre-treated with photo-Fenton. [Left axis: Low strength wastewater with 20% (v/v) sludge concentration at 27 °C] and [Right axis: High strength wastewater with 25% (v/v) sludge concentration at 27 °C]

It can be observed that in Fig. 4.64 and 4.65 the COD removal efficiency almost became stable near 4th day of aeration period and subsequently increased after 5th day. Actually, all the biodegradation experiments were performed in batch mode and the nutrients required for the growth and activity of microbes were added during the initiation of reaction. Thus, the growth and activity of microbes might get weakened due to the deficiency of nutrients in the reactor during this period. In order to maintain the required amount of nutrients during activated sludge based biological degradation, nutrients were added after 4th day of aeration period according to the COD:N:P of 100:5:1. This might be the probable reason for enhanced COD removal efficiency on 5th day of aeration period in all the biodegradation experiments.

Overall results indicated that among the utilized Fenton technologies, pre-treatment of pharmaceutical wastewater with PF lead to better mineralization and degradation efficiency with subsequent biological degradation when compared to DF treatment. Overall COD removal efficiency of the combined PF and biological treatment was over 84% for LSW and 82% for HSW. On the other hand, COD removal efficiency of the combined DF and biological treatment was over 78% for LSW and 67% for HSW. The obtained difference in the overall degradation efficiency for pre-treatments could be ascribed to the fact that efficacy of aerobic biotransformation primarily depends on the nature of the intermediates or

secondary metabolites produced during each pre-treatment method, which would be different. Conclusively, it can be considered that combined solar-induced photo-Fenton applications as pre-treatment technology and biological treatment is more proficient approach in comparison to single stage oxidation either by photo-Fenton or biological treatment.

4.7.5 Toxicity analysis

Toxicity of wastewater generated during pre-treatment as well as treated wastewater through combined treatment of Fenton's oxidation and biological treatment was tested against clinical isolates of three microorganisms viz. *E. coli, B. subtilis* and *P. aeruginosa* using zone of inhibition test.

Fig. 4.66 shows the results of toxicity analysis of treated wastewater through different Fenton technologies. Results indicated that strong zone of inhibition was observed for raw LSW and HSW against the selected microorganisms. Dark-Fenton and solar-induced photo-Fenton treated wastewater samples did not exhibited any toxicity against selected microorganisms. Toxicity assessment was conducted for the treated wastewater through Fenton technologies followed by subsequent biological treatment and the results obtained are depicted in the Fig. 4.67. These results showed that when coupled treatment of different Fenton technologies were used as pre-treatment technology to treat wastewater with different organic loads with subsequent biodegradation, a complete detoxification of wastewater was achieved indicating that hybrid treatment technology of Fenton's and biological treatment did not exhibited any toxicity against the selected microbes. However, a comprehensive study dealing with toxicity analyses of treated water using different bioassays test methods could exhibit more reliable and viable results.

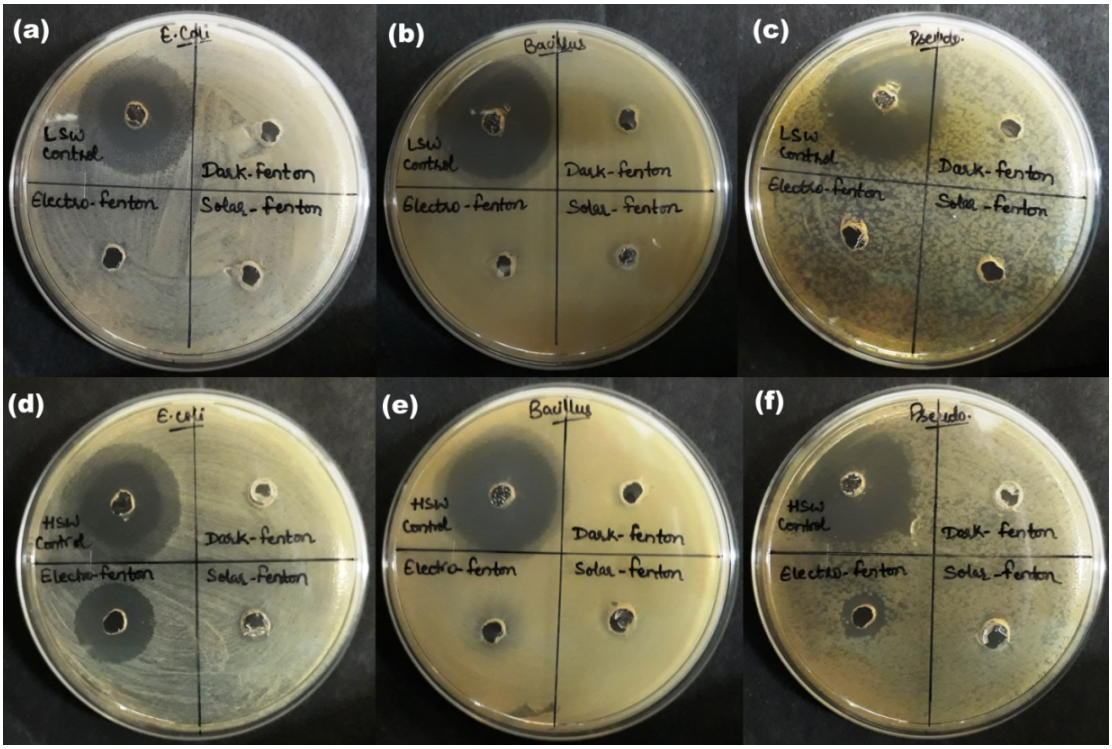

Fig. 4.66 Cytotoxic potential of (a, b and c) LSW and (d, e and f) HSW treated with Fenton treatments

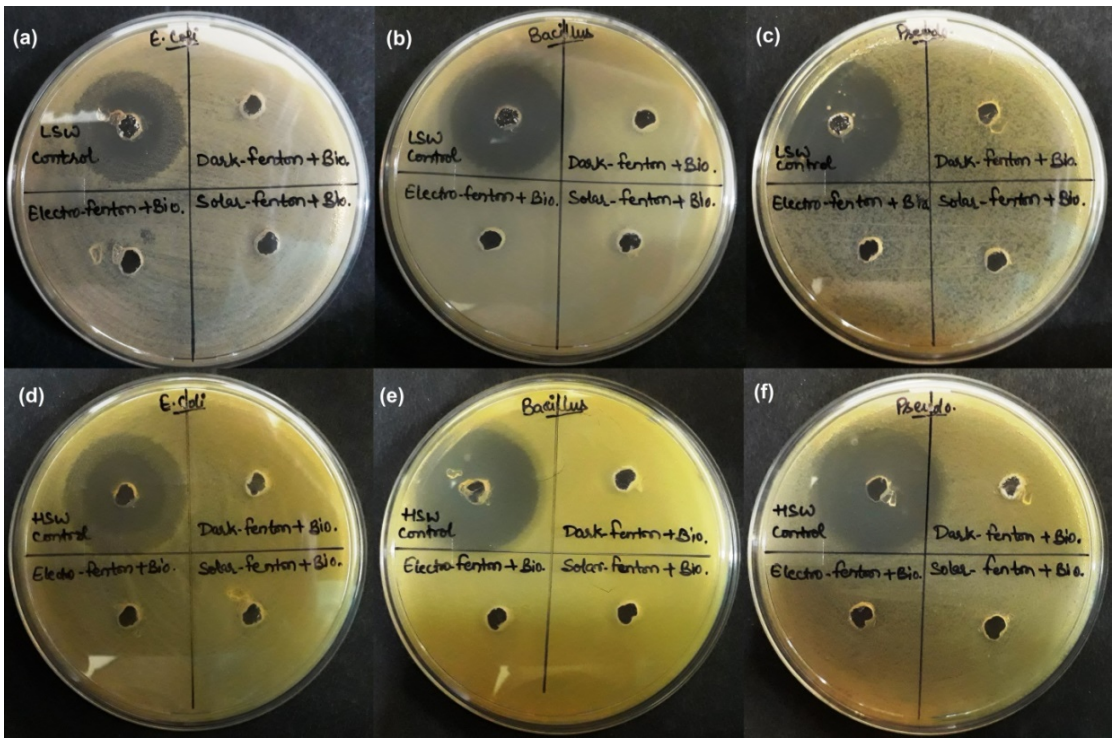

Fig. 4.67 Cytotoxic potential of (a, b and c) LSW and (d, e and f) HSW treated with Fenton treatment and subsequent biological treatment

4.8 Gamma irradiation treatment of real pharmaceutical wastewater

The collected wastewater samples *viz.* low strength (LSW) and high strength (LSW) were subjected to independent gamma irradiation treatment as well as in integrated system with aerobic biological treatment. Gamma irradiation was also employed as pre- and post-treatment to biological treatment.

4.8.1 Chemical coagulation treatment

The detailed physicochemical characteristics of wastewater indicated that raw LSW and HSW generated from the pharmaceutical manufacturing unit contains high load of organic pollutants and solids. Due to high organic load of wastewater, chemical coagulation treatment was given to LSW and HSW with various coagulants including $Ca(OH)_2$, $FeCl_3$ and $Al_2(SO_4)_3$. Table 4.24 and Table 4.25 show the physicochemical characteristics of LSW and HSW, respectively.

The type of coagulant, coagulant dosage, optimum pH and contact time for reduction in COD was investigated by varying the concentration of coagulants from 0.5 to 5 g L^{-1} for treating 100 mL of wastewater and analyzing the COD of supernatant filtered wastewater. These investigations revealed that among the used coagulants, $FeCl_3$ treatment showed better results for both LSW and HSW, and results of various coagulants with different dosages are presented as Fig. 4.68. Fig. 4.69 shows the results of optimum pH and contact time of $FeCl_3$ treatment for reduction in COD. For LSW, 35% of COD removal was obtained with 3 g L^{-1} of $FeCl_3$ at pH 8 with 180 min of contact time; whereas, 29% of COD removal was obtained for HSW at pH 8 with 120 min contact time and 4 g L^{-1} of the coagulant. Although the biodegradability index (BOD_5/COD ratio) of raw LSW and HSW were found to be >0.5, but the post-coagulant treatment of wastewater slightly increases the BOD_5/COD ratio >0.6. The pre-coagulant treated LSW and HSW were subjected to independent biological and gamma-irradiation treatment.

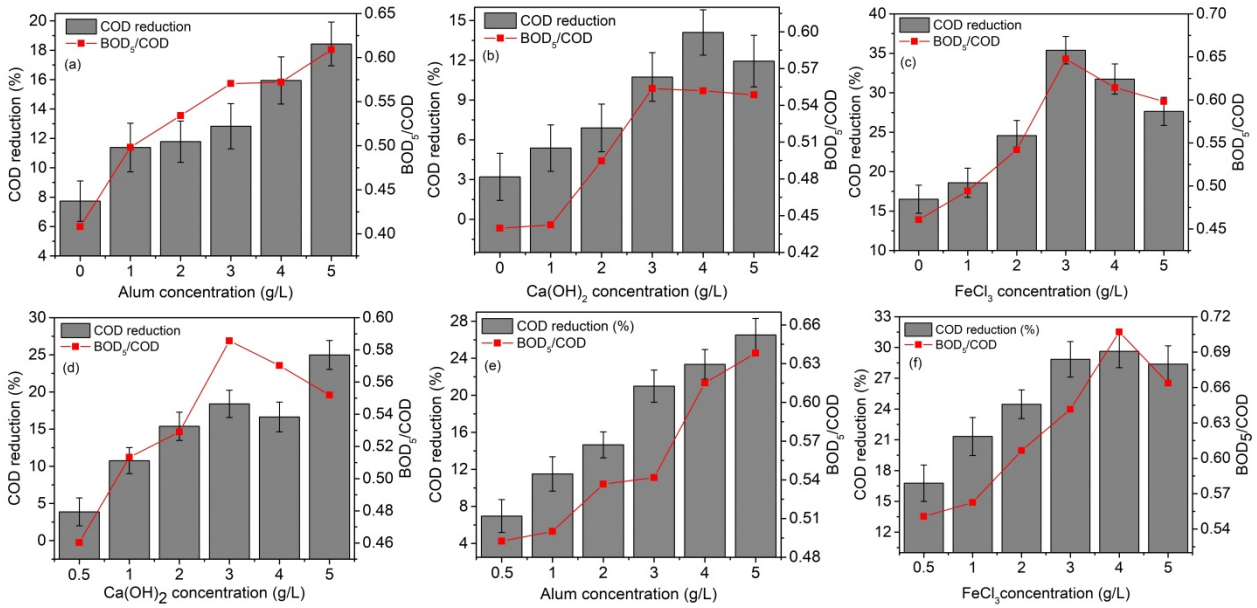

Fig. 4.68 Effect of different coagulants on COD reduction and biodegradability index of (a,d,c) Low strength wastewater and (d,e,f) high strength wastewater

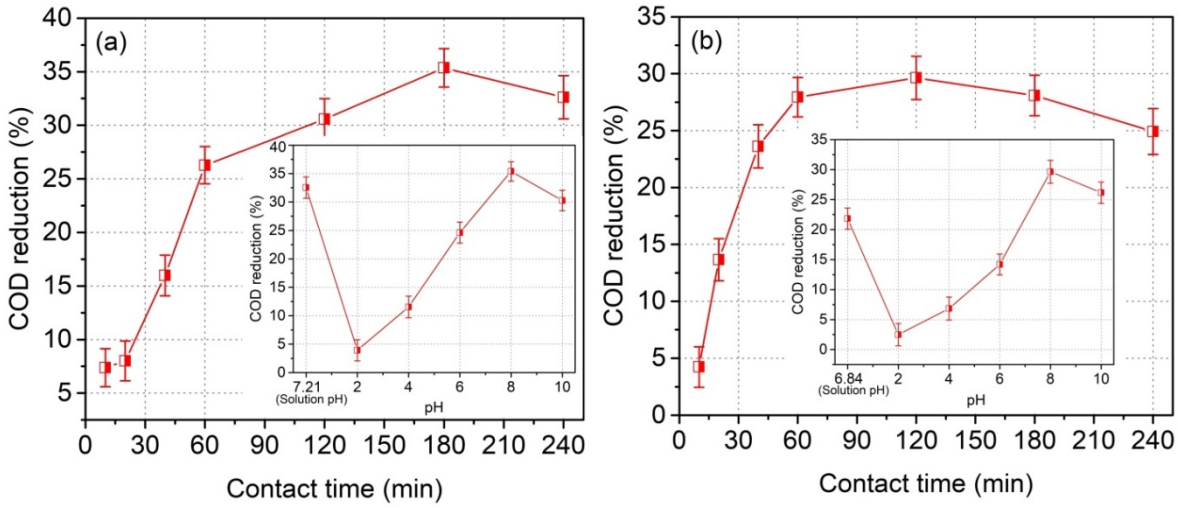

Fig. 4.69 Results of pH and contact time of $FeCl_3$ treatment of (a) LSW and (b) HSW for reduction in COD

Table 4.24 Physicochemical characteristics of low strength wastewater before and after coagulation treatment with 3 g L^{-1} of coagulant dose

S.No.	Parameter	Pre-chemical treatment	Post-chemical treatment with $Ca(OH)_2$	Post-chemical treatment with $FeCl_3$	Post-chemical treatment with Alum
		Mean ± S.D.	Mean ± S.D.	Mean ± S.D.	Mean ± S.D.
1	pH	7.21 ± 0.22	12.2 ± 0.42	12.4 ± 0.34	11.9 ± 0.57
2	Color	Light brown	Light brown	Light brown	Light brown
3	BOD_5	6550 ± 180	6223 ± 170	5210 ± 210	5989 ± 180
4	COD	12480 ± 450	11140 ± 521	8064 ± 412	10250 ± 510
5	BOD_5/COD	0.52 ± 0.04	0.55 ± 0.03	0.64 ± 0.05	0.57 ± 0.03
6	TOC	2927 ± 102	2341 ± 121	2110 ± 134	2019 ± 117
7	TSS	6330 ± 173	3812 ± 156	3754 ± 124	4387 ± 213
8	TDS	29010 ± 289	27651 ± 219	23670 ± 199	25678 ± 230
9	TKN	1040 ± 123	871 ± 89	697 ± 103	612 ± 98
10	Nitrate	14 ± 1.78	11 ± 1.54	8 ± 1.15	8 ± 1.4
11	Nitrite	21 ± 1.53	17 ± 1.11	11 ± 1.08	12 ± 1.98
12	Sulfates	3539 ± 122	2713 ± 180	2463 ± 146	3212 ± 180
13	Chloride	2025 ± 130	1920 ± 101	1822 ± 98	1856 ± 112
14	Phosphate	<0.005	< 0.005	< 0.005	< 0.005

Note: All the values except pH, color and BOD_5/COD are expressed as mg L^{-1}. All the values are expressed as mean of three values.

Table 4.25 Physicochemical characteristics of high strength wastewater before and after coagulation treatment with 4 g L^{-1} of coagulant dose

S.No.	Parameter	Pre-chemical treatment	Post-chemical treatment with $Ca(OH)_2$	Post-chemical treatment with $FeCl_3$	Post-chemical treatment with Alum
		Mean ± S.D.	Mean ± S.D.	Mean ± S.D.	Mean ± S.D.
1	pH	6.84 ± 0.12	11.9 ± 0.35	12.8 ± 0.25	12.5 ± 0.45
2	Color	Dark brown	Dark brown	Dark brown	Dark brown
3	BOD_5	27010 ± 230	24212 ± 210	23352 ± 320	24042 ± 180
4	COD	50933 ± 390	42461 ± 490	35840 ± 470	39040 ± 510

5	BOD_5/COD	0.53 ± 0.05	0.57 ± 0.04	0.65 ± 0.06	0.61 ± 0.04
6	TOC	11840 ± 176	10280 ± 154	7920 ± 180	9780 ± 195
7	TSS	12231 ± 321	3812 ± 156	3465 ± 124	4387 ± 213
8	TDS	37565 ± 672	27091 ± 380	19780 ± 450	22989 ± 375
9	TKN	4040 ± 145	2980 ± 120	2696 ± 155	3387 ± 188
10	Nitrate	27 ± 1.43	25 ± 1.12	23 ± 2.23	21 ± 1.65
11	Nitrite	87 ± 2.1	17 ± 1.11	47 ± 1.23	54 ± 312
12	Sulfates	9527 ± 233	2713 ± 180	3375 ± 1190	3212 ± 180
13	Chloride	7380 ± 154	6690 ± 120	5550 ± 78	5323± 143
14	Phosphate	1.5 ± 0.23	0.4 ± 0.04	0.07 ± 0.02	0.2 ± 0.04

Note: All the values except pH, color and BOD_5/COD are expressed as mg L^{-1}. All the values are expressed as mean of three values.

4.8.2 Integrated Bio-Gamma treatment of wastewater

The pre-coagulant treated LSW and HSW were subjected to aerobic biological degradation with activated sludge obtained from the aeration basin of ETP of pharmaceutical manufacturing unit (Derabassi, Punjab). The pH of pre-coagulant treated LSW and HSW was adjusted between 7.0 to 8.0 ±0.2 using H_2SO_4 and NaOH solutions. Due to the deficiency of nutrients in the treated wastewater, the suitable amount of nutrients (nitrogen and phosphorous) were added to keep the COD:N:P ratio to 100:5:1, respectively. Nutrients were added to support the growth of microbial population and ensuring that both microbial population and removal of organic loading would be limited only by the carbon content of wastewater. Nitrogen and phosphorous were added in the form of $(NH_4)_2SO_4$ and K_2HPO_4, respectively, in various concentrations depending upon on the COD load of feed wastewater.

As the microbial population is strongly reliant on the concentration of sludge and temperature conditions, small-scale experiments were conducted with various volumes of sludge concentrations followed by wastewater addition. For both LSW and HSW, different concentration of sludge was varied and all glass reactors were kept in incubator at different temperature conditions of 20, 27 and 37 °C. Air pumps supplied the necessary air to keep minimum dissolved oxygen concentration of 2.0 mg L^{-1}. Mixing was provided with the help of mechanical stirrer during the course of treatment. Air supply and mixing was turned off to allow sludge to settle for 30 min prior to sample withdrawal. Subsequently, samples were withdrawn at regular intervals of 12 h and syringe filtered for subsequent COD and TOC analysis.

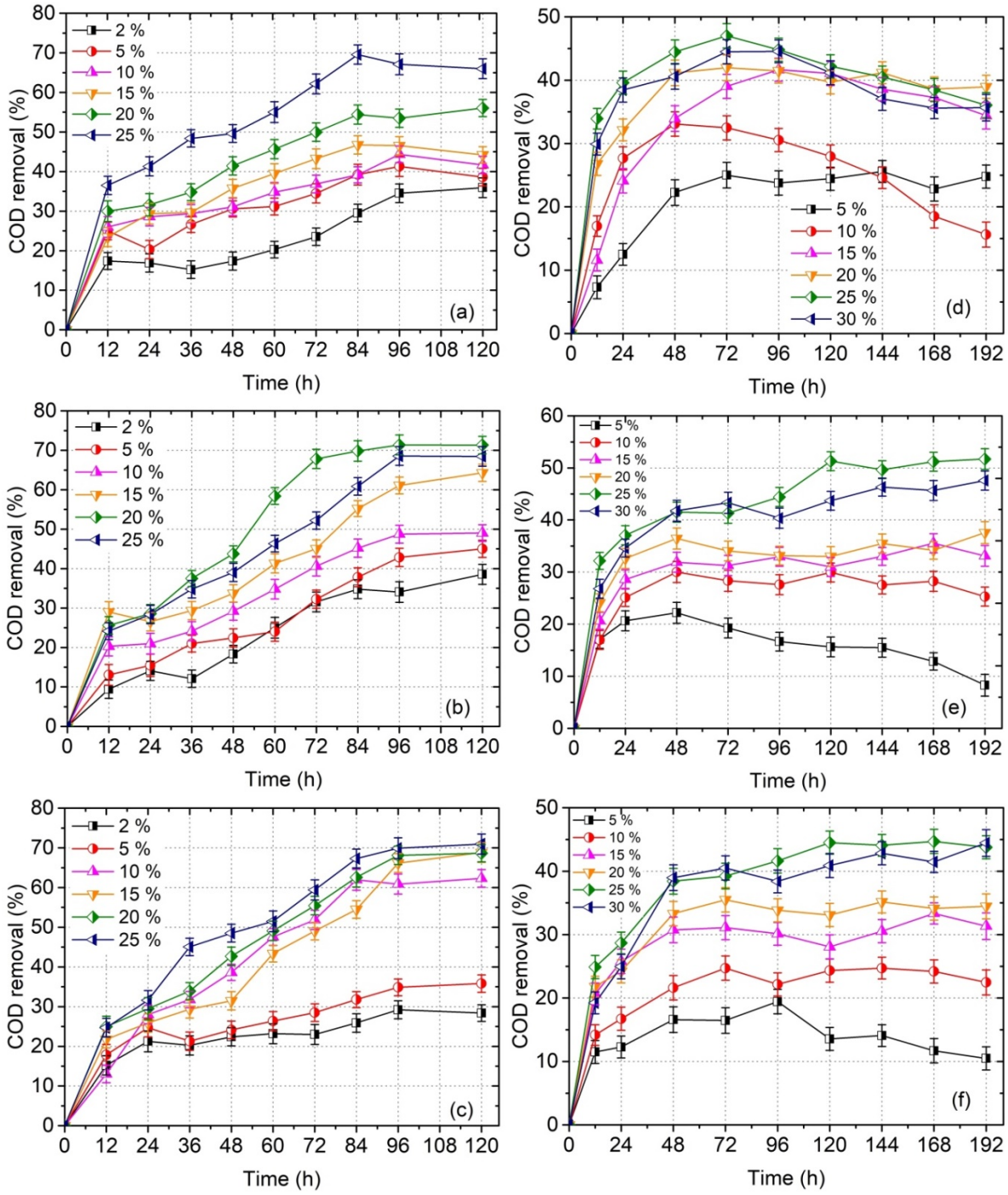

Fig. 4.70 Effect of sludge concentration and temperature on COD reduction of (a) LSW at 20 °C (b) LSW at 27 °C (c) LSW at 37 °C (d) HSW at 20 °C (e) HSW at 27 °C and (f) HSW at 37 °C

Fig. 4.70 shows the results of biological degradation of pre-coagulant treated LSW and HSW at varied sludge concentration and different temperature conditions. For LSW, sludge concentration was varied from 2 to 25% (v/v); whereas, 5 to 30% (v/v) of sludge concentration was maintained for HSW treatment. Results indicate that increase in sludge concentration from 2 to 20% for LSW and 5 to 25% for HSW led to enhanced COD removal;

however, further increase in concentration of sludge led to reduction in COD removal which might be due to increase in MLSS concentration that reduced oxygen transfer obstructing the survival of microbial population and perturbing the biomass to food ratio.

Fig. 4.71a and 4.71b show the optimized results obtained for the biological degradation of LSW and HSW, respectively. Results showed that 71.3% COD and 56.7% TOC removal was achieved for LSW with 20% (v/v) sludge concentration at 27 °C and 120 h of incubation temperature and aeration period, respectively. On the other hand, 53.4% COD and 22.1% TOC removal was achieved for HSW with 25% (v/v) sludge concentration at 27 °C and 192 h of incubation temperature and aeration period, respectively. The percentage removal of COD gradually increased with increase in aeration period for LSW; however, the removal of COD for HSW was significant up to 48 h after which only 10% reduction in COD was achieved up to 192 h of aeration period. This can be explained on the basis of higher organic load of HSW, which may be inhibitory for efficient treatment (Raj and Anjaneyulu, 2005). Moreover, it was observed that both LSW and HSW showed better results at 27 °C which might indicate that this temperature could facilitate the growth and metabolic activity of the microbial community to degrade the biodegradable organic matter present in the wastewater.

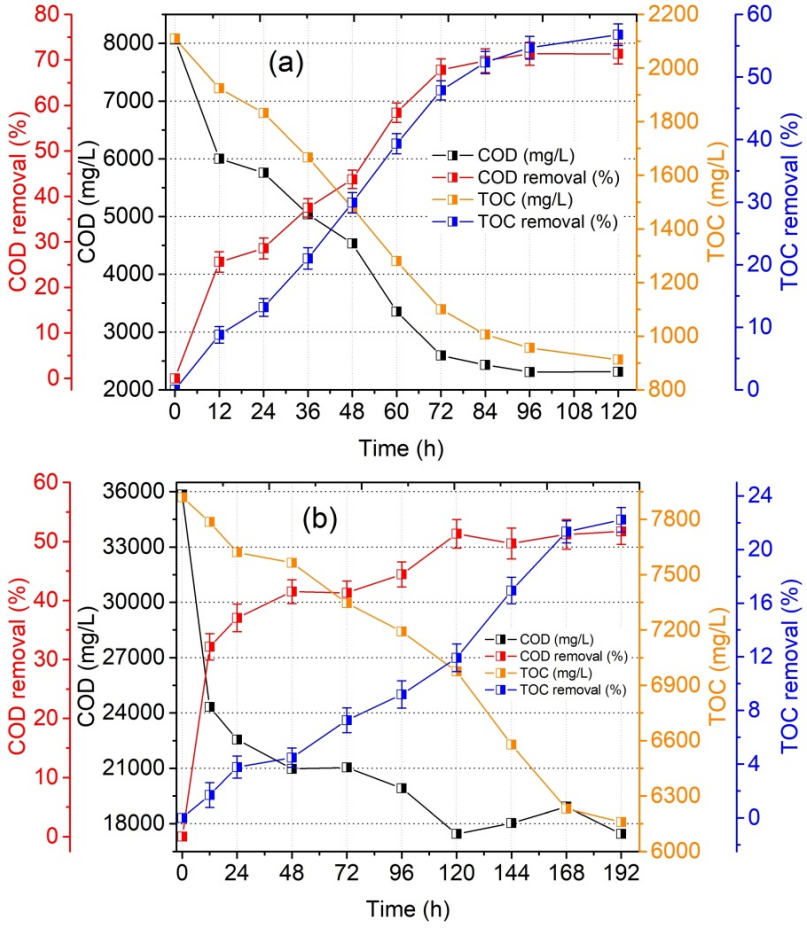

Fig. 4.71 (a) COD and TOC profile of low strength wastewater under biological degradation with 20% (v/v) sludge concentration at 27 °C (b) COD and TOC profile of high strength wastewater under biological degradation with 25% (v/v) sludge concentration at 27 °C

The biologically treated wastewaters were subjected to post-gamma irradiation treatment after being centrifuged to remove the sludge content. The parameters like pH, dose and type of oxidant like H_2O_2 and $K_2S_2O_8$ were optimized to achieve the enhanced COD and TOC removal. Gamma radiolysis of water produces three main reactive species *viz.* HO• radicals, hydrated electrons (e_{aq}^-) and hydrogen atom (H•) in the pH range 3-11. Under the atmospheric conditions, H• and e_{aq}^- react with the dissolved oxygen generating perhydroxyl radical ($HO_2^{\cdot}$) and superoxide radical anion ($O_2^{\cdot -}$). Thus, HO• are regarded as the predominant species in the aqueous solution.

The gamma radiolysis of bio-treated LSW and HSW was carried out for different doses ranging from 2.5 to 100 kGy. Fig. 4.72a and 4.72b show the results of pH effect on COD removal of bio-treated LSW and HSW under gamma radiolysis, respectively. Results indicated that acidic conditions were favourable for the efficient COD removal of

LSW and HSW when compared to neutral/alkaline conditions. 43.3, 30.3 and 34.7% of COD removal were achieved for LSW at pH 3, 7 and 11, respectively; whereas, 29.9, 14.9 and 20.8% of COD removal were achieved for HSW at pH 3, 7 and 11, respectively. Under acidic conditions, e_{aq}^- reacts with H^+ to generate $H^\bullet$, hence inhibiting the recombination of $HO^\bullet$ radicals and $e_{aq}^-$to form OH^-, allowing $HO^\bullet$ species to react with organic content of wastewaters (Guo *et al.* 2012). The increased COD removal in acidic medium and decreased COD removal in neutral/alkaline medium exhibit that the presence of $HO^\bullet$ radical is effective for COD removal during gamma radiolysis of wastewater. Moreover, the insignificant reduction of COD at an irradiation dose of 100 kGy could be due to the high content of dissolved solids in wastewater samples as presented in Table 4.23 and Table 4.24. Among the different salts contributing to high dissolved solids, carbonates and bicarbonates are considered to be scavenger of $HO^\bullet$ radicals, thereby reducing the concentration of $HO^\bullet$ radicals to react with organic matter of wastewater (Buxton *et al.* 1988).

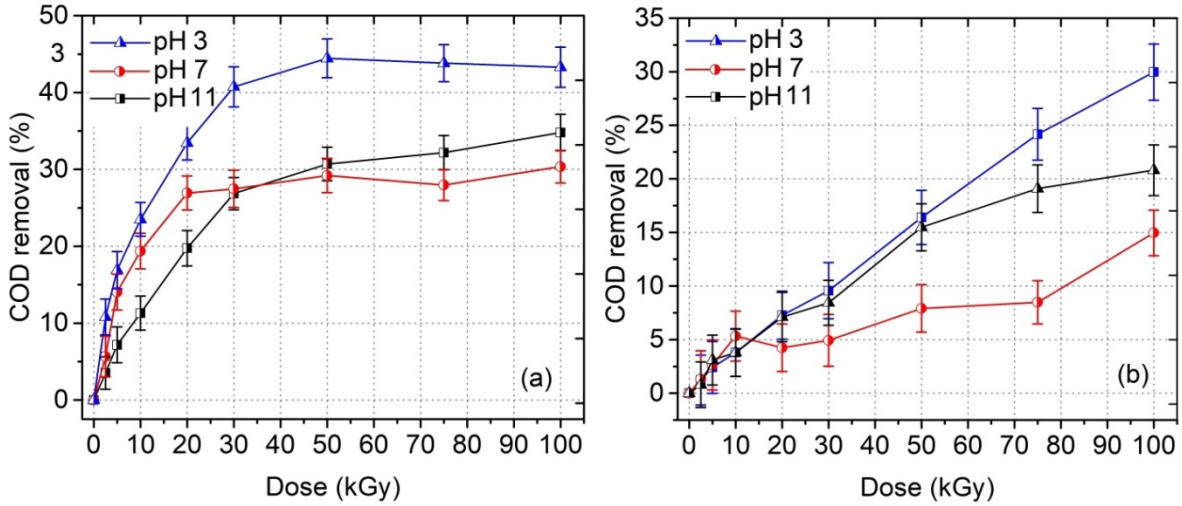

Fig. 4.72 Effect of solution pH and dose on COD removal efficiency of pre-bio treated (a) LSW and (b) HSW under gamma radiolysis

As shown in Fig. 4.64, gamma irradiation alone is ineffective in removing organic load of the wastewater; therefore different types of oxidants *viz.* H_2O_2 and $K_2S_2O_8$ were added to bio-treated LSW and HSW during gamma radiolysis and the COD and TOC removal efficiency of these wastewaters were investigated. For LSW, concentration of H_2O_2 was varied from 0.005 to 0.1 M, while concentration of $K_2S_2O_8$ was varied from 0.01 to 0.15 M. For HSW, concentration of H_2O_2 was varied from 0.025 to 0.5 M, while concentration of $K_2S_2O_8$ was varied from 0.05 to 0.2 M. Fig. 4.73 shows the effect of different concentration

of oxidants on COD and TOC removal of LSW and HSW. Fig. 4.74a and 4.74b show the COD and TOC removal of bio-treated LSW and HSW under gamma radiolysis at optimized results of oxidants, respectively. Under the optimized conditions of pH 3 and 100 kGy dose, addition of 0.05 M H_2O_2 and 0.15 M $K_2S_2O_8$ in LSW led to 79.4 and 75.1% of COD removal (Fig. 4.66a), respectively, whereas 43.7 and 41.9% of COD removal of HSW was achieved with addition of 0.1 M H_2O_2 and $K_2S_2O_8$ (Fig. 4.66b), respectively.

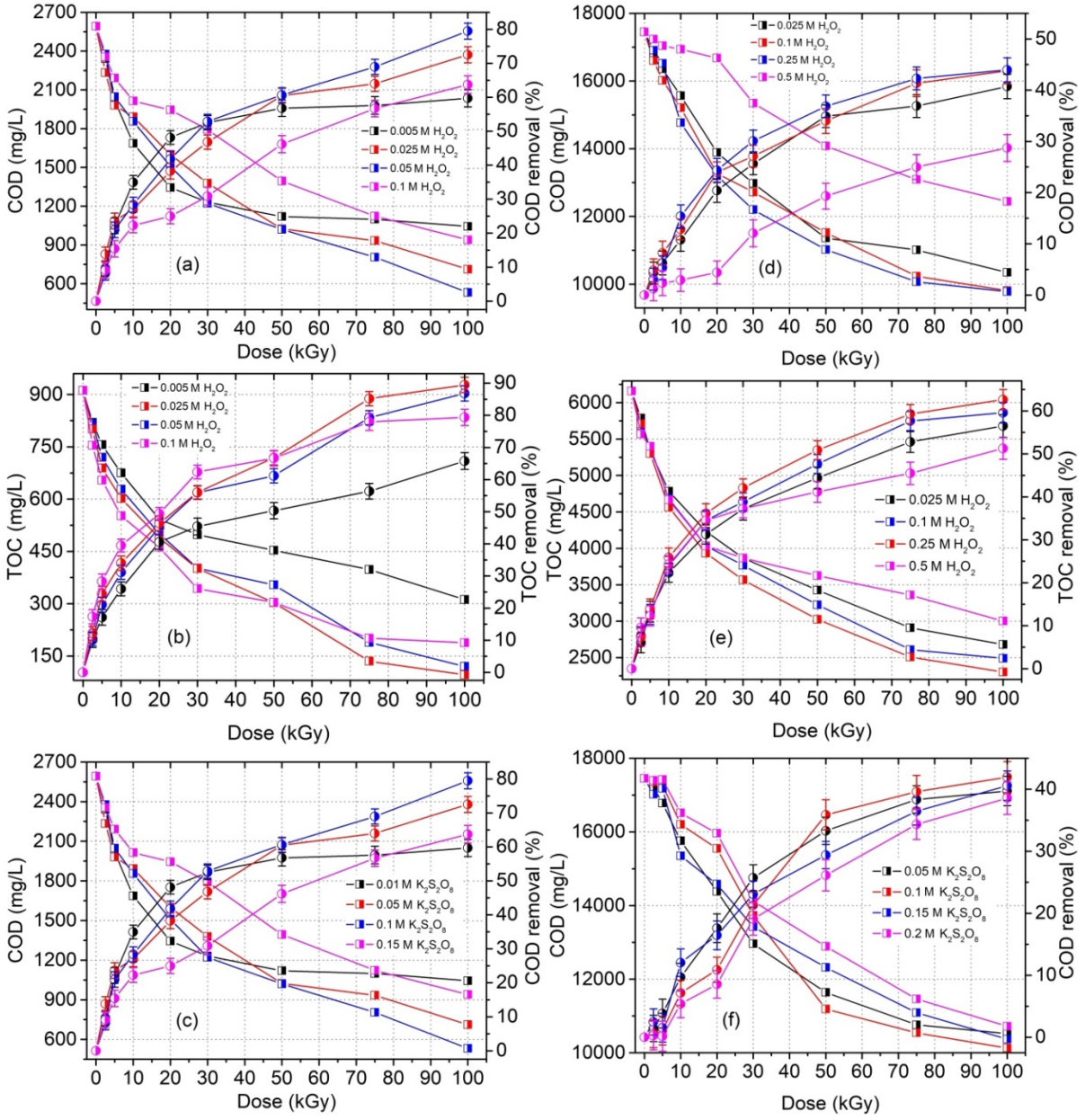

Fig. 4.73 Effect of H_2O_2 on COD and TOC removal of gamma irradiation treatment of (a & b) LSW (d & e) HSW; Effect of $K_2S_2O_8$ on COD removal of (c) LSW (f) HSW

It is expected that the addition of H_2O_2 could enhanced the degradation of organic matter. But practically, it was observed that COD of irradiated samples drastically rise with

increase in H_2O_2 concentration due to dichromate method which may be explained as: when potassium dichromate solution is added to the samples containing H_2O_2 which is acidified with sulphuric acid, a green color appears. It is generally due to the Cr^{3+} ions formed due to potassium dichromate reduction according to Eq. 4.45 (Kang *et al.* 1999). The interference of H_2O_2 on COD with the stoichiometry of the Eq. 4.45 shows, each mg L^{-1} of H_2O_2 contributes about 0.47 mg L^{-1} to the COD value on its reduction to Cr^{3+} from Cr^{6+}. Eq. 4.45 reveals that although H_2O_2 is a powerful oxidant, but in the presence of an even more powerful oxidant, i.e. the dichromate ion ($Cr_2O_7^{2-}$), H_2O_2 acts as a reductant and is itself oxidized, thereby contributing positively to the COD value. Thus, all the samples containing H_2O_2 as an oxidant were boiled for 10 min to remove the interference due to H_2O_2 prior to COD analysis.

$$K_2S_2O_8 + 4H_2SO_4 + 3H_2O_2 \rightarrow K_2SO_4 + Cr_2(SO_4)_3 + 7H_2O + 3O_2 \quad (4.45)$$

Further TOC removal at given irradiation dose was evaluated to determine the influence of H_2O_2 on the mineralization extent of LSW and HSW (Fig. 4.73). The enhanced TOC removal of LSW and HSW due to H_2O_2 is ascribed to the fact that H_2O_2 rapidly reacts with reactive species, such as e_{aq}^- and $H^\bullet$ during gamma radiolysis, and enhances the concentration of $HO^\bullet$ radical in the solution to degrade the organic content of wastewater. However, the addition of excess H_2O_2 may generate peroxyl radical species which are less reactive species in comparison to $HO^\bullet$ radical (Buxton *et al.* 1998). Under optimized conditions, 0.05 and 0.25 M H_2O_2 leads to 89.4 and 66.6% TOC reduction of bio-treated LSW and HSW, respectively under gamma radiolysis. However, the remaining TOC in the solutions is expected due to the remaining organic content in wastewaters or radiolytically degraded by-products formed during gamma irradiation of wastewater.

During the gamma radiolysis of wastewater in the presence of $K_2S_2O_8$, e_{aq}^- and $H^\bullet$ reacts with $S_2O_8^{2-}$ according to well established reactions (4.46) and (4.47) producing sulfate radical anion $SO_4^{\cdot-}$ (Bensasson *et al.*1983).

$$S_2O_8^{2-} + e_{aq}^- \rightarrow SO_4^{\cdot-} + SO_4^{2-} \quad (k = 1.2 \times 10^{10} L\, mol^{-1} S^{-1}) \quad (4.46)$$

$$S_2O_8^{2-} + H^\cdot \rightarrow SO_4^{\cdot-} + HSO_4^- \quad (k = 2.5 \times 10^{7} L\, mol^{-1} S^{-1}) \quad (4.47)$$

Like $HO^\bullet$, $SO_4^{\cdot-}$ is an oxidizing specie with redox potential of 2.43 V and is reactive towards many organic as well as inorganic compounds. Thus, degradation of organic compounds is expected to enhance due to the presence of both $SO_4^{\cdot-}$ and $HO^\bullet$ radicals. However, addition of $S_2O_8^{2-}$ ions did not exhibit any significant reduction in COD and TOC of wastewaters when compared to H_2O_2 addition. It is well established that both $SO_4^{\cdot-}$ and

HO• are scavenged by the reaction with Cl^- present in the real wastewater as given by Eqs. 4.48 - 4.50 (Liao *et al.* 2001; Lian *et al.* 2017). It can be said that, HO• radicals are scavenged by Cl^- ions producing $ClOH^{\cdot -}$ intermediate specie which again can dissociate back to HO• radicals and Cl^- with slightly higher rate constant values. However, it is worth mentioning that at optimized pH 3, $ClOH^{\cdot -}$ is rapidly converted to Cl• atom by protonation reaction as shown by Eq. 4.51 (Liao *et al.* 2001). Therefore, it can be hypothesized that more selective nature of $SO_4^{\cdot -}$ than non-selective HO• radical leads to lesser degradation of the pollutants resulting into lower COD and TOC removal efficiency of the solutions in presence of $K_2S_2O_8$ than H_2O_2 (Lian *et al.* 2017).

$$SO_4^{\cdot -} + Cl^- \rightarrow SO_4^{2-} + Cl^{\cdot} \; [k = 3.1 \times 10^8 L\,mol^{-1}s^{-1}] \quad (4.48)$$

$$HO^{\cdot} + Cl^- \rightarrow HO^- + ClOH^{\cdot -} \; [k = 4.3 \times 10^9 Lmol^{-1}s^{-1}] \quad (4.49)$$

$$ClOH^{\cdot} \rightarrow HO^{\cdot} + Cl^- \; [k = 6.1 \times 10^9 Lmol^{-1}s^{-1}] \quad (4.50)$$

$$ClOH^{\cdot -} + H^+ \rightarrow Cl^{\cdot} + H_2O \; [k = 2.1 \times 10^{10}\,Lmol^{-1}s^{-1}] \quad (4.51)$$

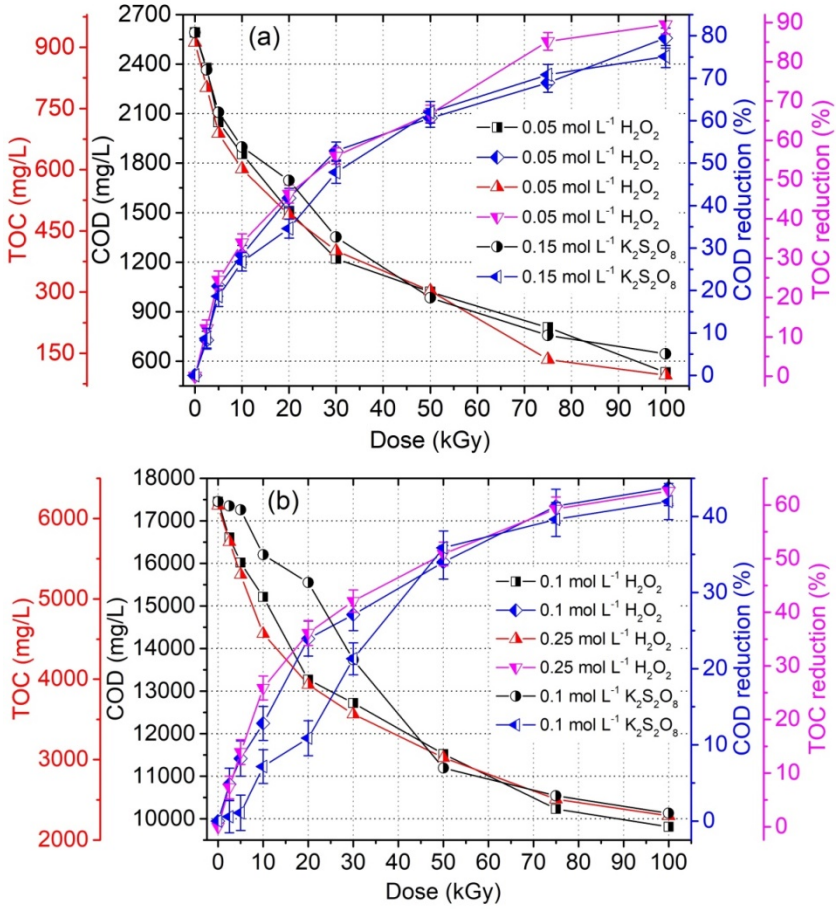

Fig. 4.74 Effect of oxidants on COD and TOC profile of pre-bio treated (a) LSW (b) HSW under gamma radiolysis

4.8.3 Integrated Gamma-Bio treatment of wastewater

The pre-coagulant treated wastewaters *viz.* LSW and HSW were subjected to gamma irradiation treatment with irradiation dose ranging from 2.5 to 100 kGy. The effect of parameters including solution pH and type of oxidants was evaluated on the COD and TOC removal extent of wastewaters. The pH of wastewater samples was adjusted using H_2SO_4 and NaOH solutions prior to irradiation. Fig. 4.75a and 4.75b display the results of solution pH on the COD removal of LSW and HSW, respectively. Results showed that 54.8, 52.4 and 49.6% of COD removal was obtained for LSW at pH 3, 7 and 11, respectively; whereas, 50.1, 39.4, and 43.2% of COD removal was achieved for HSW at pH 3, 7 and 11, respectively. Similar to the results of gamma irradiation treatment of pre-biologically treated wastewaters, the enhanced COD removal was observed at acidic conditions when compared to neutral and alkaline conditions. The increased COD removal extent in acidic medium and decreased COD removal extent in neutral and alkaline medium demonstrate that the $HO^{\bullet}$ radicals were accountable for the effective degradation of organic content present in the wastewater using gamma radiolysis (Huang *et al.* 2016). The results obtained of TOC removal showed 37, 25 and 19% of mineralization extent of LSW, whereas 37, 21.7 and 16.7% of mineralization extent of HSW was observed at pH 3, 7 and 11, respectively.

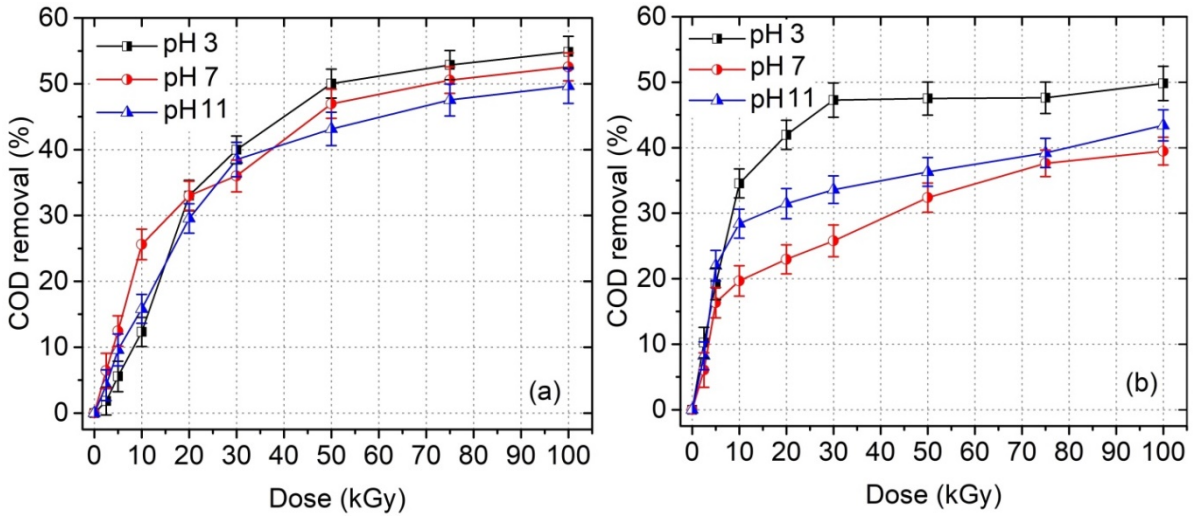

Fig. 4.75 Effect of solution pH and dose on COD removal efficiency of pre-coagulant treated (a) LSW and (b) HSW under gamma radiolysis

To elucidate the effect of oxidant on the gamma radiolytic treatment of wastewater, the addition of oxidant *viz.* H_2O_2 and $K_2S_2O_8$ with different concentrations was evaluated in

terms of COD and TOC removal. Fig. 4.76 shows the results of oxidant effect with different concentrations on the COD and TOC removal of wastewater. For LSW, concentration of H_2O_2 was varied from 0.01 to 0.5 M, while concentration of $K_2S_2O_8$ was varied from 0.01 to 0.15 M. For HSW, concentration of H_2O_2 was varied from 0.025 to 0.75 M, while concentration of $K_2S_2O_8$ was varied from 0.05 to 0.2 M.

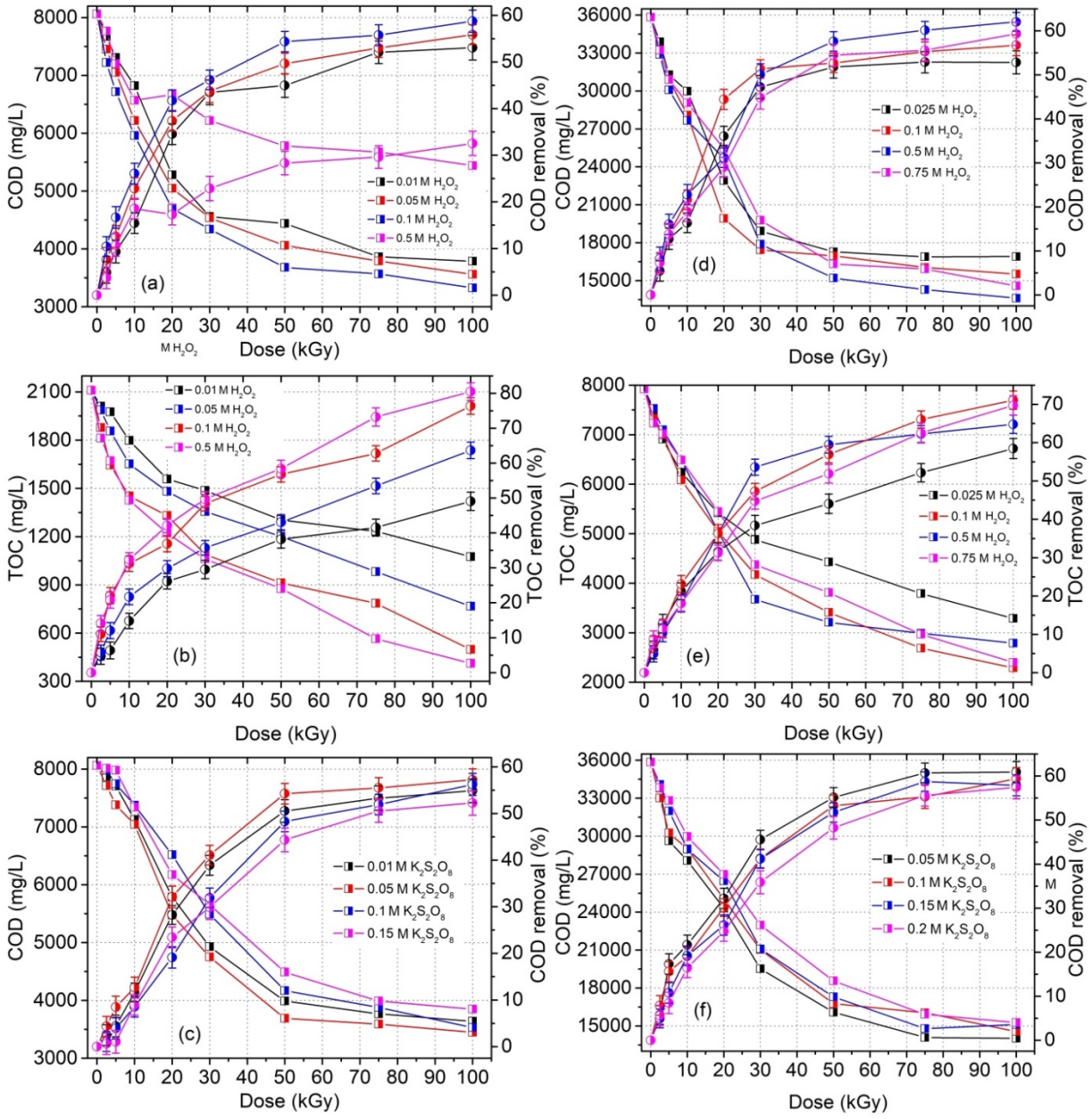

Fig. 4.76 Effect of H_2O_2 on COD and TOC removal of pre-biological and post-gamma irradiation treatment of (a & b) LSW (d & e) HSW; Effect of $K_2S_2O_8$ on COD removal of (a) LSW (b) HSW

Fig. 4.77a and 4.77b show the optimized results for LSW and HSW, respectively, obtained using oxidants mediated gamma radiolysis of wastewater. Under the optimized

conditions of pH 3 and 100 kGy dose, addition of 0.1 M H_2O_2 and 0.05 M $K_2S_2O_8$ in LSW led to 58.7 and 57.2% of COD removal, respectively; whereas, 62.3 and 61.3% of COD removal of HSW was attained with addition of 0.5 M H_2O_2 and 0.05 M $K_2S_2O_8$, respectively. Fig. 4.69a and 4.69b show the results of TOC removal extent of LSW and HSW, respectively. Results showed that addition of 0.1 M H_2O_2 and 0.05 M $K_2S_2O_8$ in LSW led to 80.4 and 66.5% of TOC removal (Fig. 4.77a), respectively; whereas, 71.0 and 65.1% of TOC removal of HSW was achieved with addition of 0.5 M H_2O_2 and 0.05 M $K_2S_2O_8$ (Fig. 4.77b), respectively. The removal efficiency of TOC was slightly higher in H_2O_2-mediated gamma radiolysis when compared to $S_2O_8^{2-}$-mediated gamma radiolysis indicating the preferential attack of non-selective HO$^{\bullet}$ radicals to further degrade the persistent pollutants in wastewater when compared to selective nature of SO_4^{-} radials in $S_2O_8^{2-}$-mediated gamma radiolysis (Liao *et al.* 2001).

It is noteworthy that removal curves of COD and TOC do not overlap each other as they do not follow the similar trend. The higher the quantity of intermediate or by-products produced during the gamma radiolysis of wastewater, the lower the number of moles of oxygen was required to oxidize the generated intermediate or by-products. Thus, the COD value of irradiation treated samples showed a significant reduction. Though, some of those oxidized products might persist in the treated solution and this is the cause of remaining TOC in the wastewater. Overall results indicated that gamma irradiation alone with optimum concentration of oxidant could degrade the organic content of pharmaceutical wastewater to significantly reduce the COD and TOC content. However, the irradiation dose required to achieve enhanced COD and TOC removal was too high, i.e. 100 kGy, which could possibly reduce the potential viability of independent gamma irradiation to treat the real pharmaceutical wastewater. The use of irradiation treatment could be explored as a pre-treatment method to enhance the biodegradability of wastewater and/or eliminate the toxicity by converting the persistent organic compounds in wastewater to easily biodegradable compounds.

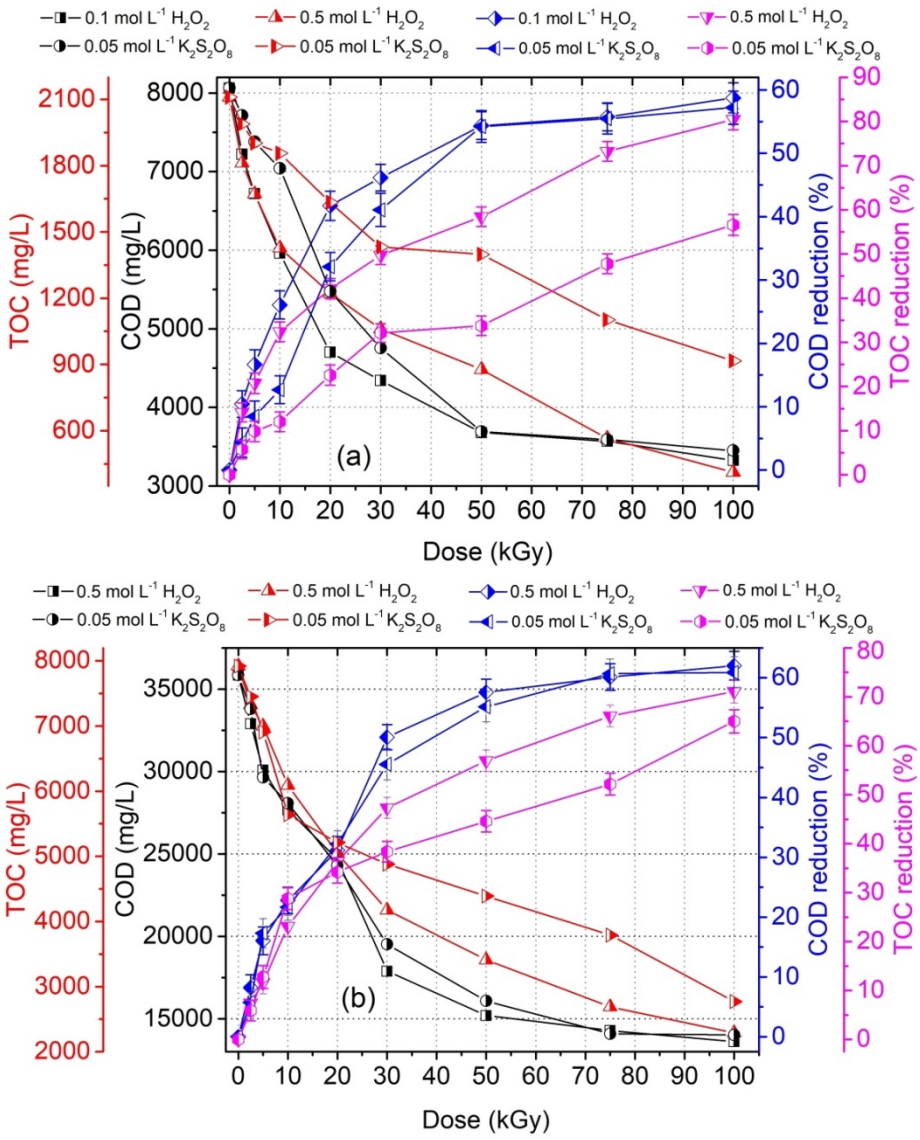

Fig. 4.77 Effect of oxidant on COD and TOC profile of pre-coagulant treated (a) LSW (b) HSW under gamma radiolysis

The irradiated samples of wastewater were given post-biological treatment to evaluate the ability of activated sludge process in further elimination of organic content of wastewater. Under optimized conditions, the irradiated samples of LSW and HSW led to 58.7 and 62.3% of COD removal efficiencies, respectively achieving final COD value of 3540 mg L^{-1} and 13610 mg L^{-1}, respectively. Moreover, biodegradability index (BOD_5/COD) was found to increase from 0.52 to 0.67 for LSW after 100 kGy of absorbed dose; whereas, BOD_5/COD value increased from 0.53 to 0.62 for HSW after 100 kGy of absorbed dose, indicating the conversion of non-biodegradable organic content of wastewater to biodegradable compounds. Since the irradiation treatment of LSW and HSW significantly enhanced the BOD_5/COD ratio, therefore irradiated samples were susceptible to biological degradation. As primary

objective was to achieve maximum degradation of organic content of wastewater with the integrated treatment, so irradiated samples of LSW and HSW were subjected to subsequent biological degradation. For LSW, concentration of sludge was varied from 2 to 25% (v/v); whereas, 5 to 30% (v/v) of sludge concentration was maintained for HSW treatment. As a result, the optimum sludge concentration and incubation temperature for LSW was found to be 15% (v/v) and 27 °C, respectively; whereas, 25% (v/v) sludge concentration and 27 °C of incubation temperature was optimized for HSW. The results of biological treatment of irradiation treated samples of LSW and HSW under the optimized conditions are depicted in Fig. 4.78.

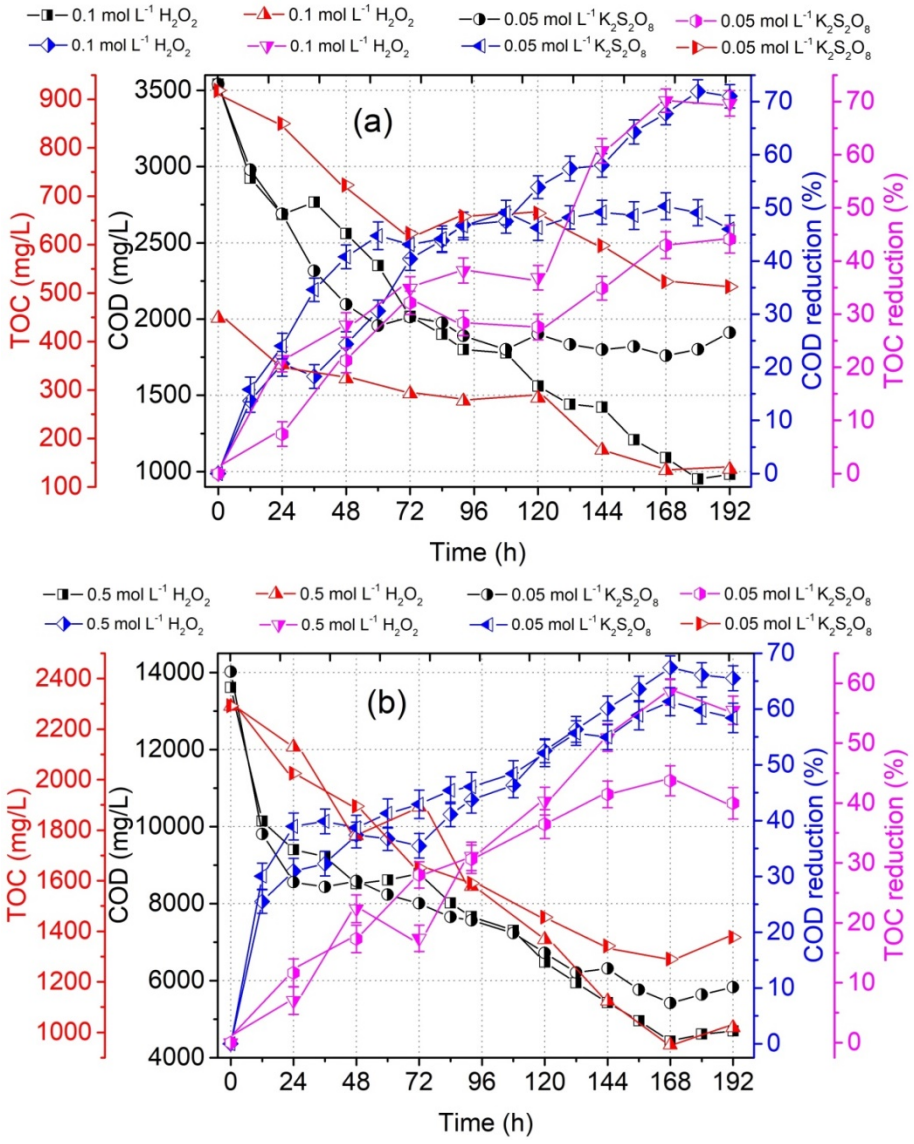

Fig. 4.78 (a) COD and TOC profile of low strength wastewater using post-biological treatment with 20% (v/v) sludge concentration at 27 °C (b) COD and TOC profile of high strength wastewater using post-biological treatment with 25% (v/v) sludge concentration at 27 °C

Results indicate that 70.9% of COD removal and 66.6% of TOC removal were achieved for LSW (irradiated with 0.1 M H_2O_2); whereas, 50.3% of COD removal and 44.1% of TOC removal were achieved for LSW (irradiated with 0.05 M $K_2S_2O_8$) with 15% (v/v) sludge concentration at incubation temperature and duration of 27 °C and 168 h, respectively. For HSW (irradiated with 0.5 M H_2O_2), 65.5 and 55.5% of COD and TOC removal were achieved, respectively; whereas, 58.4% of COD removal and 39.6% of TOC removal were achieved for HSW (irradiated with 0.05 M $K_2S_2O_8$) with 25% (v/v) sludge concentration at incubation temperature and duration of 27 °C and 168 h, respectively. A significant reduction in COD and TOC was achieved in post-biological degradation of wastewater. Furthermore, the activated sludge was of good quality as specified by the sludge volume index (SVI) value, which ranged from 55-80 and 65-95 mL g^{-1} for initial COD load of 3540 and 13160 mg O_2 L^{-1}, respectively (Tchobanoglous *et al.* 2003). Microscopical inspection of the used sludge indicated the presence of a vast variety of bacterial populations which are either freely dispersed in aqueous phase or aggregated in sludge flocs.

The overall results depict that independent coagulant treatment of LSW and HSW led to final COD value of 8110 ±175 mg L^{-1} and 35840 ±220 mg L^{-1} respectively, from the initial LSW COD of 12,480 ±450 mg L^{-1} and HSW COD of 50,933 ±390 mg L^{-1}. The independent gamma irradiation treatment of pre-coagulant treated LSW led to final COD value of 3326 ±140 mg L^{-1} and 3450 ±125 mg L^{-1} with H_2O_2 and $K_2S_2O_8$, respectively, from the initial COD of 12,480 ±235 mg L^{-1}. In case of HSW, final COD value of 13610 ±220 mg L^{-1} and 14020 ±245 mg L^{-1} with H_2O_2 and $K_2S_2O_8$, respectively, was obtained from the initial COD value of 50,933 ±390 mg L^{-1}. The pre-coagulant treatment of LSW followed by biological treatment and subsequent post-gamma-irradiation treatment led to final COD value of 532 ±85 mg L^{-1} and 645 ±90 mg L^{-1} with H_2O_2 and $K_2S_2O_8$, respectively, from the initial COD of 12,480 ±450 mg L^{-1}. In case of HSW, final COD value of 9810 ±205 mg L^{-1} and 10130 ±220 mg L^{-1} with H_2O_2 and $K_2S_2O_8$, respectively, was obtained from the initial COD value of 50,933 ±390 mg L^{-1}. On the other hand, the overall results of pre-coagulant treatment of LSW followed by gamma irradiation treatment and subsequent post-biological treatment led to final COD value of 982 ±110 mg L^{-1} and 1912 ±125 mg L^{-1} with H_2O_2 and $K_2S_2O_8$, respectively, from the initial COD of 12,480 ±390 mg L^{-1}. In case of HSW, final COD value of 4693 ±175 mg L^{-1} and 5381 ±140 mg L^{-1} with H_2O_2 and $K_2S_2O_8$, respectively, was obtained from the initial COD value of 50,933 ±390 mg L^{-1}. These results indicate that the pre-biological treatment followed by post-gamma irradiation treatment was effective in overall COD reduction of low strength wastewater; whereas, for high strength wastewater,

pre-gamma irradiation treatment followed by post-biological treatment was effective for overall COD removal. Nevertheless, the study is limited to wastewater from single pharmaceutical manufacturing unit; still the findings suggest that gamma-irradiation could be used as pre-treatment method to convert the recalcitrant and non-biodegradable organic matter present in high organic loaded pharmaceutical wastewater into easily biodegradable organic compounds which could be removed by subsequent biological treatment. However, utilization of too high irradiation dose for wastewater treatment and sample volume capacity in gamma chamber are the limiting factors for the use of gamma irradiation for practical point of view.

4.8.4 Cytotoxicity assessment of wastewater

The effectiveness of treatment technology does not rely on the degradation of organic pollutants present in the wastewater, but also on the generation of intermediates or by-products which are lesser or non-toxic in nature. Therefore, to test the cytotoxicity of raw and treated wastewater samples against the three microorganism's *viz*. *B. subtilis, P. aeruginosa* and *E. coli,* a zone of inhibition test was conducted. All the tests were performed on the results obtained under optimized conditions for LSW and HSW.

The toxicity of control (raw LSW and HSW) and the treated wastewater through pre-biological followed by post-gamma irradiation treatment at absorbed doses of 100 kGy were compared through zone of inhibition test and results are depicted in Fig. 4.79. Results showed that in almost all the petri-dishes, inhibition zone was observed for low and high strength wastewater treated with pre-biological treatment, indicating the presence of toxic organic pollutants in the wastewater. However, with subsequent gamma-irradiation treatment of pre-biological treated wastewater, inhibition zone almost disappeared in case of LSW when compared to HSW. These results clearly indicated that gamma irradiation has the potential to detoxify the toxic intermediates in the wastewater which are not eliminated by biological treatment.

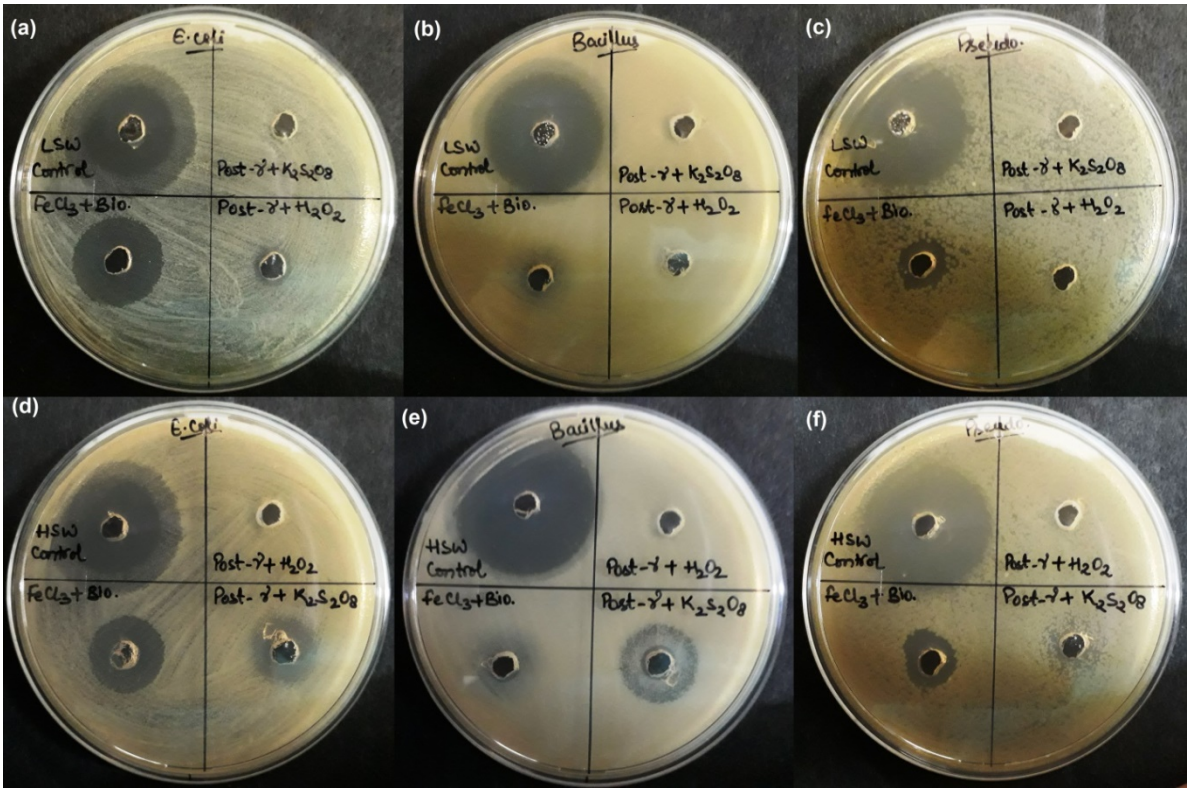

Fig. 4.79 Cytotoxic potential of (a, b and C) LSW and (d, e and f) HSW treated with pre-biological followed by post-gamma irradiation treatment

Moreover, toxicity assessment was also conducted for the treated wastewater through pre-gamma irradiation followed by post-biological treatment and the results obtained are depicted in the Fig. 4.80. These results showed that when gamma irradiation was used as pre-treatment technology to treat wastewater with different organic loads, a complete detoxification of wastewater was achieved indicating that gamma-irradiation has a potential to eliminate toxicity from real wastewater. Since the toxic nature was only tested against the clinical isolates of selected microbes, a comprehensive study dealing with toxicity analyses of actual wastewater using different bioassays test methods could exhibit more reliable and viable results.

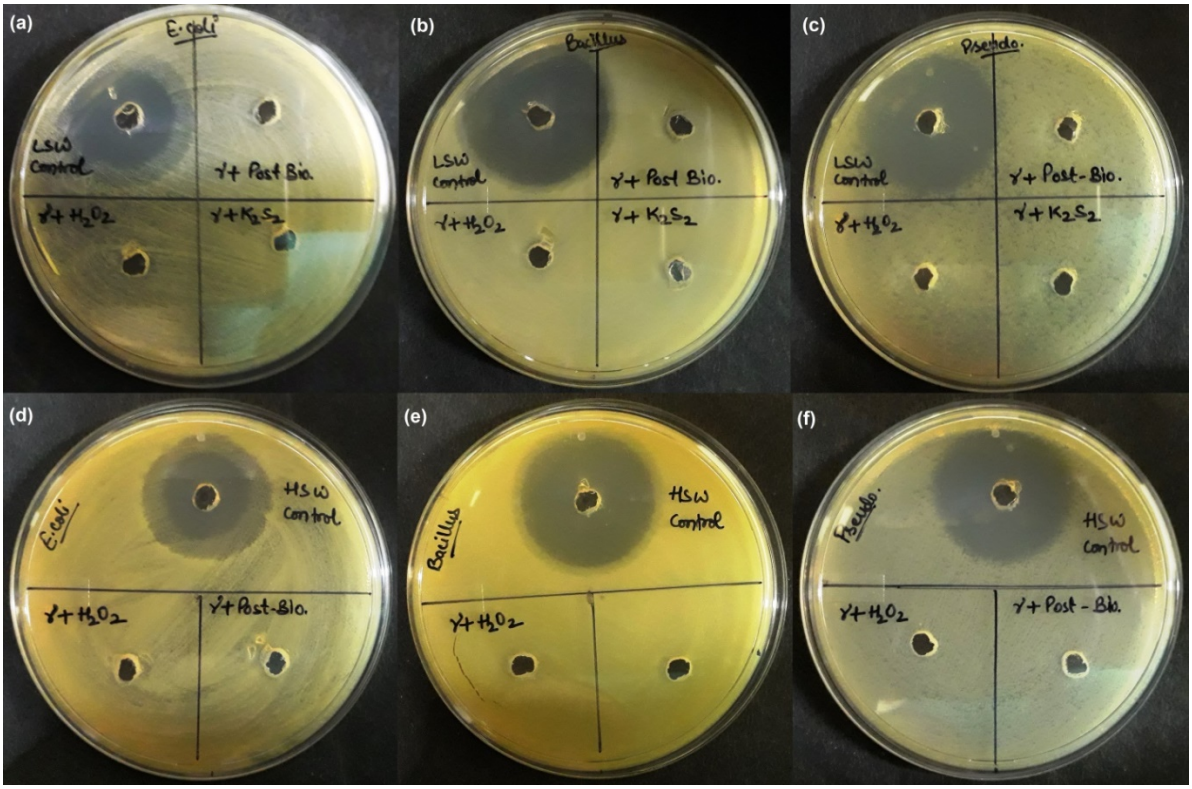

Fig. 4.80 Cytotoxic potential of (a, b and C) LSW and (d, e and f) HSW treated with pre-gamma irradiation followed by post-biological treatment

4.8.5 Cost associated with irradiation treatment for wastewater

The efficiencies of gamma radiolysis alone, gamma + H_2O_2 radiolysis and gamma + $K_2S_2O_8$ radiolysis was evaluated in terms of treatment cost including the consumption of energy and other auxiliary chemicals. Since gamma irradiation does not engage electrical energy, the cost of treatment could be calculated by accounting for five effective half-lives of ^{60}Co source according to the Eq. 4.40.

Table 4.26 The cost of energy involved in gamma radiolysis of low strength pharmaceutical wastewater

S.No.	Treatment Employed	Average treatment time (h)*	Cost of H_2O_2 used (INR m^{-3})	Cost of $K_2S_2O_8$ (INR m^{-3})**	Total ATC (INR m^{-3})	Total ATC (US \$ m^{-3})
1.	Gamma irradiation alone	4.6	NIL	NIL	63.8	0.87
2.	Gamma+H_2O_2	3.6	104	NIL	154	2.09
3.	Gamma+$K_2S_2O_8$	4.2	NIL	162	220.2	2.99

*Guided by the working dose rate during experimentations i.e., 10.9 kGy h^{-1}
**Average cost of $K_2S_2O_8$ @ 1.2 INR g^{-1}

The costs involved during gamma radiolysis of low and high strength wastewater were calculated on the basis of COD removal efficiency of 50% with gamma-irradiation as an independent technology. The total cost of gamma radiolysis alone, gamma + H_2O_2 radiolysis and gamma +$K_2S_2O_8$ radiolysis for low strength wastewater was found to be 63.8, 154 and 220.2 INR m^{-3}; whereas, for high strength wastewater, it was found to be 126.2, 560.4 and 213.3 INR m^{-3}, respectively. The results obtained are presented in Table 4.26 and 4.27.

Table 4.27 The cost of energy involved in gamma radiolysis of high strength pharmaceutical wastewater

S.No.	Treatment Employed	Average treatment time (h)*	Cost of H_2O_2 used (INR m^{-3})	Cost of $K_2S_2O_8$ (INR m^{-3})**	Total ATC (INR m^{-3})	Total ATC (US \$ m^{-3})
1.	Gamma irradiation alone	9.1	NIL	NIL	126.2	1.71
2.	Gamma+H_2O_2	2.7	523	NIL	560.4	7.61
3.	Gamma+$K_2S_2O_8$	3.7	NIL	162	213.3	2.90

*Guided by the working dose rate during experimentations i.e., 10.9 kGy h^{-1}
**Average cost of $K_2S_2O_8$ @ 1.2 INR g^{-1}

4.9 E-beam irradiation treatment of real pharmaceutical wastewater

The pre-coagulant treated wastewater samples *viz.* LSW and HSW were subjected to independent E-beam irradiation treatment as well as sequential aerobic biological treatment.

4.9.1 Chemical coagulant treatment of wastewater and its characterization

As discussed in Section 4.8.1, the physicochemical analysis revealed that among the used coagulants, $FeCl_3$ produced better results for both low and high strength wastewater of representative pharmaceutical industry. Table 4.28 shows the results of physicochemical characteristics of LSW and HSW obtained with the addition of $FeCl_3$ as a coagulant.

The result indicated that 30% of COD removal was achieved for LSW with 3 g L^{-1} of $FeCl_3$ at pH 8.0 after 180 min of contact time, whereas 25% of COD removal was obtained for HSW at pH 8.0 after 120 min contact time and 4 g L^{-1} of coagulant dose. The pre-coagulant treated wastewater samples were subjected to independent E-beam irradiation treatment followed by post-biological treatment.

Table 4.28 Physicochemical characteristics of low and high strength wastewater before and after coagulation treatment with $FeCl_3$

S.No.	Parameter	Raw LSW	Treatment of LSW with 3 g L^{-1} $FeCl_3$	Raw HSW	Treatment of HSW with 4 g L^{-1} $FeCl_3$
		Mean ± S.D.	Mean ± S.D.	Mean ± S.D.	Mean ± S.D.
1	pH	7.76 ± 0.35	12.6 ± 0.26	7.12 ± 0.35	12.8 ± 0.35
2	Color	Light brown	Light brown	Dark brown	Dark brown
3	BOD_5	6180 ± 170	5285 ± 190	25650 ± 245	23980 ± 220
4	COD	11940 ± 215	8345 ± 230	52856 ± 365	37460 ±325
5	BOD_5/COD	0.51 ± 0.04	0.63 ± 0.05	0.48 ± 0.06	0.64 ± 0.06
6	TOC	2898 ± 85	2270 ± 140	12440 ± 146	8160 ± 158
7	TSS	7130 ± 165	3980 ± 120	10560 ± 278	6570 ± 180
8	TDS	18430 ± 255	14460 ± 175	39890 ± 580	20750 ± 560
9	TKN	965 ± 120	612 ± 96	3450 ± 140	2980 ± 134
10	Nitrate	17 ± 1.25	11 ± 0.95	23 ± 1.10	20 ± 1.78
11	Nitrite	27 ± 1.50	15 ± 1.55	69 ± 3.2	43 ± 1.45
12	Sulfates	3898 ± 110	2121 ± 165	10254 ± 275	3860 ± 280
13	Chloride	2345 ± 115	1525 ± 85	9020 ± 260	6020 ± 128
14	Phosphate	<0.005	< 0.005	1.9 ± 0.32	0.2 ± 0.03

Note: All the values except pH, color and BOD_5/COD are expressed as mg L^{-1}. All the values are expressed as mean of three values.

4.9.2 E-beam irradiation treatment

The pre-coagulant treated wastewater samples of LSW and HSW were subjected to E-beam irradiation treatment under two stages. Firstly, the wastewater samples were treated in 25 mL glass petri-plates to optimize the parametric conditions like pH, irradiation dose and type of oxidant like H_2O_2 and $K_2S_2O_8$ in terms of COD and TOC removal. Secondly, the optimized conditions were utilized to treat wastewater samples with 20 L of volume in stainless steel tray under E-beam irradiation. It is well understood fact that E-beam radiolysis of water produces three primary reactive species *viz.* $HO^{\bullet}$ radicals, hydrated electrons (e_{aq}^{-}) and hydrogen atom ($H^{\bullet}$) in the pH range 3-11. Under the atmospheric conditions, e_{aq}^{-} and $H^{\bullet}$ reacts with the dissolved oxygen producing superoxide radical anion ($O_2^{\cdot -}$) and perhydroxyl radical ($HO_2^{\cdot}$). Therefore, $HO^{\bullet}$ is considered to be predominant species in the aqueous solution during water radiolysis.

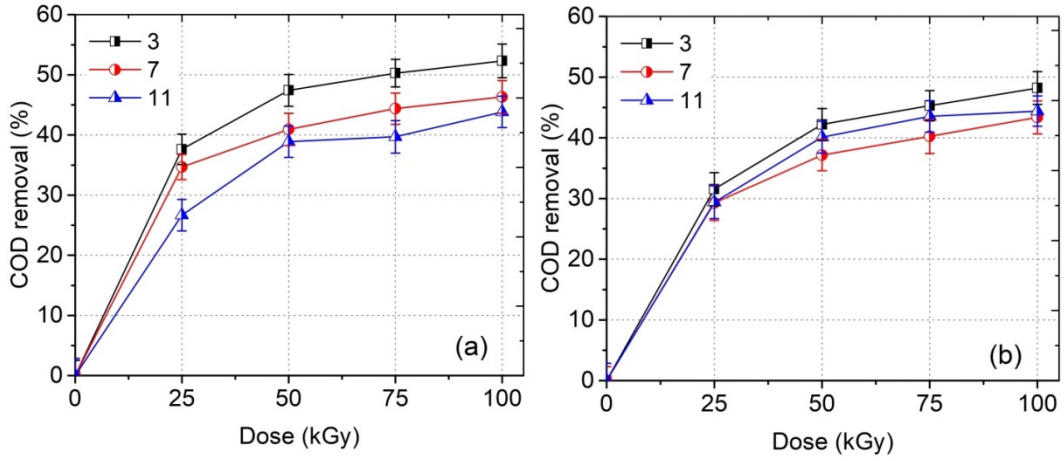

Fig. 4.81 Effect of solution pH on COD removal of (a) LSW and (b) HSW under E-beam radiolysis

The E-beam radiolysis of LSW and HSW was carried out for different doses ranging from 25 to 100 kGy. Fig. 4.81a and 4.81b shows the effect of solution pH on COD removal of LSW and HSW under E-beam radiolysis, respectively. Results showed that acidic pH solutions were slightly favourable for effective COD removal of LSW and HSW when compared to neutral and alkaline pH solutions. 52.3, 46.3 and 43.8 % of COD removal were achieved for LSW at pH 3, 7 and 11, respectively, whereas 48.1, 43.3 and 44.3% of COD removal were achieved for HSW at pH 3, 7 and 11, respectively. The increased COD removal efficiency in acidic solution and decreased COD removal efficiency in neutral and/or alkaline solution exhibit that the $HO^{\bullet}$ existence was proved to be effective for COD removal during E-beam radiolysis of wastewater. The results indicated that COD reduction was not much significant even with high irradiation dose of 100 kGy. This might be due to the presence of high amount of dissolved solids in wastewater samples. The degradation efficiency by irradiation treatment or other AOPs (generating $HO^{\bullet}$ radicals) is expected to decrease as $HO^{\bullet}$ radicals are scavenged by these salts in wastewater. Among these, carbonates and bicarbonates are considered to be strong scavenger of $HO^{\bullet}$ radicals, thereby reducing the concentration of $HO^{\bullet}$ radicals to react with organic matter of wastewater (Buxton *et al.* 1988). However, the E-beam radiation with high ionization energy (4.5 MeV) is not easily perturbed or scattered by insoluble solids, where UV radiation with low energy can be attenuated (Cantwell and Hofmann, 2011).

To investigate the effect of different types of oxidants on E-beam radiolysis of wastewater, H_2O_2 and $K_2S_2O_8$ were added to LSW and HSW at different concentrations to study their influence on COD and TOC removal efficiency. The H_2O_2 concentration was

varied from 0.01 to 0.5 M, while, $K_2S_2O_8$ concentration was varied from 0.01 to 0.15 M for LSW. For HSW, H_2O_2 concentration was varied from 0.025 to 0.75 M, while, $K_2S_2O_8$ concentration was varied from 0.05 to 0.2 M. The effect of different concentration of oxidants on COD and TOC removal efficiency of LSW and HSW is depicted in Fig. 4.82. Fig. 4.83a and 4.83b shows the optimized results of oxidant on COD and TOC removal efficiency on LSW and HSW, respectively. Results revealed that addition of 0.05 M H_2O_2 and $K_2S_2O_8$ in LSW led to 62.6 and 60.4% of COD removal (Fig. 4.83a), respectively, whereas 66.9 and 61.5% of COD removal of HSW was achieved with addition of 0.5 M H_2O_2 and 0.1 M $K_2S_2O_8$, respectively (Fig. 4.83b).

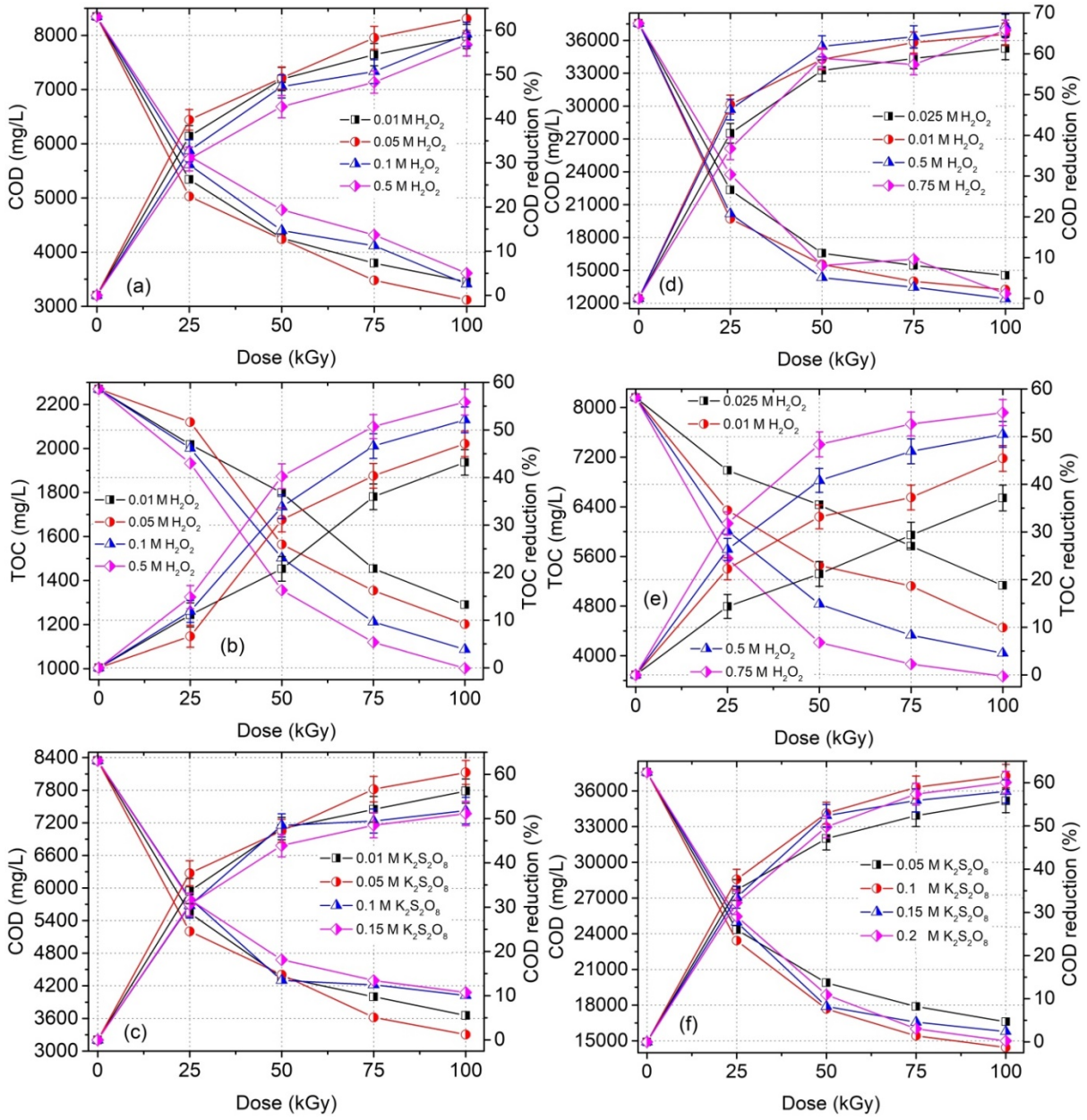

Fig. 4.82 Effect of H_2O_2 on COD and TOC removal of E-beam irradiation treatment of (a & b) LSW (d & e) HSW; Effect of $K_2S_2O_8$ on COD removal of (c) LSW (f) HSW

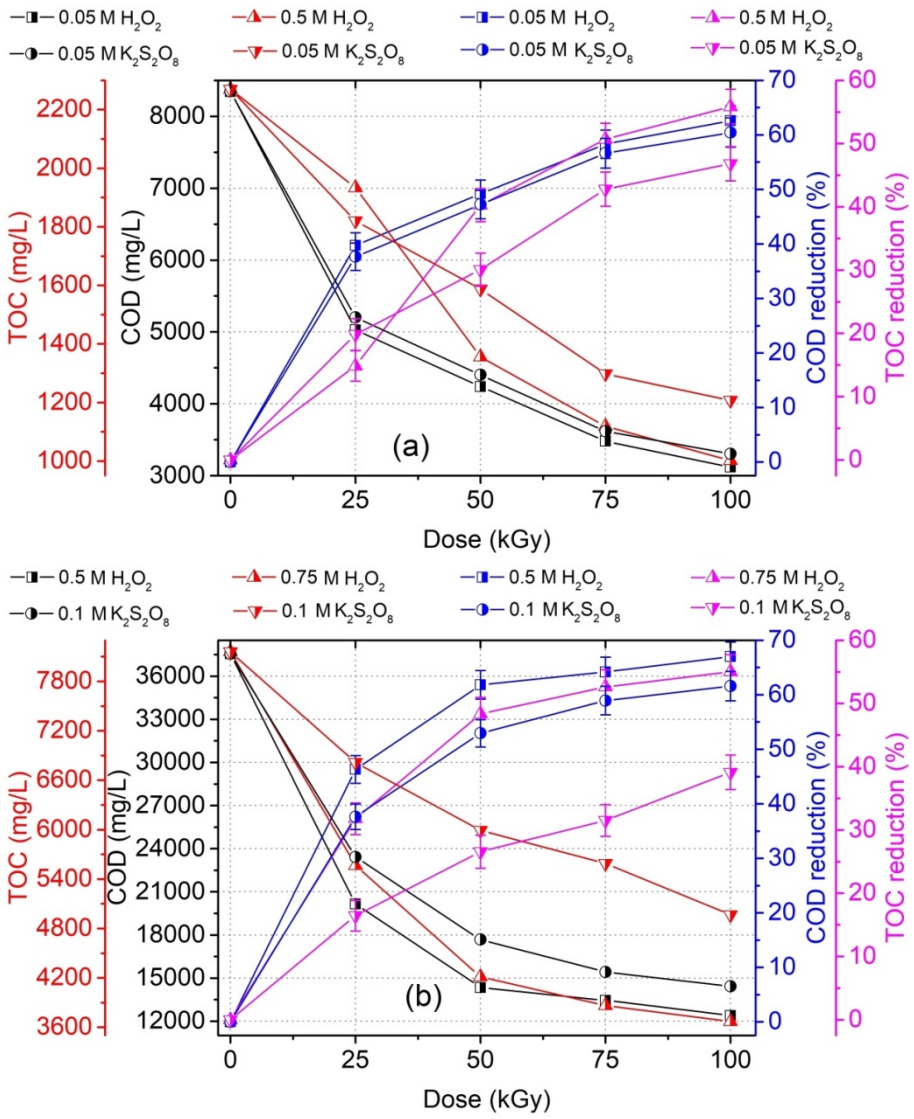

Fig. 4.83 Effect of oxidants on COD and TOC removal of (a) LSW and (b) HSW under E-beam irradiation treatment

The efficacy of E-beam radiolysis to treat wastewater is not only determined by the COD removal but also depends on the mineralization extent of recalcitrant organic compounds present in wastewater and the generated intermediates/by-products. Thus, the mineralization extent of irradiated wastewater samples was assessed to analyze the influence of different concentrations of H_2O_2 on the TOC removal (Fig. 4.82). Results indicated that addition of 0.01 M H_2O_2 led to 43.1% of TOC removal which enhanced to 55.8% with initial H_2O_2 concentration of 0.5 M in the case of LSW, whereas TOC removal efficiency enhanced from 37.1 to 55.0% with the increased H_2O_2 concentration from 0.025 to 0.75 M in case of HSW. The enhanced TOC removal of LSW and HSW with increasing H_2O_2 concentration is attributed to the fact that H_2O_2 rapidly reacts with e_{aq}^- and $H^\bullet$ during E-beam radiolysis, and

increases the HO• radical concentration in the aqueous solution to further mineralize the organic compounds and generated by-products during radiolysis. However, the presence of excess H_2O_2 may produce peroxyl radical (HO_2) species which are less reactive in comparison to HO• radical (Buxton *et al.* 1988). Fig. 4.83a and 4.83b depicts that 0.5 and 0.75 M H_2O_2 leads to 55.8 and 55.0% TOC removal of pre-coagulant treated LSW and HSW, respectively under E-beam radiolysis. However, the remaining TOC in the wastewater samples is probable due to the remaining recalcitrant organic compounds or radiolytically generated by-products during E-beam radiolysis of wastewater.

Irradiation treatment of pre-coagulant treated wastewater samples was also performed in the presence of $K_2S_2O_8$ as an oxidant. During E-beam radiolysis of wastewater in the presence of $K_2S_2O_8$, sulfate radical anion $SO_4^{\bullet-}$ are produced on reaction of e_{aq}^- and H• with $S_2O_8^{2-}$ ions according to reactions (4.46) and (4.47) (Bensasson *et al.* 1983). Like HO•, $SO_4^{\bullet-}$ is an oxidizing specie with redox potential of 2.43V and is reactive towards many organic as well as inorganic compounds. Thus, degradation of organic compounds is expected to enhance due to the simultaneous production of $SO_4^{\bullet-}$ and HO• radicals during E-beam rdaiolysis. Similar to gamma irradiation induced degradation study of wastewaters, addition of $S_2O_8^{2-}$ ions did not exhibit any significant removal of COD and TOC when compared to H_2O_2 addition. The probable reason for this trend in results could be the scavenging of $SO_4^{\bullet-}$ and HO• radicals by the Cl^- ions in the wastewater as given by Eqs. 4.48 - 4.50 (Liao *et al.* 2001; Lian *et al.* 2017). Therefore, it can be hypothesized that more selective nature of $SO_4^{\bullet-}$ than non-selective HO• radical leads to lesser degradation of the pollutants resulting into lower COD and TOC removal efficiency of the solutions in presence of $K_2S_2O_8$ than H_2O_2 (Lian *et al.* 2017).

Overall, results of oxidant presence in E-beam radiolysis of pharmaceutical wastewater achieved enhanced removal efficiency of COD with the addition of H_2O_2 when compared to $K_2S_2O_8$. Therefore, under the optimized conditions, 20 L of each LSW and HSW sample were irradiated in stainless steel tray with the addition of 0.05 and 0.5 M H_2O_2, respectively in separate experiments. The final COD values of LSW and HSW samples with an absorbed dose of 100 kGy were found to be 3175 ± 120 mg L^{-1} and 12,570 ± 225 mg L^{-1}, respectively. The irradiated samples were stored in refrigerator at 4 °C till the post-biological treatment using activated sludge process.

4.9.3 Biological treatment using lab-scale activated sludge process (ASP) reactor

Irradiated samples of LSW and HSW were subjected to aerobic biological

degradation in laboratory scale reactor using acclimatized sludge obtained from the aeration tank of ETP of pharmaceutical manufacturing unit (Derabassi, India). The pH of wastewater samples was adjusted between 7.0 to 8.0 ± 0.2 using H_2SO_4 and NaOH solutions. Due to the deficiency of nutrients in irradiated wastewater samples, nitrogen and phosphorous were added to the wastewaters to maintain the COD:N:P ratio to be 100:5:1 depending upon on the feed wastewater COD. The nutrients are required to support the growth of microbial population and securing that removal of organic load would be only limited by carbon content of wastewater. Although, the BOD_5/COD value of raw and pre-coagulant treated LSW and HSW ranged between 0.4-0.5, but irradiation treatment of LSW and HSW enhanced the BOD_5/COD in the range of 0.6 to 0.7. BOD_5/COD value was found to increase from 0.51 to 0.63 for LSW and 0.55 to 0.64 for HSW after 100 kGy of absorbed irradiation dose, indicating the conversion of non-biodegradable organic compounds of wastewater to biodegradable compounds; thereby allowing the integration of E-beam and biological treatment to achieve maximum degradation of organic matter present in wastewater.

The potential of biological treatment of LSW and HSW was examined by feeding the diluted or raw pharmaceutical wastewater, which was pre-treated with E-beam irradiation, to ASP reactor that has been previously fed and acclimatized to wastewater. Wastewater samples were continuously fed into the ASP reactor with a feed rate (Q_{feed}) of 0.15 LPH using peristaltic pump (Cole Parmer, Masterflex L/S® Model-7720062 and L/S 14 tubing). The wastewater hydraulic retention time (HRT) in the reactor was 2 days. The operation and performance of the ASP reactor was monitored in continuous mode by keeping constant Q_{feed} and HRT for both LSW and HSW individually, and variable feed COD. The system operation was studied, in sequel, using irradiated LSW dilutions with feed COD of 1000, 2000 and 3000 mg L^{-1}; whereas for HSW, feed COD was maintained to 4000, 8000 and 12000 mg L^{-1}. During the operations, parameters like pH, COD, TOC, MLVSS, MLSS and SVI of mixed liquor were monitored regularly.

4.9.3.1 Treatability studies of un-irradiated wastewater

The ASP system operation was studied, in sequel, using pre-coagulant treated L_{OSW} dilutions with feed COD of 4,000 and 8,200 mg L^{-1}; whereas for H_{OSW}, feed COD was maintained to 12,000, 24,000 and 36,000 mg L^{-1}. For the varying organic load, the COD and TOC removal efficiency was determined for L_{OSW} and H_{OSW}, and the results are represented in Fig. 4.84. The removal efficiency of COD was found to be 60.1 and 55.1% for initial feed COD of 4,000 and 8,200 mg L^{-1}, respectively, whereas TOC removal efficiency was 41.4 and

46.1%, respectively for a given feed COD. On the other hand, the removal efficiency of COD was found to be 42.5, 30.2 and 24.3% for initial feed COD of 12,000, 24,000 and 36,000 mg L^{-1}, respectively, whereas TOC removal efficiency was 41.3, 25.4 and 28.5%, respectively for a given feed COD. These results indicated that pre-coagulant treatment of samples have ability to remove organic substance present in the wastewater to some extent by making wastewater sample susceptible for subsequent microbial degradation, thereby leading to enhanced COD and TOC removal efficiency. However, the COD reduction for higher feed COD of 24,000 and 36,000 mg L^{-1} was observed to be lesser when compared to lower feed COD, which might be due to the inhibitory effect of the higher concentration of organic pollutant with increasing organic load (Fewson, 1988; Suman Raj and Anjaneyulu, 2005).

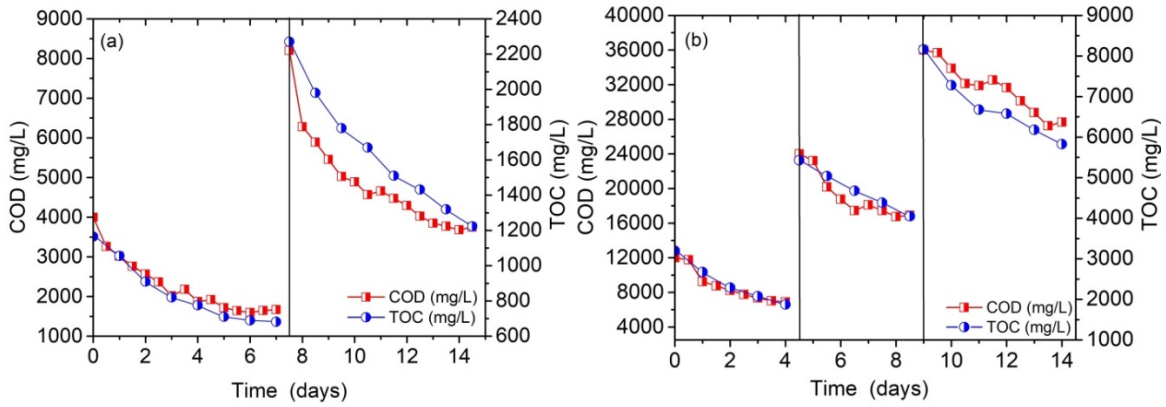

Fig. 4.84 Profile of COD and TOC concentration at the effluent of ASP reactor operating under continuous mode at constant Q_{feed} of 0.15 L h^{-1} for pre-coagulant treated (a) L_{OSW} and (b) H_{OSW}

The results indicated that sequential treatment of raw L_{OSW} with pre-coagulant treatment followed by subsequent biological treatment led to final COD value of 3,680 ±120 mg L^{-1} from the initial COD value of 8,200 ± 175 mg L^{-1}. In case of H_{OSW}, final COD value of 27,240 ± 235 mg L^{-1} was achieved when the initial COD value was 3,6000 ± 215 mg L^{-1}.

4.9.3.2 Treatability studies of irradiated wastewater

For the organic load varying from 1000 to 3000 mg L^{-1}, the pH, COD and TOC removal efficiency was determined for LSW and the results are represented in Fig. 4.85. The removal efficiency of COD was found to be 88.2, 87.2 and 78.9% for initial feed COD of 1000, 2000 and 3000 mg L^{-1}, respectively, whereas TOC removal efficiency was found to be 52.8, 62.4 and 66.8%, respectively. These results indicated that pre-treatment of samples by E-beam irradiation have ability to convert recalcitrant non-biodegradable organic substance present in the wastewater to easily removable biodegradable substances which are removed

by subsequent microbial degradation, thereby leading to enhanced COD and TOC removal efficiency. However, the COD reduction for feed COD of 3000 mg L^{-1} was observed to be lesser when compared to feed COD of 2000 mg L^{-1}, which might be due to the inhibitory effect of the higher concentration of organic pollutant with increasing organic load (Fewson *et al.* 1988; Raj and Anjaneyulu, 2005). The significant reduction of COD and TOC for LSW was supported by considerable production of MLSS and MLVSS. The values of MLSS and SVI were monitored on daily basis to understand the on-going biochemical activity and variation of feed COD concentration and results are shown in Fig. 4.86a. As a result, concentration of MLSS increased from 3500 to 3932 mg L^{-1} till 9th day of biological treatment, whereas about 87.2% of COD reduction was achieved for initial feed COD of 2000 mg L^{-1}. After 9th day, with the addition of high concentration of feed COD (3000 mg L^{-1}), MLSS concentration decreased and became consistent to ≈ 3900 mg L^{-1}. The gradual increase in MLSS concentration and insignificant decline at a specified HRT can be due to the auto oxidation of the microbial population and food to mass ratio dynamics (Sastry and Thambirajah, 1995; Raj *et al.* 2004).

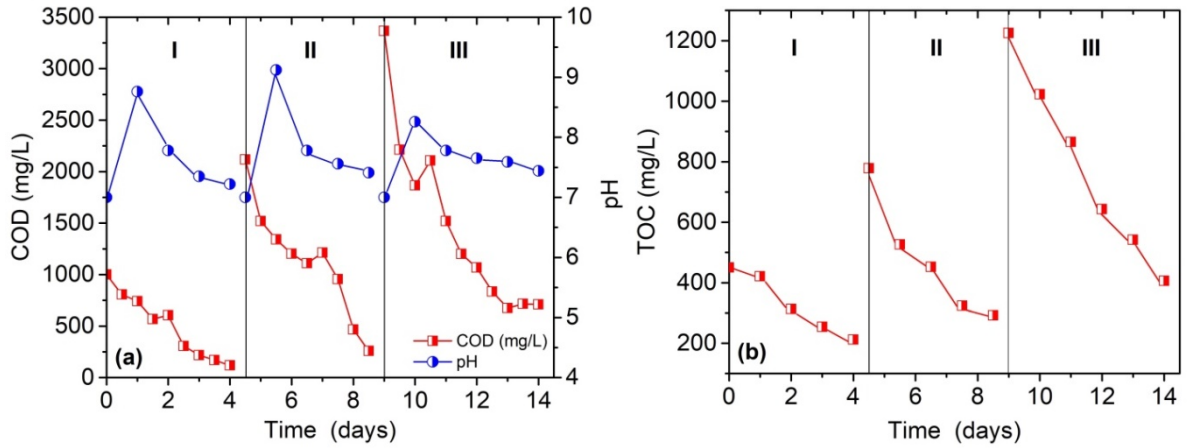

Fig. 4.85 Profile of COD concentration and pH at the effluent of ASP reactor (b) TOC profile at the effluent of ASP reactor operating in continuous mode at constant Q_{feed} of 0.15 LPH and feed COD (I) 1000 (II) 2000 and (III) 3000 mg L^{-1} LSW

For HSW, the organic load was varied from 4000 to 12000 mg L^{-1} and results of the pH, COD and TOC removal efficiency are depicted in Fig. 4.87. The COD removal efficiency was found to be 72.1, 60.1 and 52.3% for initial feed COD of 4000, 8000 and 12000 mg L^{-1}, respectively, whereas TOC removal efficiency was found to be 60.1, 65.6 and 65.3%, respectively. Herein, the COD removal efficiency decreased with the increased feed COD to the reactor which might be due to the fact that higher concentration of organic load

may induce inhibitory effect to the efficient treatment (Fewson *et al.* 1988). The maximum MLSS concentration was observed to be 4110 mg L^{-1} and after that decline in MLSS concentration was observed at a given HRT (Fig. 4.86b). From these observations, it can be considered that the decline in MLSS concentration can be attributed to the formation of secondary metabolites and intermediate products during the aerobic degradation of pharmaceutical wastewater (McCabe and Eckenfelder, 1958; Raj and Anjaneyulu 2005).

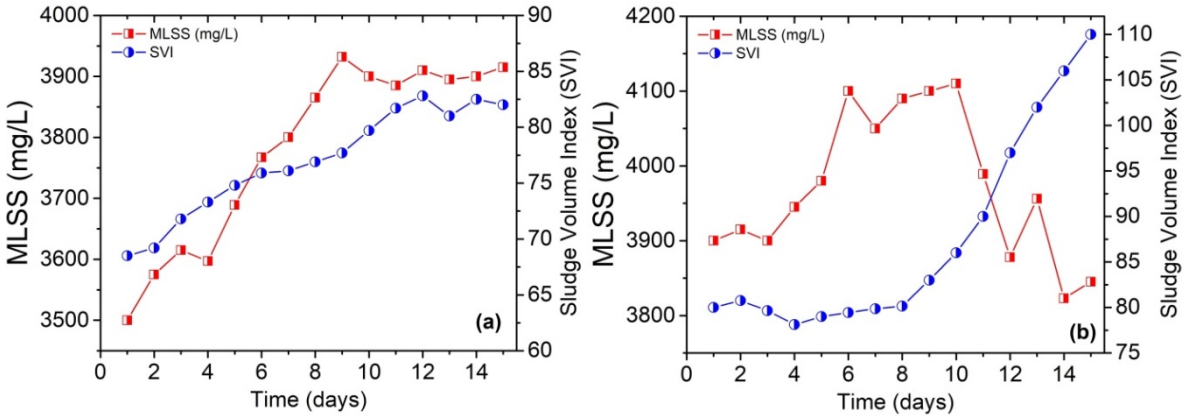

Fig. 4.86 Variation of MLSS and SVI during continuous mode operation of ASP reactor at constant Q_{feed} of 0.15 LPH and varied COD concentration for (a) LSW and (b) HSW

It was observed that for aerobic biotransformation of LSW and HSW, the pH of effluent initially increased and then remained consistent between 7.0 and 8.0 indicating that active biomass were able to manage efficiently with the imposed change of feed COD throughout the reactor operations. It is believed that rate of organic matter consumption in the aerobic biotransformation increases with the increase in concentration of microbial population in the aeration tank. The increases in MLVSS indicated the active phase of aerobic biotransformation (Metcalf, 1995). In this study, the maximum MLVSS of 3895 mg L^{-1} and 3345 mg L^{-1} were observed for reactor operation for LSW and HSW, respectively. SVI indicates the settling characteristics of activated sludge and also specifies the extent of aerobic biotransformation (McLachlan *et al.* 1936; Sharma and Chatuvedi, 1995). In the case of aerobic treatment of LSW, SVI ranged from 68 to 82; whereas it ranged between 80 and 110 in case of HSW indicating the sludge was of good quality. These results show that SVI increased with high concentration of feed COD which indicates that settling characteristics of sludge reduced due to the inhibitory effect of high strength pharmaceutical waste (Arceivala, 2007). Thus, inhibition of aerobic biotransformation at higher feed COD is due to the reduction in the microbial activity of the microbial populations in the oxidation of real

pharmaceutical wastewater. Thus, it can be considered that E-beam radiation technology has a potential to treat real industrial wastewater with high organic load and the simultaneous integration of E-beam with biological treatment could further eliminate the organic matter, thereby achieving the complete removal of organic matter from wastewater.

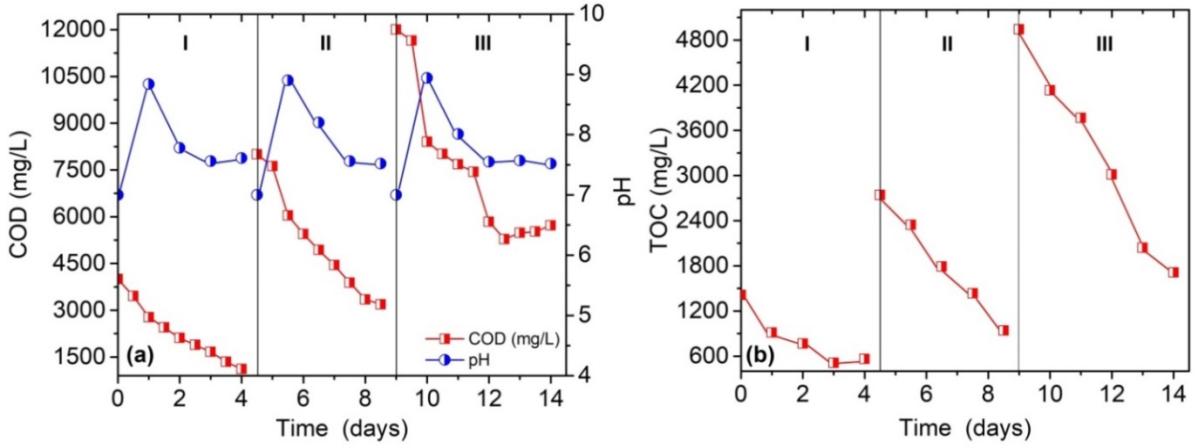

Fig. 4.87 Profile of COD concentration and pH at the effluent of ASP reactor (b) TOC profile at the effluent of ASP reactor operating in continuous mode at constant Q_{feed} of 0.15 LPH and feed COD (I) 4000 (II) 8000 and (III) 12000 mg L^{-1} HSW

Based on the results, the aerobic biological treatment of pharmaceutical wastewater of variable organic load after the pre-coagulant and irradiation-based treatment, more specifically E-beam treatment could be a promising technology in integrated wastewater management scheme at industrial or commercial scale.

4.9.4 Toxicity analysis

The toxicity of wastewater and its irradiated solutions was tested against clinical isolates of three microorganisms *viz. E. coli, B. subtilis* and *P. aeruginosa* using zone of inhibition test. Toxicity assessment was conducted for the treated LSW and HSW through sequential E-beam irradiation (100 kGy of irradiation dose) followed by biological treatment and the results obtained are depicted in the Fig. 4.88. Results showed that in almost all the petri-dishes, strong zone of inhibition was observed for raw LSW and HSW, indicating the presence of toxic organic pollutants in the wastewater. However, with E-beam irradiation treatment of wastewater followed by biological, inhibition zone almost disappeared for LSW, and small zone was observed for E-beam irradiated HSW indicating the presence of some toxic compounds or secondary products after irradiation treatment of HSW. These results showed that when E-beam irradiation was used as pre-treatment technology to treat wastewater with different organic loads, almost complete detoxification of wastewater was

achieved indicating that E-beam irradiation has a potential to eliminate cytotoxicity from real wastewater.

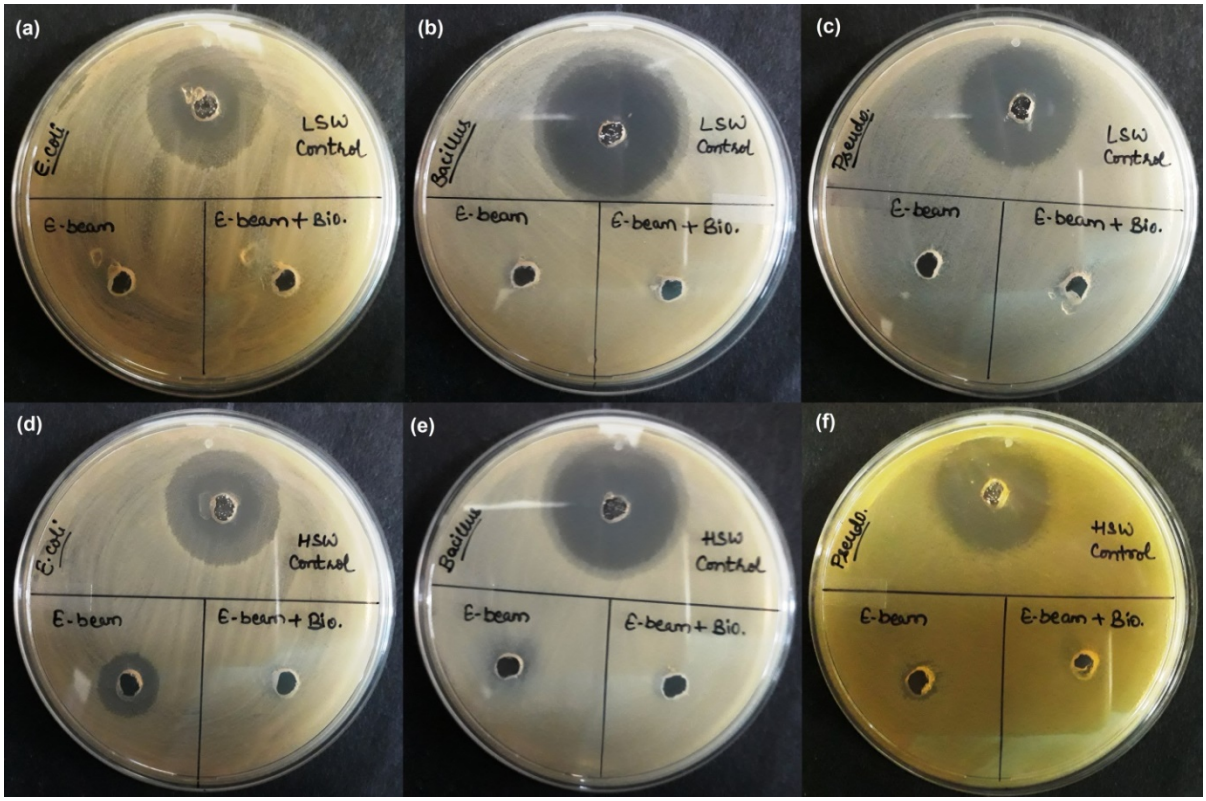

Fig. 4.88 Cytotoxic potential of (a: *E. coli*, b: *B. subtilis* and c: *P. aeruginosa*) L_{OSW} and (d: *E. coli*, e: *B. subtilis* and f: *P. aeruginosa*) H_{OSW} treated with H_2O_2-mediated E-beam irradiation followed by post-biological treatment

4.9.5 Cost analysis and environmental implications

Most of the reported studies associated with AOPs deals with the degradation of organic compound without considering the cost of the treatment and in case of real wastewater treatment, literature lacks the knowledge on overall cost associated with the treatment of real pharmaceutical wastewater using single stage oxidation or combined treatment technology. In actual, there are different types of expenses associated with the complete treatment process that must be taken into account while deciding the economic viability of process. Real costs of the process must include the reactor, reagents, chemicals, electricity consumption and operating costs. The overall cost associated with the E-beam treatment of low and high strength wastewater by excluding the cost of land is illustrated in Table 4.29 and Table 4.30. In this study, efforts were made to evaluate the overall cost of treatment at field-scale and the results are represented in Table 4.32.

The efficiencies of E-beam radiolysis alone and E-beam + H_2O_2 radiolysis was evaluated in terms or cost of electrical energy consumed and other auxiliary inputs. The cost of electrical energy employed in the E-beam radiolysis of wastewater samples was calculated using Eq. 4.44 and the results obtained are explained in Table 4.29 and 4.30. Table 4.31 represents the total operating cost of E-beam + ASP treatment of L_{OSW} and H_{OSW} wastewater.

Table 4.29 The cost of energy involved in E-beam radiolysis of low strength pharmaceutical wastewater

S.No.	Treatment Employed	Average treatment time (min)	Cost of H_2O_2 used (INR m^{-3})	Total ATC (INR m^{-3}) @INR 5/kWh*	Total ATC (USD m^{-3})#
1.	E-beam alone	4.02	NIL	47.1	0.6
2.	E-beam +H_2O_2	2.04	523	546.9	7.8

Average treatment time required for 50% COD removal was calculated by considering the dose rate @25kGy min^{-1}
*Considering the average cost of Rs 5/kWh for industrial sector (Punjab State Electricity Regulatory Commission, 2017).
#Considering the conversion factor from USD to INR to be 1 USD=71.14 INR

Table 4.30 The cost of energy involved in E-beam-radiolysis of high strength pharmaceutical wastewater

S.No.	Treatment Employed	Average treatment time (min)	Cost of H_2O_2 used (INR m^{-3})	Total ATC (INR m^{-3}) @INR 5/kWh*	Total ATC (USD m^{-3})#
1.	E-beam alone	3	NIL	35.15	0.5
2.	E-beam +H_2O_2	1.08	785	797.6	11.4

Average treatment time required for 50% COD removal was calculated by considering the dose rate @25kGy min^{-1}
*Considering the average cost of Rs 5/kWh for industrial sector (Punjab State Electricity Regulatory Commission, 2017).
#Considering the conversion factor from USD to INR to be 1 USD=71.14 INR

The volume of wastewater treated was 9.6 L as calculated using the dimensions of stainless steel tray ($80 \times 60 \times 2\ cm$). The rated power of E-beam unit was 0.702 kW. The

costs involved during E-beam radiolysis of LSW and HSW were calculated on the basis of COD removal efficiency of 50%. The total cost of E-beam radiolysis alone and E-beam + H_2O_2 radiolysis for low strength wastewater was found to be 0.6 and 7.8 USD m^{-3}; whereas, for high strength wastewater, it was found to be 0.5 and 11.4 USD m^{-3}, respectively.

Table 4.31 The total operating cost involved in E-beam radiolysis + biological treatment of pharmaceutical wastewater

(A) Costs involved during E-beam radiolysis alone of L_{OSW} (60 L) =0.6 USD m^{-3}	(1) Costs involved during E-beam radiolysis alone of H_{OSW} (60 L) =0.5 USD m^{-3}
(B) Operating cost of lab-scale ASP treatment of L_{OSW} • Total volume of L_{OSW} treated= 60 L (0.06 m^3) • Cost of activated sludge= 0 USD • Energy consumed during operation of ASP process (pumping through peristaltic pumps, air spargers, stirrer etc.) = 3270 Wh • With 50% degradation, COD removal= 1,660 mg L^{-1} (1.66 kg m^{-3}) • Energy consumed during per kg of COD removed = 3270/1.66 = 1.96 kWh • Electricity price in India = 0.072 USD/kWh • Cost of electricity consumption = **1.96** × 0.072 = 0.141 USD/kWh • Cost per m^3 of wastewater treated= 0.141/0.06 = 2.35 USD m^{-3}	(2) Operating cost of lab-scale ASP treatment of H_{OSW} • Total volume of L_{OSW} treated= 60 L (0.06 m^3) • Cost of activated sludge= 0 USD • Energy consumed during operation of ASP process (pumping through peristaltic pumps, air spargers, stirrer etc.) = 3495 Wh • With 50% degradation, COD removal= 5,940 mg L^{-1} (5.94 kg m^{-3}) • Energy consumed during per kg of COD removed = 3495/5.94 = 0.588 kWh • Electricity price in India = 0.072 USD/kWh • Cost of electricity consumption = 0.588 × 0.072 = 0.042 USD/kWh • Cost per m^3 of wastewater treated= 0.042/0.06 = 0.7 USD m^{-3}
Total operating cost of E-beam radiolysis + ASP treatment of L_{OSW} = (A) + (B) = 2.95 USD m^{-3}	Total operating cost of E-beam radiolysis + ASP treatment of H_{OSW} = (1) + (2) = 1.2 USD m^{-3}

Table 4.32 Evaluation of total cost of E-beam facility for industrial applications of wastewater treatment

Installation capacity	Application	Total cost of E-beam unit (M USD)	Shielding and maintenance cost (M USD)	Capital requirement (kUSD)	Treatment capacity (m^3 day^{-1})	Cost of treatment (USD m^{-3})
E-Beam (20 MeV, 100 kW)	Pharmaceutical wastewater treatment (For average COD of 10,000-12,000 mg L^{-1})	1.25	0.3	4500	10,000	0.3

The use of radiation technology has been considered as an emerging tool to treat groundwater, surface water, wastewater and sludge. High energy E-beam radiation-based pilots and commercial sludge treatment plants have been successfully installed in India, USA, New Mexico, Argentina, Korea and Germany (IAEA, 2007 and 2008). E-beam machine involve only one time installation and nullifies the use of any auxiliary chemicals for the treatment which further strengthen the potential applicability of E-beam irradiation as a clean, cost-effective and productive tool for water and wastewater treatments. Thus, radiation technology particularly the use of E-beam accelerators could play an imperative role in near future for the treatment of real pharmaceutical wastewater at pilot as well as commercial scale.

4.10 Comparison of treatment technologies for degradation of real wastewater

The low (LSW) and high strength wastewater (HSW) collected from the representative pharmaceutical industry were subjected to independent Fenton, gamma and E-beam irradiation treatment as well as in conjunction with biological treatment. Table 4.33 summarized the treatment results of real pharmaceutical wastewater obtained using independent Fenton, gamma and E-beam irradiation treatment. Table 4.34 summarized the treatment results of real pharmaceutical wastewater obtained using Fenton, gamma and E-beam irradiation treatment with subsequent biological treatment. The initial COD of raw LSW and HSW was 50,933 ± 390 mg L^{-1} and 12,480 ± 450 mg L^{-1}, respectively during gamma and E-beam treatment. The initial COD of raw LSW and HSW was 35,840 ± 225 mg L^{-1} and 8206 ± 190 mg L^{-1}, respectively during Fenton treatments.

Table 4.33 Comparative results of employed treatments for real wastewater

S. No.	Treatment	Type of wastewater	Optimized conditions	COD		TOC
				Reduction (%)	**Value (mg L^{-1})**	**Reduction (%)**
1.	Dark-Fenton treatment	LSW	0.25 M H_2O_2, 0.02 M Fe^{2+}, pH 3, 120 min	53	3775	23
		HSW	1 M H_2O_2, 0.15 M Fe^{2+}, pH 3, 120 min	47	18642	21
2.	Solar-photo Fenton treatment	LSW	0.25 M H_2O_2, 0.05 M Fe^{2+}, pH 3, 120 min	58	3413	26
		HSW	1 M H_2O_2, 0.1 M Fe^{2+}, pH 3, 120 min	57	15362	31
3.	Coagulation treatment	LSW	3 g L^{-1} $FeCl_3$	37	8064	27
		HSW	4 g L^{-1} $FeCl_3$	29	35840	33
4.	Gamma irradiation treatment	LSW	0.1 M H_2O_2 with 100 kGy dose	58	3326	80
			0.05 M $K_2S_2O_8$ with 100 kGy dose	57	3450	66
		HSW	0.5 M H_2O_2 with 100 kGy dose	60	13610	71
			0.05 M $K_2S_2O_8$ with 100 kGy dose	61	14090	65
5.	E-beam irradiation treatment	LSW	0.05 M H_2O_2 with 100 kGy dose	62	3120	55
			0.05 M $K_2S_2O_8$ with 100 kGy dose	60	3303	46
		HSW	0.05 M H_2O_2 with 100 kGy dose	66	12400	55
			0.1 M $K_2S_2O_8$ with 100 kGy dose	61.5	14434	39

Table 4.34 Comparative results of employed treatments for real wastewater in conjunction with biological treatment

S. No.	Treatment	Type of wastewater	Optimized conditions	COC		TOC
				Reduction (%)	**Value (mg L^{-1})**	**Reduction (%)**
1.	Dark-Fenton treatment + Bio	LSW	20 % (v/v) sludge, incubation temperature and period of 27 °C and 192 h	52	1801	35
		HSW	25 % (v/v) sludge, incubation temperature and period of 27 °C and 192 h	37	11720	31
2.	Solar-photo Fenton treatment + Bio	LSW	20 % (v/v) sludge, incubation temperature and period of 27 °C and 192 h	62	1290	49

		HSW	25 % (v/v) sludge, incubation temperature and period of 27 °C and 192 h	55	6790	51
3.	Biological treatment	LSW	20 % (v/v) sludge, incubation temperature and period of 27 °C and 120 h	71	2312	56
		HSW	25 % (v/v) sludge, incubation temperature and period of 27 °C and 192 h	53	17450	22
4.	Gamma to Bio	LSW	15 % (v/v) sludge, incubation temperature and period of 27 °C and 168 h	70	982	66
		HSW	25 % (v/v) sludge, incubation temperature and period of 27 °C and 168 h	65	4693	55
5.	Bio to gamma	LSW	0.05 M H_2O_2 with 100 kGy dose	79	532	89
			0.15 M $K_2S_2O_8$ with 100 kGy dose	75	645	-
		HSW	0.1 M H_2O_2 with 100 kGy dose	43	9810	62
			0.1 M $K_2S_2O_8$ with 100 kGy dose	41	10130	-
6.	E-beam to Bio (with ASP reactor)	LSW	Feed COD 1000 mg L^{-1}	88	118	52
			Feed COD 2000 mg L^{-1}	87	258	62
			Feed COD 3000 mg L^{-1}	78	710	66
		HSW	Feed COD 4000 mg L^{-1}	72	1113	60
			Feed COD 8000 mg L^{-1}	60	3190	65
			Feed COD 12000 mg L^{-1}	52	5721	65
7.	Sequential coagulation to gamma and subsequent biological treatment	LSW with initial COD of 12,840 mg L^{-1}		92	982	82
		HSW with initial COD of 50,933 mg L^{-1}		90	4693	91
8.	Sequential coagulation to bio and subsequent gamma	LSW with initial COD of 12,840 mg L^{-1} 92.3		95	532	94
		HSW with initial COD of 50,933 mg L^{-1} 90.7		80	9810	79
9.	Sequential coagulation E-beam and subsequent biological	LSW with initial COD of 12,840 mg L^{-1} 92.3		94	675	81
		HSW with initial COD of 50,933 mg L^{-1} 90.7		89	5280	90

According to Table 4.32, gamma and E-beam treatment with subsequent biological treatment of pharmaceutical wastewater of different organic load were effective in their degradation when compared to Fenton technologies. Considering the high dose rate of E-beam accelerators and capacity to treat large volume of wastewater when compared to gamma irradiation chamber, E-beam technology followed by conventional biological treatment could be utilized as an effective technique for the degradation of real pharmaceutical industry wastewater.

Conclusion

- The study presented the effective degradation of model compounds (OFX, AMX and ORZ) and pharmaceutical wastewater using independent gamma, E-beam and Fenton-based treatment.
- Solar-assisted Fenton process was more efficient than UV-assisted Fenton process in degrading the ORZ using hematite. Among the synthesized hematite particles, cubical shaped hematite performed better under solar and UV irradiations.
- Naturally available soil as a low cost and abundantly available resource with high content of iron oxides played a significant role for treating the pharmaceutical contaminants in batch and continuous.
- High-dispersive FeS_2 on GO possesses a relatively high oxidative capacity for degrading recalcitrant pharmaceuticals in photo-Fenton system, offering a good alternative for the treatment of aqueous organic contaminants.
- Gamma radiolysis proved to better for the treatment of model compounds due to high radiation yield when compared to E-beam and Fenton treatments.
- Under independent gamma and E-beam radiolysis, G-value increased and dose constant reduced with higher initial concentrations of model compounds. Degradation efficiency was found to be increased in acidic medium when compared to alkaline/neutral medium and followed pseudo first-order reaction kinetics model.
- Addition of H_2O_2 exhibited the synergic effect on the degradation and mineralization of model compounds in independent gamma and E-beam by promoting the production of $HO^{\bullet}$ radicals.
- Independent gamma and E-beam radiolytic degradation of model compounds in the presence of various additives revealed that the main pathway of degradation was through the $HO^{\bullet}$ oxidation.
- Cytotoxicity assessments showed that gamma as well as E-beam irradiated solutions of model compounds did not acquire any toxicity after radiation treatment. Therefore, the results encourage to employ gamma and E-beam radiolysis as an efficient and promising technology for the effective removal and mineralization of water pollutants; thus making water reusable and recyclable for various applications.
- Considering the potential applications of Fe^{2+} and Fe^{3+} ions as coagulants, the Fenton process employed in the treatment of real pharmaceutical wastewater have dual

function of coagulation as well as oxidation in minimizing the organic load of wastewater prior to biological treatment.

- Overall results indicated that among the utilized Fenton technologies, pre-treatment of pharmaceutical wastewater with photo-Fenton lead to better degradation and mineralization removal efficiency with subsequent biological degradation when compared to dark-Fenton.
- Sequential coagulation, gamma radiolysis and aerobic biodegradation lead to synergistic degradation and detoxification of both the LSW and HSW, and lead to overall improved COD and TOC removal. Gamma irradiation enabled these streams to be treated effectively by biological treatment by converting the recalcitrant and toxic wastewater to biodegradable and non-toxic.
- Sequential treatment route involving coagulation followed by E-beam irradiation and subsequent biological degradation lead to synergistic degradation and detoxification of the LSW and HSW with improved COD and TOC removal efficiencies.
- Almost similar COD and TOC removal efficiencies were obtained using gamma and E-beam radiolysis of pharmaceutical wastewaters followed by subsequent biological treatment. However, due to sample volume constrain in gamma chamber, E-beam technology could play an imperative role in near future at pilot and commercial scale for real pharmaceutical wastewater treatment.
- This study suggests that E-beam technology could be utilized as an effective technique for the remediation of real pharmaceutical industry wastewater in the common effluent treatment plant (CETP), and if used with traditional treatment technologies, it may achieve best possible treatment goals at lowest cost possible.

Future recommendations

In present study the wastewater was collected from a single pharmaceutical manufacturing unit, therefore, a comprehensive study of integrated system by taking mixed wastewater from cluster of manufacturing industries could be helpful in attaining the actual representation of existing wastewater treatment problems and signifies the practical viability of combined E-beam irradiation and biological treatment for a common effluent treatment plant. Since the toxic nature of wastewater was only tested against the clinical isolates of selected microbes, a comprehensive study dealing with toxicity analyses of actual wastewater using different bioassays test methods could exhibit more reliable and viable results.

References

1. Adityosulindro, S., Barthe, L., González-Labrada, K., Haza, U. J. J., Delmas, H., & Julcour, C. (2017). Sonolysis and sono-Fenton oxidation for removal of ibuprofen in (waste) water. *Ultrasonics Sonochemistry*, *39*, 889-896.
2. Akiba, M., Senba, H., Otagiri, H., Prabhasankar, V. P., Taniyasu, S., Yamashita, N., Lee, K., Yamamoto, T., Tsutsui, T., Joshua, D. I., Balakrishna, K., Bairy, I., Iwata, T., Kusumot, M., Kannan, K., & Guruje, K. S. (2015). Impact of wastewater from different sources on the prevalence of antimicrobial-resistant Escherichia coli in sewage treatment plants in South India. *Ecotoxicology and Environmental Safety*, *115*, 203-208.
3. Alalm, M. G., Tawfik, A., & Ookawara, S. (2015). Degradation of four pharmaceuticals by solar photo-Fenton process: kinetics and costs estimation. *Journal of Environmental Chemical Engineering*, *3*, 46-51.
4. Alaton, I. A., Balcioglu, I. A., & Bahnemann, D. W. (2002). Advanced oxidation of a reactive dyebath effluent: comparison of O_3, H_2O_2/UV-C and TiO_2/UV-A processes. *Water Research*, *36*, 1143-1154.
5. Alaton, I. A., Dogruel, S., Baykal, E., & Gerone, G. (2004). Combined chemical and biological oxidation of penicillin formulation effluent. *Journal of Environmental Management*, *73*, 155-163.
6. Alexy, R., Kümpel, T., Dörner, M., & Kümmerer, K. (2001). Effects of antibiotics against environmental bacteria studied with simple tests. In *Proceedings of the 11th Annual Meeting of SETAC Europe, Madrid* (pp. 6-11).
7. Andreozzi, R., Caprio, V., Insola, A., & Marotta, R. (1999). Advanced oxidation processes (AOP) for water purification and recovery. *Catalysis Today*, *53*, 51-59.
8. Andreozzi, R., Raffaele, M., & Nicklas, P. (2003). Pharmaceuticals in STP effluents and their solar photodegradation in aquatic environment. *Chemosphere*, *50*, 1319-1330.
9. Anumol, T., Vijayanandan, A., Park, M., Philip, L., & Snyder, S. A. (2016). Occurrence and fate of emerging trace organic chemicals in wastewater plants in Chennai, India. *Environment International*, *92*, 33-42.
10. APHA, Standard Methods for the Examination of Water and Wastewater, Twentieth ed., method 3500-Fe B.
11. APHA, Standard Methods for the Examination of Water and Wastewater, Twentieth ed., method 5220 C.

12. APHA, 1998. The Standard Methods for the Examination of Water and Wastewater, Twentieth ed., American Public Health Association, Washington, DC.
13. Arceivala, S. J., & Asolekar, S. R. (2007). *Wastewater treatment for pollution control and reuse*. Tata McGraw-Hill Education.
14. Archana, G., Dhodapkar, R., & Kumar, A. (2016). Offline solid-phase extraction for preconcentration of pharmaceuticals and personal care products in environmental water and their simultaneous determination using the reversed phase high-performance liquid chromatography method. *Environmental Monitoring and Assessment*, *188*, 512.
15. Arlos, M. J., Bragg, L. M., Parker, W. J., & Servos, M. R. (2015). Distribution of selected antiandrogens and pharmaceuticals in a highly impacted watershed. *Water Research*, *72*, 40-50.
16. Arslan-Alaton, I., & Caglayan, A. E. (2006). Toxicity and biodegradability assessment of raw and ozonated procaine penicillin G formulation effluent. *Ecotoxicology and Environmental Safety*, *63*, 131-140.
17. Arslan-Alaton, I., & Dogruel, S. (2004). Pre-treatment of penicillin formulation effluent by advanced oxidation processes. *Journal of Hazardous Materials*, *112*, 105-113.
18. Badawy, M. I., Wahaab, R. A., & El-Kalliny, A. S. (2009). Fenton-biological treatment processes for the removal of some pharmaceuticals from industrial wastewater. *Journal of Hazardous Materials*, *167*, 567-574.
19. Balakrishna, K., Rath, A., Praveenkumarreddy, Y., Guruge, K. S., & Subedi, B. (2017). A review of the occurrence of pharmaceuticals and personal care products in Indian water bodies. *Ecotoxicology and Environmental Safety*, *137*, 113-120.
20. Balcıoğlu, I. A., & Ötker, M. (2003). Treatment of pharmaceutical wastewater containing antibiotics by O_3 and O_3/H_2O_2 processes. *Chemosphere*, *50*, 85-95.
21. Baran, W., Sochacka, J., & Wardas, W. (2006). Toxicity and biodegradability of sulfonamides and products of their photocatalytic degradation in aqueous solutions. *Chemosphere*, *65*, 1295-1299.
22. Barhoumi, N., Oturan, N., Olvera-Vargas, H., Brillas, E., Gadri, A., Ammar, S., & Oturan, M. A. (2016). Pyrite as a sustainable catalyst in electro-Fenton process for improving oxidation of sulfamethazine. Kinetics, mechanism and toxicity assessment. *Water Research, 94*, 52-61.
23. Basfar, A. A., Khan, H. M., Al-Shahrani, A. A., & Cooper, W. J. (2005). Radiation induced decomposition of methyl tert-butyl ether in water in presence of chloroform: kinetic modelling. *Water Research*, *39*, 2085-2095.

24. Batt, A. L., Bruce, I. B., & Aga, D. S. (2006). Evaluating the vulnerability of surface waters to antibiotic contamination from varying wastewater treatment plant discharges. *Environmental Pollution*, *142*, 295-302.
25. Bautista, P., Mohedano, A. F., Gilarranz, M. A., Casas, J. A., & Rodriguez, J. J. (2007). Application of Fenton oxidation to cosmetic wastewaters treatment. *Journal of Hazardous Materials*, *143*, 128-134.
26. Behera, S. K., Kim, H. W., Oh, J. E., & Park, H. S. (2011). Occurrence and removal of antibiotics, hormones and several other pharmaceuticals in wastewater treatment plants of the largest industrial city of Korea. *Science of the Total Environment*, *409*, 4351-4360.
27. Benkelberg, H. J., & Warneck, P. (1995). Photodecomposition of iron (III) hydroxo and sulfato complexes in aqueous solution: wavelength dependence of OH and SO^{4-} quantum yields. *The Journal of Physical Chemistry*, *99*, 5214-5221.
28. Bensasson, R. V., Land, E. J., Truscott, T. G. (1983). Flash Photolysis and Pulse Radiolysis: Contributions to the Chemistry of Biology and Medicine, Pergamon Press, Oxford, pp.1–19.
29. Bhatia, V., & Dhir, A. (2016). Transition metal doped TiO_2 mediated photocatalytic degradation of anti-inflammatory drug under solar irradiations. *Journal of Environmental Chemical Engineering*, *4*, 1267-1273.
30. Bhatia, V., Ray, A. K., & Dhir, A. (2016a). Enhanced photocatalytic degradation of ofloxacin by co-doped titanium dioxide under solar irradiation. *Separation and Purification Technology*, *161*, 1-7.
31. Bhattacharyya, T., Chandran, P., Ray, S. K., Mandal, C., Pal, D. K., Venugopalan, M. V., Durge, S. L., Srivastava, P., Dubey, P. N., Kamble, G. K., Sharma, R. P., Wani, S. P., Rego, T. J., Pathak, P., Ramesh, V., Manna, M. C., & Sahrawat, K. L. (2008). Physical and Chemical Properties of Red and Black Soils of Selected Benchmark Spots for Carbon Sequestration Studies in Semi-Arid Tropics of India: Global Theme on Agroecosystems Report No. 35.
32. Bhuiyan, M. R., Shaid, A., Hossain, M. A., & Khan, M. A. (2016). Decolorization and decontamination of textile wastewater by gamma irradiation in presence of H_2O_2. *Desalination and Water Treatment*, *57*, 21545-21551.
33. Bila, D. M., & Dezotti, M. (2003). Pharmaceutical drugs in the environment. *Química Nova*, *26*, 523-530.

34. Bojanowska-Czajka, A., Kciuk, G., Gumiela, M., Borowiecka, S., Nałęcz-Jawecki, G., Koc, A., Garcia-Reyes, J. F., Ozbay, D. S., & Trojanowicz, M. (2015). Analytical, toxicological and kinetic investigation of decomposition of the drug diclofenac in waters and wastes using gamma radiation. *Environmental Science and Pollution Research*, *22*, 20255-20270.
35. Borrely, S. I., Morais, A. V., Rosa, J. M., Badaró-Pedroso, C., da Conceição Pereira, M., & Higa, M. C. (2016). Decoloration and detoxification of effluents by ionizing radiation. *Radiation Physics and Chemistry*, *124*, 198-202.
36. Bosela, A. A., Salamah, K. K., Alsarra, I. A., & El-Bagory, I. M. (2010). Reactivity of prednisolone to gamma radiation in aqueous and organic solutions. *Journal of Drug Delivery Science and Technology*, *20*, 225-229.
37. Bredhult, C., Bäcklin, B. M., & Olovsson, M. (2007). Effects of some endocrine disruptors on the proliferation and viability of human endometrial endothelial cells in vitro. *Reproductive Toxicology*, *23*, 550-559.
38. Brites-Nóbrega, F. F., Lacerda, I. A., Santos, S. V., Amorim, C. C., Santana, V. S., Fernandes-Machado, N. R., Ardisson, J. D., Henriques, A. B., & Leão, M. M. (2015). Synthesis and characterization of new NaX zeolite-supported Nb, Zn, and Fe photocatalysts activated by visible radiation for application in wastewater treatment. *Catalysis Today*, *240*, 168-175.
39. Bu, Q., Wang, B., Huang, J., Deng, S., & Yu, G. (2013). Pharmaceuticals and personal care products in the aquatic environment in China: a review. *Journal of Hazardous Materials*, *262*, 189-211.
40. Buffle, M. O., Schumacher, J., Salhi, E., Jekel, M., & Von Gunten, U. (2006). Measurement of the initial phase of ozone decomposition in water and wastewater by means of a continuous quench-flow system: application to disinfection and pharmaceutical oxidation. *Water Research*, *40*, 1884-1894.
41. Bui, X. T., Vo, T. P. T., Ngo, H. H., Guo, W. S., & Nguyen, T. T. (2016). Multicriteria assessment of advanced treatment technologies for micropollutants removal at large-scale applications. *Science of the Total Environment*, *563*, 1050-1067.
42. Buxton, G. V., Greenstock, C. L., Helman, W. P., & Ross, A. B. (1988). Critical review of rate constants for reactions of hydrated electrons, hydrogen atoms and hydroxyl radicals ($\cdot OH/\cdot O^-$) in aqueous solution. *Journal of Physical and Chemical Reference Data*, *17*, 513-886.

43. Calza, P., Medana, C., Carbone, F., Giancotti, V., & Baiocchi, C. (2008). Characterization of intermediate compounds formed upon photoinduced degradation of quinolones by high-performance liquid chromatography/high-resolution multiple-stage mass spectrometry. *Rapid Communications in Mass Spectrometry: An International Journal Devoted to the Rapid Dissemination of Up-to-the-Minute Research in Mass Spectrometry*, *22*, 1533-1552.
44. Cantwell, R. E., & Hofmann, R. (2011). Ultraviolet absorption properties of suspended particulate matter in untreated surface waters. *Water Research*, *45*, 1322-1328.
45. Capodaglio, A. G. (2018). Could EB irradiation be the simplest solution for removing emerging contaminants from water and wastewater? *Water Practice and Technology*, *13*, 172-183.
46. Carbajo, J. B., Petre, A. L., Rosal, R., Herrera, S., Letón, P., García-Calvo, E., Fernández-Alba, A. R., & Perdigón-Melón, J. A. (2015). Continuous ozonation treatment of ofloxacin: transformation products, water matrix effect and aquatic toxicity. *Journal of Hazardous Materials*, *292*, 34-43.
47. Carballa, M., Omil, F., Lema, J. M., Llompart, M., García-Jares, C., Rodríguez, I., Gómez, M., & Ternes, T. (2004). Behavior of pharmaceuticals, cosmetics and hormones in a sewage treatment plant. *Water Research*, *38*, 2918-2926.
48. Cavalcante, R. P., da Rocha Sandim, L., Bogo, D., Barbosa, A. M. J., Osugi, M. E., Blanco, M., Cesar de Oliveira, S., Matos, M. F. C., Machulek Jr., A., & Ferreira, V. S. (2013). Application of Fenton, photo-Fenton, solar photo-Fenton, and UV/H_2O_2 to degradation of the antineoplastic agent mitoxantrone and toxicological evaluation. *Environmental Science and Pollution Research*, *20*, 2352-2361.
49. Celiz, M. D., Pérez, S., Barceló, D., & Aga, D. S. (2009). Trace analysis of polar pharmaceuticals in wastewater by LC-MS-MS: Comparison of membrane bioreactor and activated sludge systems. *Journal of Chromatographic Science*, *47*, 19-25.
50. Celle-Jeanton, H., Schemberg, D., Mohammed, N., Huneau, F., Bertrand, G., Lavastre, V., & Le Coustumer, P. (2014). Evaluation of pharmaceuticals in surface water: Reliability of PECs compared to MECs. *Environment International*, *73*, 10-21.
51. Chan, J. Y. T., Ang, S. Y., Ye, E. Y., Sullivan, M., Zhang, J., & Lin, M. (2015). Heterogeneous photo-Fenton reaction on hematite (α-Fe_2O_3){104},{113} and {001} surface facets. *Physical Chemistry Chemical Physics*, *17*, 25333-25341.

52. Chatzitakis, A., Berberidou, C., Paspaltsis, I., Kyriakou, G., Sklaviadis, T., & Poulios, I. (2008). Photocatalytic degradation and drug activity reduction of chloramphenicol. *Water Research*, *42*, 386-394.
53. Che, H., Bae, S., & Lee, W. (2011). Degradation of trichloroethylene by Fenton reaction in pyrite suspension. *Journal of Hazardous Materials*, *185*, 1355-1361.
54. Chen, J. H., Jang, C., Adam, S., Fuhrer, M. S., Williams, E. D., & Ishigami, M. (2008). Charged-impurity scattering in graphene. *Nature Physics*, *4*, 377.
55. Chen, Y., Hu, X., Evanko, B., Sun, X., Li, X., Hou, T., Cai, S., Zheng, C., Hu, W., & Stucky, G. D. (2018). High-rate FeS_2/CNT neural network nanostructure composite anodes for stable, high-capacity sodium-ion batteries. *Nano Energy*, *46*, 117-127.
56. Che, H., & Lee, W. (2011). Selective redox degradation of chlorinated aliphatic compounds by Fenton reaction in pyrite suspension. *Chemosphere, 82,* 1103-1108.
57. Chen, Y., Yao, J., Wang, F., Zhou, Y., Chen, H., Gai, N., Chen, H., Maskow, T., Ceccanti, B., Trebse, P., & Zaray, G. (2008). Toxic effect of inorganic arsenite [As (III)] on metabolic activity of Bacillus subtilis by combined methods. *Current Microbiology*, *57*, 258-263.
58. Chmielewski, A. G. (2011). Electron accelerators for environmental protection. *Reviews of Accelerator Science and Technology, 4*, 147-159.
59. Cho, J. Y. (2010). Evaluation of degradation of antibiotic tetracycline in pig manure by electron beam irradiation. *Bulletin of Environmental Contamination and Toxicology*, *84*, 450-453.
60. Cho, J. Y., Chung, B. Y., & Hwang, S. A. (2015). Detoxification of the veterinary antibiotic chloramphenicol using electron beam irradiation. *Environmental Science and Pollution Research*, *22*, 9637-9645.
61. Chong, M. N., Jin, B., Chow, C. W., & Saint, C. (2010). Recent developments in photocatalytic water treatment technology: a review. *Water Research*, *44*, 2997-3027.
62. Chu, L., & Wang, J. (2016). Degradation of 3-chloro-4-hydroxybenzoic acid in biological treated effluent by gamma irradiation. *Radiation Physics and Chemistry*, *119*, 194-199.
63. Chu, L., Wang, J., & Liu, Y. (2015). Degradation of sulfamethazine in sewage sludge mixture by gamma irradiation. *Radiation Physics and Chemistry*, *108*, 102-105.
64. Chu, L., Yu, S., & Wang, J. (2016). Gamma radiolytic degradation of naphthalene in aqueous solution. *Radiation Physics and Chemistry*, *123*, 97-102.

65. Clara, M., Strenn, B., Gans, O., Martinez, E., Kreuzinger, N., & Kroiss, H. (2005). Removal of selected pharmaceuticals, fragrances and endocrine disrupting compounds in a membrane bioreactor and conventional wastewater treatment plants. *Water Research*, *39*, 4797-4807.
66. Cokgor, E. U., Alaton, I. A., Karahan, O., Dogruel, S., & Orhon, D. (2004). Biological treatability of raw and ozonated penicillin formulation effluent. *Journal of Hazardous Materials*, *116*, 159-166.
67. Coleman, H. M., Vimonses, V., Leslie, G., & Amal, R. (2007). Removal of contaminants of concern in water using advanced oxidation techniques. *Water Science and Technology*, *55*, 301-306.
68. Comninellis, C., Kapalka, A., Malato, S., Parsons, S. A., Poulios, I., & Mantzavinos, D. (2008). Advanced oxidation processes for water treatment: advances and trends for R&D. *Journal of Chemical Technology & Biotechnology: International Research in Process, Environmental & Clean Technology*, *83*, 769-776.
69. Cooper, W. J., Nickelsen, M. G., Mezyk, S. P., Leslie, G., Tornatore, P. M., Hardison, W., & Hajali, P. A. (2002). MTBE and priority contaminant treatment with high energy electron beam injection. *Radiation Physics and Chemistry*, *65*, 451-460.
70. Cornell, R. M., & Schwertmann, U. (2003). *The iron oxides: structure, properties, reactions, occurrences and uses*. John Wiley & Sons.
71. CPCB. 2005. Parivesh Sewage Pollution – News Letter. Central Pollution Control Board, Ministry of Environment and Forests, Govt. of India, Parivesh Bhawan, East Arjun Nagar, Delhi 110 032.
72. CPCB. 2007. Advance methods for treatment of textile industry effluents, Resource Recycling Series: RERES/&/2007. Central Pollution Control Board, India.
73. Csay, T., Rácz, G., Salik, Á., Takács, E., & Wojnárovits, L. (2014). Reactions of clofibric acid with oxidative and reductive radicals—Products, mechanisms, efficiency and toxic effects. *Radiation Physics and Chemistry*, *102*, 72-78.
74. CWC. 2010. Water and related statistics. Water Planning and Project Wing, Central Water Commission, India.
75. Dalrymple, O. K., Yeh, D. H., & Trotz, M. A. (2007). Removing pharmaceuticals and endocrine-disrupting compounds from wastewater by photocatalysis. *Journal of Chemical Technology & Biotechnology: International Research in Process, Environmental & Clean Technology*, *82*, 121-134.

76. Dantas, R. F., Contreras, S., Sans, C., & Esplugas, S. (2008). Sulfamethoxazole abatement by means of ozonation. *Journal of Hazardous Materials*, *150*, 790-794.
77. Daud, N. K., & Hameed, B. H. (2010). Decolorization of Acid Red 1 by Fenton-like process using rice husk ash-based catalyst. *Journal of Hazardous Materials*, *176*, 938-944.
78. Daughton, C. G. (2001). Emerging pollutants, and communicating the science of environmental chemistry and mass spectrometry: pharmaceuticals in the environment. *Journal of the American Society for Mass Spectrometry*, *12*, 1067-1076.
79. Daughton, C. G., & Ternes, T. A. (1999). Pharmaceuticals and personal care products in the environment: agents of subtle change? *Environmental Health Perspectives*, *107*, 907-938.
80. De la Cruz, N., Giménez, J., Esplugas, S., Grandjean, D., De Alencastro, L. F., & Pulgarin, C. (2012). Degradation of 32 emergent contaminants by UV and neutral photo-Fenton in domestic wastewater effluent previously treated by activated sludge. *Water Research*, *46*, 1947-1957.
81. de la Plata, G. B. O., Alfano, O. M., & Cassano, A. E. (2010). Decomposition of 2-chlorophenol employing goethite as Fenton catalyst. I. Proposal of a feasible, combined reaction scheme of heterogeneous and homogeneous reactions. *Applied Catalysis B: Environmental*, *95*, 1-13.
82. De Laat, J., & Le, T. G. (2006). Effects of chloride ions on the iron (III)-catalyzed decomposition of hydrogen peroxide and on the efficiency of the Fenton-like oxidation process. *Applied Catalysis B: Environmental*, *66*, 137-146.
83. De Luca, A., Dantas, R. F., Simões, A. S., Toscano, I. S., Lofrano, G., Cruz, A., & Esplugas, S. (2013). Atrazine Removal in Municipal Secondary Effluents by Fenton and Photo-Fenton Treatments. *Chemical Engineering & Technology*, *36*, 2155-2162.
84. de Souza Santos, L. V., Meireles, A. M., & Lange, L. C. (2015). Degradation of antibiotics norfloxacin by Fenton, UV and UV/H_2O_2. *Journal of Environmental Management*, *154*, 8-12.
85. De witte, B., Dewulf, J., Demeestere, K., Van De Vyvere, V., De Wispelaere, P., & Van Langenhove, H. (2008). Ozonation of ciprofloxacin in water: HRMS identification of reaction products and pathways. *Environmental Science & Technology*, *42*, 4889-4895.
86. De Witte, B., Van Langenhove, H., Hemelsoet, K., Demeestere, K., De Wispelaere, P., Van Speybroeck, V., & Dewulf, J. (2009). Levofloxacin ozonation in water: rate

determining process parameters and reaction pathway elucidation. *Chemosphere*, *76*, 683-689.

87. Deegan, A. M., Shaik, B., Nolan, K., Urell, K., Oelgemöller, M., Tobin, J., & Morrissey, A. (2011). Treatment options for wastewater effluents from pharmaceutical companies. *International Journal of Environmental Science & Technology*, *8*, 649-666.
88. Demarchis, L., Minella, M., Nisticò, R., Maurino, V., Minero, C., & Vione, D. (2015). Photo–Fenton reaction in the presence of morphologically controlled hematite as iron source. *Journal of Photochemistry and Photobiology A: Chemistry*, *307*, 99-107.
89. Diffey, B. L. (1991). Solar ultraviolet radiation effects on biological systems. *Physics in Medicine & Biology*, *36*, 299.
90. Dimitrakopoulou, D., Rethemiotaki, I., Frontistis, Z., Xekoukoulotakis, N. P., Venieri, D., & Mantzavinos, D. (2012). Degradation, mineralization and antibiotic inactivation of amoxicillin by UV-A/TiO_2 photocatalysis. *Journal of Environmental Management*, *98*, 168-174.
91. Dinh, Q. T., Alliot, F., Moreau-Guigon, E., Eurin, J., Chevreuil, M., & Labadie, P. (2011). Measurement of trace levels of antibiotics in river water using on-line enrichment and triple-quadrupole LC–MS/MS. *Talanta*, *85*, 1238-1245.
92. Doll, T. E., & Frimmel, F. H. (2003). Fate of pharmaceuticals—photodegradation by simulated solar UV-light. *Chemosphere*, *52*, 1757-1769.
93. Dong, S., Feng, J., Fan, M., Pi, Y., Hu, L., Han, X., Liu, M., Su, J., & Sun, J. (2015). Recent developments in heterogeneous photocatalytic water treatment using visible light-responsive photocatalysts: a review. *RSC Advances*, *5*, 14610-14630.
94. Du, J., Bao, J., Fu, X., Lu, C., & Kim, S. H. (2016). Mesoporous sulfur-modified iron oxide as an effective Fenton-like catalyst for degradation of bisphenol A. *Applied Catalysis B: Environmental*, *184*, 132-141.
95. Duarte, C. L., Sampa, M. H. O., Rela, P. R., Oikawa, H., Silveira, C. G., & Azevedo, A. L. (2002). Advanced oxidation process by electron-beam-irradiation-induced decomposition of pollutants in industrial effluents. *Radiation Physics and Chemistry*, *63*, 647-651.
96. el mehdi Benacherine, M., Debbache, N., Ghoul, I., & Mameri, Y. (2017). Heterogeneous photoinduced degradation of amoxicillin by goethite under artificial and natural irradiation. *Journal of photochemistry and photobiology A: Chemistry*, *335*, 70-77.

97. Elmolla, E. S., & Chaudhuri, M. (2010). Degradation of amoxicillin, ampicillin and cloxacillin antibiotics in aqueous solution by the UV/ZnO photocatalytic process. *Journal of Hazardous Materials*, *173*, 445-449.
98. Emmi, S. S., De Paoli, G., Caminati, S., Takacs, E., & Pálfi, T. (2008). *The E beam induced decomposition of pesticides in water: A gamma and pulse radiolysis investigation on carbofuran* (No. IAEA-TECDOC--1598).
99. Faust, B. C., & Hoigné, J. (1990). Photolysis of Fe (III)-hydroxy complexes as sources of OH radicals in clouds, fog and rain. *Atmospheric Environment. Part A. General Topics*, *24*, 79-89.
100. Fewson, C. A. (1988). Biodegradation of xenobiotic and other persistent compounds: the causes of recalcitrance. *Trends in Biotechnology*, *6*, 148-153.
101. Fick, J., Söderström, H., Lindberg, R. H., Phan, C., Tysklind, M., & Larsson, D. J. (2009). Contamination of surface, ground, and drinking water from pharmaceutical production. *Environmental Toxicology and Chemistry*, *28*, 2522-2527.
102. Finlayson-Pitts, B. J., & Pitts Jr, J. N. (1999). *Chemistry of the upper and lower atmosphere: theory, experiments, and applications*. Academic. US.
103. Frisch, M. J., Trucks, G. W., & Schlegel, H. B. (2003). Gaussian 03, Gaussian. *Inc., Pittsburgh, PA*.
104. Gadipelly, C., Pérez-González, A., Yadav, G. D., Ortiz, I., Ibáñez, R., Rathod, V. K., & Marathe, K. V. (2014). Pharmaceutical industry wastewater: review of the technologies for water treatment and reuse. *Industrial & Engineering Chemistry Research*, *53*, 11571-11592.
105. Garg, K. K., & Prasad, B. (2016). Treatment of multicomponent aqueous solution of purified terephthalic acid wastewater by electrocoagulation process: optimization of process and analysis of sludge. *Journal of the Taiwan Institute of Chemical Engineers*, *60*, 383-393.
106. Getoff, N. (1995). Radiation-induced degradation of water pollutants: state of the art. *Radiation Physics and Chemistry*, *46*, 1079.
107. Ghafoori, S., Mowla, A., Jahani, R., Mehrvar, M., & Chan, P. K. (2015). Sonophotolytic degradation of synthetic pharmaceutical wastewater: Statistical experimental design and modeling. *Journal of Environmental Management*, *150*, 128-137.

108. Gogate, P. R., & Pandit, A. B. (2004). A review of imperative technologies for wastewater treatment I: oxidation technologies at ambient conditions. *Advances in Environmental Research*, *8*, 501-551.
109. Golsheikh, A. M., Huang, N. M., Lim, H. N., Chia, C. H., Harrison, I., & Muhamad, M. R. (2013). One-pot hydrothermal synthesis and characterization of FeS_2 (pyrite)/graphene nanocomposite. *Chemical Engineering Journal*, *218*, 276-284.
110. González, O., Sans, C., & Esplugas, S. (2007). Sulfamethoxazole abatement by photo-Fenton: toxicity, inhibition and biodegradability assessment of intermediates. *Journal of Hazardous Materials*, *146*, 459-464.
111. Gothwal, R., & Shashidhar. (2017). Occurrence of high levels of fluoroquinolones in aquatic environment due to effluent discharges from bulk drug manufacturers. *Journal of Hazardous, Toxic, and Radioactive Waste*, *21*, 05016003.
112. Gros, M., Blum, K. M., Jernstedt, H., Renman, G., Rodríguez-Mozaz, S., Haglund, P., Andersson, P. L. & Ahrens, L. (2017). Screening and prioritization of micropollutants in wastewaters from on-site sewage treatment facilities. *Journal of Hazardous Materials*, *328*, 37-45.
113. Guimarães, B. D. S., Kleemann, N., Caldas, S. S., Costa, F. P., Silveira, M. A., Duarte, F. A., & Primel, E. G. (2014). Environmentally friendly system for the degradation of multipesticide residues in aqueous media by the Fenton's reaction. *Environmental Science and Pollution Research*, *21*, 584-592.
114. Guimaraes, I. R., Giroto, A., Oliveira, L. C., Guerreiro, M. C., Lima, D. Q., & Fabris, J. D. (2009). Synthesis and thermal treatment of cu-doped goethite: oxidation of quinoline through heterogeneous Fenton process. *Applied Catalysis B: Environmental*, *91*, 581-586.
115. Guin, J. P., Bhardwaj, Y. K., & Varshney, L. (2017). Efficient degradation of butylparaben by gamma radiolysis. *Applied Radiation and Isotopes*, *122*, 21-27.
116. Guin, J. P., Naik, D. B., Bhardwaj, Y. K., & Varshney, L. (2014). An insight into the effective advanced oxidation process for treatment of simulated textile dye waste water. *RSC Advances*, *4*, 39941-39947.
117. Guo, Z., Dong, Q., He, D., & Zhang, C. (2012a). Gamma radiation for treatment of bisphenol A solution in presence of different additives. *Chemical Engineering Journal*, *183*, 10-14.

118. Guo, Z., Zhou, F., Zhao, Y., Zhang, C., Liu, F., Bao, C., & Lin, M. (2012). Gamma irradiation-induced sulfadiazine degradation and its removal mechanisms. *Chemical Engineering Journal*, *191*, 256-262.
119. Guo, Z., Zhu, S., Zhao, Y., Cao, H., & Liu, F. (2015). Radiolytic decomposition of ciprofloxacin using γ irradiation in aqueous solution. *Environmental Science and Pollution Research*, *22*, 15772-15780.
120. Gupta, V. K., Sharma, M., & Vyas, R. K. (2015). Hydrothermal modification and characterization of bentonite for reactive adsorption of methylene blue: an ESI-MS study. *Journal of Environmental Chemical Engineering*, *3*, 2172-2179.
121. Halling-Sørensen, B., Nielsen, S. N., Lanzky, P. F., Ingerslev, F., Lützhøft, H. H., & Jørgensen, S. (1998). Occurrence, fate and effects of pharmaceutical substances in the environment-A review. *Chemosphere*, *36*, 357-393.
122. Han, B., Kim, J. K., & Kim, Y. R. (2008). Disinfection of effluent from municipal wastewater plant with electron beam. *Rad. Treat. Pollut. Water Wastewater (IEA-TECDOC-1598)*, 109-114.
123. Han, B., Kim, J. K., Kim, Y., Choi, J. S., & Jeong, K. Y. (2012). Operation of industrial-scale electron beam wastewater treatment plant. *Radiation Physics and Chemistry*, *81*, 1475-1478.
124. Hapeshi, E., Achilleos, A., Vasquez, M. I., Michael, C., Xekoukoulotakis, N. P., Mantzavinos, D., & Kassinos, D. (2010). Drugs degrading photocatalytically: kinetics and mechanisms of ofloxacin and atenolol removal on titania suspensions. *Water Research*, *44*, 1737-1746.
125. Hapeshi, E., Fotiou, I., & Fatta-Kassinos, D. (2013). Sonophotocatalytic treatment of ofloxacin in secondary treated effluent and elucidation of its transformation products. *Chemical Engineering Journal*, *224*, 96-105.
126. Hartmann, J., Bartels, P., Mau, U., Witter, M., Tümpling, W. V., Hofmann, J., & Nietzschmann, E. (2008). Degradation of the drug diclofenac in water by sonolysis in presence of catalysts. *Chemosphere*, *70*, 453-461.
127. Hassanzadeh-Khayyat, M., Lai, E. P., Kollu, K., & Ormeci, B. (2011). Degradation of diclofenac in molecularly imprinted polymer submicron particles by UV light irradiation and HCl acid treatment. *Journal of Water Resource and Protection*, *3*, 643.
128. He, S., Sun, W., Wang, J., Chen, L., Zhang, Y., & Yu, J. (2016). Enhancement of biodegradability of real textile and dyeing wastewater by electron beam irradiation. *Radiation Physics and Chemistry*, *124*, 203-207.

129. He, S., Wang, J., Ye, L., Zhang, Y., & Yu, J. (2014). Removal of diclofenac from surface water by electron beam irradiation combined with a biological aerated filter. *Radiation Physics and Chemistry*, *105*, 104-108.
130. Heberer, T. (2002). Occurrence, fate, and removal of pharmaceutical residues in the aquatic environment: a review of recent research data. *Toxicology letters*, *131*, 5-17.
131. Heberer, T. (2002a). Tracking persistent pharmaceutical residues from municipal sewage to drinking water. *Journal of Hydrology*, *266*, 175-189.
132. Hedgespeth, M. L., Sapozhnikova, Y., Pennington, P., Clum, A., Fairey, A., & Wirth, E. (2012). Pharmaceuticals and personal care products (PPCPs) in treated wastewater discharges into Charleston Harbor, South Carolina. *Science of the Total Environment*, *437*, 1-9.
133. Hirose, J., Kondo, F., Nakano, T., Kobayashi, T., Hiro, N., Ando, Y., Takenaka, H. & Sano, K. (2005). Inactivation of antineoplastics in clinical wastewater by electrolysis. *Chemosphere*, *60*, 1018-1024.
134. Homem, V., & Santos, L. (2011). Degradation and removal methods of antibiotics from aqueous matrices–a review. *Journal of Environmental Management*, *92*, 2304-2347.
135. Horovitz, I., Avisar, D., Baker, M. A., Grilli, R., Lozzi, L., Di Camillo, D., & Mamane, H. (2016). Carbamazepine degradation using a N-doped TiO_2 coated photocatalytic membrane reactor: Influence of physical parameters. *Journal of Hazardous Materials*, *310*, 98-107.
136. Hu, J., & Wang, J. (2007). Degradation of chlorophenols in aqueous solution by γ-radiation. *Radiation Physics and Chemistry*, *76*, 1489-1492.
137. Hua, W., Bennett, E. R., & Letcher, R. J. (2006). Ozone treatment and the depletion of detectable pharmaceuticals and atrazine herbicide in drinking water sourced from the upper Detroit River, Ontario, Canada. *Water Research*, *40*, 2259-2266.
138. Huang, D., Wang, Z., Zhang, J., Feng, J., Zheng, Z., & Zhang, J. (2016). Gamma radiolytic degradation of 3, 4-dichloroaniline in aqueous solution. *Separation and Purification Technology*, *170*, 264-271.
139. Huang, W., Brigante, M., Wu, F., Hanna, K., & Mailhot, G. (2013). Effect of ethylenediamine-N, N′-disuccinic acid on Fenton and photo-Fenton processes using goethite as an iron source: optimization of parameters for bisphenol A degradation. *Environmental Science and Pollution Research*, *20*, 39-50.

140. Huber, M. M., Canonica, S., Park, G. Y., & Von Gunten, U. (2003). Oxidation of pharmaceuticals during ozonation and advanced oxidation processes. *Environmental Science & Technology*, *37*, 1016-1024.
141. Huie, R. E., Clifton, C. L., & Neta, P. (1991). Electron transfer reaction rates and equilibria of the carbonate and sulfate radical anions. *International Journal of Radiation Applications and Instrumentation. Part C. Radiation Physics and Chemistry*, *38*, 477-481.
142. IAEA Scientific Report. (2007). Radiation Processing: Environmental Applications, ISBN 92-0-100507-5, International Atomic Energy Agency, Vienna.
143. IAEA. (2008). Radiation Treatment of Polluted Water and Wastewater. International Atomic Energy Agency, Industrial Application in Chemistry Section, Report IAEA-TECDOC-1598, IAEA, Vienna.
144. Ikehata, K., Jodeiri Naghashkar, N., & Gamal El-Din, M. (2006). Degradation of aqueous pharmaceuticals by ozonation and advanced oxidation processes: a review. *Ozone: Science and Engineering*, *28*, 353-414.
145. Illés, E., Takács, E., Dombi, A., Gajda-Schrantz, K., Gonter, K., & Wojnárovits, L. (2012). Radiation induced degradation of ketoprofen in dilute aqueous solution. *Radiation Physics and Chemistry*, *81*, 1479-1483.
146. Illés, E., Takács, E., Dombi, A., Gajda-Schrantz, K., Rácz, G., Gonter, K., & Wojnárovits, L. (2013). Hydroxyl radical induced degradation of ibuprofen. *Science of the Total Environment*, *447*, 286-292.
147. Iqbal, M., & Bhatti, I. A. (2015). Gamma radiation/H_2O_2 treatment of a nonylphenol ethoxylates: degradation, cytotoxicity, and mutagenicity evaluation. *Journal of Hazardous Materials*, *299*, 351-360.
148. Iqbal, M., Abbas, M., Arshad, M., Hussain, T., Ullah Khan, A., Masood, N., Tahir, M. A., Makhdoom Hussain, S., Hussain Bokhari, T., & Ahmad Khera, R. (2015). Short Communication Gamma Radiation Treatment for Reducing Cytotoxicity and Mutagenicity in Industrial Wastewater. *Polish Journal of Environmental Studies*, *24*, 2745–2750.
149. Irmak, S., Erbatur, O., & Akgerman, A. (2005). Degradation of 17β-estradiol and bisphenol A in aqueous medium by using ozone and ozone/UV techniques. *Journal of Hazardous Materials*, *126*, 54-62.

150. Ishibashi, K. I., Fujishima, A., Watanabe, T., & Hashimoto, K. (2000). Detection of active oxidative species in TiO_2 photocatalysis using the fluorescence technique. *Electrochemistry Communications*, *2*, 207-210.

151. Iyanee, F. S., Simamura, K., Prabhasankar, V. P., Taniyasu, S., Tsuruta, M., Balakrishna, K., Yamashita, N., Guruje, K. S., Akiba, M., Jishua, D. I., & Kannan, K. (2013). Occurrence of antibiotics in river water: A case study of Vrishabhavathi River near Bangalore, India. In *33rd International Symposium on Halogenated Persistent Organic Pollutants* (pp. 25-30).

152. Jagadevan, S., Dobson, P., & Thompson, I. P. (2011). Harmonisation of chemical and biological process in development of a hybrid technology for treatment of recalcitrant metalworking fluid. *Bioresource Technology*, *102*, 8783-8789.

153. Jamil, T. S., Ghaly, M. Y., El-Seesy, I. E., Souaya, E. R., & Nasr, R. A. (2011). A comparative study among different photochemical oxidation processes to enhance the biodegradability of paper mill wastewater. *Journal of Hazardous Materials*, *185*, 353-358.

154. Jia, W., He, Y., Ling, Y., Hei, D., Shan, Q., Zhang, Y., & Li, J. (2015). Radiation-induced degradation of cyclohexanebutyric acid in aqueous solutions by gamma ray irradiation. *Radiation Physics and Chemistry*, *109*, 17-22.

155. Jin, L., & Bai, R. (2002). Mechanisms of lead adsorption on chitosan/PVA hydrogel beads. *Langmuir*, *18*, 9765-9770.

156. Jones, O. A. H., Voulvoulis, N., & Lester, J. N. (2003). Analytical method development for the simultaneous determination of five human pharmaceuticals in water and wastewater samples by gas chromatography-mass spectrometry. *Chromatographia*, *58*, 471-477.

157. Jones, O. A., Lester, J. N., & Voulvoulis, N. (2005). Pharmaceuticals: a threat to drinking water?. *TRENDS in Biotechnology*, *23*, 163-167.

158. Joss, A., Keller, E., Alder, A. C., Göbel, A., McArdell, C. S., Ternes, T., & Siegrist, H. (2005). Removal of pharmaceuticals and fragrances in biological wastewater treatment. *Water Research*, *39*, 3139-3152.

159. Jung, Y. J., Kim, W. G., Yoon, Y., Kang, J. W., Hong, Y. M., & Kim, H. W. (2012). Removal of amoxicillin by UV and UV/H_2O_2 processes. *Science of the Total Environment*, *420*, 160-167.

160. Kajitvichyanukul, P., & Suntronvipart, N. (2006). Evaluation of biodegradability and oxidation degree of hospital wastewater using photo-Fenton process as the pretreatment method. *Journal of Hazardous Materials*, *138*, 384-391.
161. Kanakaraju, D., Glass, B. D., & Oelgemöller, M. (2018). Advanced oxidation process-mediated removal of pharmaceuticals from water: A review. *Journal of Environmental Management*, *219*, 189-207.
162. Kanakaraju, D., Ravichandar, S., & Lim, Y. C. (2017). Combined effects of adsorption and photocatalysis by hybrid TiO_2/ZnO-calcium alginate beads for the removal of copper. *Journal of Environmental Sciences*, *55*, 214-223.
163. Kang, S. F., Liao, C. H., & Chen, M. C. (2002). Pre-oxidation and coagulation of textile wastewater by the Fenton process. *Chemosphere*, *46*, 923-928.
164. Kang, Y. W., Cho, M. J., & Hwang, K. Y. (1999). Correction of hydrogen peroxide interference on standard chemical oxygen demand test. *Water Research*, *33*, 1247-1251.
165. Karl, W., Schneider, J., & Wetzstein, H. G. (2006). Outlines of an "exploding" network of metabolites generated from the fluoroquinolone enrofloxacin by the brown rot fungus Gloeophyllum striatum. *Applied Microbiology and Biotechnology*, *71*, 101.
166. Karthikeyan, S., Titus, A., Gnanamani, A., Mandal, A. B., & Sekaran, G. (2011). Treatment of textile wastewater by homogeneous and heterogeneous Fenton oxidation processes. *Desalination*, *281*, 438-445.
167. Katsumata, H., Kaneco, S., Suzuki, T., Ohta, K., & Yobiko, Y. (2005). Degradation of linuron in aqueous solution by the photo-Fenton reaction. *Chemical Engineering Journal*, *108*, 269-276.
168. Kaur, R., Dhir, G., Laishram, G., Ningthoujam, D., Kumar, P. (2012) Nutrient and trace metal removal efficiency of small scale (batch fed) vertical flow municipal wastewater treatment wetlands, 4th International Eco-Summit on "Ecological Sustainability-Restoring the Planets Ecosystem Services", Ohio, USA.
169. Kavitha, V., & Palanivelu, K. (2004). The role of ferrous ion in Fenton and photo-Fenton processes for the degradation of phenol. *Chemosphere*, *55*, 1235-1243.
170. Kessler, R. (2010). INDUSTRY ISSUES: pharmaceutical factories as a source of drugs in water. *Environmental Health Perspectives*, *118*, A383.
171. Khan, J. A., Shah, N. S., Nawaz, S., Ismail, M., Rehman, F., & Khan, H. M. (2015). Role of e_{aq}^-, $OH^\cdot$ and $H^\cdot$ in radiolytic degradation of atrazine: A kinetic and mechanistic approach. *Journal of Hazardous Materials*, *288*, 147-157.

172. Khataee, A., Gholami, P., & Vahid, B. (2016). Heterogeneous sono-Fenton-like process using nanostructured pyrite prepared by Ar glow discharge plasma for treatment of a textile dye. *Ultrasonics Sonochemistry*, *29*, 213-225.
173. Khattab, F. I., Ramadan, N. K., Hegazy, M. A., & Ghoniem, N. S. (2012). Stability-indicating methods for the determination of ornidazole in the presence of its degradate according to ICH guidelines. *Pharmaceut Anal Acta*, *3*, 1-8.
174. Khetan, S. K., & Collins, T. J. (2007). Human pharmaceuticals in the aquatic environment: a challenge to green chemistry. *Chemical Reviews*, *107*, 2319-2364.
175. Kıdak, R., & Doğan, Ş. (2018). Medium-high frequency ultrasound and ozone based advanced oxidation for amoxicillin removal in water. *Ultrasonics Sonochemistry*, *40*, 131-139.
176. Kidd, K. A., Blanchfield, P. J., Mills, K. H., Palace, V. P., Evans, R. E., Lazorchak, J. M., & Flick, R. W. (2007). Collapse of a fish population after exposure to a synthetic estrogen. *Proceedings of the National Academy of Sciences*, *104*, 8897-8901.
177. Kim, H. Y., Kim, T. H., Cha, S. M., & Yu, S. (2017). Degradation of sulfamethoxazole by ionizing radiation: Identification and characterization of radiolytic products. *Chemical Engineering Journal*, *313*, 556-566.
178. Kim, H. Y., Lee, O. M., Kim, T. H., & Yu, S. (2015). Enhanced biodegradability of pharmaceuticals and personal care products by ionizing radiation. *Water Environment Research*, *87*, 321-325.
179. Kimura, A., Osawa, M., & Taguchi, M. (2012). Decomposition of persistent pharmaceuticals in wastewater by ionizing radiation. *Radiation Physics and Chemistry*, *81*, 1508-1512.
180. Kitajima, N., Fukuzumi, S., & Ono, Y. (1978). Formation of superoxide ion during the decomposition of hydrogen peroxide on supported metal oxides. *The Journal of Physical Chemistry*, *82*, 1505-1509.
181. Klamerth, N., Rizzo, L., Malato, S., Maldonado, M. I., Agüera, A., Fern_andez-Alba, A. R. (2010). Degradation of fifteen emerging contaminants at mg L^{-1} initial concentrations by mild solar photo-Fenton in MWTP effluents. *Water Research, 44*, 545-554.
182. Klavarioti, M., Mantzavinos, D., & Kassinos, D. (2009). Removal of residual pharmaceuticals from aqueous systems by advanced oxidation processes. *Environment International*, *35*, 402-417.

183. Kockler, J., Kanakaraju, D., Glass, B., & Oelgemöller, M. (2012). Photochemical and photocatalytic degradation of diclofenac and amoxicillin using natural and simulated sunlight. *Journal of Sustainability Science and Management*, *7*, 23-29.

184. Kolpin, D. W., Furlong, E. T., Meyer, M. T., Thurman, E. M., Zaugg, S. D., Barber, L. B., & Buxton, H. T. (2002). Pharmaceuticals, hormones, and other organic wastewater contaminants in US streams, 1999− 2000: A national reconnaissance. *Environmental Science & Technology*, *36*, 1202-1211.

185. Kormann, C., Bahnemann, D. W., & Hoffmann, M. R. (1991). Photolysis of chloroform and other organic molecules in aqueous titanium dioxide suspensions. *Environmental Science & Technology*, *25*, 494-500.

186. Kovács, K., He, S., Mile, V., Csay, T., Takács, E., & Wojnárovits, L. (2015a). Ionizing radiation induced degradation of diuron in dilute aqueous solution. *Chemistry Central Journal*, *9*, 21.

187. Kovács, K., He, S., Míle, V., Földes, T., Pápai, I., Takács, E., & Wojnárovits, L. (2016). Ionizing radiation induced degradation of monuron in dilute aqueous solution. *Radiation Physics and Chemistry*, *124*, 191-197.

188. KPMG International., 2006. The Indian Pharmaceutical Industry: Collaboration for Growth. 2-42.

189. Kristiansson, E., Fick, J., Janzon, A., Grabic, R., Rutgersson, C., Weijdegård, B., Söderström, H., & Larsson, D. J. (2011). Pyrosequencing of antibiotic-contaminated river sediments reveals high levels of resistance and gene transfer elements. *PloS one*, *6*, e17038.

190. Kuk, S. H., Kim, S. M., Kang, W. G., Han, B., Kuksanov, N. K. & Jeong, K. Y. (2011). High-power accelerator for environmental applications. *Journal of the Korean Physical Society, 59*, 3485-3488.

191. Kulik, N., Trapido, M., Goi, A., Veressinina, Y., & Munter, R. (2008). Combined chemical treatment of pharmaceutical effluents from medical ointment production. *Chemosphere*, *70*, 1525-1531.

192. Kumar, R. M. (2003). Financing of wastewater Treatment Projects. Infrastructure Development Finance Corporation and Confederation of Indian Industries. Water Summit, Hyderabad.

193. Kümmerer, K. (2001). Drugs in the environment: emission of drugs, diagnostic aids and disinfectants into wastewater by hospitals in relation to other sources–a review. *Chemosphere*, *45,* 957-969.

194. Kümmerer, K. (2009). Antibiotics in the aquatic environment–a review–part I. *Chemosphere*, *75*, 417-434.
195. Kümmerer, K. (2010). Pharmaceuticals in the environment. *Annual Review of Environment and Resources*, *35,* 57-75.
196. Kuo, C. Y., & Lo, S. L. (1999). Oxidation of aqueous chlorobiphenyls with photo-Fenton process. *Chemosphere*, *38*, 2041-2051.
197. Kurunthachalam, S. K. (2012). Pharmaceutical substances in India are a point of great concern. *Hydrology Current Research*, *3*, 3-5.
198. Kwon, M., Yoon, Y., Cho, E., Jung, Y., Lee, B. C., Paeng, K. J., & Kang, J. W. (2012). Removal of iopromide and degradation characteristics in electron beam irradiation process. *Journal of Hazardous Materials*, *227*, 126-134.
199. Lamba, R., Umar, A., Mehta, S. K., Anderson, W. A., & Kansal, S. K. (2015). Visible-light-driven photocatalytic properties of self-assembled cauliflower-like AgCl/ZnO hierarchical nanostructures. *Journal of Molecular Catalysis A: Chemical*, *408*, 189-201.
200. Langdon, K. A., Warne, M. S. T. J., & Kookana, R. S. (2010). Aquatic hazard assessment for pharmaceuticals, personal care products, and endocrine-disrupting compounds from biosolids-amended land. *Integrated Environmental Assessment and Management*, *6*, 663-676.
201. Le Caër, S. (2011). Water radiolysis: influence of oxide surfaces on H_2 production under ionizing radiation. *Water*, *3*, 235-253.
202. Lee, C. M., Palaniandy, P., & Dahlan, I. (2017). Pharmaceutical residues in aquatic environment and water remediation by TiO_2 heterogeneous photocatalysis: a review. *Environmental Earth Sciences*, *76*, 611.
203. Lee, J. M., Kim, J. H., Chang, Y. Y., & Chang, Y. S. (2009). Steel dust catalysis for Fenton-like oxidation of polychlorinated dizo-p-dioxins. *Journal of Hazardous Materials*, *163*, 222-230.
204. Lee, M. J., Kim, T. H., & Jung, I. H. (2012). *A Demonstration Study on Decomposition of Anntibiotics and Endocrine Disrupters Contained in Sewage Effluent by Mobile Electron Beam Accelerator* (Report No. IAEA-RC--1188.2).
205. Legrini, O., Oliveros, E., & Braun, A. M. (1993). Photochemical processes for water treatment. *Chemical Reviews*, *93*, 671-698.
206. Lester, Y., Avisar, D., Gnayem, H., Sasson, Y., Shavit, M., & Mamane, H. (2014). Demonstrating a new $BiOCl_{0.875}Br_{0.125}$ photocatalyst to degrade pharmaceuticals under solar irradiation. *Water, Air, & Soil Pollution*, *225*, 2132.

207. Li, H., Priambodo, R., Wang, Y., Zhang, H., & Huang, Y. H. (2015). Mineralization of bisphenol A by photo-Fenton-like process using a waste iron oxide catalyst in a three-phase fluidized bed reactor. *Journal of the Taiwan Institute of Chemical Engineers*, *53*, 68-73.

208. Lian, L., Yao, B., Hou, S., Fang, J., Yan, S., & Song, W. (2017). Kinetic study of hydroxyl and sulfate radical-mediated oxidation of pharmaceuticals in wastewater effluents. *Environmental Science & Technology*, *51*, 2954-2962.

209. Liang, C., & Su, H. W. (2009). Identification of sulfate and hydroxyl radicals in thermally activated persulfate. *Industrial & Engineering Chemistry Research*, *48*, 5558-5562.

210. Liao, C. H., Kang, S. F., & Wu, F. A. (2001). Hydroxyl radical scavenging role of chloride and bicarbonate ions in the H_2O_2/UV process. *Chemosphere*, *44*, 1193-1200.

211. Lin, C. C., Lin, H. Y., & Hsu, L. J. (2016). Degradation of ofloxacin using UV/H_2O_2 process in a large photoreactor. *Separation and Purification Technology*, *168*, 57-61.

212. Lindqvist, N., Tuhkanen, T., & Kronberg, L. (2005). Occurrence of acidic pharmaceuticals in raw and treated sewages and in receiving waters. *Water Research*, *39*, 2219-2228.

213. Liu, L., Li, R., Liu, Y., & Zhang, J. (2016a). Simultaneous degradation of ofloxacin and recovery of Cu (II) by photoelectrocatalysis with highly ordered TiO_2 nanotubes. *Journal of Hazardous Materials*, *308*, 264-275.

214. Liu, N., Wang, T., Zheng, M., Lei, J., Tang, L., Hu, G., Xu, J., & Wu, M. (2015). Radiation induced degradation of antiepileptic drug primidone in aqueous solution. *Chemical Engineering Journal*, *270*, 66-72.

215. Liu, Q., Luo, X., Zheng, Z., Zheng, B., Zhang, J., Zhao, Y., Yang, X., Wang, J., & Wang, L. (2011). Factors that have an effect on degradation of diclofenac in aqueous solution by gamma ray irradiation. *Environmental Science and Pollution Research*, *18*, 1243-1252.

216. Liu, R., Wang, R., Lu, J., Chang, M., Jin, Q., Du, Z., Wang, S., Li, Q., & Wang, X. (2016). Degradation of AFB1 in aqueous medium by electron beam irradiation: Kinetics, pathway and toxicology. *Food Control*, *66*, 151-157.

217. Liu, W., Wang, Y., Ai, Z., & Zhang, L. (2015). Hydrothermal synthesis of FeS_2 as a high-efficiency Fenton reagent to degrade alachlor via superoxide-mediated Fe (II)/Fe (III) cycle. *ACS Applied Materials & Interfaces*, *7*, 28534-28544.

218. Liu, W., Xu, L., Li, X., Shen, C., Rashid, S., Wen, Y., Liu, W., & Wu, X. (2015a). High-dispersive FeS_2 on graphene oxide for effective degradation of 4-chlorophenol. *RSC Advances*, *5*, 2449-2456.
219. Liu, Y., & Wang, J. (2013). Degradation of sulfamethazine by gamma irradiation in the presence of hydrogen peroxide. *Journal of Hazardous Materials*, *250*, 99-105.
220. Loraine, G. A., & Pettigrove, M. E. (2006). Seasonal variations in concentrations of pharmaceuticals and personal care products in drinking water and reclaimed wastewater in southern California. *Environmental Science & Technology*, *40*, 687-695.
221. Luo, Y., Guo, W., Ngo, H. H., Nghiem, L. D., Hai, F. I., Zhang, J., Liang, S., & Wang, X. C. (2014). A review on the occurrence of micropollutants in the aquatic environment and their fate and removal during wastewater treatment. *Science of the Total Environment*, *473*, 619-641.
222. Luster, E., Avisar, D., Horovitz, I., Lozzi, L., Baker, M. A., Grilli, R., & Mamane, H. (2017). N-Doped TiO_2-Coated Ceramic Membrane for Carbamazepine Degradation in Different Water Qualities. *Nanomaterials*, *7*, 206.
223. Mackuľak, T., Mosný, M., Grabic, R., Golovko, O., Koba, O., & Birošová, L. (2015). Fenton-like reaction: A possible way to efficiently remove illicit drugs and pharmaceuticals from wastewater. *Environmental Toxicology and Pharmacology*, *39*, 483-488.
224. Magalhães, F. P. M. C., Pereira, M. C., Botrel, S. E. C., Fabris, J. D., Macedo, W. A., Mendonca, R., ... & Oliveira, L. C. A. (2007). Cr-containing magnetites $Fe_3- xCrxO_4$: the role of Cr^{3+} and Fe^{2+} on the stability and reactivity towards H_2O_2 reactions. *Applied Catalysis A: General*, *332*, 115-123.
225. Magureanu, M., Piroi, D., Mandache, N. B., David, V., Medvedovici, A., & Parvulescu, V. I. (2010). Degradation of pharmaceutical compound pentoxifylline in water by non-thermal plasma treatment. *Water Research*, *44*, 3445-3453.
226. Malato, S., Blanco, J., Cáceres, J., Fernández-Alba, A. R., Agüera, A., & Rodrıguez, A. (2002). Photocatalytic treatment of water-soluble pesticides by photo-Fenton and TiO_2 using solar energy. *Catalysis Today*, *76*, 209-220.
227. Mameri, Y., Debbache, N., el mehdi Benacherine, M., Seraghni, N., & Sehili, T. (2016). Heterogeneous photodegradation of paracetamol using Goethite/H_2O_2 and Goethite/oxalic acid systems under artificial and natural light. *Journal of Photochemistry and Photobiology A: Chemistry*, *315*, 129-137.

228. Mantzavinos, D., & Psillakis, E. (2004). Enhancement of biodegradability of industrial wastewaters by chemical oxidation pre-treatment. *Journal of Chemical Technology & Biotechnology: International Research in Process, Environmental & Clean Technology*, *79*, 431-454.
229. Marcano, D. C., Kosynkin, D. V., Berlin, J. M., Sinitskii, A., Sun, Z., Slesarev, A., Alemany, L. B., Lu, W., & Tour, J. M. (2010). Improved synthesis of graphene oxide. *ACS Nano*, *4*, 4806-4814.
230. Martınez, N. S. S., Fernández, J. F., Segura, X. F., & Ferrer, A. S. (2003). Pre-oxidation of an extremely polluted industrial wastewater by the Fenton's reagent. *Journal of Hazardous Materials*, *101*, 315-322.
231. Martınez, N. S. S., Fernández, J. F., Segura, X. F., & Ferrer, A. S. (2003). Pre-oxidation of an extremely polluted industrial wastewater by the Fenton's reagent. *Journal of Hazardous Materials*, *101*, 315-322.
232. Maruthi, Y. A., Das, N. L., Hossain, K., Sarma, K. S. S., Rawat, K. P., & Sabharwal, S. (2011). Application of electron beam technology in improving sewage water quality: An advance technique. *African Journal of Environmental Science and Technology*, *5*, 545-552.
233. Matsuo, H., Sakamoto, H., Arizono, K., & Shinohara, R. (2011). Behavior of pharmaceuticals in waste water treatment plant in Japan. *Bulletin of Environmental Contamination and Toxicology*, *87*, 31-35.
234. Matta, R., Hanna, K., Kone, T., & Chiron, S. (2008). Oxidation of 2, 4, 6-trinitrotoluene in the presence of different iron-bearing minerals at neutral pH. *Chemical Engineering Journal*, *144*, 453-458.
235. McCabe, J., & Eckenfelder, W. W. (Eds.). (1958). *Biological treatment of sewage and industrial wastes* (Vol. 2). Reinhold.
236. McKibben, M. A., & Barnes, H. L. (1986). Oxidation of pyrite in low temperature acidic solutions: Rate laws and surface textures. *Geochimica et Cosmochimica Acta*, *50*, 1509-1520.
237. McLachlan, J. A. (1936). The settlement and rising of activated sludge. *The Surveyor*, *90*, 2320.
238. Meeroff, D. E., Waite, T. D., Kazumi, J., & Kurucz, C. N. (2004). Radiation-assisted process enhancement in wastewater treatment. *Journal of Environmental Engineering*, *130*, 155-166.

239. Mehrvar, M., Anderson, W. A., & Moo-Young, M. (2001). Photocatalytic degradation of aqueous organic solvents in the presence of hydroxyl radical scavengers. *International Journal of photoenergy*, *3*, 187-191.

240. Mendez-Arriaga, F., Torres-Palma, R. A., Pétrier, C., Esplugas, S., Gimenez, J., & Pulgarin, C. (2009). Mineralization enhancement of a recalcitrant pharmaceutical pollutant in water by advanced oxidation hybrid processes. *Water Research*, *43*, 3984-3991.

241. Méndez-Medrano, M. G., Kowalska, E., Lehoux, A., Herissan, A., Ohtani, B., Bahena, D., Briois, V., Colbeau-Justin, C., Rodríguez-López, J. L., & Remita, H. (2016). Surface modification of TiO_2 with Ag nanoparticles and CuO nanoclusters for application in photocatalysis. *The Journal of Physical Chemistry C*, *120*, 5143-5154.

242. Metcalf, Eddy, 1995. Wastewater engineering, Third ed., Tata McGraw-Hill, New Delhi.

243. Michael, I., Hapeshi, E., Michael, C., & Fatta-Kassinos, D. (2010). Solar Fenton and solar TiO_2 catalytic treatment of ofloxacin in secondary treated effluents: evaluation of operational and kinetic parameters. *Water Research*, *44*, 5450-5462.

244. Miller, G. W. (2006). Integrated concepts in water reuse: managing global water needs. *Desalination*, *187*, 65-75.

245. Minh, T. B., Leung, H. W., Loi, I. H., Chan, W. H., So, M. K., Mao, J. Q., Choi, D., Lam, J. C., Zheng, G., Martin, M., & Lee, J. H. (2009). Antibiotics in the Hong Kong metropolitan area: ubiquitous distribution and fate in Victoria Harbour. *Marine Pollution Bulletin*, *58*, 1052-1062.

246. Mohammadi, R., Massoumi, B., & Eskandarloo, H. (2015). Preparation and characterization of Sn/Zn/TiO_2 photocatalyst for enhanced amoxicillin trihydrate degradation. *Desalination and Water Treatment*, *53*, 1995-2004.

247. Mohapatra, S., Huang, C. H., Mukherji, S., & Padhye, L. P. (2016). Occurrence and fate of pharmaceuticals in WWTPs in India and comparison with a similar study in the United States. *Chemosphere*, *159*, 526-535.

248. Molina, R., Segura, Y., Martínez, F., & Melero, J. A. (2012). Immobilization of active and stable goethite coated-films by a dip-coating process and its application for photo-Fenton systems. *Chemical Engineering Journal*, *203*, 212-222.

249. Mompelat, S., Le Bot, B., & Thomas, O. (2009). Occurrence and fate of pharmaceutical products and by-products, from resource to drinking water. *Environment International*, *35*, 803-814.

250. Monteagudo, J. M., Durán, A., Culebradas, R., San Martín, I., & Carnicer, A. (2013). Optimization of pharmaceutical wastewater treatment by solar/ferrioxalate photo-catalysis. *Journal of Environmental Management*, *128*, 210-219.
251. Moreira, N. F., Orge, C. A., Ribeiro, A. R., Faria, J. L., Nunes, O. C., Pereira, M. F. R., & Silva, A. M. (2015). Fast mineralization and detoxification of amoxicillin and diclofenac by photocatalytic ozonation and application to an urban wastewater. *Water Research*, *87*, 87-96.
252. Murty, M. N., & Kumar, S. (2011). Water pollution in India: an economic appraisal. *India Infrastructure Report*, *19*, 285-298.
253. Muruganandham, M., & Swaminathan, M. (2004). Decolourisation of Reactive Orange 4 by Fenton and photo-Fenton oxidation technology. *Dyes and Pigments*, *63*, 315-321.
254. Murugananthan, M., Yoshihara, S., Rakuma, T., Uehara, N., & Shirakashi, T. (2007). Electrochemical degradation of 17β-estradiol (E2) at boron-doped diamond (Si/BDD) thin film electrode. *Electrochimica Acta*, *52*, 3242-3249.
255. Mutiyar, P. K., & Mittal, A. K. (2013). Occurrences and fate of an antibiotic amoxicillin in extended aeration-based sewage treatment plant in Delhi, India: a case study of emerging pollutant. *Desalination and Water Treatment*, *51*, 6158-6164.
256. Mutiyar, P. K., & Mittal, A. K. (2014). Occurrences and fate of selected human antibiotics in influents and effluents of sewage treatment plant and effluent-receiving river Yamuna in Delhi (India). *Environmental Monitoring and Assessment*, *186*, 541-557.
257. Naddeo, V., Uyguner-Demirel, C. S., Prado, M., Cesaro, A., Belgiorno, V., & Ballesteros, F. (2015). Enhanced ozonation of selected pharmaceutical compounds by sonolysis. *Environmental Technology*, *36*, 1876-1883.
258. Ocampo-Pérez, R., Rivera-Utrilla, J., Sánchez-Polo, M., Lopez-Penalver, J. J., & Leyva-Ramos, R. (2011). Degradation of antineoplastic cytarabine in aqueous solution by gamma radiation. *Chemical Engineering Journal*, *174*, 1-8.
259. Oller, I., Malato, S., & Sánchez-Pérez, J. (2011). Combination of advanced oxidation processes and biological treatments for wastewater decontamination—a review. *Science of the Total Environment*, *409*, 4141-4166.
260. Onesios, K. M., Jim, T. Y., & Bouwer, E. J. (2009). Biodegradation and removal of pharmaceuticals and personal care products in treatment systems: a review. *Biodegradation*, *20*, 441-466.

261. Oturan, M. A., & Aaron, J. J. (2014). Advanced oxidation processes in water/wastewater treatment: principles and applications. A review. *Critical Reviews in Environmental Science and Technology, 44*, 2577-2641.
262. Pariente, M. I., Martinez, F., Melero, J. A., Botas, J. A., Velegraki, T., Xekoukoulotakis, N. P., & Mantzavinos, D. (2008). Heterogeneous photo-Fenton oxidation of benzoic acid in water: effect of operating conditions, reaction by-products and coupling with biological treatment. *Applied Catalysis B: Environmental*, *85*, 24-32.
263. Paul, J., Naik, D. B., & Sabharwal, S. (2010). High energy induced decoloration and mineralization of Reactive Red 120 dye in aqueous solution: a steady state and pulse radiolysis study. *Radiation Physics and Chemistry*, *79*, 770-776.
264. Paul, J., Naik, D. B., Bhardwaj, Y. K., & Varshney, L. (2014). Studies on oxidative radiolysis of ibuprofen in presence of potassium persulfate. *Radiation Physics and Chemistry*, *100*, 38-44.
265. Paul, J., Rawat, K. P., Sarma, K. S. S., & Sabharwal, S. (2011). Decoloration and degradation of Reactive Red-120 dye by electron beam irradiation in aqueous solution. *Applied Radiation and Isotopes*, *69*, 982-987.
266. Pauwels, B., Deconinck, S., & Verstraete, W. (2006). Electrolytic removal of 17α-ethinylestradiol (EE2) in water streams. *Journal of Chemical Technology & Biotechnology: International Research in Process, Environmental & Clean Technology*, *81*, 1338-1343.
267. Pereira, V. J., Linden, K. G., & Weinberg, H. S. (2007). Evaluation of UV irradiation for photolytic and oxidative degradation of pharmaceutical compounds in water. *Water Research*, *41*, 4413-4423.
268. Perkowski, J., & Kos, L. (1988). The purification of textile wastes by radiation and coagulation. *Przeglad Wlokienniczy*, *42*, 444-446.
269. Pi, Y., Feng, J., Sun, J., Song, M., & Sun, J. (2014). Oxidation of ofloxacin by Oxone/Co^{2+}: identification of reaction products and pathways. *Environmental Science and Pollution Research*, *21*, 3031-3040.
270. Pignatello, J. J., Oliveros, E., & MacKay, A. (2006). Advanced oxidation processes for organic contaminant destruction based on the Fenton reaction and related chemistry. *Critical Reviews in Environmental Science and Technology*, *36*, 1-84.
271. Planson, A. G., Carbonell, P., Paillard, E., Pollet, N., & Faulon, J. L. (2012). Compound toxicity screening and structure–activity relationship modeling in Escherichia coli. *Biotechnology and Bioengineering*, *109*, 846-850.

272. Pouran, S. R., Raman, A. A. A., & Daud, W. M. A. W. (2014). Review on the application of modified iron oxides as heterogeneous catalysts in Fenton reactions. *Journal of Cleaner Production*, *64*, 24-35.
273. Quintana, J. B., Weiss, S., & Reemtsma, T. (2005). Pathways and metabolites of microbial degradation of selected acidic pharmaceutical and their occurrence in municipal wastewater treated by a membrane bioreactor. *Water Research*, *39*, 2654-2664.
274. Radjenović, J., Sirtori, C., Petrović, M., Barceló, D., & Malato, S. (2009). Solar photocatalytic degradation of persistent pharmaceuticals at pilot-scale: kinetics and characterization of major intermediate products. *Applied Catalysis B: Environmental*, *89*, 255-264.
275. Raj D, S. S., Chary, N. S., Bindu, V. H., Reddy, M. R. P., & Anjaneyulu, Y. (2004). Aerobic oxidation of common effluent treatment plant wastewaters and sludge characterization studies. *International Journal of Environmental Studies*, *61*, 99-111.
276. Raj, D. S. S., & Anjaneyulu, Y. (2005). Evaluation of biokinetic parameters for pharmaceutical wastewaters using aerobic oxidation integrated with chemical treatment. *Process Biochemistry*, *40*, 165-175.
277. Ramaswamy, B. R., Shanmugam, G., Velu, G., Rengarajan, B., & Larsson, D. J. (2011). GC–MS analysis and ecotoxicological risk assessment of triclosan, carbamazepine and parabens in Indian rivers. *Journal of Hazardous Materials*, *186*, 1586-1593.
278. Ramteke, L. P., & Gogate, P. R. (2016). Treatment of real industrial wastewater using the combined approach of advanced oxidation followed by aerobic oxidation. *Environmental Science and Pollution Research*, *23*, 9712-9729.
279. Ratola, N., Cincinelli, A., Alves, A., & Katsoyiannis, A. (2012). Occurrence of organic microcontaminants in the wastewater treatment process. A mini review. *Journal of Hazardous Materials*, *239*, 1-18.
280. Ravina, M., Campanella, L., & Kiwi, J. (2002). Accelerated mineralization of the drug diclofenac via Fenton reactions in a concentric photo-reactor. *Water Research*, *36*, 3553-3560.
281. Rawat, K. P., & Sarma, K. S. S. (2013). Enhanced biodegradation of wastewater with electron beam pretreatment. *Applied Radiation and Isotopes*, *74*, 6-8.
282. Rehman, M. S. U., Rashid, N., Ashfaq, M., Saif, A., Ahmad, N., & Han, J. I. (2015). Global risk of pharmaceutical contamination from highly populated developing countries. *Chemosphere*, *138*, 1045-1055.

283. Ren, X., Li, J., Tan, X., Shi, W., Chen, C., Shao, D., Wen, T., Wang, L., Zhao, G., Sheng, G., & Wang, X. (2014). Impact of Al_2O_3 on the aggregation and deposition of graphene oxide. *Environmental Science & Technology*, *48*, 5493-5500.
284. Richardson, B. J., Lam, P. K., & Martin, M. (2005). Emerging chemicals of concern: pharmaceuticals and personal care products (PPCPs) in Asia, with particular reference to Southern China. *Marine Pollution Bulletin*, *50*, 913-920.
285. Rivera-Utrilla, J., Sánchez-Polo, M., Ferro-García, M. Á., Prados-Joya, G., & Ocampo-Pérez, R. (2013). Pharmaceuticals as emerging contaminants and their removal from water. A review. *Chemosphere*, *93*, 1268-1287.
286. Rizzo, L. (2011). Bioassays as a tool for evaluating advanced oxidation processes in water and wastewater treatment. *Water Research*, *45*, 4311-4340.
287. Rodriguez, C., Van Buynder, P., Lugg, R., Blair, P., Devine, B., Cook, A., & Weinstein, P. (2009). Indirect potable reuse: a sustainable water supply alternative. *International Journal of Environmental Research and Public Health*, *6*, 1174-1203.
288. Rosario-Ortiz, F. L., Wert, E. C., & Snyder, S. A. (2010). Evaluation of UV/H_2O_2 treatment for the oxidation of pharmaceuticals in wastewater. *Water Research*, *44*, 1440-1448.
289. Safarzadeh-Amiri, A., Bolton, J. R., & Cater, S. R. (1996). The use of iron in advanced oxidation processes. *Journal of Advanced Oxidation Technologies*, *1*, 18-26.
290. Sági, G., Csay, T., Pátzay, G., Csonka, E., Wojnárovits, L., & Takács, E. (2014). Oxidative and reductive degradation of sulfamethoxazole in aqueous solutions: decomposition efficiency and toxicity assessment. *Journal of Radioanalytical and Nuclear Chemistry*, *301*, 475-482.
291. Sági, G., Kovács, K., Bezsenyi, A., Csay, T., Takács, E., & Wojnárovits, L. (2016). Enhancing the biological degradability of sulfamethoxazole by ionizing radiation treatment in aqueous solution. *Radiation Physics and Chemistry*, *124*, 179-183.
292. Salo, J. P. K., Yli-Kauhaluoma, J., & Salomies, H. (2003). On the hydrolytic behavior of tinidazole, metronidazole, and ornidazole. *Journal of Pharmaceutical Sciences*, *92*, 739-746.
293. Sánchez-Polo, M., López-Peñalver, J., Prados-Joya, G., Ferro-García, M. A., & Rivera-Utrilla, J. (2009). Gamma irradiation of pharmaceutical compounds, nitroimidazoles, as a new alternative for water treatment. *Water Research*, *43*, 4028-4036.

294. Sanchez-Prado, L., Barro, R., Garcia-Jares, C., Llompart, M., Lores, M., Petrakis, C., Kalogerakis, N., Mantzavinos, D., & Psillakis, E. (2008). Sonochemical degradation of triclosan in water and wastewater. *Ultrasonics Sonochemistry*, *15*, 689-694.
295. Sandhwar, V. K., & Prasad, B. (2017). Comparative study of electrocoagulation and electrochemical Fenton treatment of aqueous solution of benzoic acid (BA): Optimization of process and sludge analysis. *Korean Journal of Chemical Engineering*, *34*, 1062-1072.
296. Sangion, A., & Gramatica, P. (2016). Hazard of pharmaceuticals for aquatic environment: prioritization by structural approaches and prediction of ecotoxicity. *Environment International*, *95*, 131-143.
297. Santos, J. L., Aparicio, I., & Alonso, E. (2007). Occurrence and risk assessment of pharmaceutically active compounds in wastewater treatment plants. A case study: Seville city (Spain). *Environment International*, *33*, 596-601.
298. Saritha, P., Aparna, C., Himabindu, V., & Anjaneyulu, Y. (2007). Comparison of various advanced oxidation processes for the degradation of 4-chloro-2 nitrophenol. *Journal of Hazardous Materials*, *149*, 609-614.
299. Sastry, P. A. & Thambirajah, J. J. (1995). Aerobic Biological Waste Treatment, Narosa Publishing House, New Delhi.
300. Sayed, M., Khan, J. A., Shah, L. A., Shah, N. S., Khan, H. M., Rehman, F., Khan, A. R., & Khan, A. M. (2016). Degradation of quinolone antibiotic, norfloxacin, in aqueous solution using gamma-ray irradiation. *Environmental Science and Pollution Research*, *23*, 13155-13168.
301. Schröder, P., Helmreich, B., Škrbić, B., Carballa, M., Papa, M., Pastore, C., Emre, Z., Oehmen, A., Langenhoff, A., Molinos, M., & Dvarioniene, J. (2016). Status of hormones and painkillers in wastewater effluents across several European states—considerations for the EU watch list concerning estradiols and diclofenac. *Environmental Science and Pollution Research*, *23*, 12835-12866.
302. Schuman, E., Kujawa-Roeleveld, K., & Zeeman, I. G. (2008). Fate of human pharmaceuticals in biological treatment systems treating concentrated wastewater under various environmental conditions. *Sub-department of Environmental Technology, Wageningen University*.
303. Schwartz, D. E., & Jeunet, F. (1976). Comparative pharmacokinetic studies of ornidazole and metronidazole in man. *Chemotherapy*, *22*, 19-29.

304. Sedlak, D. L., & Hoigné, J. (1993). The role of copper and oxalate in the redox cycling of iron in atmospheric waters. *Atmospheric Environment. Part A. General Topics*, *27*, 2173-2185.
305. Sellers, R. M. (1980). Spectrophotometric determination of hydrogen peroxide using potassium titanium (IV) oxalate. *Analyst*, *105*, 950-954.
306. Shanmugam, G., Sampath, S., Selvaraj, K. K., Larsson, D. J., & Ramaswamy, B. R. (2014). Non-steroidal anti-inflammatory drugs in Indian rivers. *Environmental Science and Pollution Research*, *21*, 921-931.
307. Sharma, M. C., & Chaturvedi, A. K. (1995). Simulation of biological treatment of effluents by activated sludge process at laboratory bench scale. *Indian Journal of Environment Protection*, *10*, 10-4.
308. Shemer, H., Kunukcu, Y. K., & Linden, K. G. (2006). Degradation of the pharmaceutical metronidazole via UV, Fenton and photo-Fenton processes. *Chemosphere*, *63*, 269-276.
309. Shin, H. S., Kim, Y. R., Han, B., Makarov, I. E., Ponomarev, A. V., & Pikaev, A. K. (2002). Application of electron beam to treatment of wastewater from papermill. *Radiation Physics and Chemistry*, *65*, 539-547.
310. Singh, B. K., Parwate, D. V., Sarma, I. B. D., & Shukla, S. K. (2010). Study on gamma and electron beam sterilization of third generation cephalosporins cefdinir and cefixime in solid state. *Radiation Physics and Chemistry*, *79*, 1079-1087.
311. Singh, K. P., Rai, P., Singh, A. K., Verma, P., & Gupta, S. (2014). Occurrence of pharmaceuticals in urban wastewater of north Indian cities and risk assessment. *Environmental Monitoring and Assessment*, *186*, 6663-6682.
312. Singh, P., Mittal, R., Sharma, G. C., Singh, S., & Singh, A. (2003). Ornidazole: comprehensive profile. *Profiles of Drug Substances, Excipients and Related Methodology*, *30*, 123-184.
313. Sirtori, C., Zapata, A., Gernjak, W., Malato, S., Lopez, A., & Agüera, A. (2011). Solar photo-Fenton degradation of nalidixic acid in waters and wastewaters of different composition. Analytical assessment by LC–TOF-MS. *Water Research*, *45*, 1736-1744.
314. Sirtori, C., Zapata, A., Oller, I., Gernjak, W., Agüera, A., & Malato, S. (2009). Decontamination industrial pharmaceutical wastewater by combining solar photo-Fenton and biological treatment. *Water Research*, *43*, 661-668.

315. Slegers, C., & Tilquin, B. (2005). Theoretical approach to the destruction or sterilization of drugs in aqueous solution. *Radiation Physics and Chemistry*, *72*, 363-365.
316. Slegers, C., & Tilquin, B. (2006). Final product analysis in the e-beam and gamma radiolysis of aqueous solutions of metoprolol tartrate. *Radiation Physics and Chemistry*, *75*, 1006-1017.
317. Snyder, S. A., Adham, S., Redding, A. M., Cannon, F. S., DeCarolis, J., Oppenheimer, J., Wert, E. C., & Yoon, Y. (2007). Role of membranes and activated carbon in the removal of endocrine disruptors and pharmaceuticals. *Desalination*, *202*, 156-181.
318. Soleimani, S., Ormeci, B., & Isgor, O. B. (2013). Growth and characterization of Escherichia coli DH5α biofilm on concrete surfaces as a protective layer against microbiologically influenced concrete deterioration (MICD). *Applied Microbiology and Biotechnology*, *97*, 1093-1102.
319. Solomon, W. S., Gowda, K. V., Selvan, P. S., Mandal, U., & Pal, T. K. (2008). HPLC method for quantification of ornidazole in human plasma. *Asian Journal of Chemistry*, *20*, 4361.
320. Soltani, T., & Lee, B. K. (2016). Sono-synthesis of nanocrystallized $BiFeO_3$/reduced graphene oxide composites for visible photocatalytic degradation improvement of bisphenol A. *Chemical Engineering Journal*, *306*, 204-213.
321. Song, W., Cooper, W. J., Mezyk, S. P., Greaves, J., & Peake, B. M. (2008). Free radical destruction of β-blockers in aqueous solution. *Environmental Science & Technology*, *42*, 1256-1261.
322. Sood, S., Mehta, S. K., Sinha, A. S. K., & Kansal, S. K. (2016). Bi_2O_3/TiO_2 heterostructures: synthesis, characterization and their application in solar light mediated photocatalyzed degradation of an antibiotic, ofloxacin. *Chemical Engineering Journal*, *290*, 45-52.
323. Sood, S., Umar, A., Mehta, S. K., & Kansal, S. K. (2015). Highly effective Fe-doped TiO_2 nanoparticles photocatalysts for visible-light driven photocatalytic degradation of toxic organic compounds. *Journal of Colloid and Interface Science*, *450*, 213-223.
324. Spinks, J. W. T., & Woods, R. J. (1990). An introduction to radiation chemistry. John Wiley and Sons Inc; New York, USA.
325. Sturini, M., Speltini, A., Maraschi, F., Vinci, G., Profumo, A., Pretali, L., Albini, A., & Malavasi, L. (2017). gC_3N_4-promoted degradation of ofloxacin antibiotic in natural

waters under simulated sunlight. *Environmental Science and Pollution Research*, *24*, 4153-4161.

326. Subedi, B., Balakrishna, K., Joshua, D. I., & Kannan, K. (2017). Mass loading and removal of pharmaceuticals and personal care products including psychoactives, antihypertensives, and antibiotics in two sewage treatment plants in southern India. *Chemosphere*, *167*, 429-437.
327. Subedi, B., Balakrishna, K., Sinha, R. K., Yamashita, N., Balasubramanian, V. G., & Kannan, K. (2015). Mass loading and removal of pharmaceuticals and personal care products, including psychoactive and illicit drugs and artificial sweeteners, in five sewage treatment plants in India. *Journal of Environmental Chemical Engineering*, *3*, 2882-2891.
328. Sukhdev, A., & Shubha, J. P. (2009). Kinetics and reactivities of ruthenium (III)-and osmium (VIII)-catalyzed oxidation of ornidazole with chloramine-T in acid and alkaline media: A mechanistic approach. *Journal of Molecular Catalysis A: Chemical*, *310*, 24-33.
329. Sun, J. H., Sun, S. P., Sun, J. Y., Sun, R. X., Qiao, L. P., Guo, H. Q., & Fan, M. H. (2007). Degradation of azo dye Acid black 1 using low concentration iron of Fenton process facilitated by ultrasonic irradiation. *Ultrasonics Sonochemistry*, *14*, 761-766.
330. Sun, J. H., Sun, S. P., Wang, G. L., & Qiao, L. P. (2007a). Degradation of azo dye Amido black 10B in aqueous solution by Fenton oxidation process. *Dyes and Pigments*, *74*, 647-652.
331. Sun, W., Chen, J., Chen, L., Wang, J., & Zhang, Y. (2016). Coupled electron beam radiation and MBR treatment of textile wastewater containing polyvinyl alcohol. *Chemosphere*, *155*, 57-61.
332. Swati, J., Vyas Raj, K., Prabhat, P., & Sangeeta, V. (2010). A review on fate of antiviral drugs in environment and detection techniques. *International Journal of Environmental Science, 1,* 1533-1548.
333. Symons, J. M., McKinney, R. E., & Hassis, H. H. (1960). A procedure for determination of the biological treatability of industrial wastes. *Journal (Water Pollution Control Federation)*, 841-852.
334. Tamimi, M., Qourzal, S., Barka, N., Assabbane, A., & Ait-Ichou, Y. (2008). Methomyl degradation in aqueous solutions by Fenton's reagent and the photo-Fenton system. *Separation and Purification Technology*, *61*, 103-108.

335. Tamtam, F., Mercier, F., Le Bot, B., Eurin, J., Dinh, Q. T., Clément, M., & Chevreuil, M. (2008). Occurrence and fate of antibiotics in the Seine River in various hydrological conditions. *Science of the Total Environment*, *393*, 84-95.

336. Tan, C., Huang, X., & Zhang, H. (2013). Synthesis and applications of graphene-based noble metal nanostructures. *Materials Today*, *16*, 29-36.

337. Tang, W. Z., & Chen, R. Z. (1996). Decolorization kinetics and mechanisms of commercial dyes by H_2O_2/iron powder system. *Chemosphere*, *32*, 947-958.

338. Tanizaki, T., Kadokami, K., & Shinohara, R. (2002). Catalytic photodegradation of endocrine disrupting chemicals using titanium dioxide photosemiconductor thin films. *Bulletin of Environmental Contamination and Toxicology*, *68*, 732-739.

339. Tarpani, R. R. Z., & Azapagic, A. (2018). A methodology for estimating concentrations of pharmaceuticals and personal care products (PPCPs) in wastewater treatment plants and in freshwaters. *Science of the Total Environment*, *622*, 1417-1430.

340. Tay, K. S., & Madehi, N. (2015). Ozonation of ofloxacin in water: by-products, degradation pathway and ecotoxicity assessment. *Science of the Total Environment*, *520*, 23-31.

341. Tchobanoglous, G., Burton, F. L., & Stensel, H. D. (2003). Metcalf and Eddy Wastewater Engineering: Treatment and Reuse, McGraw Hill. New York, USA.

342. Tedla, H., Díaz, I., Kebede, T., & Taddesse, A. M. (2015). Synthesis, characterization and photocatalytic activity of zeolite supported $ZnO/Fe_2O_3/MnO_2$ nanocomposites. *Journal of Environmental Chemical Engineering*, *3*, 1586-1591.

343. Teixeira, L. A. C., Junior, N. D. A. V., Yokoyama, L., & da Fonseca, F. V. (2015). Degradation of phenol in mine waters using hydrogen peroxide and commercial steel wool. *International Journal of Mineral Processing*, *138*, 15-19.

344. Tekin, H., Bilkay, O., Ataberk, S. S., Balta, T. H., Ceribasi, I. H., Sanin, F. D., Dilek, F.B., & Yetis, U. (2006). Use of Fenton oxidation to improve the biodegradability of a pharmaceutical wastewater. *Journal of Hazardous Materials*, *136*, 258-265.

345. Teophilo, G., dos Fernandes Vieira, R., dos Prazeres Rodrigues, D., & Menezes, F. R. (2002). Escherichia coli isolated from seafood: toxicity and plasmid profiles. *International Microbiology*, *5*, 11-14.

346. Ternes, T. A., Meisenheimer, M., McDowell, D., Sacher, F., Brauch, H. J., Haist-Gulde, B., Preuss, G., Wilme, U., & Zulei-Seibert, N. (2002). Removal of pharmaceuticals during drinking water treatment. *Environmental Science & Technology*, *36*, 3855-3863.

347. Theruvathu, J. A., Aravindakumar, C. T., Flyunt, R., von Sonntag, J., & von Sonntag, C. (2001). Fenton chemistry of 1, 3-dimethyluracil. *Journal of the American Chemical Society*, *123*, 9007-9014.
348. Thill, P. G., Ager, D. K., Vojnovic, B., Tesh, S. J., Scott, T. B., & Thompson, I. P. (2016). Hybrid biological, electron beam and zero-valent nano iron treatment of recalcitrant metalworking fluids. *Water Research*, *93*, 214-221.
349. Tian, M., Adams, B., Wen, J., Asmussen, R. M., & Chen, A. (2009). Photoelectrochemical oxidation of salicylic acid and salicylaldehyde on titanium dioxide nanotube arrays. *Electrochimica Acta*, *54*, 3799-3805.
350. Tireli, A. A., do Rosário Guimarães, I., de Souza Terra, J. C., da Silva, R. R., & Guerreiro, M. C. (2015). Fenton-like processes and adsorption using iron oxide-pillared clay with magnetic properties for organic compound mitigation. *Environmental Science and Pollution Research*, *22*, 870-881.
351. Tong, A. Y., Peake, B. M., & Braund, R. (2011). Disposal practices for unused medications around the world. *Environment International*, *37*, 292-298.
352. Tonnesen, H. H. (2004). *Photostability of drugs and drug formulations*. CRC Press.
353. Trivedy, R. K., & Nakate, S. S. (2001). Treatment of hospital waste and sewage in hyacinth ponds. *Low Cost Wastewater Treatment Technologies. ABD, Jaipur, India*, 132-163.
354. Trojanowicz, M., Bojanowska-Czajka, A., & Capodaglio, A. G. (2017). Can radiation chemistry supply a highly efficient AO (R) P process for organics removal from drinking and waste water? A review. *Environmental Science and Pollution Research*, *24*, 20187-20208.
355. Trojanowicz, M., Bojanowska-Czajka, A., Kciuk, G., Bobrowski, K., Gumiela, M., Koc, A., Nałęcz-Jawecki, G., Torun, M., & Ozbay, D. S. (2012). Application of ionizing radiation in decomposition of selected organic pollutants in waters. *Eur Water*, *39*, 15-26.
356. Trojanowicz, M., Drzewicz, P., Bojanowska-Czajka, A., Naleczjawecki, G., Gryz, M., Sawicki, J., Kulisa, K., Wolkowicz, S., Nichipor, H. & Zimek, Z. (2008). Application of ionizing radiation for removal of pesticides from groundwaters and wastes. *IAEA TECDOC-1598*, 115-140.
357. Trovo, A. G., Nogueira, R. F. P., Agüera, A., Fernandez-Alba, A. R., & Malato, S. (2011). Degradation of the antibiotic amoxicillin by photo-Fenton process–chemical and toxicological assessment. *Water Research*, *45*, 1394-1402.

358. Tunay, O., Samuk, B., Olmez, T., & Kabdash, I. (2004). Application of advanced oxidation to enhance biodegradability of pharmaceutical industry wastewaters. *Fresenius Environmental Bulletin*, *13*, 965-968.

359. Umar, M., Aziz, H. A., & Yusoff, M. S. (2010). Trends in the use of Fenton, electro-Fenton and photo-Fenton for the treatment of landfill leachate. *Waste Management*, *30*, 2113-2121.

360. Urkiaga, A., De las Fuentes, L., Bis, B., Chiru, E., Bodo, B., Hernández, F., & Wintgens, T. (2006). Methodologies for feasibility studies related to wastewater reclamation and reuse projects. *Desalination*, *187*, 263-269.

361. Ursachi, I., Stancu, A., & Vasile, A. (2012). Magnetic α-Fe_2O_3/MCM-41 nanocomposites: Preparation, characterization, and catalytic activity for methylene blue degradation. *Journal of Colloid and Interface Science*, *377*, 184-190.

362. Usman, M., Faure, P., Ruby, C., & Hanna, K. (2012). Remediation of PAH-contaminated soils by magnetite catalyzed Fenton-like oxidation. *Applied Catalysis B: Environmental*, *117*, 10-17.

363. Van Dijk-Looijaard, A. M., & Van Genderen, J. (2000). Levels of exposure from drinking water. *Food and Chemical Toxicology*, *38*, S37-S42.

364. Varghese, R., Aravind, U. K., & Aravindakumar, C. T. (2007). Fenton-enhanced γ-radiolysis of cyanuric acid. *Journal of Hazardous Materials*, *142*, 555-558.

365. Vasquez, M. I., Hapeshi, E., Fatta-Kassinos, D., & Kümmerer, K. (2013). Biodegradation potential of ofloxacin and its resulting transformation products during photolytic and photocatalytic treatment. *Environmental Science and Pollution Research*, *20*, 1302-1309.

366. Veach, A. M., & Bernot, M. J. (2011). Temporal variation of pharmaceuticals in an urban and agriculturally influenced stream. *Science of the Total Environment*, *409*, 4553-4563.

367. Vellinga, A., Cormican, S., Driscoll, J., Furey, M., O'Sullivan, M., & Cormican, M. (2014). Public practice regarding disposal of unused medicines in Ireland. *Science of the Total Environment*, *478*, 98-102.

368. Velo Gala, I., López Peñalver, J. J., Sánchez Polo, M., & Rivera Utrilla, J. (2013). Degradation of X-ray contrast media diatrizoate in different water matrices by gamma irradiation. *Journal of Chemical Technology & Biotechnology*, *88*, 1336-1343.

369. Verma, S., Prasad, B., & Mishra, I. M. (2010). Pretreatment of petrochemical wastewater by coagulation and flocculation and the sludge characteristics. *Journal of Hazardous Materials*, *178*, 1055-1064.
370. Vieno, N. M., Härkki, H., Tuhkanen, T., & Kronberg, L. (2007). Occurrence of pharmaceuticals in river water and their elimination in a pilot-scale drinking water treatment plant. *Environmental Science & Technology*, *41*, 5077-5084.
371. Wammer, K. H., Korte, A. R., Lundeen, R. A., Sundberg, J. E., McNeill, K., & Arnold, W. A. (2013). Direct photochemistry of three fluoroquinolone antibacterials: norfloxacin, ofloxacin, and enrofloxacin. *Water Research*, *47*, 439-448.
372. Wang, J. L., & Xu, L. J. (2012). Advanced oxidation processes for wastewater treatment: formation of hydroxyl radical and application. *Critical Reviews in Environmental Science and Technology*, *42*, 251-325.
373. Wang, J., & Wang, S. (2016). Removal of pharmaceuticals and personal care products (PPCPs) from wastewater: a review. *Journal of Environmental Management*, *182*, 620-640.
374. Wang, L., Batchelor, B., Pillai, S. D., & Botlaguduru, V. S. (2016). Electron beam treatment for potable water reuse: Removal of bromate and perfluorooctanoic acid. *Chemical Engineering Journal*, *302*, 58-68.
375. Wang, M., Yang, R., Wang, W., Shen, Z., Bian, S., & Zhu, Z. (2006). Radiation-induced decomposition and decoloration of reactive dyes in the presence of H_2O_2. *Radiation Physics and Chemistry*, *75*, 286-291.
376. Wang, S., & Wang, J. (2017). Carbamazepine degradation by gamma irradiation coupled to biological treatment. *Journal of Hazardous Materials*, *321*, 639-646.
377. Wang, Y., Gao, Y., Chen, L., & Zhang, H. (2015). Goethite as an efficient heterogeneous Fenton catalyst for the degradation of methyl orange. *Catalysis Today*, *252*, 107-112.
378. Warburton, D. W., Bowen, B., & Konkle, A. (1994). The survival and recovery of Pseudomonas aeruginosa and its effect upon salmonellae in water: methodology to test bottled water in Canada. *Canadian Journal of Microbiology*, *40*, 987-992.
379. Watkinson, A. J., Murby, E. J., & Costanzo, S. D. (2007). Removal of antibiotics in conventional and advanced wastewater treatment: implications for environmental discharge and wastewater recycling. *Water Research*, *41*, 4164-4176.
380. Watts, R. J., & Dilly, S. E. (1996). Evaluation of iron catalysts for the Fenton-like remediation of diesel-contaminated soils. *Journal of Hazardous Materials*, *51*, 209-224.

381. WHO, World Health Organization, 2011. Pharmaceuticals in Drinking-water. 1-49.
382. Woods, R. J., & Pikaev, A. K. (1994). *Applied Radiation Chemistry: Radiation Processing*. John Wiley & Sons.
383. Wu, J. J., Muruganandham, M., Yang, J. S., & Lin, S. S. (2006). Oxidation of DMSO on goethite catalyst in the presence of H_2O_2 at neutral pH. *Catalysis Communications*, *7*, 901-906.
384. Xiao, X. Y., McCalley, D. V., & McEvoy, J. (2001). Analysis of estrogens in river water and effluents using solid-phase extraction and gas chromatography–negative chemical ionisation mass spectrometry of the pentafluorobenzoyl derivatives. *Journal of Chromatography A*, *923*, 195-204.
385. Xu, L., & Wang, J. (2011). A heterogeneous Fenton-like system with nanoparticulate zero-valent iron for removal of 4-chloro-3-methyl phenol. *Journal of Hazardous Materials*, *186*, 256-264.
386. Xu, L., & Wang, J. (2012). Magnetic nanoscaled Fe_3O_4/CeO_2 composite as an efficient Fenton-like heterogeneous catalyst for degradation of 4-chlorophenol. *Environmental Science & Technology*, *46*, 10145-10153.
387. Xu, Y., Chen, L., Wang, X., Yao, W., & Zhang, Q. (2015). Recent advances in noble metal based composite nanocatalysts: colloidal synthesis, properties, and catalytic applications. *Nanoscale*, *7*, 10559-10583.
388. Xue, J., & Wang, J. (2008). Radiolysis of pentachlorophenol (PCP) in aqueous solution by gamma radiation. *Journal of Environmental Sciences*, *20*, 1153-1157.
389. Xue, X., Hanna, K., Despas, C., Wu, F., & Deng, N. (2009). Effect of chelating agent on the oxidation rate of PCP in the magnetite/H_2O_2 system at neutral pH. *Journal of Molecular Catalysis A: Chemical*, *311*, 29-35.
390. Yang, H., Ogawa, T., Hasegawa, D., & Takahashi, M. (2008). Synthesis and magnetic properties of monodisperse magnetite nanocubes. *Journal of Applied Physics*, *103*, 07D526.
391. Yang, J., Gao, Y., Liu, W., Ge, W., & Zhao, R. (2015). The degradation and mineralization of acephate by ionization irradiation. *Environmental Progress & Sustainable Energy*, *34*, 324-332.
392. Yang, L., Liya, E. Y., & Ray, M. B. (2008). Degradation of paracetamol in aqueous solutions by TiO_2 photocatalysis. *Water Research*, *42*, 3480-3488.

393. Yu, S., Hu, J., & Wang, J. (2010). Gamma radiation-induced degradation of p-nitrophenol (PNP) in the presence of hydrogen peroxide (H_2O_2) in aqueous solution. *Journal of Hazardous Materials*, *177*, 1061-1067.

394. Yuan, X., Floresyona, D., Aubert, P. H., Bui, T. T., Remita, S., Ghosh, S., Brisset, F., Goubard, F., & Remita, H. (2019). Photocatalytic degradation of organic pollutant with polypyrrole nanostructures under UV and visible light. *Applied Catalysis B: Environmental*, *242*, 284-292.

395. Zhang, D., Gersberg, R. M., Ng, W. J., & Tan, S. K. (2014). Removal of pharmaceuticals and personal care products in aquatic plant-based systems: a review. *Environmental Pollution*, *184*, 620-639.

396. Zhao, J., Yao, B., He, Q., & Zhang, T. (2012). Preparation and properties of visible light responsive Y^{3+} doped $Bi_5Nb_3O_{15}$ photocatalysts for Ornidazole decomposition. *Journal of Hazardous Materials*, *229*, 151-158.

397. Zheng, B. G., Zheng, Z., Zhang, J. B., Luo, X. Z., Wang, J. Q., Liu, Q., & Wang, L. H. (2011). Degradation of the emerging contaminant ibuprofen in aqueous solution by gamma irradiation. *Desalination*, *276*, 379-385.

398. Zheng, B. G., Zheng, Z., Zhang, J. B., Luo, X. Z., Wang, J. Q., Liu, Q., & Wang, L. H. (2011). Degradation of the emerging contaminant ibuprofen in aqueous solution by gamma irradiation. *Desalination*, *276*, 379-385.

399. Zhu, L., Santiago-Schübel, B., Xiao, H., Hollert, H., & Kueppers, S. (2016). Electrochemical oxidation of fluoroquinolone antibiotics: Mechanism, residual antibacterial activity and toxicity change. *Water Research*, *102*, 52-62.

400. Zhu, Y., Murali, S., Cai, W., Li, X., Suk, J. W., Potts, J. R., & Ruoff, R. S. (2010). Graphene and graphene oxide: synthesis, properties, and applications. *Advanced Materials*, *22*, 3906-3924.

401. Zubir, N. A., Yacou, C., Motuzas, J., Zhang, X., & Da Costa, J. C. D. (2014). Structural and functional investigation of graphene oxide–Fe_3O_4 nanocomposites for the heterogeneous Fenton-like reaction. *Scientific Reports*, *4*, 4594.

402. Zuccato, E., Calamari, D., Natangelo, M., & Fanelli, R. (2000). Presence of therapeutic drugs in the environment. *The lancet*, *355*, 1789-1790.

403. Zuccato, E., Castiglioni, S., & Fanelli, R. (2005). Identification of the pharmaceuticals for human use contaminating the Italian aquatic environment. *Journal of Hazardous Materials*, *122*, 205-209.

404. Zwiener, C. F. F. H., & Frimmel, F. H. (2000). Oxidative treatment of pharmaceuticals in water. *Water Research*, *34*, 1881-1885.

LIST OF CONTRIBUTIONS

Published:

- **Changotra, R.**, Varshney, L., Guin, J. P., & Dhir, A. (2018). Performance of hematite particles as an Iron source for the degradation of ornidazole in photo-fenton process. ***Journal of Sol-Gel Science and Technology***, *85*(1), 203-212.
- **Changotra, R.**, Rajput, H., Dhir, A., Natural soil mediated photo Fenton-like processes in treatment of pharmaceuticals: Batch and continuous approach, ***Chemosphere*** 188 (2017) 345-353.
- **Changotra, R.**, Varshney, L., Guin, J. P., Dhir, A., Assessment of reaction intermediates with gamma radiation-induced degradation of Ofloxacin in aqueous medium, ***Chemosphere*** 208 (2018) 606-613.
- **Changotra, R.**, Guin, J. P., Dhir, A., & Varshney, L. (2018). Decomposition of antibiotic ornidazole by gamma irradiation in aqueous solution: kinetics and its removal mechanism. ***Environmental Science and Pollution Research***, 25(32), 32591-32602.
- **Changotra, R.**, Guin, J. P., Khader, S. A., Varshney, L., & Dhir, A. (2019). Electron beam induced degradation of ofloxacin in aqueous solution: kinetics, removal mechanism and cytotoxicity assessment. ***Chemical Engineering Journal***, *356*, 973-984.
- **Changotra, R.**, Rajput, H., Guin, J. P., Varshney, L., Dhir, A. (2019). Hybrid coagulation, gamma irradiation and biological treatment of real pharmaceutical wastewater. ***Chemical Engineering Journal***, 370, 595–605.
- **Changotra, R.**, Rajput, H., Dhir, A. (2019). Treatment of real pharmaceutical wastewater using combined approach of Fenton applications and aerobic biological treatment. ***Journal of Photochemistry and Photobiology A: Chemistry,*** 376, 175–184.
- **Changotra, R.**, Rajput, H., Guin, J. P., Varshney, L., Dhir, A. (2020). Techno-economical evaluation of coupling ionizing radiation and biological treatment process for the remediation of real pharmaceutical wastewater. ***Journal of Cleaner Production,*** 242 118544

Communicated:

- **Changotra, R.**, Guin, J. P., Khader, S. A., Varshney, L., & Dhir, A. Assessment of efficacy of electron beam-induced degradation of ornidazole in aqueous solution: implications to kinetics, parameters, toxicity and cost evaluation (Revesion submitted)
- **Changotra, R.,** Guin, J. P., Khader, S. A., Varshney, L., Dhir, A., Comparative assessment of gamma and electron beam irradiation for the treatment of pharmaceutical wastewater.
- **Changotra, R.,** Rajput, H., Guin, J. P., Dhir, A., Enhanced catalytic degradation of antibiotics by highly-dispersive FeS_2@Graphene Oxide via heterogeneous photo-Fenton reaction.

Conferences/workshops/symposium attended:

- Poster Presentation on "Treatment of real pharmaceutical industry wastewater using photo-Fenton process" International Conference on Advanced Oxidation Processes, AOP-2016, BITS Goa. December 17-20, 2016.
- Poster Presentation on "Electron beam induced degradation of Ofloxacin in aqueous medium" International Conference on Advanced Applications of Radiation technology, NICSTAR-2018, organized by NAARRI, Mumbai and DAE, Govt. of India on March 5-7, 2018 at Mumbai.
- Poster presentation "Gamma irradiation-induced degradation of Ofloxacin in aqueous medium" at National Symposium on Applications of Radioisotopes and Radiation Technology in Industry, Healthcare and Agriculture (ARRTIHA-2016) organized by Department of Chemical Engineering, TIET, Patiala and NAARRI, Mumbai on November 28-29, 2016 at TIET, Patiala.

Annexure

1.1 List of solvents used in bulk drugs manufacturing

S. No.	Name of solvent	Chemical formula	Toxicity	Boiling point
1	Methanolic hydrochoride	CH_3OHCl	Slightly	100.8
2	Methanol	CH_3OH	Moderate	66
3	Methyl isobutyl ketone	$C_6H_{12}O$	Moderate	115.9
4	Azacyclonol	$C_{18}H_{21}NO$	-	445.5
5	Denatured salt	C_2H_5OH	Moderate	78
6	Acetic acid	$C_2H_4O_2$	Slightly	118.1
7	Methylene chloride	CH_2Cl_2	Moderate	39.75
8	Isopropyl alcohol	$CH_3CHOHCH_3$	Moderate	82.5
9	Ethyl acetate	$C_2H_5COOCH_3$	Slightly	77
10	Acetonitrile	CH_3CN	Moderate	81.6
11	Toluene	C_7H_8	Acute	110.6
12	Tri ethyl amine	$C_6H_{15}N$	Acute	88.8
13	Dimethyl amine	C_2H_7N	Acute	7-9
14	2-Eethoxy propene	$C_5H_{10}O$	Acute	66
15	Formic acid	HCOOH	Acute	110
16	Hexamethyldisilazane	$C_6H_{19}NSi_2$	Moderate	126
17	Dimethyl sulfoxide	CH_3SOCH_3	Moderate	106
18	Hydroxyl amine	NH_2OHHCl	Moderate	78
19	Chloro benzene	C_6H_5Cl	Slightly	131